Heme *b* abundance in marine particulate material and heme *b* utilization and regulation patterns in marine phytoplankton

Dissertation

ZUR ERLANGUNG DES DOKTORGRADES

DER MATHEMATISCH - NATURWISSENSCHAFTLICHEN FAKULTÄT

DER CHRISTIAN-ALBRECHTS-UNIVERSITÄT ZU KIEL

VORGELEGT VON

EVANGELIA LOUROPOULOU

KIEL, JUNI 2019

1. Gutachter: Prof. Ruth Schmitz-Streit

2. Gutachterin: Prof. Eric Achterberg

Disputationsdatum: 18.09.2019

Zum Druck genehmigt

gez. Prof. Dr. Natascha Oppelt, Dekanin

Summary

Iron (Fe) is an essential micro-nutrient for all organisms in general, including marine phytoplankton, because it is a key component of biomolecules that participate in fundamental biological processes. One of the most biologically important groups of Fe biomolecules are hemes. Hemes consist of a tetrapyrrole ring (porphyrin) and a centrally coordinated Fe atom. Heme *b* (Fe-protoporphyrin IX) is considered the most common heme in marine phytoplankton and accounts for 20% of the intracellular Fe inventory. Heme *b* is involved in photosynthesis, respiration and nitrate assimilation in marine phytoplankton. In open-ocean surface waters, the concentrations of dissolved Fe can be very low thus not sufficient to sustain phytoplankton growth. Hence, Fe limitation leads to decreases in photosynthesis and nitrogen fixation (i.e. reduction of atmospheric di-nitrogen to biologically accessible forms of nitrogen) rates of phytoplankton as well as to lack of heme-bound-Fe, so called "*Anemia*". We know that heme *b* concentrations in phytoplankton typically decline with low Fe supply, but the physical, chemical or biological processes driving heme *b* abundance in the ocean are still uncertain.

This PhD project investigates the impact of Fe limitation i) on heme *b* abundance in phytoplankton and marine particulate matter, and ii) on the production, utilization and degradation processes of heme *b* by field work and laboratory experiments. The main research questions driving this work are 1) Can heme *b* be used as a proxy of Fe limitation in field phytoplankton populations? 2) Is phytoplankton able to regulate their heme *b* pool to reduce Fe requirements under Fe limitation? 3) Does heme *b* regulation originate from a modification in the gene expression of proteins involved in its cycling?

The main findings of this study were the following:

- Sampling in the subpolar North Atlantic showed that changes in the abundance of heme *b* were mainly linked to changes in the biomass. A decoupling from the biomass-driven abundance occurred in Irminger Basin where heme *b* was low despite an elevated biomass. Comparison of the Irminger Basin to the Iceland Basin showed that dissolved-Fe concentrations were similar in these two areas and that Fe was not depleted. However, large diatoms dominated in the Irminger Basin and smaller-sized prymnesiophytes were mostly abundant in the Iceland Basin. Thus, heme *b* depletion in Irminger Basin was considered to be a regulatory response of the diatoms expressed by reduction of heme-Fe because of their size related higher Fe requirement. Similar patterns were observed in the past in prymnesiophyte populations, hence heme *b* depletion and regulation is not a class- or species-specific response but rather depends on the individual Fe requirements of each phytoplankton class. Reduction and regulation of heme *b* may thus occur in declining phytoplankton populations during the shifts from larger to smaller sized species.

- The systematic investigation of heme *b* abundance in different oceanographic regions of the Atlantic Ocean showed that heme *b* relative to biomass (as indicated by particulate organic carbon) was consistently low in areas characterized by low Fe supply (i.e. seasonally Fe limited Irminger Basin and the Subtropical South Atlantic gyre). Thus, this ratio gave a reliable indication of Fe-limited phytoplankton communities *in situ*. In addition, comparison of the measured to simulated heme *b* concentrations indicated that heme *b* could account for 0.17 to 9.1 % of the total biogenic Fe.
- Laboratory experiments in the two diazotroph species *Cyanothece* and *Trichodesmium* showed that low Fe supply restricted the production of heme *b* in both species since the abundance of protoporphyrin-IX (heme *b* precursor) declined under Fe limitation. Under Fe limitation, *Trichodesmium* reduced the overall Fe requirements by allocating the available Fe into the heme *b*- containing cytochrome b_6f and by reducing the nitrogenase production which thus resulted in declines in nitrogen fixation activity. *Cyanothece* also increased the utilization of heme *b* under Fe limitation, which however was not linked to increases in the cytochrome b_6f. Furthermore, heme oxygenase (HO), which catalyzes the degradation of heme *b*, remained downregulated under Fe limitation in both species. Interestingly, the transcripts of a second HO in *Cyanothece* increased under Fe limitation and were accompanied by an enhancement of the heme *b* relative to biomass ratios.

Overall this PhD project demonstrated that heme *b* depletion is a good indicator of Fe limited phytoplankton. Therefore, heme *b* concentrations and ratios relative to biomass can be used for mapping Fe limited areas in field studies. Furthermore, this study illustrated that many phytoplankton groups (diatoms, haptophytes and diazotrophs) are able to regulate their heme *b* pool as a response to Fe limitation in order to maintain their growth and activity, potentially via localization of Fe to non-heme Fe-proteins. It appears that there are diverse mechanisms for regulating the heme *b* pool including modifications in the production, utilization and degradation processes. This study documented that up- or downregulation of the genes encoding HO can be of primary importance for controlling heme *b* intracellular levels. Finally, the upregulation of a HO in *Cyanothece* raises the hypothesis of an existence of Fe acquisition mechanisms by prokaryotes either via internal Fe recycling or via breakdown of extracellular hemes.

This study contributes to the understanding of how the available Fe is utilized in the heme *b* pool of phytoplankton and provides information on the molecular adaptation capability of diverse phytoplankton groups to Fe limitation. This information is particularly useful for assessing phytoplankton's status in dynamically changing oceanic environments and specifically in the Atlantic Ocean because of the projected changes in atmospheric dust deposition from the Sahara desert. Knowledge of phytoplankton adaptation mechanisms can thus help us predict the implications of changing Fe supply on key biogeochemical processes in the ocean (e.g. carbon fixation, nitrogen fixation).

Zusammenfassung

Eisen ist ein essentieller Mikronährstoff für alle lebendigen Organismen der Erde, einschließlich des marinen Phytoplanktons, da Eisen in Biomolekülen eine Schlüsselrolle für grundlegende biologische Prozesse spielt. Eine der biologisch wichtigsten Gruppen von Eisen-Biomolekülen sind Häme. Häme bestehen aus einem Tetrapyrrolring (Porphyrin) und einem zentral koordinierten Eisen-Atom. Häm *b* (Fe-Protoporphyrin IX) gilt als das am häufigsten vorkommende Häm im marinen Phytoplankton und es beträgt 20% des intrazellulären Eiseninventars. Häm *b* ist an der Photosynthese, Zellatmung und Nitratassimilation im marinen Phytoplankton beteiligt. In der Oberflächenschicht des Ozeans können die Eisenkonzentrationen niedrig sein, was zu einer Limitierung des Phytoplanktonwachstums führen kann. Diese Eisenlimitierung führt zu einer Abnahme der Photosyntheseleistung und der Stickstofffixierung (d.h. Reduktion des atmosphärischen Distickstoffs zu biologisch zugänglichen Stickstoffformen) von Phytoplankton sowie zu einem Mangel an Häme-Eisen, der sogenannten "Anämie". Es ist allgemein bekannt, dass die Häm *b* Konzentration in Phytoplankton unter geringer Eisenverfügbarkeit abnimmt, aber bis jetzt sind die physikalischen, chemischen oder biologischen Prozesse, die diese Abnahme verursachen noch unbekannt.

Diese Dissertation untersucht die Auswirkungen der Eisenlimitierung auf Häm *b* Konzentrationen in Phytoplankton und auf die Bildungs-, Verarbeitungs- und Abbauprozesse von Häm *b* in Feld- und Laborexperimenten. Die wichtigsten Forschungsfragen, die diese Arbeit antreiben, sind 1) Kann Häm *b* als Proxy für die Eisenlimitierung von verschiedenen Phytoplanktongruppen im Ozean verwendet werden? 2) Ist Phytoplankton in der Lage ihren Häm *b* Pool zu regulieren, um den Eisenbedarf unter Eisenmangel zu reduzieren? 3) Reguliert Phytoplankton seine Häm *b* Konzentration durch eine Änderung der Gen-Expression der Proteine, die am Häm *b* Zyklus beteiligt sind?

Die wichtigsten Ergebnisse dieser Studie waren die folgenden:

- Die Probenahme im subpolaren Nordatlantik zeigte, dass Häm *b* Konzentrationen positiv mit der Biomasse korrelieren. Eine Entkopplung hiervon erfolgte im Irminger Becken, wo trotz hoher Biomasse-Werte die Häm *b* Konzentrationen niedrig waren. Ein Vergleich des Irminger Beckens mit dem Island Becken zeigte, dass hier gelöste Eisenkonzentrationen ähnlich waren und dass keine Eisenlimitierung vorlag. Im Irminger Becken dominierten jedoch große Kieselalgen und im Island Becken waren kleinere Prymnesiophyten am häufigsten vorhanden. Die Kieselalgen im Irminger Becken regulierten ihre Häm *b* Konzentration aufgrund ihres größenbedingten höheren Eisenbedarfs herunter, was zu einer Konzentrationsabnahme des Häm-Eisen Komplexes führte. Häm *b* Limitierung und Regulierung sind keine klassen- oder artenspezifische Eigenschaften, sondern sie

hängen von dem individuellen Eisenbedarf jeder Phytoplanktonklasse ab. Bei dem Übergang von Kieselalgen zu Prymnesiophyten als dominante Phytoplanktongruppen, kann Reduktion und Regulierung von Häm b in der schwindenden Kieselalgenpopulation auftreten.

- Systematische Untersuchungen der Häm *b* Konzentrationen in verschiedenen ozeanographischen Regionen des Atlantiks zeigten, dass das Verhältnis von Häm *b* zur Biomasse (d.h. partikulärer organischer Kohlenstoff) in Gebieten des Atlantiks konstant niedrig war, die durch eine geringe Eisenkonzentration charakterisiert waren (d.h. im saisonal Eisenlimitierten Irminger Becken und im subtropischen südatlantischen Strömungswirbel). Das Häm *b* zu Biomasse Verhältnis ist ein zuverlässiger Indikator für Eisenlimitierung im Ozean für verschiedene Phytoplanktongruppen. Darüber hinaus ergab sich aus gemessenen und mit den in einem Model simulierten Häm *b*-Konzentrationen, dass Häm *b* circa 0,17 bis 9,1 % des gesamten biogenen Eisens im Ozean ausmachen kann.
- Laborversuche mit zwei diazotrophen Phytoplanktonarten *Cyanothece* und *Trichodesmium* zeigten, dass eine geringe Eisenkonzentration die Bildung von Häm *b* in beiden Arten einschränkte, da die Protoporphyrin-IX Konzentration (Häm *b* Vorprodukt) unter Eisenlimitierung abnahm. Unter Eisenmangel reduzierten *Trichodesmia* den gesamten Eisenbedarf, indem sie das verfügbare Eisen dem im Häm *b* enthaltenden Cytochrom b_6f zuführten und die Nitrogenaseproduktion unterdrückten. Das letztere führte zu einem Rückgang der Stickstofffixierung. *Cyanothece* erhöhte die intrazelluläre Häm *b* Konzentration unter Eisenlimitierung, was jedoch nicht im Zusammenhang steht mit einem Anstieg der Cytochrom b_6f Konzentrationen in den Zellen. Darüber hinaus war die Bildung von Hämoxygenase (HO), die den Abbau von Häm *b* katalysiert, bei beiden Arten unter Eisenlimitierung unterdrückt. Überraschenderweise nahmen die Transkripte einer zweiten HO in *Cyanothec*e unter Eisenlimitierung zu und führte zu einer Verbesserung des Häm *b* zu Biomasse Verhältnisses.

Zusammenfassend hat diese Dissertation gezeigt, dass geringe Häm *b* Konzentrationen ein guter Indikator für Eisenlimitierung in Phytoplankton ist. Folglich könnten Häm *b*-Konzentrationen und das Häm *b* zu Biomasse Verhältnis zur Kartierung von eisenlimitierten Gebieten verwendet werden. Darüber hinaus hat diese Studie gezeigt, dass viele Phytoplanktonklassen (Kieselalgen, Haptophyten und Diazotrophen) in der Lage sind, ihr Häm *b* Inventar als Reaktion auf die Eisenlimitierung zu regulieren, um damit ihr Biomasse-Wachstum und ihre biologische Aktivität aufrechtzuerhalten, indem das knapp vorhandene Eisen nur überlebenswichtigen Proteinen zugewiesen wird. Es scheint, dass es verschiedene Mechanismen zur Regulierung des Häm *b*-Pools gibt, einschließlich Anpassungen in den Bildungs-, Verarbeitungs- und Abbauprozessen. Diese Studie zeigt, dass die Regulierung des Genpools, die die HO kodieren, von primärer Bedeutung für die Kontrolle des intrazellulären Häm *b* Levels sein kann. Schließlich wirft die Hochregulation der HO in *Cyanothece* die Frage auf, ob es weitere

Eisen-Akquisitionsmechanismen von Prokaryonten gibt, entweder über internes Eisenrecycling oder über den Abbau von extrazellulären Hämen.

Diese Studie trägt zum Verständnis bei, wie das verfügbare Eisen im Häm *b* Pool genutzt wird, und liefert Informationen über die molekularen Anpassungsmöglichkeiten verschiedener Phytoplanktongruppen auf Eisenmangel. Diese Informationen sind besonders wertvoll, um die Reaktion von Phytoplankton auf sich dynamisch verändernde Bedingungen im Ozean abzuschätzen. Hierzu zählt insbesondere der Atlantische Ozean, der unter dem Einfluss eines sich veränderenden atmosphärischen Eintrags von Staub aus der Sahara steht. Dieses vertiefte Wissen über Adaptionsmechnismen von Phytoplankton kann uns helfen, die Auswirkungen einer veränderten Eisenverfügbarkeit für wichtige biogeochemische Prozesse im Ozean (z.B. Kohlenstofffixierung, Stickstofffixierung) vorherzusagen.

Acknowledgements

First and foremost I would like to express my sincere gratitude to my two main supervisors, Dr. Martha Gledhill and Prof. Ruth Schmitz-Streit for offering me the opportunity to do research as a doctoral candidate and to realize this PhD dissertation.

I would like to especially thank Dr. Martha Gledhill, primarily for trusting me and initiating this project with me and for contributing to its funding. Mostly I would like to thank her for her constant support and encouragement both on a scientific and personal level and for her supervision, her interest and active participation, her substantial guidance of my project and the stimulating discussions that allowed me to grow as a research scientist.

I am deeply grateful to Prof. Ruth Schmitz-Streit for undertaking the supervision of my PhD project, for supporting it financially and for her guidance throughout my reseach and writing of my dissertation which motivated me to widen my research to different perspectives. Also I would like to thank her for being always supportive and for giving me the opportunity to work in innovative techniques at her lab which opened for me new horizons and gave me valuable experience.

I would also like to offer special thanks to Prof. Eric Achterberg who provided valuable guidance throughout the project but also for his financial contribution. His insightful comments allowed me to improve the way I worked and helped me think of the bigger picture of my research.

Special thanks to Prof. Julie LaRoche for co-supervising my project, for welcoming me in her lab at Dalhousie University and for exchanging ideas and data with me that added a different perspective to my research and improved the final outcome.

I would also like to express my appreciation to the HOSST graduate school for the financial support but primarily for giving me the opportunity to start this journey as a member of a multidisciplinary international community and for offering me the means via seminars, summer schools, conferences and a research stay at Dalhousie University to evolve as a scientist. I specially thank Dr. Christel Van den Bogaard for her support right from the beginning of my project in administrative issues. Also, I thank all my fellow HOSSTies and TOSSTies for sharing the enthusiasm for our PhD projects.

Also I thank Dr. Nancy Weiland-Bräuer and Nicole Pinnow of AG. Schmitz-Streit for all the scientific and technical support they provided and for helping me in the development of analytical methods even at times when I thought it was impossible. Without their precious help it would not be possible to conduct this research.

I thank my colleague, labmate and friend Dr. Alexandra Marki for the stimulating discussions that made our endless hours in the lab entertaining, for always keeping my moral high and for all the fun we have had in the last years.

Thanks to all members of the AG. Achterberg at GEOMAR for the wonderful collaboration. Special thanks to my officemate Felix Geißler for creating an excellent working environment and for helping me with German-language issues. Also thanks to Tim de Groot, Jennifer Clarke and Matthew Patey for the help in sampling during the research cruises and for making the long days on the ship enjoyable.

On a personal level, I thank my friends Kirsten, Ben, Hajar, Lisa, Tatum, Kriste for all the good time we had in last years and Penny, Christina, Julia, Georgina, Afroditi and Olga for supporting me spiritually while being in Greece. Also, special thanks to my good friend Amaryllis who convinced me to pursue a PhD project abroad and actively contributed to my application for funding.

Last but not least, this project would not have been possible without the constant support of my family throughout my time as a PhD student and my life in general; I would like to deeply thank my husband Tronje for his patience, his help in every-day issues, his spiritual support, his positive thinking that helped me believe in myself when I was in doubt and finally for proofreading my thesis. I am deeply grateful to my parents Costas and Kitty, who always inspired me and gave me a vision of contribution to the society through science and who never stopped supporting me in all possible ways when pursuing my dreams. Finally, I want to specially thank both Alexandros and Afroditi for their emotional support, for cheering me up and helping have fun during this stressful period.

Thank you all for your contribution to this PhD project!

Content

Abbreviations

AMT	Ammonium Transporters
AnC	Angola Current
ATP	Adenosine Triphosphate
AU	Arbitrary Units
BnC	Benguella Current
BR	Bilirubin
BV IXα	Biliverdin IXα
BVR	Biliverdin Reductase
C	Carbon
Ca^{2+}	Calcium ion
cDNA	complementary DNA
chl *a*	Chlorophyll *a*
Cl^-	Clorid ion
CO_2	Carbon dioxide
cp	Chloroplast
CS	Celtic Sea
CTD	Conductivity Temperature Depth sensor
CTNA	Coastal Tropical North Atlantic
cyt b_6f	Cytochrome b_6f
DAD	Diode Array Detection
DCM	Deep Chlorophyll Maximum
DFe	Dissolved iron
DNA	Desoxyribonukleinsäure
EGC	East Greenland Current
ESI	Electrospray Ionisation
ESI-MS	Electrospray Ionisation Mass Spectrometry
ESNAG	Eastern Subtropical North Atlantic Gyre
F_0	Minimal fluroscence values
Fe	Iron

Fe(II)	Ferrous Iron
Fe(III)	Ferric Iron
Fe(III)PTP	Fe(III) protoporphyrin IX chloride
Fe_{bio}	Biogenic iron
FeMo	Ironmolybdenum
Fe-S	Iron(II)sulfide
F_m	Maximal fluroscence values
FRRF	Fast Repetition Rate Fluorometry
F_v:F_m	Apparent PSII Photochemical Efficiency
GSH	Greenland Shelf
HCl	Hydrochlorid acid
hmo1	Gene encoding Heme Oxygenase 1 in *Cyanothece*
hmo2	Gene encoding Heme Oxygenase 2 in *Cyanothece*
hmox	Gene encoding Heme Oxygenase in *Trichodesmium*
HNO_3	Nitric acid
HO	Heme Oxygenase
HO1	Heme Oxygenase 1
HO2	Heme Oxygenase 2
HPLC	High Performance Liquid Chromatography
IC	Irminger Current
IceB	Iceland Basin
ICP-MS	Inductively Coupled Plasma – Mass Spectrometry
IrmB	Irminger Basin
ITCZ	Intertropical Convergence Zone
IUE	Carbon-specific Iron Use Efficiencies
K^+	Potassium ion
LC	Labrador Current
LS	Labrador Sea
Mg^{2+}	Magnesium ion
MLD	Mixed layer depth

MS	Mass Spectrometry
N_2	di-nitrogen
Na^+	Sodium ion
NAC	North Atlantic Current
NH_4^+	Ammonium
$NH_4(OH)$	Ammonium hydroxide
nifH	Gene encoding Fe-subunit of nitrogenase
NO_3^-	Nitrate
OGP	Octyl β-D-Glucopyranoside
OTU	Operational Taxonomic Unit
P	Phosphorus
PCR	Polymerase Chain Reaction
petB	Gene encoding of b_6 subunit of cytochrome b_6f
PFe	Particulate iron
PO_4^{3-}	Phosphate
POC	Particulate organic carbon
PON	Particulate organic nitrogen
POP	Particulate organic phosphorus
PSI	Photosystem I
PSII	Photosystem II
PTP	Protoporphyrin
QRT-PCR	Quantitative Realtime Polymerase Chain Reaction
ROS	Reactive Oxygen Species
SD	Standard deviation
SI	Supplementary Information
$Si(OH)_4$	Silicic acid
Si*	Silicate tracer
SML	Surfaced Mixed Layer
SNAG	Subtropical North Atlantic Gyre
SO_4^{2-}	Sulfate ion

SSAG	Subtropical South Atlantic Gyre
STSF	Subtropical Shelf Front
TN	Total Nitrate
TNA	Tropical North Atlantic
TSA	Tropical South Atlantic
Vnfix	Nitrogen-specific growth rate via nitrogen fixation
Φ_{sat}	Satellite-derived quantum yield of fluorescence

1. Introduction

1.1 Motivation and thesis outline

Iron (Fe) is the fourth most abundant element in the Earth's crust and is essential for life. On a cellular level, all organisms produce and employ specialized proteins (termed enzymes) to catalyze biochemical processes required for functioning, growth and survival. Iron is important because it constitutes one of the most common chemical components (i.e. metal cofactors) of proteins. In marine phytoplankton, all these Fe-containing proteins are associated with diverse fundamental biological processes, necessary for functioning, such as photosynthesis, respiration, di-nitrogen (N_2) fixation, reduction of oxidized nitrogen species (Geider and La Roche, 1994; Morel and Price, 2003; Raven et al., 1999).

Iron uptake by phytoplankton occurs directly from seawater in dissolved or colloidal forms. Despite the high abundance of Fe in the Earth's crust, the concentrations of dissolved Fe (DFe) in open ocean surface waters can be very low (<0.10 nmol L^{-1}) (Boyd and Ellwood, 2010; Sunda and Huntsman, 1995). This occurs for three reasons; i) precipitation, ii) scavenging and iii) biological uptake. In well-oxygenated surface waters and under seawater pH values of around 8, the dissolved ferrous iron - Fe(II) oxidizes rapidly to ferric iron - Fe(III), which subsequently forms insoluble Fe oxy-hydroxides that precipitate to deeper waters (Liu and Millero, 1999, 2002). In addition, Fe is removed from surface seawater due to scavenging, which refers to the removal of colloidal Fe by adsorption onto large settling particles falling down from surface waters. Finally, uptake of Fe by phytoplankton contributes to declines in the concentrations of Fe in surface seawater. Hence, the supply of Fe to surface waters from atmospheric deposition and deep mixing entrainment of sub-surface Fe pools can often not compensate for the losses via precipitation, scavenging and biological uptake (Tagliabue et al., 2017).

Iron deficiency is a condition reported for various organisms. Hence, in a similar manner to mammals and higher plants, many phytoplankton groups also suffer when Fe supply is low. Studies have well documented that low Fe availability can cause a decline in growth rates and other fundamental biological functions of phytoplankton. These include disruptions in carbon dioxide uptake and nitrogen fixation rates, with consequent impact on the global biogeochemical cycles of these two elements (e.g. Greene et al. 1992; Geider & La Roche 1994; Kolber et al. 1994; Sunda & Huntsman 1997; King & Barbeau 2007; Shi et al. 2007).

On a molecular level, atoms of Fe form small chemical structures with other elements and these structures are called cofactors. Cofactors bind to larger biomolecules (polypeptide chains) forming proteins as an end product. Heme *b* is the most common

Fe cofactor within an organism; it consists of a tetrapyrrole ring and a centrally coordinated Fe atom, and combined with polypeptide chains it forms hemoproteins (da Silva and Williams, 2001). For phytoplankton, heme *b* is a key component of photosynthesis and other critical metabolic processes (Hogle et al., 2014).

Anemia originates from the Greek word "*Αναιμία"* which literally translates as deficiency of Fe bound in heme molecules (thereon heme-Fe). Anemia can be a severe condition that occurs when Fe supply to cells is low and is expressed by reduction of the hemoprotein levels. Phytoplankton faces a similar problem since hemoproteins and their heme cofactors are of primary importance because they participate in critical metabolic processes. Although the impact of Fe limitation on phytoplankton activity is well documented, relatively few studies have reported the effects of Fe deficiency on the abundance of heme *b* containing proteins (e.g. Strzepek and Harrison 2004; Shi et al. 2007; Richier et al. 2012; Honey et al. 2013; Nunn et al. 2013; Gledhill et al. 2015; Snow et al. 2015a).

The aim of this PhD thesis is to advance the research regarding the impact of Fe limitation i) on the abundance of heme *b* in field and cultured phytoplankton populations, and ii) on heme *b* production, utilization and degradation processes. In the field, this study aims to identify the physical, chemical and biological processes that drive heme *b* distribution in oceanic environments. For phytoplankton in culture, this study aims to shed light on the Fe utilization strategies in the hemoprotein pool and identify its fate during Fe limitation.

Background information about the role of Fe in phytoplankton, the hemoproteins and their functions, the heme *b* cofactor as well as the state of research regarding the impact of Fe limitation on the heme *b* containing proteins are presented in Section 1.2 to 1.5. Based on the state of research, the hypotheses formulated for this dissertation are presented in Section 1.6. This dissertation is written in a cumulative form consisting of three manuscripts (Chapters 2, 3 and 4) aiming for publication to peer-reviewed scientific journals.

The dissertation has two research aspects; **1)** the investigation of heme *b* abundance in the field (Chapters 2 and 3), and **2)** the investigation of the heme *b* cycling in cultured phytoplankton (Chapter 4).

Chapter 2 examines the utility of heme *b* as a proxy for Fe limitation in the sub-polar and sub-tropical North Atlantic while it also provides the link between heme *b* abundance and microbial community composition. Thus this chapter also identifies how heme *b* behaves in extant phytoplankton groups during Fe limitation.

Chapter 3 provides a compilation of datasets and presents large-scale distribution patterns of heme *b* in the Atlantic Ocean. The heme *b* data presented in this chapter are gathered from different regions of the Atlantic Ocean varying in terms of physical,

chemical and biological oceanographic characteristics. Thus this chapter examines a series of factors that potentially drive heme *b* distribution in the ocean.

Chapter 4 presents a lab study in two common diazotroph species (*Cyanothece* and *Trichodesmium*) and examines the abundance of heme *b* and its production, utilization and degradation processes under different Fe treatments in culture. This chapter also incorporates transcriptomic studies thus it provides insights into the patterns of Fe utilization in the hemoprotein pool and its regulation under Fe limitation.

Chapter 5 presents an overview of the findings, the overall conclusions of the dissertation and provides suggestions for future studies required to fill in gaps in the existing state of research and answer scientific questions arising from the current project.

1.2 The role of oceanic phytoplankton

The term phytoplankton refers to photosynthetic organisms which function in a similar manner to terrestrial plants - they contain chlorophyll and require sunlight to grow. Phytoplankton occupies the upper parts of the ocean because of light availability. Phytoplankton species can be grouped into prokaryotes and eukaryotes. Marine cyanobacteria (e.g. *Prochlorococcus, Synechococcus, Trichodesmium, Crocosphaera, Cyanothece, Richelia*) belong to the prokaryotic phytoplankton. Eukaryotes include among others the Chlorophyta (green algae), Rhodophyta (red algae), Haptophyta, Bacillariophyta (diatoms) and Dinophyta (dinoflagellates) (Reynolds, 2006).

Phytoplankton requires chemical elements and compounds, also known as nutrients, in order to grow and function. Nutrients are used as energy sources or as components to build up cellular structures and molecules involved in the basic metabolism for survival, growth and reproduction (Reynolds, 2006). However, nutrients cannot be synthesized in the cells of phytoplankton and must be obtained from the environment. Nutrients can be grouped into inorganic macronutrients (carbon, nitrogen, phosphorus, silicon), major ions (Na^+, K^+, Mg^{2+}, Ca^{2+}, Cl^-, and SO_4^{2-}) and metals and metalloids such as iron, manganese, zinc, cobalt, copper, molybdenum and selenium (Sunda et al., 2005).

Oceanic phytoplankton plays a key role in the biogeochemical cycling of carbon and nitrogen on a global scale (Sarmiento and Gruber, 2004). One very important biochemical process occurring in the ocean is nitrogen fixation; some marine cyanobacteria known as marine diazotrophs are able to convert the biologically unavailable atmospheric di-nitrogen (N_2) gas to biologically accessible forms of nitrogen (NH_4). This process is crucial for the oceanic ecosystem because marine diazotrophs supply their environment with new nitrogen which is lost through denitrification and anammox processes in oxygen deficient waters (Ward et al., 2007; Zehr and Ward, 2002). Through exudation, and following death, they provide a nutrient so that other organisms are able to grow and function (Fig. 1.1).

In addition to nitrogen fixation that only some phytoplankton species are able to perform, all phytoplankton species sequester carbon dioxide (CO_2) from the atmosphere by performing photosynthesis. Oceans contribute up to approximately half of the photosynthetic carbon fixation on Earth (Field et al., 1998). Photosynthesis is closely associated with nitrogen fixation as phytoplankton requires nitrogen to sequester CO_2 (Fig. 1.1). During geological periods (e.g. during the last interglacial-glacial maximum) characterized by high nitrogen fixation activity, photosynthesis rates were also increased, while CO_2 in the atmosphere exhibited low concentrations (Falkowski, 1997). Therefore, oceanic phytoplankton plays an important role in the global atmospheric carbon dioxide removal and contributes to the regulation of the global climate (Charlson et al., 1987; Falkowski, 1994).

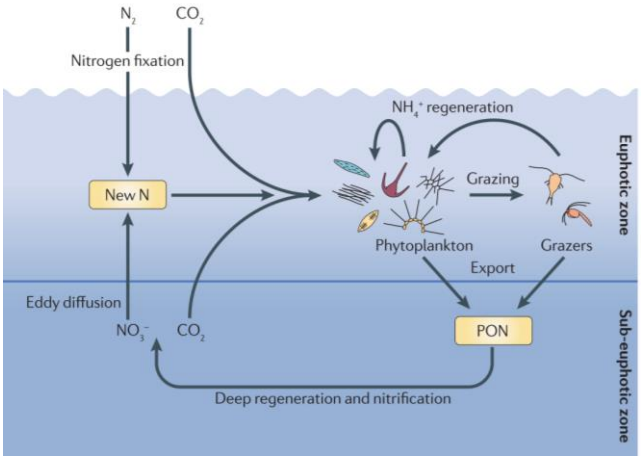

Fig. 1.1: Overview of the importance of nitrogen fixation in the ocean after (Sohm et al., 2011). The export of organic material from surface into deeper waters is dependent on the amount of CO_2 fixation (primary production) that is based on new nitrogen inputs (N_2 fixation or nitrate diffusion from deep waters). Alternatively, some primary productivity is based on the regeneration of organic material to ammonia in surface waters. PON stands for particulate organic nitrogen.

In order to perform nitrogen fixation and photosynthesis, all phytoplankton species require iron (Fe). Iron is a component of biomolecules linked to fundamental metabolic processes. In the 1980s, the 'iron hypothesis' suggested that an enhanced Fe supply to the Southern Ocean would result in increases in CO_2 sequestration rates during glacial periods (Martin, 1990). Since then studies have successfully demonstrated that Fe supply determines nitrogen fixation and photosynthesis in large parts of the world's ocean (e.g. Joos et al. 1991; Falkowski 1997; de Baar et al. 2005; Boyd et al. 2007; Moore et al. 2009).

1.3 Iron uptake and utilization by phytoplankton

The concentration of Fe in surface waters is controlled by physical, chemical and biological processes (Morel and Price, 2003; Tagliabue and Arrigo, 2006; Wells et al., 1995). Iron enters oceanic surface waters primarily via wet and dry deposition of mineral particles derived from dessert dusts (Jickells et al., 2005; Mahowald et al.,

2009). Volcanic eruptions (Achterberg et al., 2013; Duggen et al., 2010), riverine transport (Rijkenberg et al., 2014), glacial melting (Gerringa et al., 2012), hydrothermal vents (Resing et al., 2015) and sediments (Elrod et al., 2004) are also considered significant sources of Fe in the ocean. However, the Fe that enters surface waters is not readily available for uptake by phytoplankton since Fe-bioavailability depends on multiple factors like Fe speciation and kinetics, phytoplankton physiology and biochemistry or even physical parameters (Shaked and Lis, 2012).

Regarding Fe speciation, Fe solubility from aerosol particles largely depends on their origin (Baker and Croot, 2010) and on physicochemical processes such as redox reactions, inorganic and organic complexation, adsorption and precipitation that occur in seawater (Liu and Millero, 2002). Dissolved Fe (DFe) occurs in seawater in two oxidation states, Fe(II) and Fe(III), either as free ions or complexed with inorganic and organic ligands (Liu and Millero, 2002). Thermodynamically, in well oxygenated surface waters and under alkaline seawater pH, the dissolved Fe(II) oxidizes to Fe(III) (Millero et al., 1987, 1995; Stumm and Morgan, 1995). In turn, the Fe(III) reacts with water and forms insoluble Fe oxy-hydroxides which precipitate to deeper waters thus leading to low DFe concentrations in the surface (Liu and Millero, 1999, 2002).

Phytoplankton can acquire Fe directly from seawater in the dissolved form while particulate Fe (PFe) is unavailable for uptake. Free inorganic DFe can be used in both oxidation states (i.e. Fe(II) and Fe(III)) by phytoplankton and are the most readily available forms of Fe (Anderson and Morel, 1982; Morel, 2008; Shaked and Lis, 2012). However, in most cases Fe is not free in the marine environment but complexed by one or more organic ligands (Gledhill and Buck, 2012; Rue et al., 1997). The biological availability of the organic complexed Fe is still uncertain although some studies demonstrated that a fraction of the organically complexed Fe pool is bioavailable to phytoplankton (Gledhill and Buck, 2012; Lis et al., 2015; Maldonado and Price, 1999; Shaked and Lis, 2012; Soria-Dengg and Horstmann, 1995). It has also been suggested that the bioavailability of organically complexed Fe strongly depends on ligands (Hutchins et al., 1999; Maldonado et al., 2005; Maldonado and Price, 1999).

Regarding the Fe uptake mechanisms of phytoplankton from seawater, two major pathways have been described: a siderophore mediated Fe acquisition and a reductive Fe uptake pathway (Shaked and Lis, 2012). Siderophore mediated Fe uptake involves the synthesis and secretion of Fe(III) iron chelators which are capable of solubilizing, capturing, and delivering Fe(III) to the cell (e.g. Goldman et al. 1983; Kraemer 2004; Butler 2005; Butler and Theisen 2010). The reductive Fe uptake pathway applies to both free and organically complexed Fe(III) (Allnutt and Bonner, 1987; Maldonado and Price, 2001; Shaked et al., 2005). In this case, Fe(III) dissociates from its chelating ligand, transforms into Fe(II) by ferric reductases and is then transported as free Fe into the cell and reduced to Fe(II) by ferric reductases (Shaked and Lis, 2012).

Table 1.1: Iron (Fe) components of the electron transport chains in nitrogen fixation, assimilation and photosynthetic apparatus. Adapted from *Shi et al. 2007* and including data from *Raven 1988*.

Complex	Fe-containing cofactor	Number of Fe atoms per monomer
Nitrogen Fixation		
Nitrogenase	1[4Fe-4S]	4
	1 P cluster ([8Fe-7S])	8
	1 FeMoCo ([7Fe-9S-Mo])	7
Nitrogen Assimilation		
Nitrate Reductase	1 heme	1
Nitrite Reductase	2 hemes	2
Sulfur assimilation		
Sulfite reductase	1 [2Fe-2S]	2
	1 siroheme	1
Photosynthetic Apparatus		
PSII	1 non-heme iron	1
	1 heme	1
	1 heme	1
Cyt b_6f	3 hemes	3
	1 hemes	1
	1 [2Fe-2S]	2
	$1F_X$ ([4Fe-4S])	4
	$1F_A$ ([4Fe-4S])	4
	$1F_B$ ([4Fe-4S])	4
Other		
Cyt c_{553}	1 heme	1
Ferredoxin	1 [2Fe-2S] centre	2

These reductases may operate in conjunction with permease–oxidases that re-oxidize the Fe(II) as it is transported into the cell (Maldonado et al., 2006; Terzulli and Kosman, 2010). Finally, some heterotrophic bacteria are known to utilize the Fe-containing biomolecules hemes (for heme, see Section 1.4) as a direct source of Fe via heme-transport components and heme-membrane receptors (Hopkinson et al., 2008; Roe et al., 2013). Shaked and Lis (2012) proposed that the occurrence of either of these Fe uptake pathways is a result of environmental rather than taxonomic factors. Once in the cell, Fe is released in the cytoplasm and is distributed to the enzymes where it is required whilst the excess Fe is stored as ferritin (da Silva and Williams, 2001). Figure 1.2 illustrated the pathway of Fe uptake and its subsequent controlled distribution and metabolism.

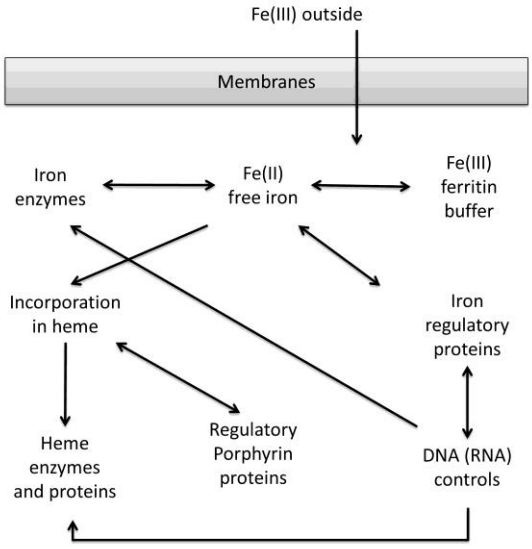

Fig. 1.2 Uptake of Fe and its subsequent controlled distribution and metabolism after *da Silva and Williams (2001)*.

Iron binds to other elements forming small chemical structures called cofactors. Iron-containing cofactors can be divided into heme (Section 1.4) and non-heme cofactors. This division is based on the Fe coordination and chemical bonds with the other elements within the molecule. These cofactors associate with longer chemical structures within the cell, polypeptide chains, thus forming proteins or the enzymes that undertake biochemical processes on a cellular level. In general, Fe - containing proteins are involved in oxidation-reduction processes, acid-base reactions as well as transport, control and storage of chemical elements (da Silva and Williams, 2001).

In marine phytoplankton, Fe is utilized in proteins of the photosynthetic and nitrogen fixation or nitrogen assimilation apparatus (Table 1.1). The photosynthetic apparatus requires the largest amount of Fe in photosynthetic organisms (Raven, 1988). The photosynthetic apparatus consists of the major protein complexes of photosystem II (PSII), cytochrome b_6f, photosystem I (PSI) and the smaller proteins ferredoxin and

cytochrome c_{553}. In total, 23-24 Fe atoms are utilized per photosynthetic unit in these complexes (Raven, 1990; Shi et al., 2007).

Nitrogen fixation and nitrogen accumulation are processes where Fe is also required. One "Fe-expensive" Fe-containing molecule is nitrogenase; marine cyanobacterial diazotrophs employ nitrogenase to catalyze the conversion of N_2 gas to fixed nitrogen (NH_4). The nitrogenase complex is composed of a dimeric Fe protein, which contains four Fe atoms per monomer, and a heterotetrameric Fe-molybdenum (FeMo) protein which contains fifteen Fe atoms per monomer (Dos Santos et al., 2004; Zehr, 1997). As a consequence marine diazotrophs require larger amounts of Fe in comparison to other marine phytoplankton species (Kustka et al., 2003). For the non-diazotrophic phytoplankton, the use of nitrite and nitrate adds a significant Fe cost (Raven, 1988, 1990) since nitrate and nitrite reductases contain one and four Fe atoms per monomer, respectively. In general, the computed Fe requirement for nitrogen assimilation increases in the order ammonium < nitrate < dinitrogen (Raven, 1988). Sulfur (S) assimilation by phytoplankton also requires Fe; sulfite reductases catalyze the reduction of sulfite to sulfide and contain per monomer two Fe atoms in the Fe-S cluster and an Fe atom in a siroheme complex (Crane et al., 1995).

1.4 Iron bound in heme cofactors

The Fe-cofactors consisting of a tetrapyrrole ring, also known as porphyrin and a centrally coordinated Fe(II) atom are called hemes (Chapman et al., 1997). These molecules are non-protein compounds but act as prosthetic groups (i.e. cofactors) in hemoproteins. The physical and chemical properties of the iron-porphyrins allow them to act as electron source/sink and as a binding site for small molecules (da Silva and Williams, 2001; Hogle et al., 2014). Hence, hemes are involved in crucial biological activities including electron transfer reactions, oxygen transport and storage, oxygen reduction to the level of hydrogen peroxide or water, oxygenations of organic substrates, and the reduction of peroxides (Chapman et al., 1997).

1.4.1 Heme biosynthesis

Hemes are produced via the tetrapyrrole synthesis pathway, in a similar manner to chlorophyll *a* (chl *a*) and siroheme/vitamin B12 pathways (Milgrom, 1997). Figure 1.3 illustrates briefly the heme biosynthesis pathway whilst all compounds participating in the biosynthesis are presented in Fig. 1.4. The synthesis is a multistep procedure and starts with a 5-aminolevulinic acid (ALA) complex, which is a universal precursor of tetrapyrroles in all organisms (Dailey et al., 2017; Hogle et al., 2014). The synthesis of ALA may differentiate among organisms and two common pathways have been described; a C4 pathway from succinyl-CoA commonly found in alphaproteobacteria and a C5 pathway of ALA from L-glutamate reported for other bacteria, eukaryotic marine algae, archaea and plants (Dailey et al., 2017; Hogle et al., 2014).

As a next step, asymmetric condensation of two ALA molecules by the action of the enzyme porphobilinogen synthase (PbgS) leads to the formation of monopyrrole porphobilinogen (Frankenberg et al., 1999; Jaffe, 1995, 2004). Hydroxymethylbilane synthase (HmbS) converts the monopyrrole into an intermediate tetrapyrrole called hydroxymethylbilane (Hart et al., 1987). Then, the enzyme uroporphyrinogen synthase (UroS) transforms hydroxymethylbilane into uroporphyrinogen III (Hart and Battersby, 1985; Shoolingin-Jordan, 1995).

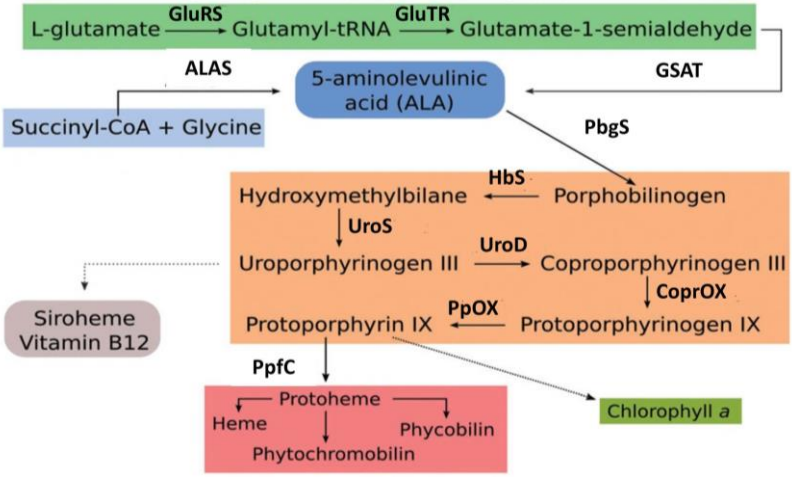

Fig. 1.3 Heme biosynthesis pathway after (Hogle et al., 2014). Dashed lines indicate multiple enzymatic steps. Abbreviations in bold letters indicate the enzyme responsible for each reaction; ALAS: ALA synthase; CoprOX, coproporphyrinogen oxidase; GluRS: glutamyl-tRNA synthetase; GluTR: glutamyl-tRNA reductase; GSAT: glutamate-1-semialdehyde aminotransferase; HbS: hydroxymethylbilane synthase; PbgS: porphobilinogen synthase; PpfC: ferrochelatase; PpoX: protoporphyrinogen IX oxidase; UroD: uroporphyrinogen decarboxylase; UroS: uroporphyrinogen III synthase.

From uroporphyrinogen III, there are two possible pathways; one leading to siroheme, heme *d1*, vitamin B12 and coenzyme F430 production and one leading to heme production. In the first case, the enzyme uroporphyrinogen III methyltransferase transforms uroporphyrinogen III into precorrin-2. Precorrin-2 is a precursor for heme d1, vitamin B12, coenzyme F430 and siroheme (Frankenberg et al., 2003).

The enzyme uroporphyrinogen III decarboxylase (UroD) catalyses the conversion of uroporphyrinogen III into coproporphyrinogen III (Elder and Roberts, 1995). Then, a classic pathway leading to heme production starts with coproporphyrinogen III which is oxidatively decarboxylated at two propionate groups by the enzyme coproporphyrinogen III oxidase (CoprOX) (Layer et al., 2006) and produces an intermediate product protoporphyrinogen IX. This intermediate is then oxidized to protoporphyrin IX by protoporphyrinogen IX oxidase (PpoX) (Koch et al., 2004; Poulson and Polglase, 1975) and is converted into heme upon insertion of an Fe atom by ferrochelatase (PpfC) (Ferreira, 1999). The Fe(II) is then bound to four coordinated nitrogen atoms in the protoporphyrin ring system. Similarly, chl *a* is produced by insertion of a magnesium (Mg) atom into a porphyrin ring by the enzyme magnesium chelatase (Cornah et al., 2003).

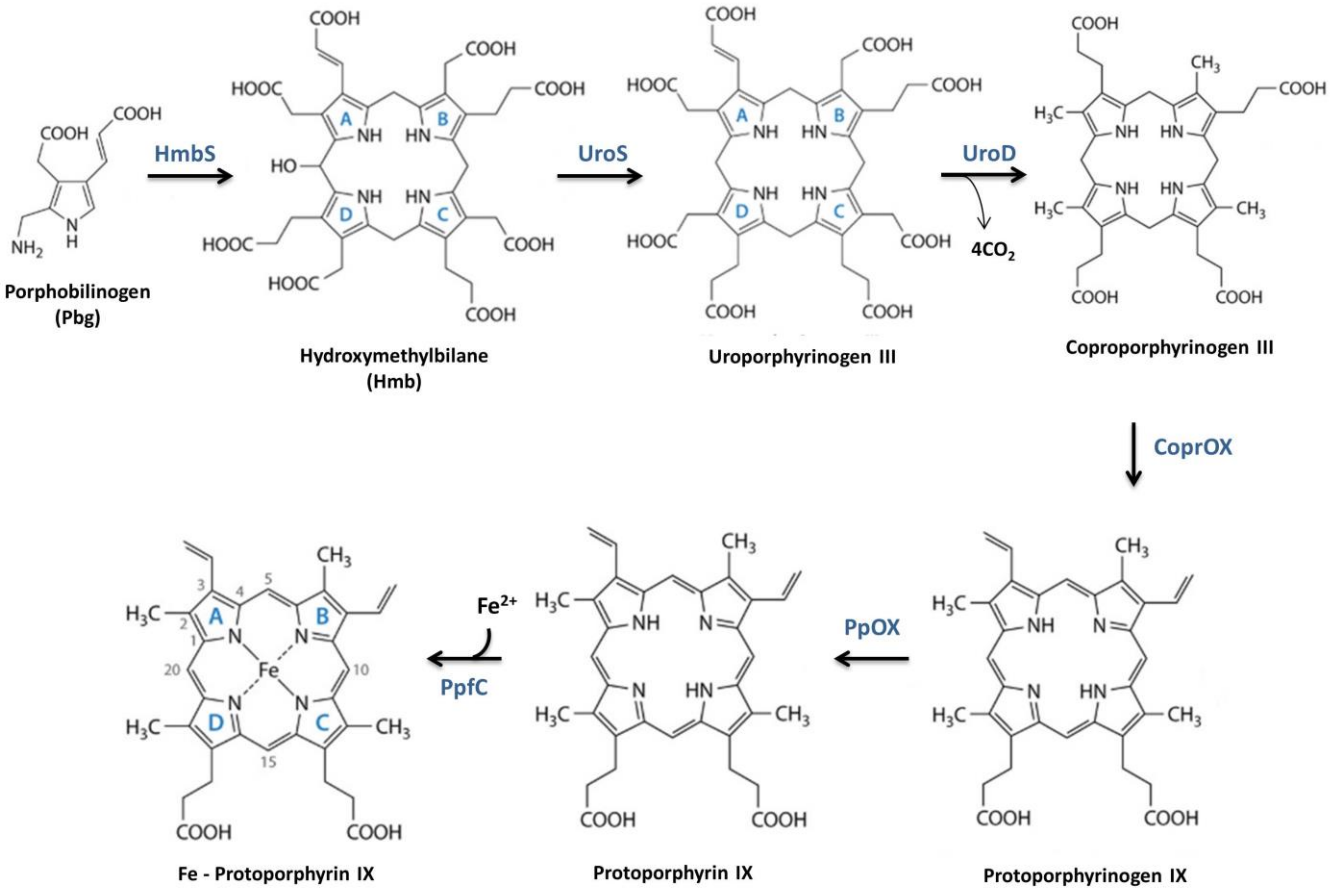

Fig. 1.4: Heme biosynthesis pathway; Abbreviations in bold letters indicate the enzyme responsible for each reaction; HmbS: Hydroxymethylbilane synthase; UroS: uroporphyrinogen synthase; UroD: uroporphyrinogen III decarboxylase; CoprOX: coproporphyrinogen III oxidase; PpOX: protoporphyrinogen IX oxidase; PpfC: ferrochelatase.

The protoporphyrin pathway was considered the sole mechanism for heme biosynthesis until recently, and is referred to as the "classic" pathway. This is the single pathway utilized in eukaryotes whilst among prokaryotes, it is found only within Gram-negative bacteria (Dailey et al., 2017). Two alternative pathways are commonly found in prokaryotes for heme production which use siroheme or coproporphyrin as precursors for the synthesis of Fe-protoporphyrin IX (Dailey et al., 2017). The common precursor of all three possible pathways is the Fe-protoporphyrin IX (or heme *b*), the product after insertion of the Fe atom. These alternative routes are considered evolutionary transitions between the siroheme pathway found first in archaea and the classical pathway found in Gram-negative bacteria and eukaryotes (Dailey et al., 2015, 2017; Dailey and Gerdes, 2015; Lobo et al., 2015).

The tetrapyrrole synthesis in eukaryotes is restricted to heme, siroheme, chlorophyll and bilins whereas prokaryotes are able to produce additionally corrinoids, heme *d1* and the coenzyme F430 (Frankenberg et al., 2003; Vavilin and Vermaas, 2002). The synthesis of hemes is partly controlled by free Fe (II) levels at the insertion step in mitochondria (da Silva and Williams, 2001). Cyanobacteria follow the protoporphyrin biosynthesis (i.e. classic) pathway for heme production (Dailey et al., 2017).

The end steps of heme biosynthesis diverge in all organisms (Milgrom, 1997) as the organic substituents bound in the outer part the porphyrin ring are not fixed. This feature allows the binding of various molecules with different chemical and physical properties onto the Fe-porphyrin structure thus resulting in various heme structures with diverse functions Fig. 1.5 (da Silva and Williams, 2001). Free hemes are highly toxic to cells (Espinas et al., 2012). Therefore, any produced heme molecules are incorporated as a prosthetic group in apoproteins (i.e. proteins without the cofactors) leading to the production of the hemoproteins. Hence, heme abundance is tightly linked to hemoprotein abundance within an organism (Espinas et al., 2012).

The multiple combinations of heme structures and polypeptide chains constituting the apoproteins result in a variety of hemoproteins with diverse biological functions (Chapman et al., 1997). In most hemoproteins, heme is coordinated to the protein via the central Fe atom (Chapman et al., 1997). Hemes *a*, *b*, *c*, *d1* and siroheme are some of the most commonly found hemes (Fig. 1.5). Heme *b* (also known as protoporphyrin IX) is the most versatile heme within an organism and has two vinyl ($-CH=CH_2$) groups on C2 and C4 and one methane group on C8 bound on the porphyrin ring (Caughey et al., 1973). Heme *b* is a prosthetic group of hemoglobin, myoglobin, catalase, most peroxidases, the *b*-type cytochromes and the cytochrome P-450 (Chapman et al., 1997). In contrast to heme *b*, heme *c* is covalently linked to the protein via thioether linkages which form between the thiol groups of cysteine residues on the protein and carbon atoms of vinyl groups at positions 2 and 4 of the porphyrin ring (Caughey et al., 1973; Chapman et al., 1997). Heme *c* is the prosthetic group in the *c*-type cytochromes performing electron transfer (Bowman and Bren, 2008). Heme *a* consists of a

hydroxyethylfarnesyl (-HFAR) sidechain on C2 of the porphyrin ring and a formyl group on C8 (Caughey et al., 1975). Heme *a* performs electron transfer in *a*-type cytochromes (Chapman et al., 1997; Malatesta et al., 1995). In contrast to hemes *a*, *b* and *c*, heme *d1* and siroheme have saturated bonds and carboxylic acid groups in the ring which make these molecules more water soluble compared to the other heme groups (Chapman et al., 1997; Hogle et al., 2014). Heme *d1* is utilized within heme-containing nitrite reductases, whilst siroheme is a component of sulfite and nitrite reductases (Stroupe and Getzoff, 2009; Tripathy et al., 2010).

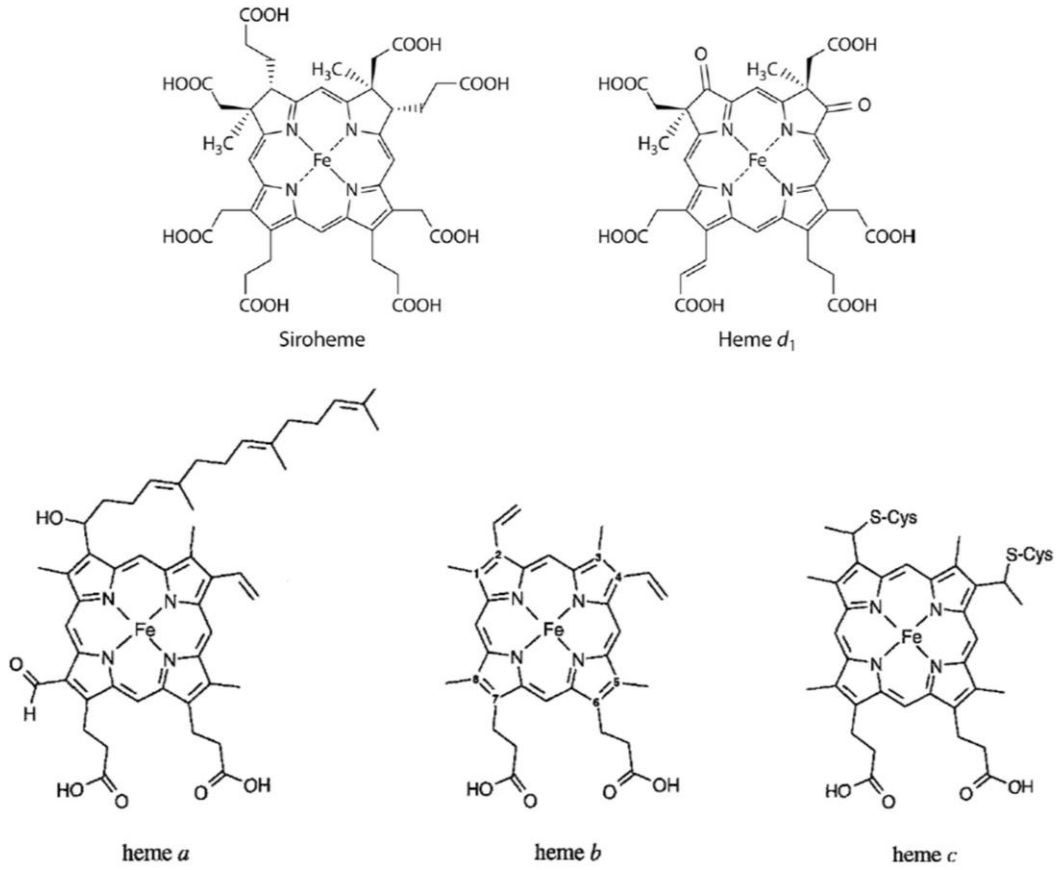

Fig. 1.5 *Structures of hemes commonly found in organisms modified from* Chapman et al. (1997) and Dailey et al. (2017).

1.4.2 Heme functions in marine phytoplankton

The heme molecule differs from simple Fe ions in terms of physical and chemical properties due to the presence of organic substituents on the porphyrin ring and the variety of Fe spin-states (da Silva and Williams, 2001). As cofactors in proteins, hemes have the ability to function as electron source and sink and as binding sites for small molecules. Thus, hemoproteins exhibit diverse biological functions which include electron transfer reactions and redox reactions, oxygenations of organic substrates, reduction of peroxides and divalent gas transport and storage (Chapman et al., 1997). Regarding the location of hemoproteins within a cell (Fig. 1.6), in eukaryotes they are located in major cellular organelles such as the mitochondrion and the chloroplast. In

bacteria these proteins may be either in the cytosol, periplasm, or inner and outer membranes whilst in cyanobacteria, photosynthetic and respiratory cytochromes reside in the thylakoid membrane (Hogle et al., 2014).

In marine phytoplankton, hemoproteins are involved in two of the most important biological processes; respiration and photosynthesis. Hemes are central components of the cytochromes involved in respiration and thus perform the electron transport required for the production of the Adenosine Triphosphate (ATP) (Richardson, 2000; Richter and Ludwig, 2009). Similarly, hemes undertake electron transport during oxygenic photosynthesis (Hohmann-Marriott and Blankenship, 2011). The D1 subunit of photosystem II (PSII) consists of the heme-containing cytochrome b_{559}, which is a heterodimer composed of PsbE (alpha) and PsbF (beta) subunits (Guskov et al., 2009). In addition, during photosynthesis, cytochrome b_6f shuttles electrons from PSII to PSI; cytochrome b_6f consists of a Rieske protein [2Fe-2S] and four heme groups (Kurisu, 2003).

Hemes are also components of enzymes linked to nutrient uptake in marine phytoplankton. Assimilatory nitrate reductase is a heme *b*- containing protein that undertakes the reduction of nitrate to nitrite (Fischer et al., 2005). Nitrate reductase is localized in the cytoplasm in marine diatoms (Allen et al., 2005; Gao et al., 1993). Ferredoxin nitrite reductases have also been reported for diatoms, which have one siroheme and one [4Fe-4S] cluster as cofactors (Bowler et al., 2009; Nakano et al., 2012). Similarly, for sulfite assimilation, sulfite reductases contain siroheme and Fe-S cofactors, they are located in the plastid and participate in the conversion of sulfite to sulfide (Giordano et al., 2005; Takahashi et al., 2011). Ferric reductases catalyze the reduction of Fe(III) to Fe(II) thus also promoting the solubilisation of extracellular complexed Fe (Schröder et al., 2003). Cytochrome b_{558}, cytochrome b_5 and cytochrome b_{561} are heme-containing ferric reductases involved in Fe mobilization in organelles and at the plasma membrane (Blaby-Haas and Merchant, 2012; Hogle et al., 2014).

Hemes are the prosthetic groups of catalases, peroxidases and catalase-peroxidases. These are all antioxidant enzymes which means that they degrade hydrogen peroxide and other organic hydroperoxides by breaking oxygen-oxygen bonds (Bernroitner et al., 2009; Hogle et al., 2014; Zamocky et al., 2008). Hydrogen peroxide and other reactive oxygen species (ROS) occur naturally in seawater after photochemical oxidation of dissolved organic matter and may inhibit critical metabolic processes in phytoplankton (Diaz and Plummer, 2018). Thus the management of these compounds in microbial cells is a highly important procedure. Although in higher plants peroxidases and catalases are localized in peroxisomes and vacuoles, respectively, the exact location within the cells of algae is not confirmed (Hogle et al., 2014).

Finally, in bacteria another major role of hemes is sensing and signalling (Chapman et al., 1997), which is a feature that induces changes in the expression of specific proteins and coordinates cellular metabolism (Wang and Lei, 2018). Heme sensor proteins can

bind the diatomic O_2, NO and CO that activate sensor protein domains capable of modifying gene expression and thus metabolism (Hogle et al., 2014; Mayfield et al., 2011). Interestingly, since the identification of a protein called Fe response regulator (Irr), it has been reported that heme can also be a sensed entity for some bacterial species (Singleton et al., 2010; Yang et al., 2006). The Irr protein binds heme after biosynthesis but also senses their intracellular concentrations, and thus regulates Fe utilization (Yang et al. 2006; Singleton et al. 2010).

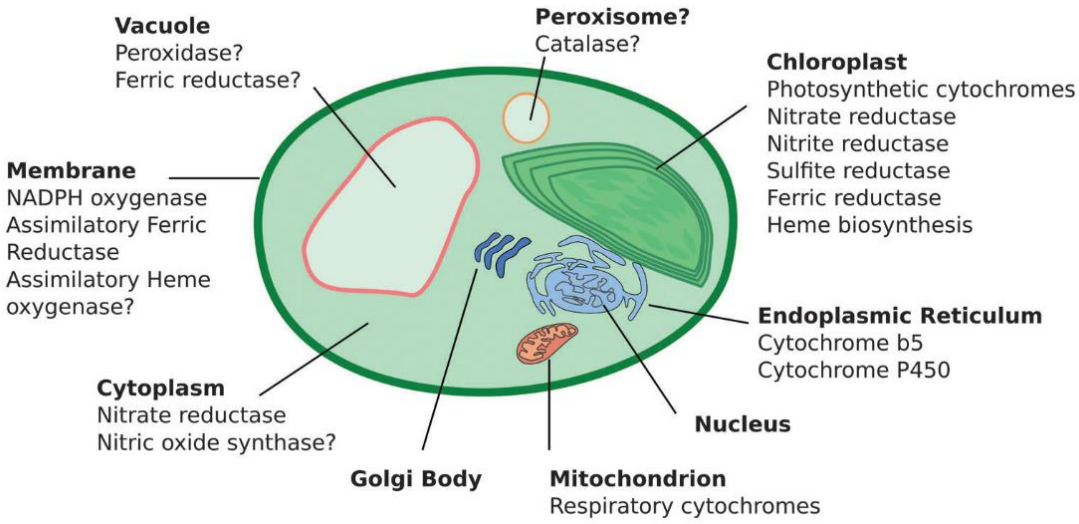

Fig. 1.6. Distribution of the major proteins containing heme-like cofactors in a hypothetical diatom after (Hogle et al., 2014). Question marks indicate hypothetical/unconfirmed presence in the cell. The major cellular organelles are listed in boldface and the proteins with heme or siroheme cofactors (and the heme biosynthesis pathway) are listed beneath them. In bacteria these proteins may be either in the cytosol, periplasm, or inner and outer membranes. In cyanobacteria, photosynthetic and respiratory cytochromes reside in the thylakoid membrane.

1.4.3 Heme metabolism and biosynthesis of phycobilins

Under normal growth conditions, hemes are degraded by the enzyme heme oxygenase (HO) to produce phytobilins (Beale and Yeh, 1999). Phytobilins are linear tetrapyrrole molecules acting as precursors of chromophores for the light-harvesting phycobiliproteins and the photoreceptor phytochrome (Beale, 1993). Hence, the deconstruction of heme is a process of primary importance for plants, algae, and cyanobacteria (Milgrom, 1997).

The production of phytobilins starts with the opening of the tetrapyrrole ring from a heme molecule in the α-meso carbon and removal of the Fe atom. This reaction is catalysed by an enzyme called HO and results in the production of biliverdin (BV IXα) (Frankenberg-Dinkel, 2004). This reaction requires a total of three oxygen molecules and seven electrons and yields apart from BV IXα, Fe^{2+} and carbon monoxide (Ortiz de Montellano, 2000). Cleavage of the porphyrin ring in the β- and δ- carbon has also been reported (Frankenberg-Dinkel, 2004). Then, BV IXα is further converted by biliverdin reductase (BVR) into bilirubin (BR) (Whitby et al., 2002) and by other

enzymes into phycocyanobilin, phycoerythrobilin and phycochromobilin (Fig. 1.7) (Frankenberg-Dinkel, 2004).

After production, the phytobilins are bound to apoproteins via single or double covalent bonds which can be further modified thus producing a variety of pigments called phycobiliproteins (Frankenberg-Dinkel, 2004). Two major classes of phycobiliproteins are phycocyanins and the phycoerythrins, which are respectively colored blue and red (Beale, 1993). These pigments are largely responsible for the characteristic colors of the organisms which contain them (i.e. blue-green cyanobacteria, red-algae rhodophytes) and the different colors arise from slightly different phytobilin chromophores (Beale, 2007).

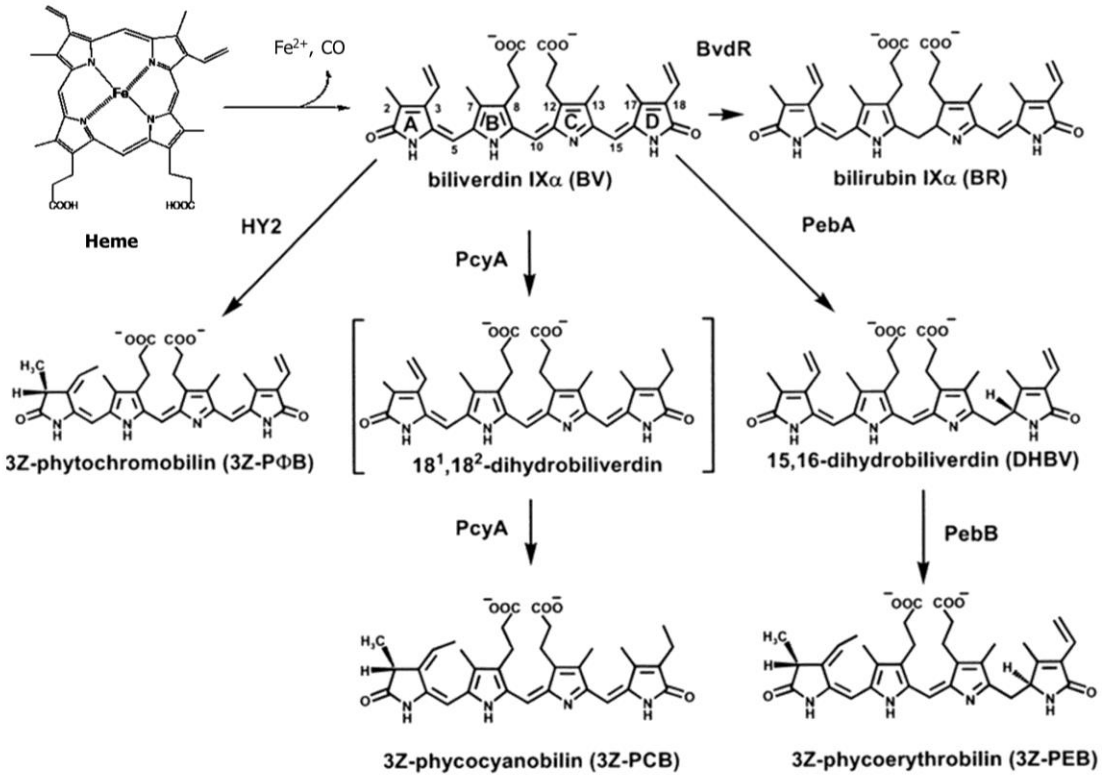

Fig. 1.7: Biosynthesis pathway of phytobilins in plants and cyanobacteria adapted from (Frankenberg-Dinkel, 2004). Synthesis starts with cleavage of the heme at the α-meso carbon position yielding biliverdin BV IXa. BV IXa is subsequently reduced by ferredoxin-dependent or NADPH-dependent reductases. Enzyme abbreviations used are: phytochromobilin – synthase (HY2), 3Z phycocyanobilin – ferredoxin – oxidoreductase (PcyA), 15,16 – dihydrobiliverdin – ferredoxin – oxidoreductase (PebA), 3Z – phycoerythrobilin – ferredoxin – oxidoreductase (PebB), biliverdin IXα – NAD(P)H – oxidoreductase (BvdR).

Heme oxygenase is the enzyme responsible for the conversion of heme to biliverdin in algae, cyanobacteria and higher plants. Similarly to mammalian HOs (Unno et al., 2007), algal HOs are highly ubiquitous and occur in several isoforms (Shekhawat and Verma, 2010). In contrast to the well characterized mammalian HOs (Wilks, 2002), the information about structures and functions of phytoplankton HOs is restricted to some cyanobacteria, cryptophytes and red algae (Beale and Cornejo, 1984; Cornejo et al., 1998; Cornejo and Beale, 1988, 1997; Migita et al., 2003; Muramoto, 2002; Rhie and

Beale, 1992, 1995; Richaud and Zabulon, 1997; Sugishima et al., 2004). The HOs are localized in the plastids (Migita et al., 2003; Muramoto, 1999; Terry et al., 2002) or the cytoplasm in prokaryotes (Hopkinson et al., 2008; Roe et al., 2013; Septer et al., 2011; Weaver et al., 2003) whereas in eukaryotes HOs are in chloroplast (Shekhawat and Verma, 2010).

On the bases of genomic organization, the cyanobacterial and algal HOs can be distinguished in two subfamilies (HO1-like and HO2-like) whilst the isoforms HO1, HO2, HO3 and HO4 were present in eukaryotic photosynthetic organisms (Frankenberg-Dinkel, 2004; Shekhawat and Verma, 2010). In general, known bacterial HO isoforms are HO1, HO2, PigA, Isd, HmuO and BphO (Frankenberg-Dinkel, 2004). The isoforms HO1 and HO2 were identified in the cyanobacterium *Synechocystis* sp. (Cornejo et al., 1998) and are encoded by two different genes *ho1* and *ho2*, respectively. The genes encoding HO1 and HO2 in other cyanobacterial species including *Anabaena*, *Thermosynechococcus* and *Nostoc* spp. have also been identified (Frankenberg-Dinkel, 2004). Furthermore, some studies showed that pathogenic bacteria (*Pseudomonas aeruginosa* and *Neisseriae menigitides*) employ HO in order to utilize heme from their host as an Fe source (Ratliff et al., 2001; Zhu et al., 2000). A similar behavior was observed for the marine bacteria *Microscilla marina* (Hopkinson et al., 2008) and *Ruegeria sp*. (Roe et al., 2013), thus suggesting that HO activity may be linked to Fe-acquisition processes also in the marine environment (Schmitt, 1997).

1.5 Heme *b* in the marine environment

Heme *b* is the most versatile heme structure within an organism (Chapman et al., 1997) and as mentioned in previous sections is a component of catalases, peroxidases, the *b*-type cytochromes and the cytochrome P-450 in marine phytoplankton (Mochizuki et al., 2010). Hence, in marine phytoplankton heme *b* is a key component electron transport chains in the respiration and photosynthesis (Hogle et al., 2014). This means that disruptions in heme *b* production, utilization and breakdown processes, potentially influence crucial biochemical processes including CO_2 uptake in the ocean.

Despite their importance in the marine environment, there was no published study regarding heme *b* abundance in phytoplankton until 2007 (Gledhill, 2007). In the past, analytical methods allowed for the determination of heme containing proteins in human tissues, higher plants and cyanobacteria using spectrophotometric techniques (Lübben and Morand, 1994; Wolf et al., 1984; Zander et al., 1984). Gledhill (2007) published a method for the quantification of heme *b* in marine particulate material using separation with HPLC and detection with diode array (DAD) after extraction with a non-ionic detergent. The method was later optimized and quantification of heme *b* was achieved by electrospray ionisation mass spectrometry (ESI-MS) thus avoiding interferences from other pigments and increasing sensitivity (Gledhill, 2007, 2014). The development of this analytical technique allowed for the determination of heme *b* in both field and

cultured marine phytoplankton thus improving our knowledge about heme *b* abundance and behavior in the oceanic environment.

1.5.1 Heme *b* in cultured phytoplankton populations

According to theoretical calculations, hemoproteins make up approximately 40% of the intracellular Fe pool whilst hemoproteins containing heme *b* contribute approximately half of this amount (Raven, 1990). The first extensive study regarding heme *b* abundance in phytoplankton was carried out in the eukaryotes *Dunaliella tertiolecta, Emiliania huxleyi, Thalassiosira oceanica* and the prokaryote *Synechococcus sp*. (Honey et al., 2013). This study showed that heme *b* accounts on average for 18±14% of total intracellular Fe inventory (Honey et al., 2013), thus confirming the theoretical calculations of Raven (1990). However, this proportion varied amongst species and growth conditions and ranged from 1 to 40 % (Honey et al., 2013). For example, under low DFe conditions (<0.50 nmol L), 6 to 26% of the available Fe in the media was incorporated into heme *b* for species from temperate ocean areas (Honey et al., 2013), whereas this percentage ranged from 0.2 to 16% for species from high latitude areas (Gledhill et al., 2015). Furthermore, fluctuations in heme *b* concentrations among different phytoplankton classes and species also implied that heme *b* abundance in the natural environment could potentially vary according to phytoplankton community composition (Gledhill et al., 2013, 2015; Honey et al., 2013).

Heme *b* quota is defined as the heme *b* quantity per unit carbon (e.g. ratio heme *b*:C) and constitutes a similar parameter to the Fe quota, which describes the quantity of Fe per unit carbon (ratio Fe:C) (Raven, 1990). Hence, the heme *b* quota refers only to the proportion of Fe bound in heme *b* cofactors. Heme *b* quotas were variable among species and growth conditions in cultured eukaryotic and prokaryotic phytoplankton (Gledhill et al., 2015; Honey et al., 2013). In general, the heme *b* quotas increased in nutrient replete cultures and resulted in increased growth rates (Honey et al., 2013).

The general trend suggested that increased heme *b* concentrations and quotas indicate a healthy status for phytoplankton (Honey et al., 2013). However, similarly to Fe:C ratios and Fe use efficiencies, which indicate how many units carbon (i.e. biomass) are produced per unit Fe per unit time (Raven, 1988), the fluctuations of heme *b* relative to carbon and PFe did not always correspond to declines in fundamental biological functions (Gledhill et al., 2015). Hence, there are likely diverse mechanisms of Fe utilization in the hemoprotein pool and that phytoplankton has the flexibility to adapt to changing nutrient and particularly Fe supply.

1.5.2 Heme *b* in field phytoplankton populations

A recent mesocosm experiment showed that the abundance of heme *b* (i.e. heme *b* concentrations) changes with bloom progression under nutrient replete conditions (Bellworthy et al., 2017) and follows similar trends with other biomass stocks

(particulate organic carbon - POC and chl *a*). However, heme *b* concentrations decreased rapidly post bloom (Bellworthy et al., 2017).

Regarding the abundance of heme *b* in the world's Oceans, to date there is published information about the Atlantic (Gledhill et al., 2013, 2015; Honey, 2012; Honey et al., 2013) and Southern Oceans (Gledhill et al., 2013, 2015). In the subtropical North Atlantic Ocean, heme *b* was associated with chl *a* whilst their depth profiles followed similar patterns (Honey et al., 2013). Hence, similarly to chl *a*, the concentrations of heme *b* were higher in shallower waters and decreased with depth. Heme *b* increased with depth only in deep chlorophyll maxima (DCM) (Honey et al., 2013). Thus, these results confirmed the link between heme *b* and the photosynthetic apparatus.

In general, heme *b* concentrations increased in areas with high biomass in the North Atlantic (Gledhill et al., 2013; Honey et al., 2013) and Southern Oceans (Gledhill et al., 2013, 2015). The spatial variability of heme *b* concentrations implied that increases and decreases were linked to different environmental conditions of each sub-region which include macronutrient (NO_3^-, PO_4^{3-}) and Fe availability. Hence, heme *b* concentrations were lower in the sub-tropical North Atlantic Gyre compared to the coastal areas of the Tropical Atlantic (Honey, 2012). The lowest heme *b* concentrations in the field were determined in the post-bloom Iceland Basin in 2007 (Gledhill et al., 2013) and in the Southern Ocean (Gledhill et al., 2015). Furthermore, a comparison of data from two different research cruises in the Tropical Atlantic Ocean implied that the temporal variability of heme *b* concentrations was associated with changes in the Fe fluxes via atmospheric deposition in this region (Honey, 2012; Schlosser et al., 2014).

Overall, these observations suggested that Fe availability potentially drives heme *b* abundance in the ocean and raised the hypothesis that heme *b* decreases in low Fe environments and can therefore serve as an indicator of Fe limitation (Gledhill et al., 2013; Honey et al., 2013).

1.5.3 Impact of iron limitation on heme *b* abundance

The biological demand for Fe by phytoplankton is high due to the various Fe-containing proteins they possess, thus Fe supply is the driving factor of the microbial community structure in 40 % of the world's ocean (Boyd and Ellwood, 2010). In surface waters DFe is often depleted because of the limited supply, bioavailability and increased biological uptake whilst its concentrations increase in deeper waters (Ussher et al., 2004). The condition when DFe concentrations are not sufficient to sustain phytoplankton growth is described as Fe limitation.

Several studies in the past decades documented the adverse effects of Fe limitation in phytoplankton growth and metabolic functions (e.g. Chappell et al., 2012; Geider and La Roche, 1994; Greene et al., 1992; King and Barbeau, 2007; Kolber et al., 1994; Shi et al., 2007; Sunda and Huntsman, 1997). Under Fe limiting conditions, the abundances of several Fe-containing proteins declined, a trend observed also for nitrogenase and

proteins of the photosynthetic apparatus (Allen et al., 2008; Bibby et al., 2001; Marchetti and Cassar, 2009; Peers and Price, 2006; Richier et al., 2012; Saito et al., 2011; Schorsch et al., 2018; Strzepek and Harrison, 2004). Furthermore, eukaryotic phytoplankton is known to switch from nitrate to ammonium utilization during Fe limitation (Price et al., 1991; Timmermans et al., 1994). Therefore, changes in the photosynthetic and/or nitrogen assimilation systems lead to changes in the abundance of hemoproteins and heme *b*.

Regarding heme *b*, in the field, low heme *b* concentrations were determined in the Iceland Basin in August 2007 (Gledhill et al., 2013). Parallel studies confirmed that during the sampling time, Iceland Basin was Fe limited (Poulton et al., 2010; Ryan-Keogh et al., 2013) thus implying that the heme *b* concentrations in the extant phytoplankton groups decreased due to low Fe availability.

Laboratory experiments performed in a wide range of phytoplankton species (eukaryotes and prokaryotes) showed that heme *b* cellular contents fall below 1.0 pmol L^{-1} under low DFe (≤0.5 nmol L^{-1}) (Gledhill et al., 2015; Honey, 2012; Honey et al., 2013). In the case of diatoms isolated from temperate and coastal regions (*Thalassiosira weissflogii*, *Thalassiosira. oceanica*, *Phaeodactylum tricornutum* and *Chaetoceros calcitrans*) and cyanobacteria (*Synechococcus sp.*), low heme *b* concentrations were also associated with declines in growth rates and other biomass stocks. However, experiments on open ocean prymnesiophytes (*Emiliania huxleyi, Phaeocystis antarctica*) and diatoms (*Chaetoceros brevis*) demonstrated that these species were capable of maintaining their biomass stocks (e.g. growth rates, chl *a* and POC) despite reduced intracellular heme *b* concentrations at low DFe concentrations (≤0.5 nmol L^{-1}) (Gledhill et al., 2015). Hence, these findings suggested that some species are able to regulate their cellular heme *b* concentrations by employing preferential allocation of Fe away from the hemoprotein pool in order to efficiently exploit the available Fe, reduce the overall Fe requirements and maintain growth (Gledhill et al., 2015).

Iron availability also appears to influence the expression of the HOs and thus the heme *b* degradation patterns. Under Fe limiting conditions, HO1 of *Synechocystis sp.* was downregulated whereas levels of HO2 remained unchanged (Singh et al., 2003) implying declines in the degradation of hemes. Indeed, Bibby et al. (2001) confirmed that phycobiliproteins decrease under Fe limitation in *Synechocystis*. However upregulation of some HOs has also been reported for Fe limited phytoplankton, as in the case of the red algae *Rhodella violacea* (Richaud and Zabulon, 1997). Hence, the impact of Fe limitation on HO gene expression and heme degradation patterns is still uncertain.

1.5.4 Heme *b* in diazotrophs

Diazotrophs have an additional need for Fe compared to other cyanobacteria and phytoplankton species due to the enzyme nitrogenase which catalyzes the conversion of

N_2 to biologically accessible forms of nitrogen (Section 1.3). It is thus established that due to their high Fe requirements, Fe supply regulates the geographical abundance of cyanobacterial diazotrophs in the ocean whilst elevated Fe atmospheric inputs are associated with increases in nitrogen fixation rates (Chappell et al., 2012; Luo et al., 2012; Moore et al., 2009; Moore and Doney, 2007; Snow et al., 2015b; Sohm et al., 2011).

Regarding the impact of Fe limitation on diazotrophs, nitrogen fixation rates decline when Fe supply is not sufficient (Berman-Frank et al., 2001a; Fu and Bell, 2003; Jacq et al., 2014; Kupper et al., 2008; Paczuska and Kosakowska, 2003; Richier et al., 2012; Saito et al., 2011; Shi et al., 2007; Snow et al., 2015a). The impact of Fe limitation on heme *b* content of marine diazotrophs is to date not well documented. Honey (2012) studied heme *b* behavior in monocultures of the unicellular *Crocosphaera* and filamentous *Trichodesmium*. The heme regulation in *Crocosphaera* was comparable to other phytoplankton species since concentrations of heme *b* decreased with low Fe supply. In contrast, *Trichodesmium* exhibited a unique regulation behavior as heme *b* concentrations remained low throughout the experiments and did not vary among Fe treatments. This trend was also observed in the field in the Tropical Atlantic Ocean, area where *Trichodesmium* is highly abundant. Hence, Honey (2012) proposed that *Trichodesmium* potentially possess a relatively low quantity of *b*-type hemoproteins because the available Fe is utilized primarily in nitrogenase and in photosystem I in order to accommodate electron transport for the Mehler activity (Bergman et al., 2013; Milligan et al., 2007).

1.6 Thesis objectives and hypotheses

This thesis investigates the abundance of heme *b* in cultured and field phytoplankton populations aiming to advance the knowledge on how the available Fe is utilized in heme *b* and hemoprotein pools.

To date there is limited data regarding the spatial distribution patterns of heme *b* in the natural environment and the impact of Fe limitation on the heme *b* cofactor. This dissertation systematically examines the abundance of heme *b* in the Atlantic Ocean and investigates the factors driving the distribution of heme *b* via two case studies (Chapters 2 and 3). The Atlantic Ocean is a region that has drawn the scientific interest in the past decades because it is subject to fluctuations in Fe supply (Boyd and Ellwood, 2010) that potentially influence the nitrogen, carbon and phosphorus cycles (Dutkiewicz et al., 2005; Mills et al., 2004; Moore et al., 2002; Tagliabue et al., 2017) and the global climate (Jickells et al., 2005).

The first case study (Chapter 2) examines the utility of heme *b* as a proxy for the identification of Fe limited phytoplankton in the post bloom sub-polar North Atlantic gyre, which is known for seasonal Fe limitation (Achterberg et al., 2018; Macey et al., 2014; Nielsdóttir et al., 2009; Poulton et al., 2010; Ryan-Keogh et al., 2013). The author

also reports for the first time a link between field heme *b* concentrations and phytoplankton community composition for the identification of potential Fe utilization strategies employed by extant phytoplankton groups.

The second case study (Chapter 3) includes an extensive dataset of heme *b* gathered from the Atlantic Ocean aiming to identify the physical, chemical or biological processes that drive its spatial distribution. Furthermore, previous laboratory measurements (Gledhill et al., 2015; Honey et al., 2013) provided an estimation of the proportion of heme *b* relative to the biogenic Fe, which is the fraction of Fe derived from biogenic particles. A comparison of these laboratory measurements with field data is also presented in this chapter thus providing information about the proportion of Fe that is utilized in heme *b* by different phytoplankton populations *in situ*. Hence, in this chapter the applicability of heme *b* as an approximate indicator for the biogenic Fe pool in field studies is examined.

Although there is some information regarding heme *b* behavior in diazotrophs under varying Fe conditions (Section 1.5.4), the knowledge about heme *b* abundance, production, utilization and degradation is still uncertain. Chapter 4 examines the patterns of heme *b* cycling in two common diazotrophs, the unicellular *Cyanothece* and the globally significant, filamentous *Trichodesmium*. The investigation incorporates transcriptomic studies since heme *b* concentrations are potentially regulated by modifications in the gene expression of heme- associated proteins under certain Fe conditions. Finally, according to the information obtained so far, heme *b* in cultured *Trichodesmium* exhibited very low concentrations which were invariable with Fe supply. Hence, the author investigates also whether this behavior is associated with heme *b* degradation from HOs on a transcriptional level.

Overall, the field and laboratory experiments of the current study are conducted to address the following hypotheses:

1. The overall distribution of heme *b* concentrations and quotas in the Atlantic Ocean is a consequence of Fe availability.
2. Heme *b* concentrations in the Atlantic Ocean decrease in low Fe regimes thus heme *b* can act as a proxy for Fe-limited phytoplankton
3. Low heme *b* concentrations in the Atlantic Ocean are not necessarily associated with decrease in key biological functions suggesting optimization of Fe use by the extant phytoplankton species.
4. Heme *b* provides a first order indication of the biogenic Fe pool in the field.
5. Heme *b* concentrations are low in tropical Atlantic due to the abundance of *Trichodesmium*.
6. Heme *b* concentrations and production and degradation processes decline under Fe limiting conditions in both *Cyanothece* and *Trichodesmium*.
7. Heme *b* degradation is regulated by HO gene expression under varying Fe treatments.

8. Heme *b* concentrations are low in *Trichodesmium* Fe-replete cultures due to increased HO expression.

The following objectives are set in order to test the hypotheses mentioned above:

1. The impact of Fe limitation in field phytoplankton populations and the optimization potential of Fe utilization by extant phytoplankton groups will be assessed by collecting samples in the high productive Subpolar North Atlantic Ocean (GEOVIDE cruise) during the spring bloom. Samples will be analyzed for heme *b*, other background parameters indicative of growth (e.g. POC, chl *a*) and for the determination of the microbial community composition (16S rRNA amplicon sequencing).
2. The impact of DFe availability on heme *b* abundance and the overall distribution of heme *b* concentrations and quotas through the Atlantic Ocean will be investigated by synthesis of datasets obtained by research expeditions. Datasets will cover various regions of the Atlantic Ocean and will include previously published and newly analyzed/ unpublished data. Existing datasets cover the Subtropical North Atlantic Gyre, Celtic Sea and Tropical Atlantic. New samples and datasets will be obtained from the Subpolar North Atlantic (GEOVIDE cruise) and from the South Atlantic (cruises M121, M124).
3. To assess, if heme *b* can function as an indicator of the biogenic Fe pool in the field, the observed field heme *b* concentrations will be compared to the total biogenic Fe and predicted heme *b* concentrations calculated by a global biogeochemical model (PISCES v2).
4. Culturing experiments will be conducted in *Cyanothece* and *Trichodesmium*. Both species will grow in different DFe treatments for the investigation of the impact of DFe availability on heme *b* concentrations, quotas and cycling.
5. Targeted molecular analysis (i.e. Quantitative Real Time Polymerase Chain Reaction) will be implemented for the identification of changes in the expression of heme *b* (e.g. cytochrome b_6f) or other Fe-containing proteins (e.g. nitrogenase) and of the HOs.

2. Regulation of the phytoplankton heme *b* iron pool during the North Atlantic spring bloom

Evangelia Louropoulou[1,2*], Martha Gledhill[1], Thomas J. Browning[1], Dhwani K. Desai[3], Jan-Lukas Menzel Barraqueta[1,4], Manon Tonnard[5,6,7], Géraldine Sarthou[5], Hélène Planquette[5], Andrew R. Bowie[6,7], Ruth A. Schmitz[2], Julie LaRoche[3], Eric P. Achterberg[1]

Accepted in *Frontiers in Aquatic Microbiology*

[1] GEOMAR Helmholtz Centre for Ocean Research Kiel, Kiel, Germany

[2]Institute for General Microbiology, Christian-Albrechts-Universität, Kiel, Germany

[3] Department of Biology, Dalhousie University, Halifax, NS, Canada

[4] Earth Sciences Department, Stellenbosch University, Stellenbosch, South Africa

[5] LEMAR (Laboratoire des Sciences de l'environnement marin), CNRS, Univ. Brest, IRD, Ifremer, Plouzané, France

[6] Antarctic Climate and Ecosystems – Cooperative Research Centre, Hobart, TAS, Australia

[7] Institute for Marine and Antarctic Studies, University of Tasmania, Hobart, TAS, Australia

Abstract. Heme *b* is an iron-containing co-factor in hemoproteins. Heme *b* concentrations are low (<1 pmol L^{-1}) in iron limited phytoplankton in cultures and in the field. Here, we determined heme *b* in marine particulate material (>0.7 μm) from the North Atlantic Ocean (GEOVIDE cruise - GEOTRACES section GA01), which spanned several biogeochemical regimes. We examined the relationship between heme *b* abundance and the microbial community composition, and its utility for mapping iron limited phytoplankton. Heme *b* concentrations ranged from 0.16 to 5.1 pmol L^{-1} (median=2.0 pmol L^{-1}, n=62) in the surface mixed layer (SML) along the cruise track, driven mainly by variability in biomass. However, in the Irminger Basin, the lowest heme *b* levels (SML: median=0.53 pmol L^{-1}, n=12) were observed, whilst the biomass was highest (particulate organic carbon, median= 14.2 μmol L^{-1}, n=25; chlorophyll *a*: median= 2.0 nmol L^{-1}, n=23) pointing to regulatory mechanisms of the heme *b* pool for growth conservation. Dissolved iron (DFe) was not depleted (SML: median= 0.38 nmol L^{-1}, n=11) in the Irminger Basin, but large diatoms (*Rhizosolenia sp.*) dominated. Hence, heme *b* depletion and regulation is likely to occur during bloom progression when phytoplankton class-dependent absolute iron requirements exceed the available ambient concentration of DFe. Furthermore, high heme *b* concentrations found in the Iceland Basin and Labrador Sea (median= 3.4 pmol L^{-1}, n=20), despite having similar DFe concentrations to the Irminger Basin, were attributed to an earlier growth phase of the extant phytoplankton populations. Thus, heme *b* provides a snapshot of the cellular activity *in situ* and could both be used as indicator of iron limitation and contribute to understanding phytoplankton adaptation mechanisms to changing iron supplies.

Keywords. Heme *b*, North Atlantic, Phytoplankton, Diatoms, Iron, Limitation, GEOTRACES, GEOVIDE

2.1 Introduction

Iron (Fe) is an essential micro-nutrient for marine phytoplankton as it is associated with several key biochemical processes including photosynthesis, respiration, reduction of oxidized nitrogen species and di-nitrogen (N_2) fixation (Geider and La Roche, 1994; Morel and Price, 2003; Raven et al., 1999). Iron uptake by phytoplankton occurs directly from seawater and the availability of Fe in the surface ocean is largely controlled by rates of supply from atmospheric deposition, continental margins, upwelling and deep mixing entrainment of sub-surface Fe pools, relative to losses via scavenging and biological uptake (Geider, 1999; Sunda and Huntsman, 1995; Tagliabue et al., 2017). Dissolved Fe (DFe) concentrations in the open ocean surface waters can be very low (<0.1 nmol L^{-1}) (Achterberg et al., 2018; Boyd and Ellwood, 2010; Sunda and Huntsman, 1995) and it has been well documented that low Fe availability can limit phytoplankton growth, N_2 fixation rates, and influence community structure (e.g. Greene et al. 1992; Geider & La Roche 1994; Kolber et al. 1994; Sunda & Huntsman 1997; King & Barbeau 2007; Shi et al. 2007).

In proteins, Fe is bound in Fe-sulfur clusters, Fe-oxygen-Fe clusters, or in Fe-porphyrin complexes also known as hemes (Hogle et al., 2014). Hemes function as prosthetic groups of the hemoproteins (Chapman et al., 1997) and are involved in electron transfers for example during photosynthesis, respiration, nitrate reduction as well as in control, storage and transport of oxygen (Hogle et al., 2014). Hemes are produced in a similar manner to chlorophyll via the tetrapyrrole synthesis pathway and several heme structures are present within an organism (Chapman et al., 1997). The cellular heme quota is tightly coordinated, since free hemes are toxic (Espinas et al., 2012). Furthermore heme can act as an Fe source for bacteria (Hogle et al., 2016; Roe et al., 2013)

Heme *b* (Fe protoporphyrin IX) is the most versatile heme in organisms (Espinas et al., 2012) and is a constituent of the *b* type cytochromes, catalases, peroxidases, cytochrome p450, globin and nitrate reductase (Mochizuki et al., 2010; Hogle et al., 2014). Culturing experiments involving eukaryotes and prokaryotes (*Dunaliella tertiolecta, Emiliania huxleyi, Thalassiosira oceanica, Synechococcus sp*.) have shown that heme *b* accounts for 18±14% of total cellular Fe inventory (Honey et al., 2013).

The information regarding heme *b* abundance in the oceans is limited, with only a few studies that have reported heme *b* concentrations in surface waters of the Atlantic and Southern Oceans (Gledhill et al., 2013, 2015; Honey et al., 2013). Increased heme *b* concentrations were associated with high biomass in the North Atlantic and Southern Oceans (Gledhill et al., 2013). Recent work has also shown that the relative abundance of heme *b* and biomass stocks, as indicated by particulate organic carbon (POC) and chlorophyll *a* (chl *a*) concentrations, changes with bloom progression under Fe replete conditions (Bellworthy et al., 2017). Hence, heme *b* was observed to decrease rapidly post bloom in a mesocosm experiment, although this effect might be dampened in open

ocean environments by a lower Fe availability (Bellworthy et al., 2017). In Fe deplete regions, heme *b* concentrations decreased in marine particulate material (Honey et al., 2013) suggesting that heme *b* could potentially be used as a proxy for Fe limitation in field studies. Furthermore, fluctuations in heme *b* concentrations among different phytoplankton classes and species also imply that heme *b* abundance in the ocean could potentially vary according to the phytoplankton community composition (Gledhill et al., 2013, 2015; Honey et al., 2013).

Laboratory experiments performed on diatoms isolated from temperate and/or coastal regions (*Thalassiosira weissflogii*, *Thalassiosira. oceanica*, *Phaeodactylum tricornutum* and *Chaetoceros calcitrans*) and cyanobacteria (*Synechococcus sp.*) showed that decreases in the heme *b* cellular contents were resulted in decreased biomass stocks under low DFe (≤0.5 nmol L^{-1}) (Gledhill et al., 2015; Honey et al., 2013). In contrast, experiments on prymnesiophytes (*Emiliania huxleyi*, *Phaeocystis antarctica*) and diatoms (*Chaetoceros brevis*), all abundant in the open ocean, showed that these species were capable of maintaining their biomass stocks (e.g. growth rates, chl *a* and POC) despite reduced intracellular heme *b* concentrations at low DFe concentrations (≤0.5 nmol L^{-1}) (Gledhill et al., 2015). These findings suggest that both diatoms and prymnesiophytes possess heme *b* regulation mechanisms which are expressed by a preferential allocation of Fe away from the hemoprotein pool in order to efficiently exploit the available Fe, reduce the overall Fe requirements and maintain growth (Gledhill et al., 2015). It is likely that such a regulation mechanism reflects an overall reduction in cellular Fe requirement until a subsistence Fe quota is obtained, below which growth can no longer occur.

In the current study we determined heme *b* in particulate material (>0.7 µm) sampled in the subtropical and subpolar North Atlantic Ocean during the GEOVIDE (GEOTRACES section G01) research expedition (Sarthou et al., 2018). The North Atlantic Ocean is an area of high phytoplankton productivity and enhanced CO_2 sequestration rates (Henson et al., 2009). Several biogeochemical regimes exist in the North Atlantic Ocean; in the temperate subtropics, nitrate limits phytoplankton growth (Moore et al., 2008, 2013). At higher latitudes in the subpolar areas, during spring and summer, light is no longer a limiting factor for phytoplankton due to the lengthening of daylight period, while nitrate and phosphate are in excess (Harrison et al., 2013; Henson et al., 2009). However, DFe concentrations can become depleted (<0.1 nmol L^{-1}) (Achterberg et al., 2018) and these regions can thus become Fe limited during late spring and summer months (Moore et al., 2008; Nielsdóttir et al., 2009). Specifically, Fe-limitation has been observed after the peak spring bloom in the Iceland Basin (Macey et al., 2014; Nielsdóttir et al., 2009; Ryan-Keogh et al., 2013), Irminger Basin (Macey et al., 2014; Ryan-Keogh et al., 2013; Sanders et al., 2005) and Labrador Sea (Fragoso et al., 2017; Harrison et al., 2013). Furthermore, shifts in phytoplankton assemblages in the high latitude North Atlantic during the spring-summer bloom are

potentially induced by the individual requirements for Fe of each phytoplankton class (e.g. Boyd et al., 2012; Ryan-Keogh et al., 2013, 2017; Strzepek et al., 2012).

Our hypothesis was that the heme *b* abundance in the subtropical and subpolar North Atlantic Ocean would vary according to biomass, and that low heme *b* concentrations would be an indicator of low Fe regimes. A reduction in the ratios of heme *b* relative to biomass would imply optimization of the heme *b* - containing Fe pool by phytoplankton in order to maintain carbon fixation. Furthermore, we hypothesized that Fe concentrations at which optimization is observed would vary among phytoplankton groups and also depend on the stage of the bloom. Finally, this is study also connects the heme *b* variability with data on phytoplankton community composition and thus contributes to our understanding of how available Fe is utilized by different phytoplankton groups.

2.2 Methods

2.2.1 Study area and field sampling

We collected samples in the subpolar and subtropical North Atlantic Ocean during the GEOVIDE (GEOTRACES-GA01 section) research cruise which took place in May-June 2014. Discrete samples were collected from a total of 32 stations (Fig. 2.1) located in the Eastern Subtropical North Atlantic Gyre (Stations 1-26), Iceland Basin (Stations 29-38), Irminger Basin (Stations 40-49 and 60), along the Greenland Shelf (Stations 53-56 and 61-64) and in the Labrador Sea (Stations 68-78).

2.2.2 Temperature, salinity and mixed layer depth

Temperature and salinity data were obtained during the voyage using CTD sensors (SBE911 equipped with SBE-43) on a stainless steel hydrographic rosette frame. The SML was calculated from the CTD data as described by Tonnard et al. (2018) applying the density criterion ($\Delta\sigma_t$ = 0.125 kg m^{-3}) with an increase in density relative to the surface density of less than $\Delta\sigma_t$ for the whole mixed layer (Kara et al., 2000). We also calculated the SML using the temperature-based criterion (ΔT = 0.5 °C) (Monterey and Levitus, 1997). Where a discrepancy was observed, we used the SML that most closely coincided with the nutricline and ferricline.

2.2.3 Heme *b*

Seawater was sampled from up to 6 depths per station (<200 m). Particles were filtered onto glass fiber filters (nominal pore size 0.7 μm, Fisherbrand, MF300), and the filters were stored at -80 ^{o}C prior to analysis.

For the determination of heme *b*, the method developed by Gledhill (2014) was followed with slight modifications. Briefly, 1 mL of the extraction solution consisting of 2.5% w:v Octyl β-D-Glucopyranoside-OGP (Sigma-Aldrich®, ≥98% GC Grade) in

0.02 mol L^{-1} NH_4OH (HPLC Grade, Fisher) was added to each filter. Samples were vortexed for 10 seconds, ultrasonicated on ice for 45 seconds using an ultrasonic probe (Bandelin Sonopuls UW70, 20kHz, 40% amplitude) and finally filtered using centrifuge tube filters (Corning® Costar® Spin-X®, cellulose acetate, 0.22 μm) for 10 min at 5°C at 6,800 x g. In parallel, a set of standard solutions of ferric iron - Fe(III) protoporphyrin IX chloride (Fe(III)PTP) (Hemin, Frontier Scientific Discovery Chemicals) was prepared for calibrations. The concentration of the calibration standards ranged from 0 to 16.3 nmol L^{-1} Fe(III)PTP. Both the extraction solution and the calibration standards were made fresh daily due to the reduced chemical stability of OGP (Gledhill, 2007).

The quantification of heme *b* was performed using separation with High Performance Liquid Chromatography (PLRP-S column 2.1 x 100 mm, 300 Å, 3 μm, Agilent Technologies) and detection by Electrospray Ionization using a Q Exactive™ Mass Spectrometer (ThermoFisher). Conditions were similar to those previously described (Bellworthy et al., 2017; Gledhill, 2014) except for the following modifications. In this study, formic acid was used as a mobile phase modifier since our test runs indicated a more stable signal and reproducible results for consecutive days of analysis. The aqueous phase (Solvent A) consisted of isopropanol (Optima® LC/MS Grade, Fisher Chemical), acetonitrile (Optima®, LC/MS Grade, Fisher Chemical), Milli-Q and formic acid (Optima®, LC/MS Grade, Fisher Chemical) in a ratio 0.5:0.5:90:0.1 % (v:v:v:v) whereas the organic phase (Solvent B) consisted of a mixture of isopropanol (Optima® LC/MS Grade, Fisher Chemical), acetonitrile (Optima® LC/MS Grade, Fisher Chemical) and formic acid (Optima®, LC/MS Grade, Fisher Chemical) in a ratio 50:50:0.1 % v:v:v. The flow rate of the HPLC was 400 μL min^{-1} and the starting conditions of the HPLC were 60% solvent A: 40% solvent B with a linear gradient increase of Solvent B to 100% over 10 minutes. The column temperature was 21°C.

In this study the high resolution (70,000 at m/z=200) ESI-MS Orbitrap detector allowed for quantification of heme *b* using the exact mass of the M^+ ion (m/z = 616.177). The injection volume was 25 μL and the heme *b* peak eluted between 2.0 and 3.0 min. The higher resolution (5 ppm) of the mass spectrometer eliminated isobaric interferences encountered with previous MS analysis (Gledhill, 2014). The analytical detection limit for 25 μL injection volume was calculated to be 32 pmol heme *b* L^{-1} determined as 3 times the standard deviation of the lowest standard (4.1 nmol heme *b* L^{-1}). This detection limit does not account for the pre-concentration factor resulting from filtration and extraction. Taking into account the pre-concentration factor, results in detection limits ranging from 0.01 to 0.02 pmol L^{-1} of heme *b* for field samples. Finally, heme *b* could not be detected in the blank extraction solution.

2.2.4 Microbial community composition

DNA samples were collected by vacuum (20 to 30 kPa) filtering 2 L of seawater onto a polycarbonate filter (Millipore's Isopore 0.2 μm 47mm - GTTP04700) and stored in a cryovial at -80 C until analysis in the laboratory.

DNA was extracted using the QIAGEN DNeasy Plant Mini Kit as directed by the manufacturer, with the following modification to improve cell lysis at the initial step of the procedure. Briefly, 50 μL of lysozyme solution (5 mg mL^{-1} in TE buffer), 45 μL of ProteinaseK solution (20 mg mL^{-1} in deionized (MilliQ) PCR grade water) and 400 μL of AP1 lysis buffer from the QIAGEN DNeasy Plant Mini Kit were added to the filter in the cryovial and incubated at 52°C on an orbital shaker (300 rpm) for 1 hour before continuing as directed by the manufacturer. DNA concentration and purity were assessed with NanoDrop 2000 (Thermo Scientific, USA) and then stored at -80 °C.

The microbial community was characterized by next generation sequencing (NGS) of the 16S rRNA gene V6-V8 variable region on an Illumina MiSeq instrument, following the Microbiome Amplicon Sequencing Workflow (Comeau et al., 2017). Samples were amplified using dual-indexing Illumina fusion primers that targeted the 438 bp V6-V8 region with the forward and reverse primers B969F 5'-ACGCGHNRAACCTTACC and BA1406R 5'-ACGGGCRGTGWGTRCAA (Comeau et al., 2012).

The DNA reads from each sample were processed using the QIIME pipeline version 1.8.0 (Caporaso et al., 2010b) following and established workflow (Comeau et al., 2017). Paired-end sequences were demultiplexed and merged by PEAR version 0.9.6 (Zhang et al., 2014). Sequences less than 400 bp in length or with a quality less than 30 over 90% of bases were discarded and VSEARCH was used to remove chimeric sequences (Rognes et al., 2016). The quality-controlled paired reads were assigned to Operational Taxonomic Units (OTUs) by clustering at the 97% similarity using *sortmerna* (Kopylova et al., 2012) for reference picking using the Greengenes version 13.8 database (McDonald et al., 2012). De novo picking of reads not assigned with Greengenes was carried out with *sumaclust* (Mercier et al., 2013). Singletons and low-confidence OTUs were removed using PyNAST (Caporaso et al., 2010a). Chloroplast (cp) 16S rRNA gene sequences were further classified using the PhytoRef database (Decelle et al., 2015).

The relative abundance of taxa was based on an OTU matrix rarified at 1290 reads for bacterial 16S rRNA and 100 reads cp 16S rRNA sequences, in order to allow meaningful comparison of the community structure that included all of the relevant samples. All 16S rRNA gene sequences are available on the Supplementary Information. The accession numbers of the cp 16S rRNA sequences are presented on SI Table 2.

2.2.5 Supporting variables

We collected discrete samples of seawater from the CTD rosette or trace metal rosette (TMR) from different depths for the determination of nitrate, POC, chl *a* and dissolved Fe (DFe).

Nitrate concentrations were measured using standard colorimetric techniques with an auto-analyzer as described by Aminot and Kerouel (2007) and are published in Sarthou et al. (2018). Phytoplankton chl *a* was determined after extraction with 100% methanol by HPLC analysis following the protocol of Ras et al. (2008) and details are published in Tonnard et al. (2018).

Seawater was filtered for the determination of POC on pre-combusted glass fiber filters (MF300, Fisherbrand) which were rinsed with deionized water to remove salts and then dried at 60°C. Data are published in Sarthou et al. (2018). Prior to analysis, dried filters were fumed with hydrochloric acid to remove inorganic carbon. The POC was determined using an elemental analyzer (ThermoQuest, Flash 1112 series) as described in Lorrain et al. (2003).

The method used for analysis of DFe is described in Tonnard et al. (2018). Briefly, seawater was sampled using a trace metal clean polyurethane powder-coated aluminum frame rosette (TMR) equipped with 12 L, Teflon lined GO-FLO bottles. Seawater samples were analyzed for DFe using a SeaFAST-pico™ coupled to an Element XR HR-ICP-MS (Tonnard et al., 2018).

2.2.6 Data handling

The Mass Spectrometry data were processed using the Thermo Xcalibur™ Software v.3.0.33. Section and contour plots were produced using the Ocean Data view v.4.7.9. software (Schlitzer, 2018). Further data processing and visualization were performed by R Statistical Software (R Core Team, 2016). The Shapiro-Wilk test was performed to check the normality of the distributions and indicated non-parametric distribution for the whole dataset ($p<0.05$). The association between parameters was determined using the Spearman's rank correlation coefficient. Finally, the non-parametric ANOVA Kruskal-Wallis and the post hoc Dunn’s test were used to identify significant differences among the sub-regions of the transect. Due to the non-normal distribution of the dataset, the ranges and the median values of each parameter are reported.

2.3 Results and discussion

2.3.1 Sampling region and hydrography

Temperature and salinity profiles of the section for the top 200 m of the water column are presented in Fig. 2.2. Regarding the surface waters, the North Atlantic Current (NAC) carries warm and saline water in the Eastern North Atlantic. The NAC causes

the formation of the Subarctic Front between stations 26 and 29 which separates the warm waters of the subtropical gyre with colder waters in the subpolar gyre. Following a cyclonic circulation, the NAC feeds the Irminger Current (IC) that flows west of the Reykjanes Ridge into the Irminger Basin. The East Greenland Current (EGC) carries cold and fresh Arctic water southwards around the Greenland Shelf into the Labrador Sea and finally merges with the Labrador Current (LC) flowing west in the subpolar gyre.

The depths of the SML was chosen according to a density criterion, however for station 63 on the Greenland Shelf we selected the temperature criterion since the depth coincided better with the nutricline and the ferricline. Overall, the SML depth ranged between 13.4 – 69.5 m with a median value of 33.5 m across the section. There were no significant differences for the SML depth among the sub-regions of the section (Kruskal-Wallis-Test, $p>0.05$).

We divided our dataset between samples located within the SML and those below it. Furthermore, we also defined five oceanographic regions (Fig. 2.1) according to the geographical position of the stations, temperature, salinity and nitrate distributions (Fig. 2.2). The five oceanographic regions consist of the Eastern Subtropical North Atlantic Gyre (ESNAG), the Iceland Basin (IceB), the Irminger Basin (IrmB), the Greenland Shelf (GSH) and the Labrador Sea (LS).

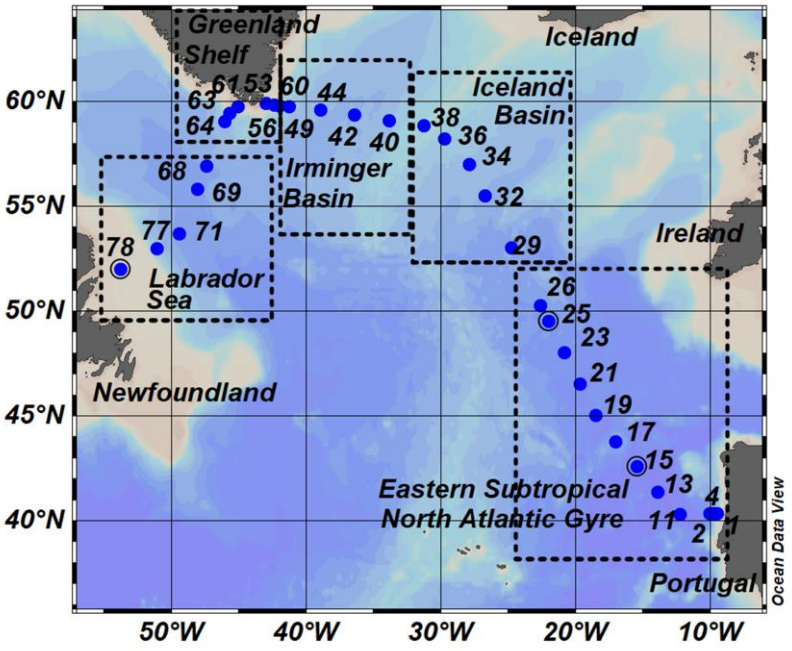

Fig. 2.1: Map of sampling stations occupied during GEOVIDE Cruise (GEOTRACES - section GA01). Dots represent sampling stations and number annotations indicate the station identification numbers. The transect is divided into 5 sub-regions: the Eastern Subtropical North Atlantic Gyre (ESNAG), Iceland Basin (IceB), Irminger Basin (IrmB), the Greenland Shelf (GSH) and the Labrador Sea (LS).

2.3.2 Nitrate and dissolved iron distributions

Nitrate concentrations were low in the SML of the ESNAG (median= 1.6 µmol L^{-1}, n= 19) and the LS (median= 0.23 µmol L^{-1}, n=6) and intermediate on the GSH (median= 5.06 µmol L^{-1}, n=7) (Fig. 2.3A). Nitrate was elevated in IceB and IrmB exhibiting median concentrations of 7.39 µmol L^{-1} (n=10) and 9.40 µmol L^{-1} (n=9), respectively. The depth distribution of nitrate (Fig. 2.2C) indicated a clear nutricline at approximately 50 m depth for the subtropical areas and 40 m for subpolar areas.

Dissolved Fe ranged from 0.09 to 2.14 nmol L^{-1} (median= 0.41 nmol L^{-1}, n=59) (Fig. 2.3B) in the SML across the transect (Tonnard et al., 2018). The spatial distribution of DFe indicated statistically significant lower concentrations (<0.5 nmol L^{-1}) within the ESNAG compared to the subpolar areas (IceB, IrmB, GSH and LS). Higher DFe concentrations (>0.75 nmol L^{-1}) were also determined close to the continental margins (Iberian and GSH). Furthermore, the concentrations of DFe during the time of our study in the IrmB (SML: range 0.22 to 1.33 nmol L^{-1}, median=0.38 nmol L^{-1}, n=11) were elevated compared to observations obtained in the spring (April-May, mean= 0.124 ± 0.06 nmol L^{-1}, n=21) and summer (mean= 0.087 ± 0.234 nmol L^{-1}, n=48) in 2010 (Achterberg et al., 2018).

The ratio of DFe:nitrate ranged from 0.02 to 38.6 mmol mol^{-1}(Tonnard et al., 2018) overall along the transect, with the lowest values in the IceB and IrmB (mean= 0.05 mmol mol^{-1}) (Fig. 2.3C).

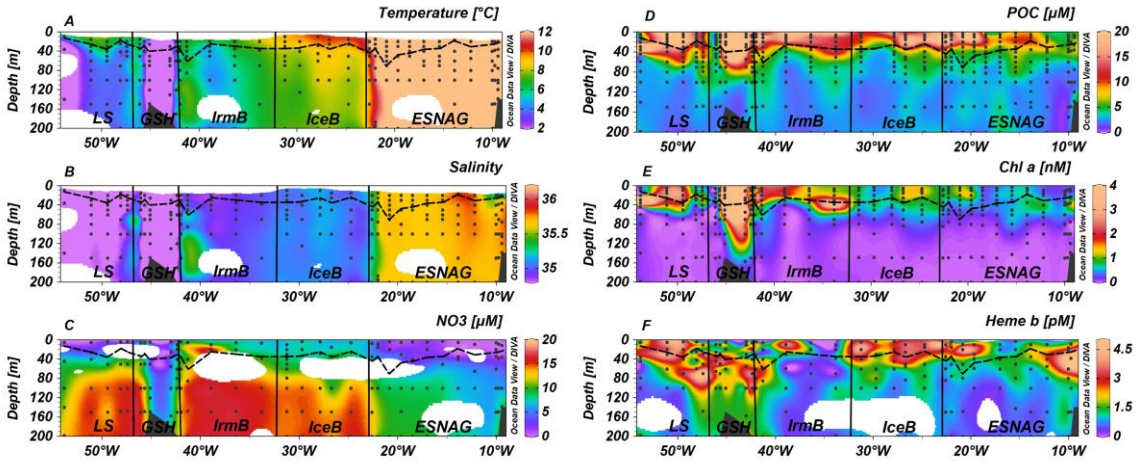

Fig. 2.2: Sections of A) Temperature, B) Salinity, C) Nitrate, D) Particulate Organic Carbon (POC), E) chlorophyll *a* (Chl *a*) and F) heme *b* across the GEOVIDE transect. Dashed lines indicate the Mixed Layer Depth and dots indicate the stations and depths where samples were taken. Letter annotations indicate the five oceanographic regions; Eastern Subtropical North Atlantic Gyre (ESNAG), Iceland Basin (IceB), Irminger Basin (IrmB), Greenland Shelf (GSH) and Labrador Sea (LS).

2.3.3 Particulate organic carbon and chlorophyll *a* as biomass-indicative parameters

The section of POC showed enhanced concentrations in the SML for most regions (Fig. 2.2D, Fig. 2.3D). Overall, POC ranged from 1.72 to 40.0 µmol L^{-1} in the SML (median=

11.6 µmol L^{-1}, n=140). The lowest concentrations of POC were observed in the ESNAG, where the median value was 8.45 µmol L^{-1} in the SML (n=52) and 3.09 µmol L^{-1} below the SML (n=80). Statistically significant differences were observed for POC among the five oceanographic regions according to the Kruskal-Wallis-Test (Fig. 2.3D). A pairwise comparison showed that they were attributed mainly to differences between the low biomass ESNAG and the remaining regions (Fig. 2.3D).

Figure 2.2E illustrates the section for chl *a*, with concentrations ranging from 0.14 to 7.44 nmol L^{-1} within the SML (median= 0.71 nmol L^{-1}, n=134). The highest concentrations in the SML were observed in the high latitude regions of IrmB, GSH and LS (Median = 1.66 nmol L^{-1}, n=61), whereas lower chl *a* was measured in the ESNAG and the IceB (median= 0.60 nmol L^{-1}, n= 70). Statistically significant differences were observed for chl *a* between the oceanographic regions (Fig. 2.3E, Kruskal-Wallis, p<0.01). Chlorophyll *a* correlated well with POC (Spearman's rho, r= 0.88, n=296, p<0.01) (SI Table 1).

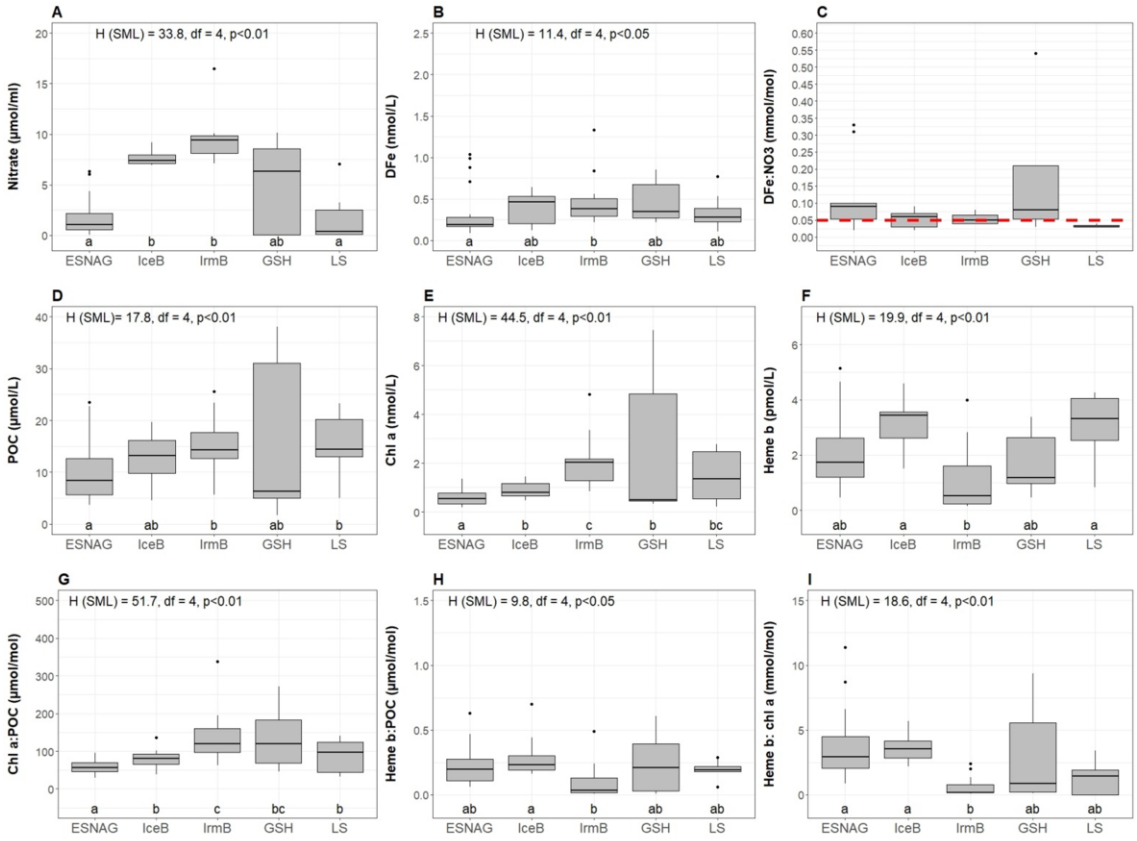

Fig. 2.3: Boxplots of distributions in the surface mixed layer (SML) of A) Nitrate, B) Dissolved iron (DFe), C) DFe:nitrate, D) Particulate Organic Carbon (POC), E) Chlorophyll *a* (Chl *a*), F) Heme b, G) Chl a:POC, H) Heme b:POC and I) Chl *a*:heme *b* for the five oceanographic regions; Eastern Subtropical North Atlantic Gyre (ESNAG), Iceland Basin (IceB), Irminger Basin (IrmB), Greenland Shelf (GSH) and Labrador Sea (LS). On top of sub-plots A, B, D, E, F, G, H and I the result of the Kruskal-Wallis test is annotated. Letters (letters a to c) below the boxes indicate the Compact Letter Display (cld) of the statistically significant different groups in the SML after a Post-hoc test for multiple comparisons of groups. The red dashed line in plot C marks the threshold value 0.01 mmol mol^{-1} for the assessment of Fe-stressed phytoplankton (Ho et al., 2003; Nielsdóttir et al., 2012; Sunda and Huntsman, 1995).

Stratification of the water column can lead to the formation of a Deep Chlorophyll Maximum (DCM) in oligotrophic waters and post-bloom during the summer in temperate (Cullen 1982; Hickman et al. 2012; Mignot et al. 2014 etc.) and Polar regions (Holm-Hansen and Hewes, 2004). A DCM was observed in the oligotrophic ESNAG and in the GSH at approximately 60 m depth, in IrmB (station 40) at 40 m depth and in the Newfoundland Shelf (station 78) of the LS (Fig. 2.2E).

2.3.4 Heme *b* concentrations and distribution

The vertical distribution of heme *b* (Fig. 2.2F) indicated enhanced concentrations in the SML, which decreased in general with depth, with the exception of stations where a DCM was present. Overall heme *b* concentrations ranged from 0.16 to 5.13 pmol L^{-1} (median= 2.17 pmol L^{-1}, N=65) within the SML. Below the SML (down to 200 m depth), the median concentration of heme *b* was 1.14 pmol L^{-1} (N=107). In the DCM of the ESNAG and GSH, heme *b* reached concentrations up to 5.67 pmol L^{-1}, whereas no increase was observed in the DCMs of the IrmB and LS. Across the section, the lowest concentrations of heme *b* were detected in the IrmB (SML: median = 0.53 pmol L^{-1}, n=12), and the Kruskal-Wallis-Test confirmed a statistically significant difference in the distribution of heme *b* among the sub-regions and particularly between the IrmB and IceB (Fig. 2.3F).

Our results were generally consistent with previously published data (Table 2.1). In 2010, heme *b* averaged 1.3 ± 0.60 pmol L^{-1} in the subtropical North Atlantic (Honey et al., 2013), which is comparable to the average of 1.5 ± 1.2 pmol L^{-1} that we determined in our study for the same region. However, heme *b* concentrations in the IceB were slightly higher during the GEOVIDE cruise (mean= 2.1 ± 1.1 pmol L^{-1}) compared to data from July-August 2007 (mean= 1.1 ± 0.7 pmol L^{-1}) (Gledhill et al., 2013) (Table 2.1), which is probably due to the sampling in different seasons (spring vs. late summer) and to the different phytoplankton bloom stages.

Heme *b* correlated weakly with both POC (Spearman's rho, r= 0.41, n=165, p<0.01) and chl *a* (Spearman's rho, *r*= 0.41, n=153, *p*<0.01) (SI Table 1), in agreement with previous observations (Gledhill, 2007; Gledhill et al., 2013, 2015; Honey et al., 2013). Heme *b* did not exhibit any statistically significant relationship with nitrate or DFe (SI Table 1).

2.3.5 Ratios of heme *b*, chlorophyll *a* and particulate organic carbon

We calculated the ratios of heme *b*:POC, chl *a*:POC and heme *b*: chl *a* in order to examine how heme *b* and chl *a* abundances changed relative to biomass. Heme *b*:POC and chl *a*:POC ratios represent, respectively, the heme *b* and chl *a* per unit carbon derived from the total organic matter (i.e. phytoplankton, zooplankton, bacteria, detritus). In addition, we used the ratio heme *b*: chl *a* to avoid conflation by zooplankton and dead matter since it is a proxy for the biomass of phytoplankton only.

The chl *a*:POC ratio (Fig. 2.3G) was comparable in the ESNAG and IceB where it ranged from 29.0 μmol mol^{-1} to 137 μmol mol^{-1} in the SML (median= 61.4 μmol mol^{-1}, n=65). Prominent variations in the ratio were observed for the IrmB, GSH and LS where the chl *a*: POC ranged from 32.1 μmol mol^{-1} to 339 μmol mol^{-1} (median= 115 μmol mol^{-1}, n=61). Enhanced chl *a*: POC ratios were also observed in the DCMs (depth down to 80 m; range: 6.8 to 412 μmol mol^{-1}, median= 92.0 μmol mol^{-1}) (SI Fig. 1A). Increases in the chl *a*: POC ratios in the SML of the IrmB, GSH and LS and in the DCMs pointed to low-light acclimated phytoplankton communities in the subpolar regions (Fragoso et al., 2016, 2017; Harrison et al., 2013; Henson et al., 2009) and below the surface waters respectively.

Table 2.1: Comparison table of heme *b*, chlorophyll *a* and dissolved iron concentrations observed in the North Atlantic Ocean (May-June 2014) to date. The data here are reported chronologically based on the sampling year. Adapted from Bellworthy et al. (2017).

Study area	Month/Year	Heme b (pmol L^{-1})	Chlorophyll *a* (nmol L^{-1})	Dissolved iron (nmol L^{-1})	References
Celtic Sea	July-August 2005	3.8±1.7	0.5±0.3	0.8–2.1	(Honey et al., 2013; Ussher et al., 2007)
Iceland Basin	July-August 2007	1.1±0.7	1.2±0.8	<0.03–0.22	(Gledhill et al., 2013; Nielsdóttir et al., 2009)
Scotia Sea	January-February 2008	5.1±4.8	1.9±1.7	<0.03–0.6	(Gledhill et al., 2013; Nielsdóttir et al., 2012)
Tropical North Atlantic	January-February 2008	2.3±1.7	0.25±0.13	<0.1–0.37	(Gledhill et al., 2013; Rijkenberg et al., 2012)
Subtropical North Atlantic	January-February 2010	1.3 ± 0.60	0.17 ± 0.11	NA	(Honey et al., 2013)
Gullmar Fjord	March-June 2013	66±45	1.2±0.6	4–40	(Bellworthy et al., 2017; Stolpe and Hassellöv, 2009)
Eastern Subtropical North Atlantic Gyre	May-June 2014	1.44±1.12	0.30±0.27	0.12-1.04	Current study
Eastern North Atlantic	May-June 2014	1.62±1.27	0.49±0.41	0.09-0.75	Current study
Iceland Basin	May-June 2014	2.09±1.14	0.50±0.37	0.12-2.23	Current study
Irminger Basin	May-June 2014	1.07±1.00	1.10±1.07	0.22-1.33	Current study
Greenland Shelf	May-June 2014	2.04±1.15	1.66±2.21	0.22-1.39	Current study
Labrador Sea	May-June 2014	2.16±1.50	1.08±1.79	0.11-0.77	Current study

The heme *b*:POC ratio in the SML (Fig. 2.3H) was significantly (Kruskal-Wallis test, H=9.8, $p<0.05$) lower in IrmB (median=0.04 μmol mol^{-1}, n=12) and intermediate in ESNAG, GSH and LS (median= 0.19 μmol mol^{-1}, n=40) when compared to IceB (median=0.28 μmol mol^{-1}, n=7). Furthermore, the sections of heme *b*:POC showed an increase in the ratio in the DCMs (median = 0.30 μmol mol^{-1}, n=50) (SI Fig. 1B). The heme *b:* chl *a* ratio followed a similar trend as the heme *b*:POC ratio (Fig. 2.3I) and was lowest in IrmB (median=0.19 mmol mol^{-1}, n=11), intermediate in GSH and LS (median= 1.45 mmol mol^{-1}, n=17) and significantly higher in ESNAG and IceB (median= 3.10 mmol mol^{-1}, n=30).

In general, the correlation of heme *b* with POC suggested that changes in both vertical and spatial distributions of heme *b* were driven primarily by changes in biomass, as reported previously (Bellworthy et al., 2017; Gledhill et al., 2013; Honey et al., 2013). Hence, higher biomass resulted in higher heme *b* concentrations. The high variability in POC, chl *a* and heme *b* and their ratios on the GSH suggested fluctuating biomass linked to submesoscale processes in these coastal waters (Hopwood et al., 2018; Swart et al., 2015; Thomas et al., 2013). Heme *b* deviated from the biomass-driven distribution in two cases; in the DCMs and the IrmB (Fig. 2.2).

Regarding the DCMs, heme *b*: POC ratios increased and followed a similar trend as chl *a*:POC thus indicative of low-light acclimated cells (Moore et al., 2006b) (SI Fig. 1B). Heme *b* is contained in the *b*-type hemoproteins present in the photosystems (i.e. cytochromes *b559* and *b6*) (Hogle et al., 2014). Hence, the changes in the photosynthetic apparatus due to light availability lead also to changes in the vertical distribution of heme *b* (Honey et al., 2013) independent of biomass. However, the light-driven adaptation of heme *b*: POC was not observed in IrmB; heme *b*:POC exhibited its lowest values while chl *a*: POC increased. The increasing low-light acclimation and chl *a* concentrations in the high latitude IrmB were not accompanied by general increases in the proteins of the photosynthetic apparatus (e.g. heme *b*).

The IceB and IrmB showed statistically significant contrasts in heme *b*: POC and heme *b*:chl *a* ratios. In IceB, heme *b*:POC exhibited a median ratio of 0.28 μmol mol^{-1} (n=7) and heme *b*:chl *a* median ratio of 3.6 mmol mol^{-1} (n=11) in the SML. In contrast, low heme *b*: POC (<0.1 μmol mol^{-1}) and heme *b*:chl *a* (<1 mmol mol^{-1}) ratios characterized the IrmB, with previous studies reporting values in the same range for Fe-limited field and cultured phytoplankton (Gledhill et al., 2013, 2015; Honey et al., 2013). This contrasting behavior between the IrmB and the IceB is particularly noteworthy since the DFe (IceB; median= 0.52 nmol L^{-1}, IrmB; median= 0.38 nmol L^{-1}) and nitrate concentrations (IceB; median= 7.4 μmol L^{-1}, IrmB; median= 9.4 μmol L^{-1}) (Fig. 2.3B) were similar in the two regions. Furthermore, both regions had DFe:nitrate ratios of <0.05 mmol mol^{-1} indicative of Fe limitation, since values between 0.05 and 0.9 mmol mol^{-1} are considered to be optimal for nutrient replete growth (Ho et al., 2003; Sunda and Huntsman, 1995; Twining et al., 2004). In the past, both the IceB and IrmB have been shown to be seasonally Fe limited following the spring bloom (Macey et al., 2014; Nielsdóttir et al., 2009; Ryan-Keogh et al., 2013), exhibiting similarly low DFe:nitrate with residual nitrate concentrations. Although these studies were undertaken during the late summer after the bloom peak (Achterberg et al., 2018; Macey et al., 2014; Mohamed et al., 2011; Moore et al., 2013; Nielsdóttir et al., 2009; Poulton et al., 2010; Ryan-Keogh et al., 2013), suboptimal supply of Fe relative to nitrate during winter overturn has been hypothesized to drive the onset of seasonal Fe limitation in IceB and IrmB.

In our study, the absolute concentrations of DFe and nitrate in IceB and IrmB suggested that both systems were DFe and nitrate replete. Therefore, we assumed that the contrast in heme *b* and its ratios arose because of different dominant phytoplankton groups. Furthermore, given that the bloom in the subpolar North Atlantic progresses from east to west (Olsen et al., 2008), such differences in heme *b* may also be attributed to different phases of the spring bloom between the two regions.

2.3.6 Linking heme *b* concentrations with microbial community composition

Sequencing and analysis of the 16S rRNA and cp16S rRNA showed the relative abundance of prokaryotes (Fig. 2.4A) and photosynthetic eukaryotes (Fig. 2.4B) along the GEOVIDE section. Proteobacteria made up most of the prokaryotic pool (35-93%, median= 74%, n=283) across the five oceanographic regions in the upper 100 m. Among the proteobacteria, alphaproteobacteria (mean= 84%, n= 283) were mostly abundant in all regions with representative species the *Pelagibacter* sp.. Gammaproteobacteria accounted for 15% (mean, n=283) of the proteobacteria pool. Cyanobacteria ranged from 0 to 11% (mean= 1.1%, n= 283) overall, but were mostly present in the ESNAG (Mean= 2.3 %, n=85). Since prokaryotes have only a small contribution to the total heme *b* pool (Gledhill, 2007), we proceeded with further data processing using the phytoplankton composition.

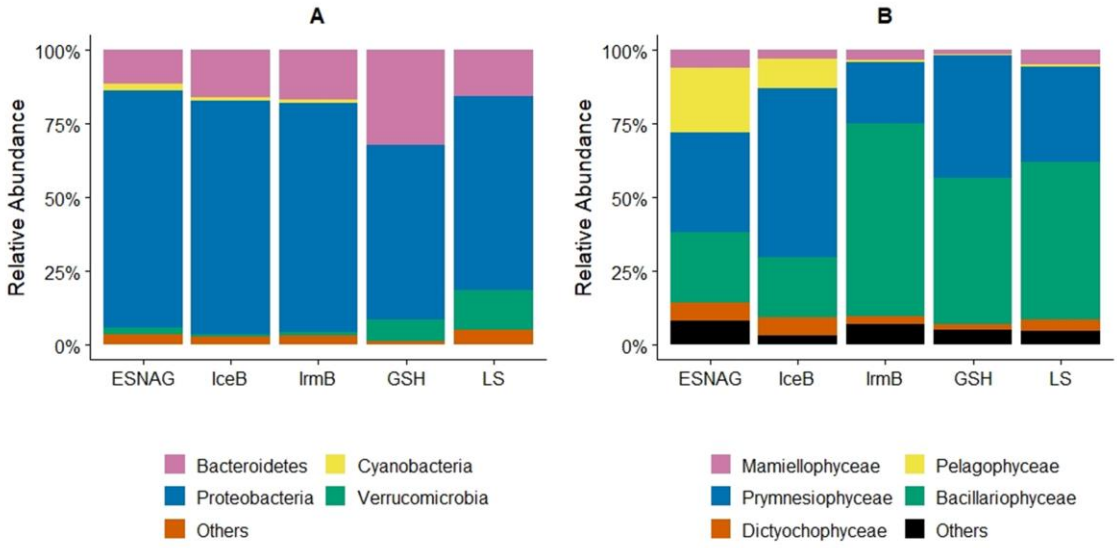

Fig. 2.4: Relative abundance of A) Prokaryotes, and B) Eukaryotes across the GEOVIDE transect in the five oceanographic regions; Eastern Subropical North Atlantic Ocean (ESNAG), Iceland Basin (IceB), Irminger Basin (IrmB), Greenland Shelf (GSH) and Labrador Sea (LS).

Mixed phytoplankton communities were present in all five oceanographic regions (Fig. 2.4B). Overall, prymnesiophyceae (Mean= 36%, n= 245), bacillariophyceae (diatoms) (Mean= 40%, n= 245) and pelagophyceae (Mean= 8%, n=245) were most abundant in the upper 100 m during the GEOVIDE expedition (May-June 2014). However, the percentage of each class varied among the regions (Fig. 2.4B). In the ESNAG, pelagophyceae and prymnesiophyceae were the most abundant classes. In IceB,

prymnesiophyceae dominated the eukaryotic phytoplankton community whereas in IrmB, GSH and LS bacillariophyceae were most abundant.

More detailed analysis of the sequences allowed for a more precise taxonomic identification of the dominant phytoplankton families and species in each oceanographic region. Concerning the prymnesiophyceae, the most abundant families were Phaeocystaceae (Fig. 2.5A), Noelaerhabdaceae (Fig. 2.5B) and Chrysochromulinaceae (Fig. 2.5C). The *Phaeocystis sp.* dominated the LS and the GSH while the *Emiliania sp.* (Noelaerhabdaceae) were mostly abundant in the eastern part of IrmB and in IceB. *Chrysochromulina sp.* were detected in ESNAG, IceB and LS. We also identified several families and species of bacillariophyceae (diatoms), including the Bacillariaceae (Fig. 2.5E), the Rhizosoleniaceae (Fig. 2.5F), the Chaetocerotaceae (Fig. 2.5G) and the Coscinodiscaceae (Fig. 2.5H) families. The large diatoms *Rhizosolenia sp.* (e.g. diameter = 4 - 20 µm, Length = 100 – 500 µm) and *Coscinodiscus sp.* (e.g. diameter 30-500 µm) were dominant in the IrmB while the smaller Bacillariaceae and Chaetocerotaceae were present in the other four oceanographic regions (ESNAG, IceB, GSH and LS). Finally, the Pelagomonadaceae (Fig. 2.5D) family was present mostly in the ESNAG (*Pelagomonas sp.*).

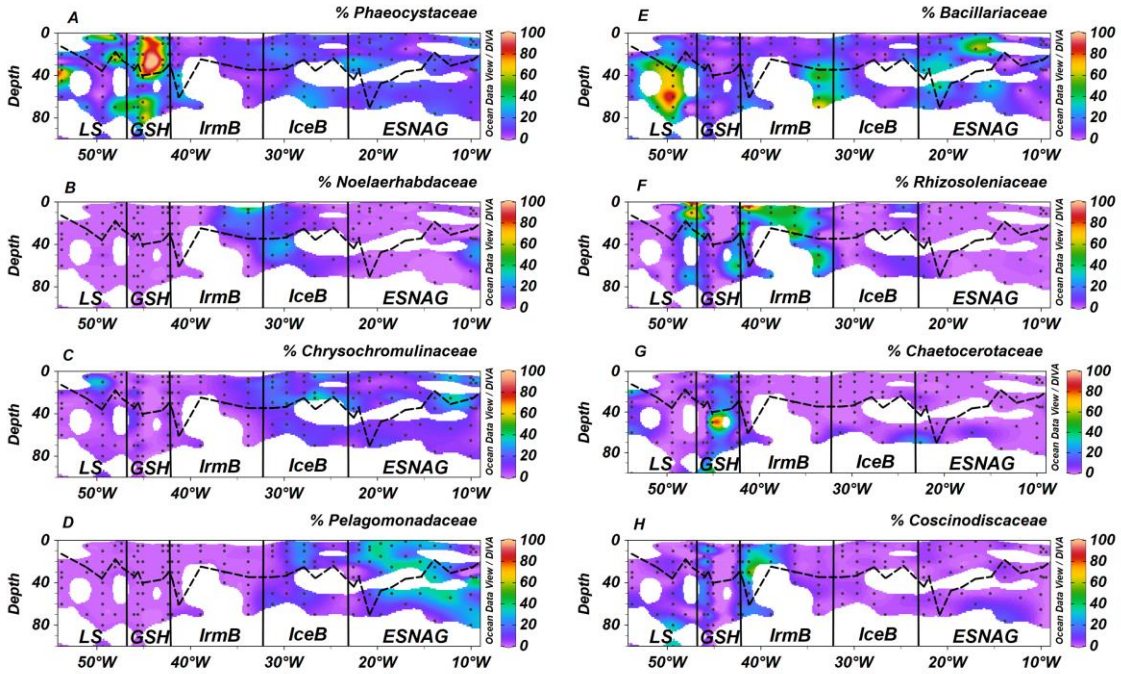

Fig. 2.5: Sections of relative abundance of major phytoplankton eukaryotic families A) Phaeocystaceae, B) Noerlaerhabdaceae, C) Chrysochromulinaceae, D) Pelagomonadaceae, E) Bacillariaceae, F) Rhizosoleniaceae, G) Chaetocerotaceae, and H) Coscinodiscaceae across the GEOVIDE transect. Dashed lines indicate the Mixed Layer Depth and dots indicate the stations and depths where samples were taken. Letter annotations indicate the five oceanographic regions; Eastern Subropical North Atlantic Ocean (ESNAG), Iceland Basin (IceB), Irminger Basin (IrmB), Greenland Shelf (GSH) and Labrador Sea (LS).

Heme *b* depletion relative to biomass in IrmB thus points to an Fe-limited diatom-dominated phytoplankton community. In culture, both diatoms and prymnesiophytes

can respond to Fe limitation by reducing heme *b* quotas (Gledhill et al., 2015; Honey et al., 2013). Despite the low heme *b* in IrmB, the biomass stocks (as indicated by POC and chl *a*) remained elevated pointing to regulation mechanisms of the hemoprotein pool which were likely employed by phytoplankton in order to efficiently reallocate the available Fe and conserve growth under the suboptimal DFe:nitrate conditions.

2.3.7 Heme *b* depletion due phytoplankton Fe -requirements

Diatoms are known for a high Fe demand (Boyd et al., 2012; Sarthou et al., 2005; Sunda and Huntsman, 1995) because of their relatively low surface area to volume ratio (Boyd et al., 2000; Timmermans et al., 2001b), while smaller-sized phytoplankton like prymnesiophytes have lower Fe requirements (Sunda et al., 1991; Sunda and Hardison, 2010; Sunda and Huntsman, 1995). Indeed half-saturation constants for Fe uptake (K_m), indicating the external concentration of Fe required to support growth, range between 0.00059 nmol L^{-1} to 1.2 nmol L^{-1} (Mean= 0.35 ± 0.44 nmol L^{-1}) with larger diatom species exhibiting higher K_m values (Sarthou et al., 2005; Timmermans et al., 2001a, 2004). In contrast, the K_m value for the prymnesiophytes *Phaeocystis sp.* range from 5.0 pmol L^{-1} to 258 pmol L^{-1} DFe (Coale et al., 2003). Furthermore, the degree of Fe stress varies among phytoplankton classes, with smaller sized phytoplankton consistently found to experience less severe Fe stress (Cullen 1991; Price et al. 1994; Macey et al. 2014; Ryan-Keogh et al., 2013).

Iron and nitrate availabilities are higher at the beginning of the growing season (March-June) in the subpolar North Atlantic following Fe supply through deep convective mixing in winter, and the faster growing diatoms are first to bloom (Lochte et al., 1993). Later in the season when Fe concentrations decline, the bloom shifts to prymnesiophytes due to their lower Fe-demand (Lochte et al., 1993; Ryan-Keogh et al., 2013, 2017; Strzepek et al., 2011, 2012). Further subsequent decline of the available Fe during the bloom progression could then lead to Fe limiting conditions for the prymnesiophytes.

The contrast in heme *b* between the IrmB and the IceB in our study likely arises because of the individual Fe requirements and the growth phase of the extant phytoplankton groups. Therefore, the large diatom dominated IrmB (e.g. *Rhizosolenia sp.* size typically 100 - 500 μm length and 4 - 20 μm width) showed signs of Fe limitation despite relatively elevated Fe concentrations (SML: median= 0.38 nmol L^{-1}, n=11) because of their higher Fe-requirements compared to the prymnesiophytes (*Phaeocystis, Emiliania* and *Chyrsochromulina spp.*) in the IceB (Sunda and Huntsman, 1995). In contrast, the haptophytes of IceB had not yet reached Fe -limited conditions at the time of the sampling (May-June 2014), probably because they were at an earlier growth stage compared to the diatoms in the IrmB (Henson et al., 2006).

We suggest that a reduction in heme *b* quota represents a general response of phytoplankton to the declining Fe concentrations over the course of the high latitude

North Atlantic growth season, since it has now been observed in the field for both diatom (current study) and prymnesiophyte (Gledhill et al., 2013; Poulton et al., 2010) (Table 4.1). The reduction in heme *b* quota, could indicate heme *b* regulation, driven by a suboptimal Fe supply and characterized by depletion relative to biomass. Regulation potentially occurs in both the declining diatom and prymnesiophyte populations but at a different time point with respect to ambient Fe concentrations as a result of differences in the absolute Fe requirements of each phytoplankton class. We suggest that once the subsistence heme *b* quotas (and related Fe quota) can no longer be supported, the extant population becomes Fe limited. The whole community will become progressively limited only when the species with the lowest Fe requirement can no longer satisfy its subsistence Fe quota. However, to fully establish the patterns of heme *b* abundance and their relationship to community composition and Fe availability relative to other nutrients during the bloom progression determination of heme *b* in concert with community composition over the course of an open ocean phytoplankton bloom is required.

Heme *b* regulation mechanisms likely include reduction in the abundance of the heme *b*-containing (Hogle et al., 2014) cytochromes b_6f and b_{559} of the PSII apparatus (Greene et al., 1992; Strzepek and Harrison, 2004) which in turn result in increases in chl *a*:PSII ratios as observed later in the growth season in the IrmB (Macey et al., 2014). Indeed, transcriptomic and proteomic analysis in other diatom species (*Thalassiosira pseudonada, Thalassiosira oceanica and Pseudo-nitzschia granii*) showed downregulation of the heme *b*-containing cytochrome b_6f and conservation of the PSII proteins expression (Cohen et al., 2018; Lommer et al., 2012; Nunn et al., 2013). Another regulatory mechanism of heme *b* could be linked to the switch from nitrate to ammonium utilization (Price et al., 1991; Timmermans et al., 1994) which would in turn lead to decreases in the heme *b*-containing nitrate reductase in eukaryotes. Studies have demonstrated via molecular analyses in field and cultured diatom populations that the gene expression and activity of nitrate reductases decreased under low Fe conditions and that the abundance of ammonium transporter (AMT) proteins increased (Cohen et al., 2017; Marchetti et al., 2012; Nunn et al., 2013; Timmermans et al., 1994). We propose that the diatoms of the IrmB had likely shifted to ammonium utilization and followed a similar nitrate reductase regulation strategy for Fe conservation. Finally, Smith et al. (2016) showed via transcriptomic analysis that the expression of the gene encoding heme oxygenase (HO) increased during Fe limitation in the diatom *Phaodactylum tricornutum*. Heme oxygenase is an enzyme that catalyzes the conversion of hemes to bilirubin thus producing Fe^{2+} and bile pigments (Frankenberg-Dinkel, 2004). Hence, the upregulation of HO may be linked to intracellular Fe recovery processes from other porphyrins (Smith et al., 2016).

2.3.8 Heme *b* as method for mapping iron limited phytoplankton

Several methods and proxies have been proposed for the identification of Fe limited oceanic regions and phytoplankton communities. These methods include i) the DFe:nitrate ratio (Browning et al., 2017a; Nielsdóttir et al., 2009; Tonnard et al., 2018), ii) the modified Si^* tracer (Si* = [µmol silicic acid L^{-1}] - ([µmol nitrate L^{-1}]) (Brzezinski et al., 2015; Hogle et al., 2018; Sarmiento et al., 2003), iii) the apparent PSII photochemical efficiency (F_v:F_m ratio) (Greene et al., 1994; Kolber et al., 1998), iv) the satellite-derived quantum yield of fluorescence Φ_{sat} (Behrenfeld et al., 2009; Browning et al., 2014b), and v) bioassay incubation experiments (Moore et al., 2006a, 2007). However, these methods can be subject to changes driven by the microbial community composition or provide an integrated picture of the nutrient status of oceanic regions, thereby missing Fe stress in phytoplankton populations that occurs over shorter temporal scales.

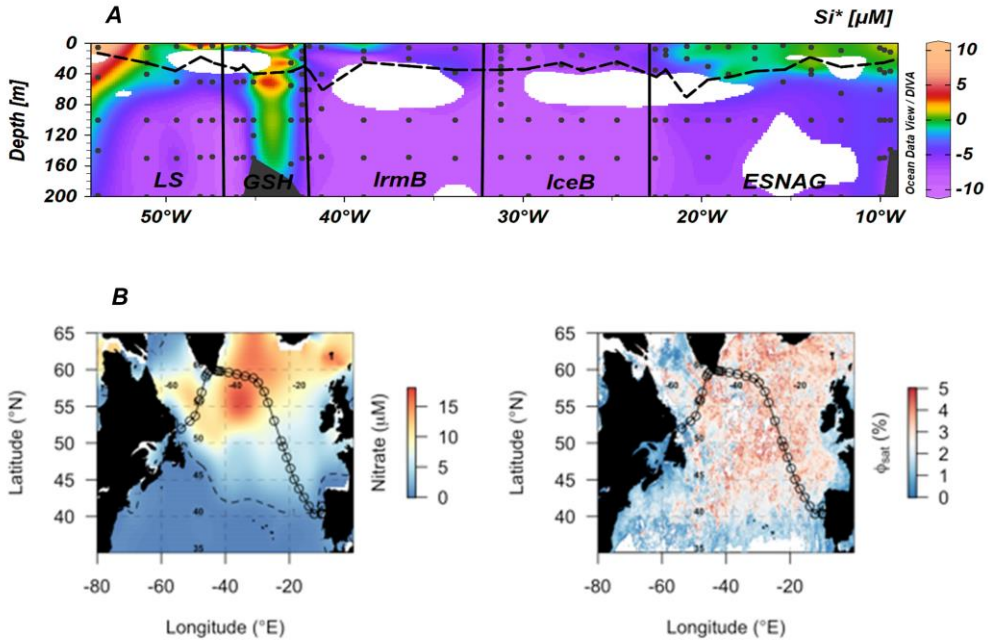

Fig. 2.6: Comparison of different approaches for mapping of Fe-limited regions. A) Si* tracer (Si* = [µmol silicic acid L^{-1}] - ([µmol nitrate L^{-1}]) (Sarmiento et al. 2003). Negative values indicate potential growth limiting nutrients while positive values indicate an excess of $Si(OH)_4$ after complete biological uptake of nitrate. Dashed lines indicate the Mixed Layer Depth and dots indicate the stations and depths where samples were taken. Letter annotations indicate the five oceanographic regions; Eastern Subtropical North Atlantic Gyre (ESNAG), Iceland Basin (IceB), Irminger Basin (IrmB), Greenland Shelf (GSH) and Labrador Sea (LS). B) Satellite-derived quantum yield of fluorescence (Φ_{sat}) averaged for May-June 2014, calculated as in Browning et al. (2014b). Higher quantum yields (red colors) potentially indicate higher Fe stress and correlate with regions of residual nitrate (May-June climatological surface ocean values from World Ocean Atlas; dashed line indicates the 1 µmol nitrate L^{-1} contour).

The parameter F_v:F_m has been shown to vary among phytoplankton classes and species (Moore et al., 2005; Suggett et al., 2009), while the Si^* represents the silicic acid uptake and growth only of the diatom communities under Fe limitation and cannot serve as a community-wide Fe limitation index (Hogle et al., 2018). Furthermore, the DFe:nitrate ratio provides an overall assessment of which nutrient is more likely to be limiting the

phytoplankton community (Moore et al., 2013; Nielsdóttir et al., 2009). Bioassay incubation experiments successfully show the positive responses of Fe-limited phytoplankton following Fe additions (e.g. Moore et al. 2006; Moore et al. 2007; Nielsdóttir et al. 2009; Nielsdóttir et al. 2012; Ryan-Keogh et al. 2013; Browning et al. 2017). However, since the incubation bottles contain seawater of mixed microbial communities, faster growing organisms (such as diatoms) can produce a positive response to nutrient additions even when the slower growing organisms, which may be more representative of the ambient population, are not Fe limited (Price et al., 1994). Finally, although the Φ_{sat} proxy has the potential for mapping Fe limitation and has high utility in terms of spatial and temporal coverage, it also provides an integrated picture of the degree of community-level Fe limitation. In addition, Φ_{sat} is potentially subject to uncertainties associated with short and longer term changes in irradiance (Behrenfeld et al., 2009; Huot et al. 2013; Browning et al. 2014).

Here we compare the heme *b* method for mapping Fe-limited regions and phytoplankton communities with DFe:nitrate (Fig. 2.3C), Si* (Fig. 2.6A) and Φ_{sat} (Fig. 2.6B). In general, the DFe:nitrate, Si* and Φ_{sat} methods showed good agreement and suggested that the phytoplankton communities in the IceB, IrmB and LS had the potential to be Fe-limited during the time of our study. However, we observed depleted heme *b* only in the IrmB. The discrepancy can be attributed to the fact that heme *b* represents a molecular level snapshot of the cellular activity *in situ* at the time of sampling, whilst DFe:nitrate and Si* indicate which nutrient is likely to be limiting for the phytoplankton community and Φ_{sat} integrates over a longer time scale (here two months) and may thus miss short term fluctuations in community Fe limitation brought about by changes in community composition. Combined use of different approaches can thus lead to a fuller picture of the factors influencing phytoplankton productivity.

We showed that changes in heme *b* relative to POC and chl *a* were linked to the stage of the phytoplankton bloom as a result of the absolute Fe requirements of each phytoplankton class. In addition, we observed large fluctuations of heme *b* relative to biomass in GSH and LS. We thus further suggest that in dynamic shelf environments phytoplankton can experience high variability in Fe stress over short temporal and spatial scales. Hence, heme *b* quotas provide further information on the level of Fe stress experienced by different phytoplankton groups and could lead to an improved understanding of the influence of Fe on community composition in productive environments.

2.4 Conclusions

In this study, we determined heme *b* concentrations in the different biogeochemical regions of the GEOVIDE section in order to identify the factors that drive the distribution of the heme *b* Fe pool in the ocean and examine its utility as a proxy for identifying Fe-limited phytoplankton communities *in situ*. Furthermore, this study

systematically examines the relationship between heme *b* abundance and phytoplankton group assemblages.

We showed that biomass variability mainly drove the heme *b* distribution and that low heme *b* quotas characterized Fe-limited phytoplankton communities (case of Irminger Basin). Our data suggest that reduction of heme *b* is not a class or species specific response to Fe limitation and that different phytoplankton groups are able to regulate heme *b* in order to optimize Fe use.

Optimization of the hemoprotein pool may be considered as an adaptation mechanism of phytoplankton to changing ambient Fe conditions. The high variability in stoichiometric ratios (e.g. Fe:C) suggest diverse mechanisms that phytoplankton employs to utilize the available nutrients during replete or limiting conditions (Moore et al., 2013). The ability to optimize Fe use and the resultant flexibility in Fe requirements needs to be accounted for when assessing areas as Fe limited or when considering the impact of Fe limitation on marine productivity and the impact of changes in Fe fluxes to the ocean in the past and future.

Direct comparison of the heme *b* method with other iron-stress biomarkers (e.g. flavodoxin, ferredoxin and IdiA) (LaRoche et al., 1996; Pankowski and McMinn, 2009; Saito et al., 2014; Webb et al., 2001) and/or bioassay incubation experiments (Browning et al., 2014a; Moore et al., 2008; Nielsdóttir et al., 2009) would reinforce the current observations that heme *b* is a good indicator of Fe limitation. Hence, heme *b* Heme *b* alongside other genetic (Allen et al., 2008) and proteomic (LaRoche et al., 1996; Saito et al., 2014) signatures, could be used as a reliable tool for mapping Fe limited areas and give an overview of the cellular activity of marine microbes *in situ*. Thus a broader application of heme *b* could provide information on the molecular adaptation responses of diverse phytoplankton groups to low Fe environments. This information is particularly valuable for the dynamically changing ocean and specifically in the Atlantic Ocean because of the projected altered atmospheric fluxes from the Sahara (Jickells et al., 2005; Mahowald and Luo, 2003; Tegen et al., 2004). Knowledge of phytoplankton adaptation mechanisms could thus help us predict the implications of changing Fe fluxes on key biogeochemical processes in the ocean (e.g. carbon fixation, nitrogen fixation) and their impact on global climate.

2.5 Acknowledgments

The authors would like to thank Pascale Lherminier (coPI of the GEOVIDE project together with GS). We would also like to thank Manon Le Goff, Emilie Grossteffan, Morgane Gallinari and Paul Tréguer for providing the nutrient data, Jérémy Devesa for the POC analyses, and Céline Dimier, Joséphine Ras, Hervé Claustre for the pigment analyses. We also acknowledge the support of Pierre Branellec, Michel Hamon, Catherine Kermabon, Philippe Le Bot, Stéphane Leizour, Olivier Ménage, Floriane Desprez de Gésincourt, Fabien Pérault, and Emmanuel de Saint-Léger during CTD

deployments and of Catherine Schmechtig for the GEOVIDE database management. Finally, we thank the Helmholtz Research School for Ocean System Science and Technology (HOSST) for the financial support to EL.

3. Heme *b* distributions through the Atlantic Ocean; evidence of "anemic" phytoplankton populations

Evangelia Louropoulou[1,2], Martha Gledhill[1], Eric P. Achterberg[1], Thomas J. Browning[1], David J. Honey[3], Ruth A. Schmitz[2], Alessandro Tagliabue[4]

Submitted in *Nature Scientific Reports*

[1] GEOMAR Helmholtz Centre for Ocean Research Kiel, Kiel, Germany
[2] Institute for General Microbiology, Christian-Albrechts-Universität, Kiel, Germany
[3] School of Ocean and Earth Science, University of Southampton, Southampton, UK
[4] School of Environmental Sciences, University of Liverpool, Liverpool, UK

Abstract. Heme *b* is an iron-containing cofactor in hemoproteins that participates in the fundamental processes of photosynthesis and respiration in phytoplankton. Heme *b* concentrations typically decline in waters with low iron concentrations but due to lack of field data, the distribution of heme *b* in particulate material in the ocean is poorly constrained. Here we report particulate heme *b* distributions across the Atlantic Ocean (59.9°N to 34.6°S). Heme *b* concentrations in surface waters ranged from 0.10 to 33.7 pmol L^{-1} (median=1.47 pmol L^{-1}, n=974) and were highest in regions with a high biomass. The ratio of heme *b* to particulate organic carbon (POC) exhibited a mean value of 0.44 μmol heme *b* mol^{-1} POC. Based on the population distribution, we identified the ratio of 0.10 μmol heme *b* mol^{-1} POC as the cut-off between heme *b* replete and heme *b* deficient (anemic) phytoplankton. By this definition, we observed anemic phytoplankton populations in the Subtropical South Atlantic and Irminger Basin. Comparison of observed and modelled heme *b* suggested that heme *b* could account for between 0.17-9.1% of biogenic iron. Our large scale observations of heme *b* relative to biomass demonstrate the impact of changes in iron supply on phytoplankton iron status.

Keywords. Heme *b*, iron, limitation, Atlantic Ocean

3.1 Introduction

Iron constitutes one of the most important nutrients for phytoplankton (Sunda et al., 2005) because it is a component of biomolecules, termed cofactors, that participate in fundamental metabolic processes such as photosynthesis, respiration, nitrogen and sulfur assimilation (Geider and La Roche, 1994; Morel and Price, 2003). The iron-containing cofactors are grouped based on the coordination and chemical bonds of iron with other elements within the molecule, and one major group of iron cofactors are hemes (da Silva and Williams, 2001).

Hemes are iron-containing porphyrins of different structures that act as cofactors (i.e. prosthetic groups) in hemoproteins (Chapman et al., 1997), and are produced via the tetrapyrrole synthesis pathway (Chapman et al., 1997). Ambient iron concentrations control heme biosynthesis and thus intracellular heme concentrations (da Silva and Williams, 2001). Heme *b* (iron protoporphyrin IX) is considered the most common heme structure within an organism (Espinas et al., 2012) and is a constituent of the *b* type cytochromes, catalases, peroxidases, cytochrome P450, globins and nitrate reductase (Hogle et al., 2014; Mochizuki et al., 2010). Hence, heme *b* is involved in electron transport and catalysis of hydrogen and other peroxides as well as oxygen control, oxygen-storage and oxygen-transport (Hogle et al., 2014). Some marine bacteria are known to use dissolved hemes in seawater as a direct source of iron (Hogle et al., 2016; Hopkinson et al., 2008; Roe et al., 2013). In cyanobacteria, rhodophytes and cryptophytes, hemes are further metabolized to phycobilins via heme oxygenase (Beale, 1993). Phycobilins function as chromophores in the light-harvesting phycobiliproteins and the photoreceptor phytochrome (Beale, 1993; Cornejo and Beale, 1997).

Hemoproteins make up approximately 40% of the intracellular iron pool in phytoplankton, with hemoproteins containing heme *b* contributing towards approximately half of this amount (Raven, 1990). Honey, *et al.*(Honey et al., 2013) demonstrated that heme *b* accounts for between 1 to 40 % of the total biogenic iron pool in marine phytoplankton (mean 18 ± 14%). At low iron concentrations in culture media ($\leq$0.50 nmol L^{-1}), 6 to 26% of the available iron was utilized for production of heme *b* cofactors for species from temperate ocean areas (Honey et al., 2013). This percentage ranged from 0.2 to 16% for species from high latitude ocean regions (Gledhill et al., 2015). These findings suggested that, similarly to iron-use efficiencies (Raven, 1990), the heme *b* quota required for growth is also variable amongst species and growth conditions (Gledhill et al., 2015; Honey et al., 2013).

To date, several studies have documented that low oceanic iron concentrations (<0.20 nmol L^{-1}) lead in general to a decrease in growth, photosynthesis and nitrogen fixation rates of phytoplankton (Chappell et al., 2012; Geider and La Roche, 1994; Greene et al., 1992; King and Barbeau, 2007; Kolber et al., 1994; Shi et al., 2007; Sunda and Huntsman, 1997). Although a number of studies have documented the declines in the

abundance of several iron proteins in cultured phytoplankton (Allen et al., 2008; Bibby et al., 2001; Marchetti and Cassar, 2009; Peers and Price, 2006; Richier et al., 2012; Saito et al., 2011; Schorsch et al., 2018; Strzepek and Harrison, 2004), only a few studies report the abundances of such proteins in the field (Erdner and Anderson, 1999; Gledhill et al., 2013; LaRoche et al., 1996; Pankowski and Mcminn, 2008; Saito et al., 2014).

Iron deficiency in higher organisms is expressed by decreases in hemoprotein levels (e.g. hemoglobin). This condition is commonly described as "anemia" which literally refers to heme-iron deficiency. In a similar manner, reduced iron supply in the surface waters in the ocean leads to anemic phytoplankton. Hence, in both cultured and field phytoplankton populations, the concentrations of heme *b* tend to fall below 1.0 pmol L^{-1} (Gledhill et al., 2013, 2015; Honey et al., 2013; Louropoulou et al.) under low iron ($\leq$ 0.5 nmol L^{-1}) conditions. However, certain eukaryotes (*Phaeocystis*, *Chaeotoceros*, *Rhizosolenia spp.*) appear able to maintain growth despite the low heme *b* concentrations (Gledhill et al., 2015; Louropoulou et al.). These species are considered to regulate and reduce intracellular heme *b* concentrations by allocating the available iron away from the hemoprotein pool in order to maintain other metabolic processes (Gledhill et al., 2015; Louropoulou et al.). Heme *b* regulation is considered a response of phytoplankton to declining ambient iron concentrations that depends on species-specific requirements in iron and thus may be observed in the field during the iron-induced shifts (Ryan-Keogh et al., 2013) from larger- to smaller-sized phytoplankton populations (Louropoulou et al.).

In this study we present an extensive dataset of heme *b* abundance in the Atlantic Ocean. We synthesise previously published (Gledhill et al., 2015; Honey et al., 2013; Louropoulou et al.) and new field data covering areas from the subpolar North Atlantic to the subtropical South Atlantic. Since the factors driving the heme *b* distribution in the natural environment are still uncertain, our aim was to examine physical, chemical and biological processes that potentially influence heme *b*. The Atlantic Ocean is a good study region for this purpose as it consists of several provinces that exhibit contrasting abundances of iron and macronutrients. In particular, the Atlantic Ocean is an area of scientific interest as it is subject to large spatial variability in iron supply (Boyd and Ellwood, 2010; Rijkenberg et al., 2014) with potential impacts on primary productivity, nitrogen and phosphorus cycling (Browning et al., 2014a, 2017b, 2017a; Mills et al., 2004; Moore et al., 2006a, 2009), and carbon export (Pabortsava et al., 2017). Furthermore, low iron supply in the Atlantic Ocean has been connected to reductions in primary productivity (Falkowski et al., 2011; Sanders et al., 2014), oceanic CO_2 uptake rates by phytoplankton (Falkowski et al., 2011) and nitrogen fixation rates (Moore et al., 2009) with potential consequences for the global climate (Jickells et al., 2005).

Finally, taking into account the laboratory experiments that showed that heme *b* makes up a significant portion of the total biogenic iron pool in marine phytoplankton, heme *b*

could potentially provide an assessment of iron utilization *in situ*. Hence, the second part of our study examines 1) the comparability of field heme *b* concentrations to predicted heme *b* from the total biogenic iron pool using a global biogeochemical model, and 2) the potential utility of heme *b* as an indicator of the magnitude of the biogenic iron pool in the field.

3.2 Results and discussion

3.2.1 Study region

We compiled newly analyzed (unpublished) and previously published data from the Atlantic Ocean collected over a time span from 2005 to 2016. We present here new data from the research cruises M121 (2015) and M124 (2016) in the South Atlantic. We further obtained published data for the research cruises CD173 (Gledhill et al., 2015), D346 (Honey et al., 2013), D361 (Honey, 2012) and GEOVIDE (Louropoulou et al.). Details on the expeditions are listed in Table 3.1 in chronological order and a map of the sampling areas and stations is shown in Fig. 3.1.

Table 3.1: List of the research cruises in the Atlantic Ocean included in this study. References indicate previous studies where heme *b* data were published.

Cruise ID	Oceanographic Area	Year	Month(s)	Research Vessel	References
CD173	Celtic Sea	2005	July-August	RRS Charles Darwin	(Gledhill et al., 2015)
D346	Subtropical North Atlantic Gyre	2010	January-February	RRS Discovery	(Honey et al., 2013)
D361	Tropical North Atlantic Tropical South Atlantic	2011	February-March	RRS Discovery	(Honey, 2012)
GEOVIDE	Subpolar and Subtropical North Atlantic Ocean	2014	May-June	RV Pourquoi Pas?	(Louropoulou et al., submitted)
M121	(Sub)-Tropical South Atlantic, Benguela Upwelling, Angola Dome – Congo Plume	2015	December	FS Meteor	This study
M124	Subtropical South Atlantic	2016	February-March	FS Meteor	This study

These research expeditions and thus datasets cover several biogeochemical provinces of the Atlantic Ocean. For statistical analysis, data interpretation and discussion, we grouped the sampled stations into sub-regions according to the geographical location and the chlorophyll *a* (chl *a*) distribution. Here we list these regions in geographical order (north to south); Labrador Sea, Irminger Basin, Iceland Basin, Celtic Sea, Subtropical North Atlantic Gyre, Tropical North Atlantic, Coastal Tropical North Atlantic, Tropical South Atlantic, Angola Current, Subtropical South Atlantic Gyre and Benguela Current.

3.2.2 Particulate organic carbon and chlorophyll *a*

Particulate Organic Carbon (POC) concentrations ranged from 0.14 to 63.5 µmol L^{-1} (median= 3.1 µmol L^{-1}, n=1137) for all oceanographic regions from the surface down to 220 m depth. The highest concentrations of POC were determined in the high latitude North Atlantic Ocean (Labrador Sea, Irminger Basin, Iceland Basin; median= 5.6 µmol L^{-1}, n=203) and the coastal areas (Celtic Sea, Coastal Tropical North Atlantic, Angola Current, Benguela Current; median= 8.0 µmol L^{-1}, n=195). Concentrations of POC were lowest in both subtropical gyres (North Atlantic Gyre, South Atlantic Gyre) and open ocean stations of the Tropical North and South Atlantic with a median value of 2.4 µmol L^{-1} (n=752).

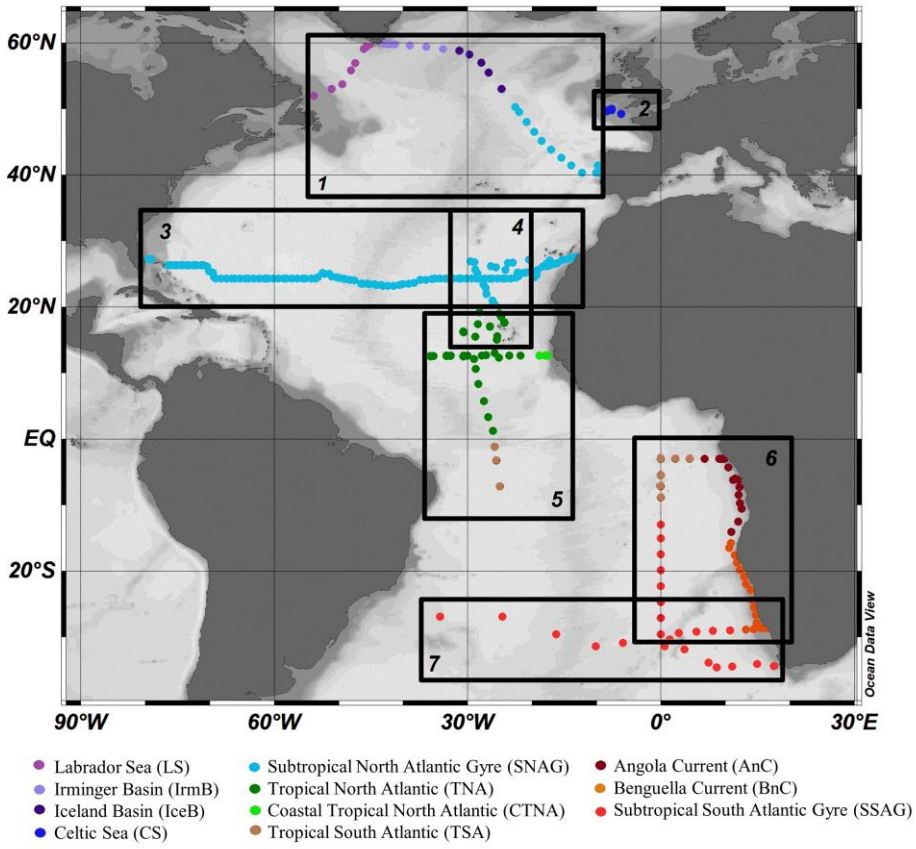

Fig. 3.1: Sampling map of research cruises from 2005 to 2015 included in this study, listed here geographically from North to South. Boxes mark the region and track of each research cruise; 1) GEOVIDE cruise (GEOTRACES – GA01 section) in May-April 2014, 2) CD173 in July-August 2005, 3) D346 in January-February 2010, 4) D361 (GEOTRACES – GA06 section) in February-March 2011, 5) M121 (GEOTRACES – GA08 section) in December 2015, and 6) M124 in February-March 2016. Dots indicate the sampled stations. Colours indicate the oceanographic regions listed geographically from North to South; Labrador Sea (LS), Irminger Basin (IrmB), Iceland Basin (IceB), Celtic Sea (CS), Subtropical North Atlantic Gyre (SNAG), Tropical North Atlantic (TNA), Coastal Tropical North Atlantic (CTNA), Tropical South Atlantic (TSA), Angola Current (AnC), Benguella Current (BnC) and Subtropical South Atlantic Gyre (SSAG).

Table 3.2: Statistics summary table of heme *b*, chlorophyll *a* (chl *a*), particulate organic carbon (POC), heme *b*:POC and heme *b*:chl *a* in the eleven oceanographic regions in the Atlantic Ocean from 2005 to 2015.

Region	Stats	Heme *b* (pmol L^{-1})	Chl *a* (nmol L^{-1})	POC (µmol L^{-1})	Heme *b*:POC (µmol mol^{-1})	Heme *b*:chl *a* (mol mol^{-1})
Labrador Sea	Median	2.5	1.2	13.5	0.20	1.9
	Range	0.82 ± 4.3	0.20 ± 7.4	1.7 ± 40.0	0.03 ± 0.41	0.18 ± 7.5
	No. samples	(16)	(31)	(34)	(16)	(14)
Irminger Basin	Median	0.53	2.0	14.3	0.03	0.20
	Range	0.16 ± 4.0	0.32 ± 4.8	5.4 ± 36.4	0.01 ± 0.61	0.07 ± 9.4
	No. samples	(17)	(30)	(33)	(17)	(15)
Iceland Basin	Median	3.2	0.77	10.9	0.28	3.8
	Range	1.5 ± 4.6	0.47 ± 1.2	4.6 ± 19.7	0.16 ± 0.70	2.2 ± 5.7
	No. samples	(9)	(18)	(14)	(7)	(9)
Celtic Sea	Median	4.1	0.47	10.1	0.43	9.8
	Range	3.1 ± 5.3	0.21 ± 0.72	8.2 ± 12.2	0.28 ± 0.60	7.8 ± 16.3
	No. samples	(12)	(29)	(9)	(9)	(12)
Eastern Subtropical North Atlantic Gyre	Median	1.2	0.15	2.3	0.52	8.3
	Range	0.30 ± 5.1	0.05 ± 1.4	0.16 ± 23.5	0.06 ± 6.2	0.88 ± 22.7
	No. samples	(296)	(340)	(313)	(273)	(296)
Tropical North Atlantic	Median	0.6	0.21	1.3	0.37	2.9
	Range	0.23 ± 3.0	0.10 ± 0.57	0.73 ± 3.0	0.13 ± 3.1	0.77 ± 79.6
	No. samples	(30)	(51)	(49)	(27)	(30)
Coastal Tropical North Atlantic	Median	4.2	2.3	15.2	0.27	1.4
	Range	0.89 ± 15.7	1.42 ± 6.6	4.6 ± 22.6	0.09 ± 1.49	0.47 ± 7.8
	No. samples	(14)	(13)	(14)	(14)	(14)
Tropical South Atlantic	Median	0.55	0.08	6.0	0.16	10.0
	Range	0.22 ± 1.5	0.02 ± 0.23	1.0 ± 10.2	0.05 ± 0.70	1.8 36.3
	No. samples	(20)	(22)	(20)	(20)	(20)
Angola Current	Median	1.6	0.12	6.2	0.25	9.7
	Range	1.60 ± 7.5	0.01 ± 0.79	1.4 ± 13.1	0.01 ± 0.98	1.5 ± 217
	No. samples	(24)	(24)	(24)	(23)	(23)
Benguela Current	Median	6.2	0.91	22.0	0.31	6.1
	Range	0.25 ± 33.7	0.05 ± 7.4	5.6 ± 63.5	0.02 ± 1.5	0.9 ± 138
	No. samples	(35)	(34)	(35)	(35)	(35)
Subtropical South Atlantic Gyre	Median	0.51	0.03	4.9	0.09	12.7
	Range	0.20 ± 4.5	0.01 ± 1.6	2.4 ± 13.6	0.04 ± 0.67	0.32 ± 45.6
	No. samples	(29)	(36)	(33)	(27)	(28)

Chlorophyll *a* concentrations ranged from <0.01 to 10.7 nmol L^{-1} (median=2.0 nmol L^{-1}, n=1272) overall (0-220 m depth). Similar to POC, chl *a* was highest in the subpolar North Atlantic (Labrador Sea, Irminger Basin, Iceland Basin; median= 0.50 nmol L^{-1}, n=186) and the coastal areas (Celtic Sea, Coastal Tropical North Atlantic, Angola Current, Benguela Current; median= 0.38 nmol L^{-1}, n=311). Lower concentrations of chl *a* were determined in tropical areas (Tropical North Atlantic, Tropical South Atlantic; median= 0.21 nmol L^{-1}, n=128) and in the subtropical gyres (North Atlantic Gyre, South Atlantic Gyre; median= 0.13 nmol L^{-1}, n=66).

Depth profiles (SI Fig. 3) of POC and chl *a* indicated generally higher concentration within the surface mixed layer (SML) that decreased with depth (Wilcoxon Rank Sum test, $p<0.01$). However, clear Deep Chlorophyll Maxima (DCM) were present in the Labrador Sea, Celtic Sea and Benguela Current (SI Fig. 3C). A summary of the median concentrations and the ranges of POC and chl *a* in the SML is reported on Table 3.2. Plots A and B in Fig. 3.2 illustrate the median concentrations of POC and chl *a* respectively for each sampling station across the Atlantic Ocean. Chlorophyll *a* correlated with POC (Spearman's rho, r=0.58, n=559, p <0.01) in the SML (SI Fig. 4A). The Kruskal-Wallis test confirmed statistically significant differences among the oceanographic regions (H = 334, p<0.01).

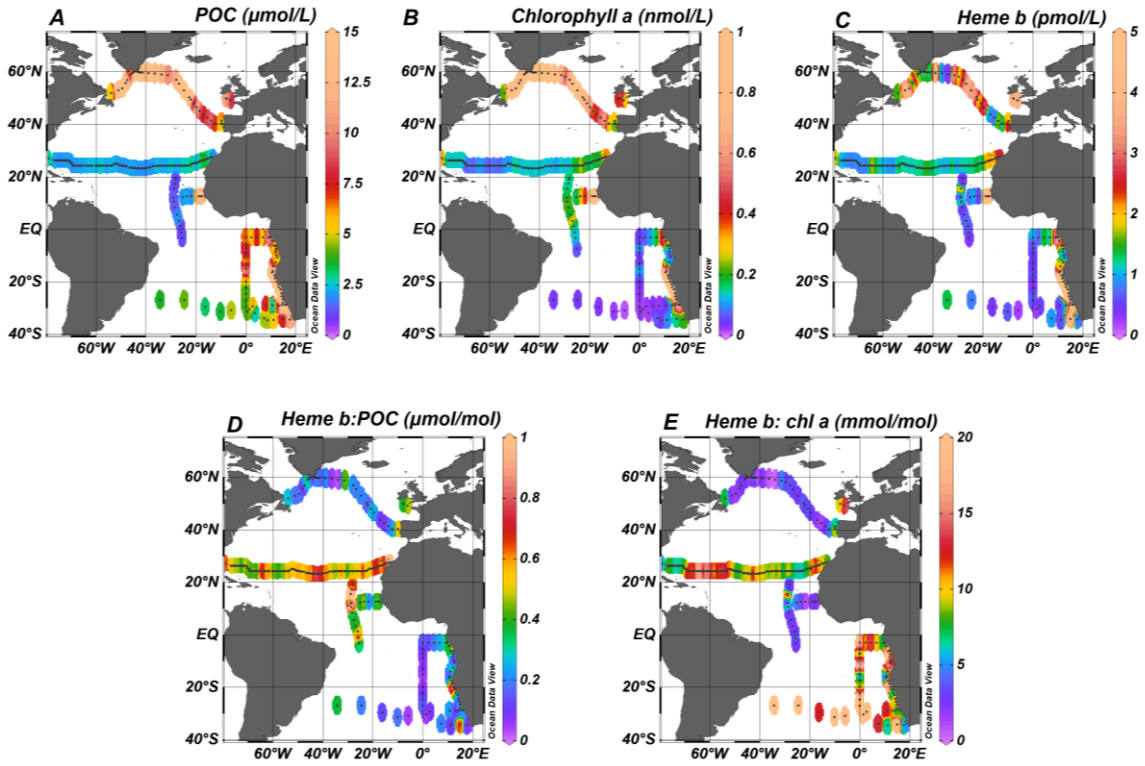

Fig. 3.2: Surface plot of the median values in the Surface Mixed Layer (SML) of A) Particulate organic carbon (POC), B) chlorophyll *a* (chl *a*), C) heme *b*, D) heme *b*:POC, and F) heme *b*:chl *a*. Dots indicate the sampled stations.

3.2.3 Heme *b* concentrations and ratios

Heme *b* concentrations ranged from 0.10 to 33.7 pmol L^{-1} (median= 1.16 pmol L^{-1}, n=974) from the surface layer down to 200 m depth. The depth profiles of heme *b* (SI Fig. 3C) indicated that heme *b* was typically higher in the SML (SML: median= 1.23 pmol L^{-1}, n=502) and decreased with depth (Wilcoxon rank sum test, $p<0.01$) except for the cases where a DCM was present (Labrador Sea, Celtic Sea and Benguela Current).

Statistically significant differences were observed in the spatial distribution of heme *b* for the various oceanographic regions (Kruskal-Wallis, H= 206, $p < 0.01$). Significantly higher concentrations were observed in the SML of the coastal regions (Celtic Sea, Coastal Tropical North Atlantic, Angola Current, Benguela Current), ranging from 0.10 to 33.7 pmol L^{-1} (median= 4.1 pmol L^{-1}, n=85). These regions include two upwelling areas (Coastal Tropical North Atlantic and Benguela Current) and the Congo river plume located in the Angola region; hence, heme *b* was highest in the Benguela area (median=6.2 nmol L^{-1}, n=14) (Fig. 3.3) followed by the Coastal Tropical North Atlantic (median= 4.2 nmol L^{-1}, n=14) (Table 3.2). In addition, heme *b* was also enhanced in the highly productive subpolar areas (Iceland Basin, Greenland Shelf and Labrador Sea) which were sampled during the spring bloom in 2014 (range 0.16 – 4.6 pmol L^{-1}, median= 2.2 pmol L^{-1}, n=48) (Louropoulou et al.). However, the Irminger Basin deviated from this pattern, despite being sampled in the same season, exhibiting the lowest heme *b* concentrations (median= 0.53 pmol L^{-1}, n=17) (Louropoulou et al.), along with the Subtropical South Atlantic Gyre (median= 0.51 pmol L^{-1}, n=29) and the offshore stations in the tropical Atlantic (Tropical South Atlantic and Tropical North Atlantic, median= 0.58 pmol L^{-1}, n=50).

Due to the systematic differences in heme *b*, POC and chl *a* ratios in the Irminger Basin and the Subtropical South Atlantic Gyre (SI Fig. 6), we excluded both areas from pairwise correlations between parameters. Heme *b* correlated well with both POC (Spearman's rho, r=0.56, n= 468, $p<0.01$) and chl *a* (Spearman's rho, r=0.63, n=491, $p<0.01$) (SI Fig. 4B,C). These results along with the average depth profiles of heme *b*, chl *a* and POC (SI Fig. 2A,B,C) suggest that both the spatial and the vertical distribution of heme *b* concentrations in the Atlantic Ocean were strongly influenced by biomass, as observed previously (Honey et al., 2013).

In order to examine the changes of heme *b* relative to biomass as indicated by POC and chl *a*, we calculated the ratios of heme *b*:POC and heme *b*: chl *a* (Gledhill et al., 2013, 2015). The heme *b*:POC ratio represents the heme *b* per unit carbon derived from the total particulate organic matter and previous field studies showed that this ratio varied as a result of iron availability (Gledhill et al., 2013, 2015; Honey et al., 2013; Louropoulou et al.). The ratio heme *b*: chl *a* corresponds to organic matter originating from phytoplankton, but because of intracellular chlorophyll variability, can also be influenced by light-driven changes in photoacclimation state.

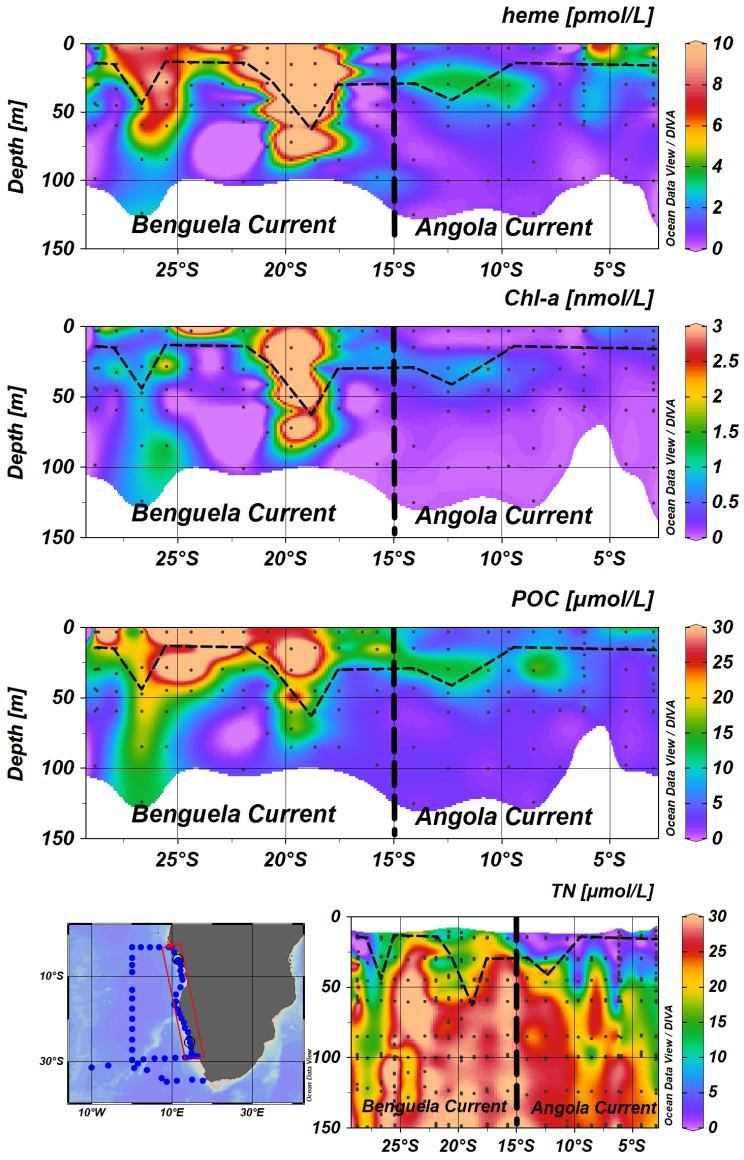

Fig. 3.3: Section plots of heme *b*, chlorophyll *a* (chl *a*), particulate organic carbon (POC) and total nitrate (TN) along the coast of Africa during the M121 cruise (December 2015). Dashed lines indicate the Mixed Layer Depth (MLD) and dots indicate the sampled stations and the data points available. Letter annotations indicate the two oceanographic regions encountered which were the Benguella Current and Angola Current regions.

In this study, heme *b*: POC ranged overall from 0.01 to 6.2 µmol mol^{-1} (median= 0.39 µmol mol^{-1}, n=907) when both SML and DCM were considered. However, the difference in values between the two layers was statistically significant (Wilcoxon Rank Sum test, $p<0.01$), with heme *b*: POC significantly higher in the DCM. Statistically significant differences were observed for the SML for the various oceanographic regions in for both heme *b*:POC (Kruskal-Wallis, H= 153, $p < 0.01$) (SI Fig. 6A). The lowest values of heme *b*:POC were determined in the Irminger Basin (SML: median= 0.03 µmol mol^{-1}, n=17) and the Subtropical South Atlantic Gyre (SML: median= 0.08 µmol mol^{-1}, n=27) suggesting a decoupling of heme *b* from POC in these regions. Similarly, we observed statistically significant differences among the oceanographic regions for the heme *b*:chl *a* ratio (Kruskal-Wallis, H= 146, $p < 0.01$) (SI Fig. 6B).

Heme *b*:chl *a* ratios ranged overall from 0.07 to 327 mmol mol^{-1} (median= 7.3 mmol mol^{-1}, n=942) and followed a different pattern of spatial distribution in the SML compared to heme *b*:POC (Fig. 3.2E). Hence, heme *b*: chl *a* was lowest in the SML of the Irminger Basin (SML: median= 0.20 mmol mol^{-1}, n=15) and highest in the Subtropical South Atlantic Gyre (SML: median= 12.7 mmol mol^{-1}, n=28) suggesting community driven differences in photoacclimation and/or hemoprotein regulation patterns.

3.2.4 Identification of heme *b* based criteria for iron limited phytoplankton

In laboratory studies, values of heme *b*:POC below 0.10 μmol mol^{-1} were indicative of iron-limited phytoplankton (Gledhill et al., 2015; Honey et al., 2013), and similar values have been determined for field phytoplankton communities in the iron - limited post-bloom Iceland Basin (Gledhill et al., 2013) and low-iron Southern Ocean (Gledhill et al., 2013, 2015). In case of Irminger Basin, Louropoulou et al. (in review) showed heme *b* depletion (median= 0.53 pmol L^{-1}, n=17) in a large diatom-dominated community in May-June 2014 despite relatively high iron concentrations (≥ 0.30 nmol L^{-1}), indicating iron limitation resulting from the high iron requirements of the extant phytoplankton population.

In this study, we report a similar pattern of low heme *b* concentrations (<1 pmol L^{-1}) and low heme *b*:POC ratios (<0.1 μmol mol^{-1}) in the eastern and in the central Subtropical South Atlantic Gyre, which point to iron-limited phytoplankton communities in these areas. Our observations are confirmed by bioassay experiments that showed the eastern boundary of the Subtropical South Atlantic Gyre was nitrate-iron co-limited during the period of the cruise (Browning et al., 2017a). The good agreement between the heme *b* measurements and the bioassay experiments of Browning, *et al.*(Browning et al., 2017a) reinforces previous comparisons with other approaches for mapping iron-limited phytoplankton communities (Louropoulou et al. in review) that included the dissolved iron:nitrate ratio (Nielsdóttir et al., 2009), modified Si^* tracer (Brzezinski et al., 2015; Hogle et al., 2018; Sarmiento et al., 2003) and satellite-derived quantum yield of fluorescence Φ_{sat} (Behrenfeld et al., 2009; Browning et al., 2014b). Heme *b* measurements thus appeared to successfully map iron limited phytoplankton by depicting the momentary condition of the phytoplankton cells *in situ*.

We constructed a histogram of all our SML heme *b*:POC data in order to investigate overall trends in Atlantic Ocean phytoplankton populations. The distribution of the heme *b*:POC data (Fig. 3.4A) was skewed to the right with a median value of 0.44 μmol mol^{-1} (n=468) and a mean value of 0.47 ± 0.42 μmol mol^{-1} (n=468). Furthermore, both the Irminger Basin and the Subtropical South Atlantic Gyre exhibited an exponential distribution and their medians (0.03 μmol mol^{-1} and 0.09 μmol mol^{-1} respectively) deviated from the median of the distribution (Fig. 3.4A). Taking into account laboratory studies and field observations of heme *b*: POC ratios and their relationship to iron

limitation, we suggest that 0.10 µmol mol^{-1} is a reasonable estimate for defining an anemic, iron limited phytoplankton community in the Atlantic Ocean. Hence, the data appearing in the left tail (break 0.10 µmol mol^{-1}, n=50) (Fig. 3.4A) of the distribution point to iron limited phytoplankton communities in these areas. Thus, by this definition, the southern stations of Tropical South Atlantic were iron limited and iron co-limitation is predicted to extend to the central parts of the subtropical gyre (Fig. 3.2, cruise M124, sampling February-March 2016).

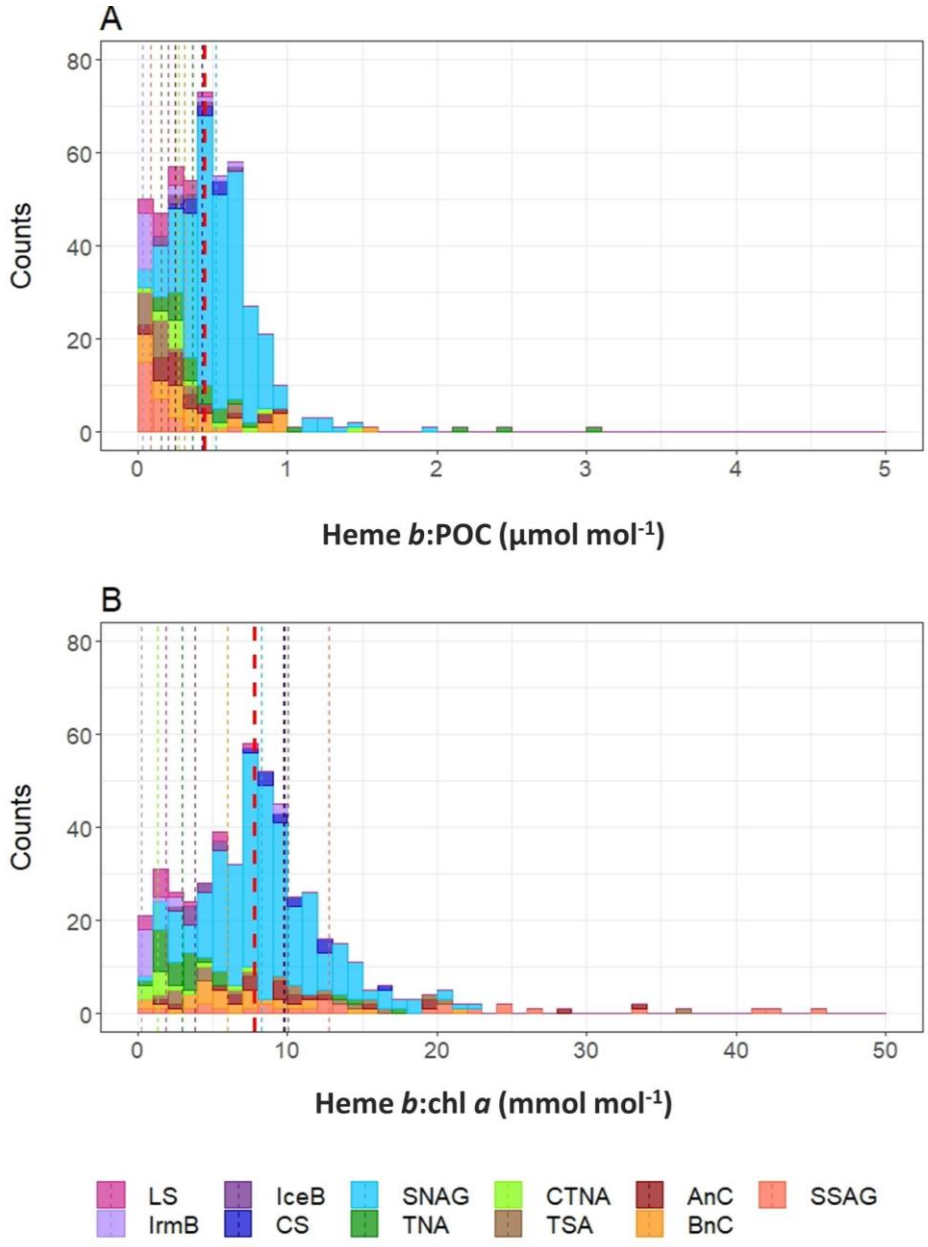

Fig. 3.4: Histograms of A) heme *b*:POC (n=468), and B) heme *b*: chl *a* (n=491) distributions in the surface mixed layer (SML) during the research cruises from 2005 to 2015 included in this study. Colours indicate the oceanographic regions; Labrador Sea (LS), Labrador Sea (LS), Irminger Basin (IrmB), Iceland Basin (IceB), Celtic Sea (CS), Subtropical North Atlantic Gyre (SNAG), Tropical North Atlantic (TNA), Coastal Tropical North Atlantic (CTNA), Tropical South Atlantic (TSA), Angola Current (AnC), Benguella Current (BnC) and Subtropical South Atlantic Gyre (SSAG). The thick red dashed line marks the median of the each distribution while the coloured thinner dashed lines indicate the medians of each oceanographic region.

In contrast, the western boundaries of the Subtropical South Atlantic Gyre were characterized by slightly higher heme concentrations (1.36 pmol L^{-1}) and heme *b*:POC ratios (0.37 μmol mol^{-1}) compared to the eastern and central Subtropical South Atlantic Gyre. These results suggest that this area was not iron limited; indeed Rijkenberg et al. (2014) reported iron concentrations up to 6.1 nM in the upper 800 m off shore of Brazil in the Subtropical Shelf Front (STSF), which is formed by the southward flowing Brazil Current and the norward flowing Malvinas Current (Piola et al., 2008). The iron enrichment was attributed to aeolian deposition and transport by the STSF, and to offshore export of iron from Brazilian shelf waters and the Rio de la Plata river (Piola et al., 2008; Rijkenberg et al., 2014).

The heme *b*:POC values of the open ocean stations in the Tropical North Atlantic, (SML; median= 0.26 μmol mol^{-1}) do not point towards iron-limited phytoplankton communities, even though heme *b* concentrations were low (SML; median= 0.59 pmol L^{-1}); we attribute this trend to low biomass at the time of sampling. In general, the location of the Intertropical Convergence Zone (ITCZ) defines the dust derived iron supply to surface waters (Jickells et al., 2005) and thus influences the biogeochemical status and bloom progression between the northern and the southern oligotrophic waters around the Equator (Schlosser et al., 2014; Snow et al., 2015b). In February-March 2011, when sampling was performed, Schlosser, *et al.*(Schlosser et al., 2014) reported that the ITCZ was at ~1°N and the Tropical North Atlantic was receiving significant amounts of atmospheric deposition whilst the Tropical South Atlantic had low atmospheric dust concentrations. In addition, Snow, *et al.*(Snow et al., 2015b) reported increased nitrogen fixation rates due to the abundance of *Trichodesmium sp.* between 15°N and 7°S which have high iron requirements relative to non-nitrogen fixing phytoplankton.

3.2.5 Heme *b* regulation strategies?

Similar to the heme *b*:POC ratio, the distribution of the population for the heme *b*:chl *a* ratio (Fig. 3.4B) was also skewed to the right with median value of 7.77 mmol mol^{-1} and a mean value 8.98 mmol mol^{-1} (n=491). However, we observed a contrasting behavior in the ratios of the two iron limited areas Irminger Basin ($median_{SML}$= 0.20 mmol mol^{-1}, n=20) and Subtropical South Atlantic Gyre ($median_{SML}$= 12.7 mmol mol^{-1}, n=28), despite the similar trend in heme *b*:POC. The medians of heme *b*:chl *a* for these two areas deviated from the overall median of the distribution and located either on left (Irminger Basin) or the right (Subtropical South Atlantic Gyre) tail. Heme *b* exhibited the same trend for the two areas which implies that changes in chl *a* quotas drove the differences in the ratio. Hence, we ascribed this contrast to different extant phytoplankton groups and to different photoacclimation status.

The low heme *b*:chl *a* observed in Irminger Basin implied that the heme *b* containing proteins of the photosynthetic apparatus decreased whilst chl *a* was conserved. In

culture, several diatoms and prymnesiophytes exhibited decreased heme *b*:chl *a* ratio under low iron conditions (<0.50 nmol L^{-1}) (Gledhill et al., 2015; Honey et al., 2013) implying allocation of iron away from the hemoprotein pool (Gledhill et al., 2015). This behavior was considered an adaptation strategy of phytoplankton that would allow a reduction of the overall iron requirements and a more efficient utilization of the available iron in order to sustain growth (Gledhill et al., 2015). Here, this pattern was also observed in the field in the Irminger Basin (GEOVIDE, May-June 2014) for diatom populations that likely employed heme *b* regulation (Louropoulou et al.) in order to adapt to declining iron concentrations during bloom progression. For example, allocating the iron away from the hemoproteins would lead to decline of the heme *b*-containing cytochromes b_6f and b_{559} of the PSII apparatus (Greene et al., 1992; Hogle et al., 2014; STRZEPEK and Harrison, 2004), which in turn would be accompanied by increases in the chl *a*:PSII ratios. Indeed this was observed by Macey, *et al.*(Macey et al., 2014) in the post-bloom iron-limited Iceland Basin. Particularly for the eukaryotes, another strategy of reducing iron requirements is switching from nitrate to ammonium utilization (Cohen et al., 2017; Price et al., 1991; Timmermans et al., 1994) which induces the reduction of heme *b*-containing nitrate reductase.

We observed very high heme *b*:chl *a* in the Subtropical South Atlantic Gyre which was driven by low concentrations of chl *a* in the area (SML median=0.03 nmol L^{-1}) (Fig. 3.2E). Hence, we further examined how chl *a* varied in this region according to biomass (as indicated by POC) and found that the ratio chl *a:*POC (SI Fig. 7) was 7.68 μmol mol^{-1} (n=32) pointing to lower photoacclimation of the dominant phytoplankton groups. At the time of the study, haptophytes and the picophytoplankton species *Synechococcus* and *Prochlorococcus* were most dominant in the eastern parts of the gyre (Browning et al., 2017a). Similar community composition characterizes the Subtropical North Atlantic Gyre (Zubkov et al., 1998). Therefore, we made a comparison of the trends in chl *a*:POC between these two regions; in the Subtropical North Atlantic Gyre, the chl *a*:POC was higher compared to the Subtropical South Atlantic Gyre reaching a median value of 65.0 μmol mol^{-1} (n=312). The contrasting behavior in chl *a*:POC can be ascribed to differences in light climate, which is known to strongly influence chl *a*:POC ratios (Behrenfeld et al., 2005). Higher light conditions in the Subtropical South Atlantic Gyre in comparison to the Subtropical North Atlantic Gyre, as a result of both higher incident irradiance and shallower mixed layers (SI Fig. 7), would be expected to result in the lower chlorophyll-to-carbon ratios observed. This result highlights the variability of chl *a* independent from iron availability, due photoacclimation.

3.2.6 Comparison of field heme *b* concentrations with model-based predictions

Both theoretical estimates and direct measurements suggest heme *b* represents an important amount of the total cellular iron pool in phytoplankton (mean 18±14%) (Honey et al., 2013; Raven, 1988, 1990) thus the second part of our study aimed to

examine to what extent the heme *b* field data were comparable to heme *b* estimated from the biogenic iron pool as predicted from a global biogeochemical model. Here we used the PISCES-v2 (Pelagic Interactions Scheme for Carbon and Ecosystem Studies volume 2) biogeochemical model to estimate the biogenic iron pool which is determined based on Michaelis Menten uptake kinetics, further regulated by a maximum iron-to-carbon (Fe:C) cellular quota and enhanced iron uptake under iron limitation (Aumont et al., 2015; Tagliabue et al., 2018; Tagliabue and Resing, 2016). Figuge 3.5A illustrates the biogenic iron (Fe_{bio}) pool from the model which corresponds to sum of the diatom and nanophytoplankton iron pools extracted at the same geographic position and month as the field data. Values represent the monthly means for the upper most layer of the model (depth 10 m) and ranged from 9.20 to 285 pmol L^{-1} (median= 78.8 pmol L^{-1}, n=254). Although a direct comparison of the absolute values is questionable due to the large uncertainties associated with model predictions of the ocean iron cycle (Tagliabue et al., 2016), there are similar trends between the Fe_{bio} and heme *b* abundance in the Atlantic Ocean. In particular, both parameters were highest in the subpolar North Atlantic (Labrador Sea, Iceland Basin), along the continental margins (Celtic Sea, Angola Current) and in the upwelling areas (Coastal Tropical North Atlantic, Benguela Current), whilst the lowest values were determined in the oligotrophic Subtropical South Atlantic Gyre.

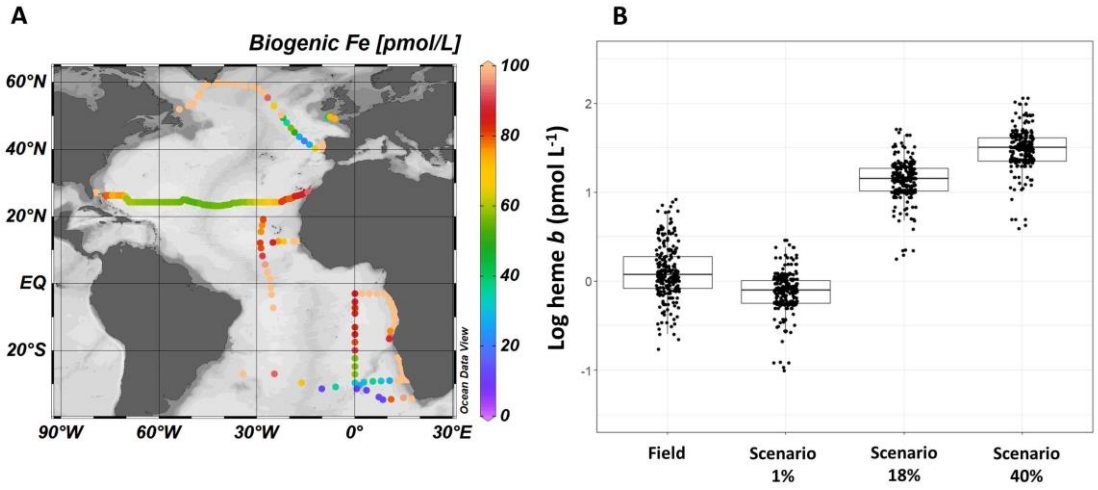

Fig. 3.5: A) Model-based estimation the biogenic iron (Fe) pool deriving from the sum of the nanophytoplankton and diatom iron pools in pmol/L. Values represent the monthly mean for the upper most layer of the model at the same time as sampling (depth 10m). B) Actual field heme *b* measurements and predicted heme *b* concentrations calculated from the total biogenic iron concentration in the SML of each station. Calculations follow three scenarios of heme *b* proportion relative to the total biogenic iron according to observations from cultured phytoplankton (Honey et al., 2013); heme *b* accounts for 1%, 18%, and 40%.

According to phytoplankton culture experiments with different phytoplankton species, heme *b* accounts for between 1 and 40% of the particulate Fe (PFe) (averaging 18 ±14 %) (Gledhill, 2007; Honey et al., 2013; Raven, 1990). We calculated the predicted heme *b* concentrations (in pmol L^{-1}) from the modelled Fe_{bio} of each station in the SML using three scenarios (values) 1%, 18% and 40% that represent the range and mean of heme

b:PFe observed in laboratory cultures. We used the formula heme *b* = [Fe_{bio} * [heme *b*/ PFe] $_{lab}$]/100, where [heme *b* / PFe]$_{lab}$ denotes the proportion of heme *b* relative to PFe determined for cultured phytoplankton under various growing conditions.

Predicted heme *b* concentrations were lowest for the 1% scenario and highest for the 40% scenario (Fig. 3.5B) with the 1% scenario corresponding more closely to the field observations reported in this study. This trend was further supported by the ratio heme *b*:Fe_{bio} calculated from the mean heme *b* concentrations (in the SML) and the model-based Fe_{bio} which ranged from 0.17% to 9.1 % (median= 1.8 %, n=234). Taken together with heme *b*:POC, these results suggest that, as far as heme *b* is concerned, field populations were comparable to laboratory observations for species with low heme *b* content. Furthermore, the ratio of 1% was determined in cultures where iron (0.50 nmol L^{-1}) or nitrate supply had been exhausted, thus perhaps better representing the natural environment. Therefore, the model prediction of Fe_{bio} and the *in situ* heme *b* concentrations were consistent with previous laboratory observations (Gledhill et al., 2015; Honey et al., 2013). The differences in the proportion of heme *b* relative to Fe_{bio} likely arose because of the microbial community composition of each region and the interspecific differences in hemoprotein processes.

Biogenic iron and iron-to-carbon (Fe:C) ratios are critical for linking the iron and carbon cycles in the ocean and constraining phytoplankton iron requirements within biogeochemical models (King et al., 2012). Currently, the biogenic iron pool can be assessed by radioisotope uptake experiments (Bowie et al., 2008; King et al., 2012), single-cell synchrotron x-ray fluorescence (King et al., 2012; Lampe et al., 2018; Twining and Baines, 2013) and determination of particulate iron after careful removal of or correction for lithogenic iron (Bowie et al., 2009; Chever et al., 2010; King et al., 2012; Sarthou et al., 2008). Whilst all these techniques provide complimentary and useful information on particulate iron, single cell iron-to-phosphorus ratios or community wide Fe:C uptake rates, none provide a definitive estimate of average *in-situ* biogenic iron quotas within phytoplankton populations. Furthermore, none of the above methods were applied consistently on larger scale field expeditions. The good agreement of heme *b* observational and model-based data suggests that heme *b* could potentially serve as an indicator of the biogenic iron for field studies and provide an assessment of the proportion of iron used in the heme *b* and the hemoprotein pools in marine phytoplankton, although further comparison of heme *b* abundance with established methods of assessing biogenic iron are required.

3.3 Conclusions

In this study, we demonstrated that the ratio heme *b*:POC can serve as a reliable indicator of iron limitation since it appeared not to be influenced by species- specific processes which potentially involve modifications in the hemoprotein and/or other protein pools. A comparison of the heme *b* method with already established protocols,

such as bioassay experiments (Browning et al., 2014a; Moore et al., 2008; Nielsdóttir et al., 2009) and iron-stress biomarkers (e.g. flavodoxin, ferredoxin and IdiA) (Allen et al., 2008; LaRoche et al., 1996; Pankowski and McMinn, 2009; Saito et al., 2014; Webb et al., 2001), would validate this simple method for mapping iron limited phytoplankton in small or large scale field expeditions. Although determination of heme *b* in marine particulate material requires specialist analytical instruments, sample collection is straightforward and utilizes the same approaches routinely applied for collection of pigment samples. Importantly, sampling for heme *b* does not require trace metal clean conditions, significantly widening the potential for assessment of iron limitation in the field. Furthermore, heme *b* is a ubiquitous biomolecule and is thus not dependent on the presence of particular phytoplankton species.

The variability of the heme *b* to biomass ratios suggested that phytoplankton 1) employ diverse mechanisms to utilize the available iron in the hemoprotein pool, and 2) are able to regulate the hemoproteins under iron limiting conditions. Expanding the field and laboratory research in hemoprotein abundance and cycling would contribute to the identification of such iron utilization and regulation strategies. One aspect could be the transcriptomic and proteomic analyses of biomolecules involved in the heme *b* cycling pathways. These include the proteins associated with the utilization of the heme *b* cofactor, such as the components of the photosynthetic or nitrate assimilation apparatus, as well as the components of the biosynthesis and breakdown pathways. The information about iron-utilization in hemoproteins and about regulation of the hemoprotein pool would shed light on the molecular response and adaptation of phytoplankton to iron limitation. This information will be particularly useful in the future due to projected alterations in desert dust supply (Jickells et al., 2005; Mahowald et al., 2009) and thus, to iron availability in the ocean, with potential impacts on carbon sequestration and climate. Finally, application of the heme *b* method in oceanic regions other than the Atlantic Ocean would enhance the estimates of the magnitude of the biogenic iron pool and expand our knowledge on phytoplankton physiological status in relation to iron.

3.4 Methods

3.4.1 Sampling

During all research cruises sampling of seawater was performed by a stainless steel CTD rosette equipped with Niskin bottles for the determination of heme *b*, POC and chl *a*. We sampled 279 stations and 4 to 6 different depths per station (typically down to 300 m deep) in order to study heme *b* abundance in the Atlantic Ocean.

3.4.2 Heme *b*

Marine particulate material (>0.7 μm) was collected after filtration of seawater on glass fiber filters (GF/F, pore size 0.7 μm, MF300, Fisherbrand™) for the determination of

heme *b*. The filters were stored at -80^{o}C prior to analysis. Heme *b* was quantified by High Performance Liquid Chromatography (HPLC) – Diode Array Detection (DAD) – Electrospray Ionisation (ESI) Mass spectrometry (MS) after extraction by 2.5% w:v Octyl β-D-glucopyranoside-OGP solution (Sigma-Aldrich®, ≥98% GC Grade) (Gledhill, 2007, 2014). Regarding the analytical procedure and the instruments used, we followed the protocol described by Gledhill (2007) for the samples from the CD173 cruise and Gledhill (2014) for the samples from cruises D346, D361 and M124. Good agreement was obtained between the two analytical methods (Gledhill, 2014). Slight modifications were applied to the analysis of the samples from GEOVIDE and M121 as described in Louropoulou et al., submitted.

Quantification of heme *b* for D346, D361, GEOVIDE, M121 and M124 was performed from the MS data on a m/z ratio of 616.122, since the PDA detector is known to have interferences from other pigments co-eluting with heme *b* and absorbing at a wavelength of 401 nm (Gledhill, 2014). The analytical detection limits were defined as three times the standard deviation of the lowest calibration standard for each of the methods followed and were 1.57 nM (CD173), 190 pmol heme *b* L^{-1} (D346, D361 and M124) and 32 pmol heme *b* L^{-1} (GEOVIDE and M121). Heme *b* could not be detected in the blank extraction solution in either utilised method.

3.4.3 Particulate organic carbon and chlorophyll *a*

Seawater was filtered through pre-combusted GF/F for the determination of POC and acidified either with sulfurous acid - H_2SO_3 (cruises D346, D361, M121, M124) or with hydrochloric acid - HCl (GEOVIDE) for the removal of inorganic carbon following published protocols (Lorrain et al., 2003; Verardo et al., 1990). POC in samples and several blank filters was quantified by elemental NC analyser using acetanilide as the calibration standard (Verardo et al., 1990).

Chl *a* was determined for the cruises CD173, D346, D361 and M124 via fluorometry after extraction with 90% (v:v) acetone in the dark (Welschmeyer, 1994). For the GEOVIDE and M121 cruises, chl *a* was determined after extraction with 100% methanol and sonication followed by High Performance Liquid Chromatography quantification (Ras et al., 2008).

3.4.4 Data handling

Data processing, statistical analysis and visualization were carried out using R Statistical Software (R Core Team 2016). The SML was calculated from the CTD data (obtained by sensors on the rosettes) using the temperature-based criterion (ΔT = 0.5 °C) (Monterey and Levitus, 1997). We checked the normality of the data distribution by applying the Shapiro-Wilk test which showed a non-normal distribution for all parameters ($p<0.05$). Hence, we used the Kruskal–Wallis test for analysis of variance, the Wilcoxon rank sum test to identify differences in the distributions in and below the

SML and the Spearman's rank correlation to check the association between parameters. Surface and section plots were produced using the Ocean Data View v.4.7.9 (Schlitzer, R. Ocean Data View. 2018).

3.5 Acknowledgements

The authors would like to thank the ship crews, PIs and research scientists of all research expeditions (GEOVIDE, CD173, D346, D361, M121 and M124). We would like to acknowledge the contribution of Tim de Groot in sampling procedures during the M124 expedition. This project was funded by the UK Natural Environment Research Council (NE/K001973/1, NE/G015732/1, NE/H00475/1). The cruise in the SE Atlantic Ocean (M121) was funded by the Deutsche Forschungsgemeinschaft (DFG). AT was funded by the European Research Council (grant #724289). TJB received funding from a Marie Skłodowska-Curie Postdoctoral European Fellowship (OceanLiNES; project ID 658035). EL was financially supported by the Helmholtz Research School for Ocean System Science and Technology (HOSST).

4. Regulation of the heme *b* pool in two cyanobacterial diazotrophs during iron limitation

Evangelia Louropoulou[1,2], Alexandra Marki[1], Martha Gledhill[1], Nancy Weiland-Bräuer[2], Julie LaRoche[3], Eric P. Achterberg[1], Ruth A. Schmitz[2]

in preparation for *Marine Ecology Progress Series*

[1] GEOMAR Helmholtz Centre for Ocean Research Kiel, Kiel, Germany
[2] Institute for General Microbiology, Christian-Albrechts-Universität, Kiel, Germany
[3] Department of Biology, Dalhousie University, Halifax, NS, Canada

Abstract. Heme *b* is the most versatile iron (Fe) containing co-factor of hemoproteins in marine phytoplankton participating in photosynthesis and respiration. Although it is established that heme *b* concentrations decrease in various phytoplankton species under low Fe (<0.50 nmol L^{-1}) conditions, the impact of Fe limitation on heme *b* production, utilization and degradation in marine diazotrophs is currently unknown. Here, we examined the abundance and cycling of heme *b* under varying dissolved Fe (DFe) treatments (1, 4 and 40 nmol L^{-1}) in *Cyanothece* and *Trichodesmium* in order to identify how Fe is utilized and potentially optimized during Fe limitation. The precursor of heme *b*, protoporphyrin IX (PTP-IX), exhibited a highest abundance during late (*Cyanothece*) and mid (*Trichodesmium*) exponential phases in Fe-replete cultures (40 nmol L^{-1} DFe), providing evidence that Fe limitation led to decreases in the production of heme *b*. Regarding heme *b* utilization patterns, the gene *petB* encoding the heme-*b* containing cytochrome b_6f was downregulated in *Cyanothece* and upregulated in *Trichodesmium* under low Fe (1 and 4 nmol L^{-1}) conditions. This finding implied that heme *b* and Fe utilization in the photosynthetic apparatus increased in *Trichodesmium* and decreased in *Cyanothece*. Indeed the photochemical efficiencies (F_v:F_m) of *Trichodesmium* were invariable across DFe treatments whereas the photochemical efficiencies of *Cyanothece* decreased in Fe depleted cultures. We showed that modifications in the gene expression of heme oxygenases (HOs) likely control intracellular heme *b* concentrations; hence, the transcripts of HOs (genes *hmox* for *Trichodesmium*, *hmo2* for *Cyanothece*) declined under low Fe suggesting that low Fe supply led to also to decreases in heme *b* metabolism in both species. However, a second HO in *Cyanothece* (gene *hmo1*) exhibited 1.9 to 161 fold higher transcripts in Fe-deplete compared to Fe-replete cultures. An increase in the heme *b* relative to particulate organic carbon (POC) accompanied the upregulation of *hmo1* suggesting that the activation of this HO was linked to Fe acquisition processes. This study demonstrated that both diazotrophs have the ability to regulate their hemoprotein pool under Fe limitation. The modification in the expression of genes encoding HOs appeared to be critical so that both diazotrophs conserve their intracellular heme *b* content and thus survive. Since, HO are responsible for heme breakdown via cleavage of the porphyrin ring and release of ferrous Fe, activation of HOs under Fe limitation may be linked on Fe acquisition mechanisms by prokaryotes either via internal Fe recycling or from external sources and simultaneous release of ferrous Fe. This study demonstrated some of the diverse strategies employed by diazotrophs for Fe conservation during Fe limitation and enhanced previous assumptions on bacterial Fe-acquisition processes.

Keywords. Heme *b*, iron, limitation, heme oxygenase, *Cyanothece*, *Trichodesmium*

4.1 Introduction

Iron (Fe) is an essential micronutrient for phytoplankton growth and functioning as it is a component of proteins undertaking fundamental metabolic activities (Geider and La Roche, 1994). Iron is bound in proteins either in Fe-sulfur clusters, Fe-oxygen-Fe clusters or in hemes (da Silva and Williams, 2001). Hemes are porphyrin structures which contain a centrally coordinated Fe atom and act as co-factors in hemoproteins (Chapman et al., 1997). Hemes are produced via a tetrapyrrole synthesis pathway from a precursor, protoporphyrin IX (Frankenberg et al., 2003). In phytoplankton, hemes undertake electron transfer during photosynthesis and respiration (Hogle et al., 2014) but other functions related to oxidative stress are also reported (Chapman et al., 1997). There are several heme structures within an organism, but heme *b* (Fe protoporphyrin IX) is considered the most versatile structure and is incorporated into a wide variety of proteins (Espinas et al., 2012). The degradation of hemes by heme oxygenase (HO) results in the production of biliverdin, a precursor of phycobilins and bilirubin (Frankenberg-Dinkel, 2004). Phycobilins function as chromophores of phycobiliproteins in cyanobacteria, rhodophytes and cryptophytes (Beale and Cornejo, 1991; Cornejo et al., 1998; Cornejo and Beale, 1997). Several isoforms of bacterial HOs have been identified (Frankenberg-Dinkel, 2004), and in some marine bacteria, HO is thought to participate in direct Fe acquisition from hemes (Hogle et al., 2016; Hopkinson et al., 2008; Roe et al., 2013; Wandersman and Delepelaire, 2004).

Marine cyanobacterial diazotrophs largely regulate the supply of biologically accessible (fixed) nitrogen to the ocean (Capone, 2001). Nitrogen is considered the primary limiting nutrient for phytoplankton in many ocean regions (Moore et al., 2013), thus marine nitrogen fixation regulates oceanic primary productivity and the gross capacity of the biological carbon pump to remove atmospheric carbon (Sohm et al., 2011; Zehr, 2011). There is evidence that, during geological time periods characterized by high nitrogen fixation rates, atmospheric concentrations of carbon dioxide (CO_2) declined (Falkowski, 1997), suggesting a link between nitrogen fixation and climate change (Zehr, 2011).

A key issue for marine cyanobacterial diazotrophs is the need for Fe, which arises from the number of Fe-containing biomolecules they possess, require and employ on a cellular level to perform fundamental biochemical processes (Kustka et al., 2003; Sohm et al., 2011). Nitrogenase is the enzyme responsible for catalyzing the reduction of dinitrogen (N_2) to ammonium (Falkowski, 1997). Nitrogenase is a protein complex and consists of two Fe-containing proteins; one dimeric protein where Fe is bound in an Fe-S cluster and a heterotetrameric protein where Fe is bound in an Fe-molybdenum (FeCo) (Howard and Rees, 1996). Hence each nitrogenase molecule requires a total of 30 atoms of Fe (Howard and Rees, 1996; Shi et al., 2007). In addition, the photosynthetic apparatus, which includes the photosystem II (PSII), photosystem I (PSI) and the cytochrome b_6f complex (Cyt b_6f), contains a total of 23-24 atoms of Fe per

monomer (Raven, 1988; Richier et al., 2012; Shi et al., 2007). Whilst all Fe in nitrogenase is present in complex Fe-S and FeMo (Fe-molybdenum) clusters, in the photosynthetic apparatus, photosynthetic proteins contain one heme *b* (i.e. 1 Fe atom) in cytochrome b_{559} (cyt b_{559}) and three heme *b* structures (i.e. 3 Fe atoms) in cyt b_6f (Hogle et al., 2014; Shi et al., 2007). Consequently, the Fe demand of diazotrophs is high, thus in the ocean Fe supply regulates the geographical abundance of cyanobacterial diazotrophs (Chappell et al., 2012; Luo et al., 2012; Moore et al., 2009; Moore and Doney, 2007; Snow et al., 2015b; Sohm et al., 2011).

In culture, studies documented decreases in growth, nitrogen fixation rates and primary productivity, and increase of Fe-stress proteins in several cyanobacterial diazotroph species (Berman-Frank et al., 2001a; Fu and Bell, 2003; Jacq et al., 2014; Kupper et al., 2008; Paczuska and Kosakowska, 2003; Richier et al., 2012; Saito et al., 2011; Shi et al., 2007; Snow et al., 2015a). However, there is evidence that cyanobacterial diazotrophs possess mechanisms to deal with low Fe supply by optimizing the use of available Fe under Fe limitation conditions (Berman-Frank et al., 2001a; Kupper et al., 2008; Saito et al., 2011). Modifications of the proteome (Richier et al., 2012), transcriptome (Pfreundt et al., 2014; Shi et al., 2007) and elemental composition (Berman-Frank et al., 2001a) are considered adaptation mechanisms of diazotrophs to Fe-limitation. For example, Fe-stress in *Trichodesmium* (Chappell and Webb, 2010; Shi et al., 2007) leads to upregulated expression of the genes encoding Fe-stress induced proteins (i.e. *isiA*, Webb et al., 2001), enhancement of the photosystem proteins (Chappell and Webb, 2010; Shi et al., 2007) and downregulation of genes encoding nitrogenase (Chappell and Webb, 2010; Shi et al., 2007). These mechanisms likely arise from the ability of *Trichodesmium* to grow in oligotrophic environments with fluctuating Fe supply. For unicellular cyanobacterial diazotrophs, diurnal oscillations in nitrogen fixation and carbon fixation, driven by the need to separate nitrogenase from oxygen, have also been shown to allow for Fe recycling (*Crocosphaera*) and regulation of the hemoprotein pool (Saito et al., 2011).

In this study, we examined whether Fe limitation has an effect on heme *b* production, utilization and breakdown processes in the two common marine diazotroph species *Cyanothece sp.* (ATCC 51142) and *Trichodesmium erythraeum* (IMS101), which grow in different environments. The unicellular *Cyanothece sp*. (strain ATCC 51142) typically grows in coastal habitats (Reddy et al., 1993). In contrast, the filamentous multicellular *Trichodesmium sp*. is highly abundant in tropical and sub-tropical oligotrophic regions (Capone et al., 2005) and significantly contributes to the global marine nitrogen fixation rates (Capone, 1997; Finzi-Hart et al., 2009; Karl et al., 2002). We compare the responses to Fe limitation of two species with potentially different Fe utilization efficiencies arising from their cell morphology and different nitrogen fixation strategies (Sunda, 2012).

We examine potential differences between the two diazotrophs in Fe utilization efficiencies and how the available Fe is allocated into heme production under varying Fe treatments. One of the heme *b* containing proteins in both *Cyanothece* and *Trichodesmium* is cytochrome b_6f (Snow et al., 2015a; Vu et al., 2012). Cytochrome b_6f complex has been shown in the past to be more sensitive to Fe availability than PSII (Behrenfeld et al., 1996; Fraser et al., 2013; Greene et al., 1992; Vassiliev et al., 1995), we therefore investigated regulation of cyt b_6 in parallel to determination of heme *b* abundance. Furthermore, we assumed that Fe-limitation triggers a regulation of the heme pool for Fe conservation on the transcriptional level by downregulating expression of genes encoding HOs. *Cyanothece* possesses two HOs (HO1, HO2) whilst *Trichodesmium* only possesses a single HO. To our knowledge, there is no detailed study regarding the impact of Fe limitation on abundance and cycling of heme *b* in prokaryotes. This is the first study to report on changes in the gene expression of HO under Fe limitation in marine cyanobacterial diazotrophs while linking heme *b* abundance to production, use and breakdown patterns.

4.2 Materials and methods

4.2.1 Experimental setup

The cyanobacteria *Trichodesmium erythraeum (IMS101)* and *Cyanothece sp.* (ATCC 51142) were grown in batch cultures at 25˚C with a 12 : 12 hours light:dark cycle at 110-140 μmol m^{-2} s^{-1} photons in the nitrogen-free YBCII media (Chen et al., 1996) at a final concentration of phosphate of 5 μmol L^{-1} and at three different nominally dissolved Fe (DFe) concentrations. The YBCII media was modified to contain recently identified important trace nutrients and increase metal buffering capacity (Ho, 2013; Shi et al., 2012). Deionized water (Milli-Q, Millipore®) was used to prepare the growth medium and reagents of Analytical Reagent grade (p.a. ACS grade) which were purchased either from Carl Roth or Sigma Aldrich. For the experiments, we set up three different DFe treatments by adding different concentrations of Fe-EDTA to the medium resulting in three different nominally final DFe concentrations; 1 nM, 4 nM and 40 nM. After the DFe additions, the medium was filter-sterilized (0.2 μm, Stericup, Nalgene) prior to inoculation. The cultures of both species were maintained in an exponential growth phase and acclimated for at least five generations before the setup and start of our experiments.

Culture aliquots from both species and all three DFe treatments were inoculated to achieve a final volume of 1.9 L, and a filament-density of approximately 80 filaments mL^{-1} *Trichodesmium* and about 20,000 cells mL^{-1} for *Cyanothece*, resulting in three independent biological replicates per DFe treatment per species. We defined the day of inoculation as day-0 and monitored the cultures for 14 days for *Trichodesmium* and 11 days for *Cyanothece*, with the endpoint corresponding to the stationary phase.

Growth parameters (i.e. cell and filament counts and variable fluorescence/photosynthetic parameters) were monitored over the course of the experiment. We collected samples from both species during the early exponential phase, the mid exponential phase (*Trichodesmium*) and the late exponential phase (*Cyanothece*) in order to monitor the expression patterns of genes encoding nitrogenase, cytochrome b_6f, HO as well as abundance of heme *b* and heme-associated pigments. In addition, the background parameters particulate organic carbon (POC), particulate organic nitrogen (PON) and chlorophyll *a* (chl *a*) were also monitored on these sampling points (early and mid/late exponential phases). Finally, the content in particulate organic phosphorus (POP) and Fe was determined during the mid and late exponential phase for *Trichodesmium* and *Cyanothece* respectively.

4.2.2 Growth parameters

The growth of *Cyanothece sp.* cultures was monitored by counting cell numbers daily over the course of the experiment using a CellLab Quanta MPL (Beckman Coulter). For *Trichodesmium sp.* cultures, filament counts were performed every other day using an epifluorescence microscope (Zeiss, Axio vision) after vacuum-filtration of 50 mL culture on 0.2 μm track-etch filters (25 mm diameter, Nuclepore) and staining with fluorescent 4′,6-diamidino-2-phenylindole (DAPI).

The variable fluorescence and photosynthetic parameters for both species were determined using Fast Repetition Rate Fluorometry (FRRF) starting on Day 0 (initiation of the experiment) at approximately two hours after the start of the light cycle. All samples were dark acclimated for 30 min prior to in vivo fluorescence analysis with a FastOcean Fast Repetition Rate fluorometer (Chelsea Technologies Group). Fluorescence transients were fit automatically using FastPro8 software, which employs the model of Kolber et al., 1998, to determine minimal (F_0) and maximal (F_m) fluorescence values. The apparent photosynthetic efficiency of PSII was calculated using the formula $F_v{:}F_m = (F_m - F_0)/ F_m$. Fluorescence of sterile YBCII media was used as blank, and subtracted from F_0 and F_m prior to calculations of $F_v{:}F_m$.

The growth rates (μ, d^{-1}) were calculated for both species by performing linear regression analyses on the natural logarithm (ln) of F_0 (Sunda et al., 2005) versus time for the three independent biological replicates of each DFe treatment.

4.2.3 Particulate organic carbon, nitrogen and chlorophyll *a*

For POC and PON analysis, cells were collected by vacuum-filtration onto pre-combusted (450˚C, 6 h) glass fiber filters (25 mm, 0.7 μm, VWR) and stored frozen at -20˚C. Samples were dried (45˚C, 24 hours), prior to pelleting in tin cups. Samples and several blank filters were analyzed with an elemental analyzer (Euro Elemental Analyser) using acetanilide as calibration standard (Verardo et al., 1990).

We determined the chl *a* content of the cultures via fluorometry (Welschmeyer, 1994). A volume 20 mL of each culture replicate was filtered onto glass fiber filters (25 mm, 0.7 µm, VWR) and extracted with 6 mL 90% acetone at -20˚C for at least 24 h. Samples were brought to room temperature in the dark prior to determination of fluorescence at wavelengths 430 nm (excitation)/ 670 nm (emission) (Cary Eclipse) and corrected for phaeopigments.

4.2.4 Elemental stoichiometry

For the determination of the elemental stoichiometry, we filtered 150 mL from each culture replicate onto acid washed (0.1 M HCl) 25 mm, 0.22 µm polyethersulfone (PES) membrane filters. Filters were stored in -80°C prior to analysis. We performed a digestion of the filters in acid-cleaned perfluoralkoxy (PFA) vials (Nalgene) overnight on a hot plate at 110°C using 2 mL concentrated nitric acid (HNO_3) (Honey et al., 2013). After evaporation of the HNO_3, the residual material was redissolved in 0.3 M HNO_3.

We analyzed the samples for phosphorus (P) and Fe by inductively coupled plasma – mass spectrometry (ICP-MS) (X-series, Thermo Scientific) using an external calibration. Indium (1 µg L^{-1}) was used to correct for instrument drift. Filter blanks, determined by following the above procedure on acid washed filters were subtracted from concentrations determined by ICP-MS.

We calculated carbon specific Fe use efficiencies (IUE) on day 8 (late exponential phase) using the formula (1) (Kustka et al., 2002; Strzepek et al., 2011) and derived from the theoretical Fe use efficiency suggested by Raven, 1988. IUE is defined as the number of moles of carbon assimilated per mole of trace metal per second (mol Fe (mol C)$^{-1}$ s^{-1}), according to the formula

$$\mathrm{IUE} = \mu * \left(\frac{\mathrm{Fe}}{\mathrm{POC}}\right)^{-1} \quad (1)$$

where µ denotes the growth rate (s^{-1}) and POC represents the POC pool.

4.2.5 Nitrogen fixation rates

We conducted 24 h incubations during the early exponential phase (Day 3 to Day 4) and mid/late exponential phase (Day 7 to Day 8) in order to determine the nitrogen fixation rates for *Trichodesmium* and *Cyanothece spp.* for different DFe treatments and growth phases. Following the method of direct addition of $^{15}N_2$ tracer-enriched seawater (Mohr et al., 2010), 5 mL of $^{15}N_2$ were injected and dissolved into 1 L previously degassed (Membrana Mini Module G543) YBCII medium (Mohr et al., 2010). Prior to the incubations, 125 mL were transferred from each biological replicate of the main culture into sterilized and acid-washed (10% HCl) polycarbonate bottles (Nalgene, Thermo Scientific). Then, 3 mL of the $^{15}N_2$ – enriched YBCII was added to each bottle; the bottles were sealed using septum closures (MPS-159-010V, Fisher Scientific) and placed into the culture cabinet for further incubation in parallel with the other culture

bottles. After 24 h, 125 mL were vacuum - filtered from each bottle onto pre-combusted (450˚C, 6 h) glass fiber filters (25 mm, 0.7 μm, VWR). The PON concentration and the isotopic composition of the samples were measured along with several blanks using the elemental analyzer coupled to an isotope ratio mass spectrometer (Thermo Delta Plus). Finally, isotopic composition of the N_2 enriched water was also determined (Isotope Ratio Mass Spec – IRMS). Finally, nitrogen fixation rates were calculated according to (Montoya et al., 1996).

4.2.6 Heme *b* and pigments

At every sampling point, cells were collected from each culture replicate onto glass fiber filters by gentle vacuum filtration (pore size 0.7 μm, MF300, Fisherbrand™). The filters were stored at -80^{o}C prior to analysis. Heme *b* was extracted from the filters using 2.5% w:v Octyl β-D-glucopyranoside-OGP solution (Sigma-Aldrich®, ≥98% GC Grade) and quantified by separation of pigments via High Performance Liquid Chromatography (PLRP-S column 2.1 x 100 mm, 300 Å, 3 μm, Agilent Technologies) and detection by high resolution (70,000 at m/z=200) Electrospray Ionization Q Exactive™ Mass Spectrometer (ThermoFisher) following a protocol of Gledhill (2007, 2014) with slight modifications described in Louropoulou et al., submitted.

Quantification of heme *b* was performed from MS data on the exact mass of the M^+ ion (m/z = 616.177). The analytical detection limit was calculated as three times the standard deviation of the lowest calibration standard. For 25 μL injection volume, the detection limit was 0.03 nmol heme *b* L^{-1}. Heme *b* could not be detected in the blank extraction solution.

Alongside heme *b*, we also monitored the relative abundance of protoporphyrin IX (PTP-IX). PTP-IX (retention time = 8.90 min) was detected by monitoring $[M+H]^+$ ions (m/z = 563.265). The peak areas for PTP-IX were normalized to filtration volume of each sample.

4.2.7 RNA sampling, extraction, purification and cDNA synthesis

For both *Cyanothece* and *Trichodesmium*, 150 mL of each biological replicate was filtered onto 0.22 μm Polyethersulfone (PES) membrane filters using a 25 mm vacuum filtration manifold (Millipore®) at a maximum pressure of 200 mbar. All filters were flash-frozen in liquid nitrogen and stored into -80°C prior to analysis.

RNA was isolated from the filters after addition of 2 mL of a phenol-guanidine-triton-hydroxyquinoline (PGTX) solution (Pinto et al., 2009), incubation at 65°C for 15 min, followed by a phase extraction procedure described by (Pfreundt et al., 2012). In the final stage, a RNA pellet was air-dried and resuspended in 35 μL of sterilized, RNase- and DNase- free and diethyl pyrocarbonate (DEPC) -treated water (Roth, Karlsruhe, Germany). The quantity of RNA was determined by a Nanodrop ND-2000 instrument (PEQLAB Biotechnologie GmbH, Erlangen, Germany).

In order to eliminate genomic DNA contamination, RNA was purified using a TURBO DNA-free™ Kit (Ambion®) following the manufacturer's protocol for rigorous treatment. To check the purity of the RNA after the DNase treatment, we carried out PCR using a GoTaq® DNA Polymerase (Promega) for amplification of the hypervariable V1-V2 region of the 16 S rRNA gene (95°C for 3 min, 30 cycles of 95°C for 30 sec, 50°C for 30 sec and 72°C for 30 sec, followed by 72°C for 10 min). We checked all reactions in 2% agarose gel and confirmed the absence of DNA. The quantity of the purified RNA was also determined using the Nanodrop ND-2000 instrument.

cDNA was generated for both species (3 biological replicates per Fe treatment per species) using a First Strand cDNA synthesis kit (K1612 Thermo Fisher) following a procedure suggested by the manufacturer for specific primers. We designed the primer sets for the key genes *hmox* and *petB* for *Trichodesmium* and *nifH*, *hmo1*, *hmo2* and *petB* for *Cyanothece* while we also used previously published primer sequences for *nifH* (*Trichodesmium*, Langlois et al., 2008), *rnpB* (*Trichodesmium,* Chappell and Webb, 2010) and *16S rRNA* (*Cyanothece,* Gaudana et al., 2013). The primer sets used for the cDNA synthesis are displayed in Table 4.1. All cDNA samples were purified after synthesis using the NucleoSpin Gel and PCR Clean-up kit (Macherey-Nagel, Düren, Germany) and the cDNA concentration was measured using a Nanodrop ND-2000 instrument.

4.2.8 Quantitative Real-Time Polymerase Chain Reaction

Gene expression was determined by real time quantitative polymerase chain reaction (QRT-PCR) using the previously constructed cDNA samples as templates and a Platinum® SYBR® Green qPCR SuperMix-UDG with ROX kit. All reactions were performed in 12 μL final volume in a mixture without Mg^{2+} addition as described by the manufacturer. Each biological replicate (i.e. three biological replicates for each DFe treatment for each species) was analyzed in three independent technical replicates for each gene on a ViiA™ 7 Real-Time PCR System (LifeSciences) along with several negative controls. The primers used for the amplifications of the genes under investigation are shown in Table 4.1. The *hmo2* of *Cyanhothece* and *hmox* of *Trichodesmium* are homologous whilst there was no similarity between *hmo1* (*Cyanothece*) and *hmox* (*Trichodesmium*) (BLAST, NCBI database (https://blast.ncbi.nlm.nih.gov/Blast.cgi)). Regarding reference genes used in this study, our preliminary tests confirmed that the expression of the *rnpB* gene is relatively stable for *Trichodesmium sp.* under various DFe conditions (data not shown) as observed previously (Chappell et al., 2012; Chappell and Webb, 2010; Shi et al., 2007) which was then used as reference gene for *Trichodesmium*. On the contrary, for *Cyanothece sp.*, we observed a large variably in the expression of the *rnpB* gene (data not shown), we thus chose to use the *16S rRNA* (Krishnakumar et al., 2013) as the reference gene for further calculations.

All genes and technical replicates for each biological replicate were run on the same plate. For *Trichodesmium sp.* a concentration of 30 ng cDNA in the final reaction for *nifH, hmox, petB* and *rnpB* was used and running conditions were 50°C for 2 min, 95°C for 10 min followed by 40 cycles of 95°C for 15 sec, 60°C for 30 sec and 72°C for 30 sec, and finally, a dissociation step of 95°C for 15 sec, 55°C for 30 sec and 95°C for 15 sec. For *Cyanothece sp.* a concentration of 5% DMSO and of 20 ng cDNA were added to the final reaction for *nifH, hmo1, hmo2, petB* and *16S rRNA* and the running conditions were 50°C for 2 min, 95°C for 10 min followed by 40 cycles of 95°C for 30 sec and 60°C for 1 min, and finally, a dissociation step of 95°C for 15 sec, 55°C for 30 sec and 95°C for 15 sec.

Table 4.1: Description and sequences of forward and reverse primers for our target genes.

Species/ Gene	Description	Forward Primer (5'-3')	Reverse Primer (5'-3')	Reference
Cyanothece				
nifH	Iron-containing subunit of nitrogenase	CAAGCGAGAATCAACTATGC	GAATCAGCTTTAGGGTCACA	This study
petB	Subunit b6 of Cytochrome b6f complex	GCGGAATTACCTTAGTTTGC	ATAGAACGGATCAACCAACC	This study
hmo1	Heme Oxygenase	CTGAGTTATTAGCAGCCCAT	GCTTTTTCATCGGAAATGGT	This study
hmo2	Heme Oxygenase	ATGTTAAAGAAGCCATCGGT	ATTCGGCAATAGCTACACTG	This study
16S rRNA		CCCTGGGCTACACACGTACT	TCTCGAGTTGCAGAGAGCAA	(Gaudana et al., 2013)
Trichodesmium				
nifH	Iron-containing subunit of nitrogenase	TGGCCGTGGTATTATTACTG	GCTTTGTTTTCACGGATAGG	(Langlois et al., 2008)
petB	Subunit b6 of Cytochrome b6f complex	CTGCAATAAACCAGGGTAGT	TGCAATTCCATTTGTTGGTC	This study
hmo	Heme Oxygenase	GTGCGCTTTCTTGTTAAAGT	GAATAACTATCGTCAGGCCA	This study
rnpB	Subunit of RNA polymerase	ACCAACCATTGTTCCTTCG	CAAGCCTGCTGGATAACG	(Chappell and Webb, 2010)

The relative change in gene expression was calculated using the method of Livak and Schmittgen (2001) based on the Ct values from a minimum of five technical replicates among three biological replicates. As endogenous control, the Ct values of the genes of interest (*nifH, hmox, hmo1, hmo2, petB*) were first normalized to the corresponding Ct values of the *rnpB* gene for *Trichodesmium sp.* and the *16S rRNA* for *Cyanothece sp*. resulting into the ΔCt values. To examine changes in gene expression due to DFe treatment and growth phase, we used the ΔCt values of the 40 nM DFe treatment on the early exponential phase (Day 4) to calculate the ΔΔCt values for each gene.

4.2.9 Data processing

Mass spectrometry data were processed using the Xcalibur software (v. 3.0.63, Thermo Scientific). The RT-PCR data were processed QuantStudio (v.1.3 Applied Biosystems,

Thermo Fisher Scientific). General data processing, statistical analysis and visualization were carried out using R Statistical Software (R Core Team, 2016). Mean values of biogeochemical parameters (i.e. cell/filament numbers, POC, PON, heme *b*, chl *a*) were calculated from three individual biological replicates per Fe treatment for each of the species, unless stated otherwise.

4.3 Results and discussion

4.3.1 Declines in growth rates during Fe limitation

Cell and filament numbers increased in *Cyanothece* and *Trichodesmium* cultures over the course of the experiment (Fig. 4.1A,B) and for both species maximum numbers of cells and filaments were determined in the highest DFe treatments (i.e. 40 nM). In *Cyanothece* the impact of Fe limitation on cell numbers (Fig. 4.1A) was evident two days after the start of the experiment. In contrast, differences in filament numbers in *Trichodesmium* between Fe-deplete and Fe-replete cultures became apparent after eight days into the experiment. We observed similar trends in minimum fluorescence F_0 (Fig. 4.1C, D), which is also indicative of biomass (Falkowski and Kiefer, 1985; Falkowski and Kolber, 1995), meaning that F_0 increased with DFe supply in *Cyanothece* already from the early exponential phase whilst differences in F_0 according to DFe of *Trichodesmium* were observed after the mid exponential phase (Fig. 4.1C,D).

Sampling for biochemical measurements was performed on day 4 and 8 for both species. Hence for data interpretation, we refer to the day 4 as early exponential for both species whereas day 8 corresponds to late exponential for *Cyanothece* and mid exponential for *Trichodesmium*.

For *Cyanothece sp*., growth rates ranged from 0.115 d^{-1} to 0.526 d^{-1} and for *Trichodesmium sp*. from 0.198 d^{-1} to 0.558 d^{-1} (Fig. 4.2, Table 4.2). The lowest growth rates were observed for both species in the 1nM DFe treatment. Growth rates increased with increasing DFe (Fig. 4.2). Hence, the differences between growth rates in relation to DFe concentrations were statistically significant for both *Cyanothece* ($F_{(2,6)} = 336$, $p< 0.01$) and *Trichodesmium* ($F_{(2,6)} = 12.6$, $p<0.01$). Furthermore, the growth rates of both species were similar to previously reported values in relation to DFe availability (Berman-Frank et al., 2001a, 2007).

4.3.2 Different Fe use efficiencies of *Cyanothece* and *Trichodesmium* influence nitrogen fixation rates

The mean (± SD) concentrations POC and PON for both species and all DFe treatments are presented on Table 4.2. Similarly to F_0, both POC and PON increased gradually over the course of the experiment and differences in both POC and PON were evident since the early exponential phase in *Cyanothece* and mid exponential phase for *Trichodesmium*. The analysis of variance of POC and PON according to DFe

concentration showed statistically significant differences only for *Cyanothece* (POC: $F_{(2,15)} = 6.8$, $p<0.01$; PON: $F_{(2,15)} = 8.9$, $p<0.01$).

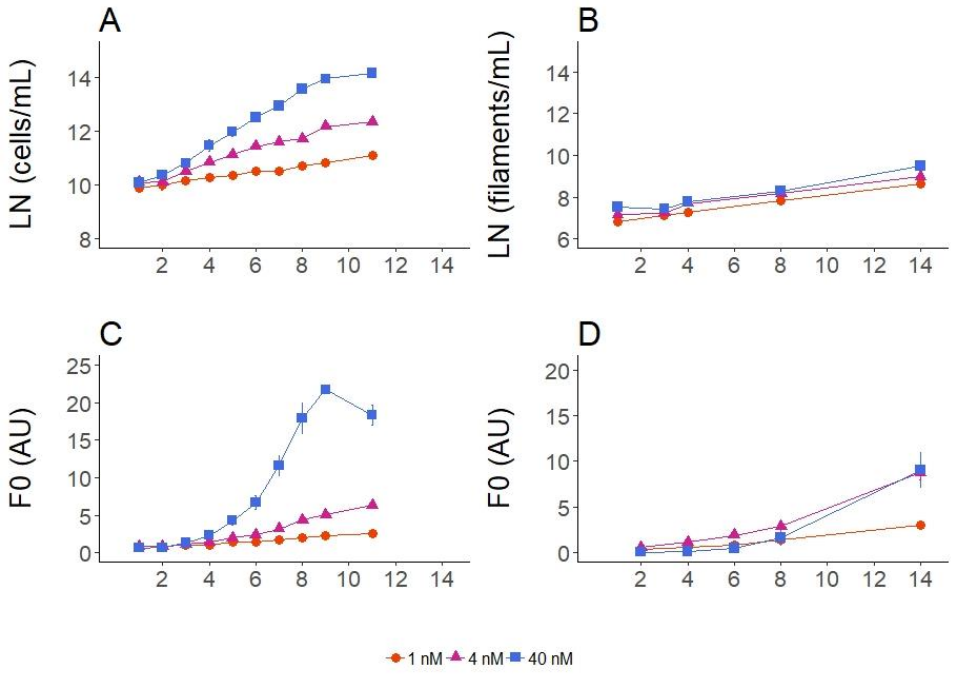

Fig. 4.1: Growth parameters of *Cyanothece* and *Trichodesmium* cultures monitored over the course of the experiment (Day 1 to 14, x axis). Subplots A and B depict the cell numbers for *Cyanothece* and the filament numbers for *Trichodesmium*, respectively. Subplots C and D depict the minimal fluorescence (F0) in arbitrary units (AU) as measured using Fast Repetition Rate Fluorometry (FRRF) for *Cyanothece* and *Trichodesmium* respectively. Dots represent the mean values of three individual biological replicates per DFe treatment and whiskers represent the standard deviation (± SD). Colors indicate the concentration of DFe in the culture media.

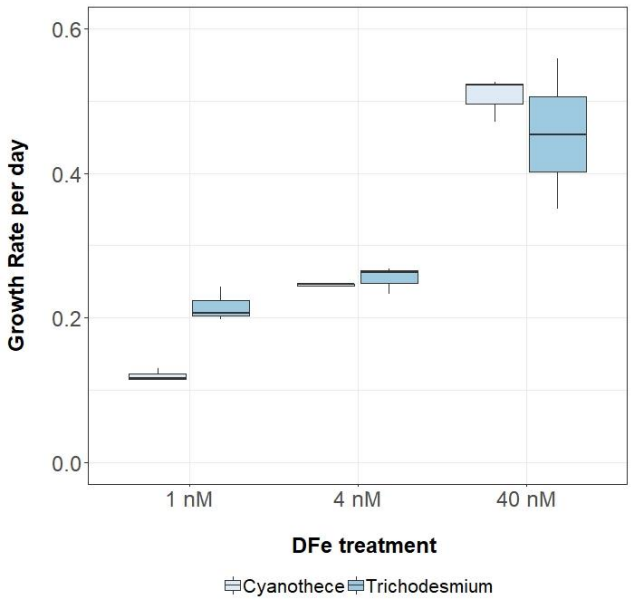

Fig. 4.2: Growth rates (μ, day-1) for *Cyanothece* and *Trichodesmium* under three dissolved iron (DFe) treatments (1, 4 and 4 nM DFe) calculated using linear regression analyses on the natural logarithm (ln) of F0 (Sunda et al., 2005) versus time. Values represent three independent biological replicates per DFe treatment for both species.

Carbon-to-nitrogen ratios (POC:PON) were similar amongst the three DFe treatments were determined in the mid exponential phase for *Trichodesmium* (Fig. 4.3A) with values around 6.0 mol mol^{-1}. In contrast, the POC:PON of *Cyanothece* in the late exponential phase was approximately 2- and 3-fold higher (~18 mol mol^{-1}) in the 1 nM Fe treatment compared to the POC:PON of the 4 nM and 40 nM DFe treatment (Fig. 4.3A). The differences were statistically significant according to the analysis of variance for *Cyanothece*, ($F_{(2,6)} = 1157$, $p<0.01$).

Particulate Fe (PFe) yields demonstrated that both *Cyanothece* and *Trichodesmium* assimilated virtually all supplied Fe in the 1 and 4 nM Fe treatments in the late and mid exponential phase (Table 4.2). *Cyanothece* assimilated nearly 70 % of nominal DFe in the 40 nM treatment but exhausted all available phosphorus (i.e. 50 µmol L^{-1} nominal concentrations). The Fe-replete *Trichodesmium* assimilated only ~ 20 % of available Fe and ~22% of the available phosphorus which further supports that these cultures were still in the exponential phase. Furthermore, normalization of Fe to carbon intracellular quotas (Fe:POC) (Fig. 4.3B) demonstrated relatively constant values for *Cyanothece* among the DFe treatments, but a pronounced increase with DFe supply for *Trichodesmium*. The differences among the DFe treatments were statistically significant only in *Trichodesmium* cultures (ANOVA, $F_{(2,5)} = 16.1$, DF=2, $p<0.01$).

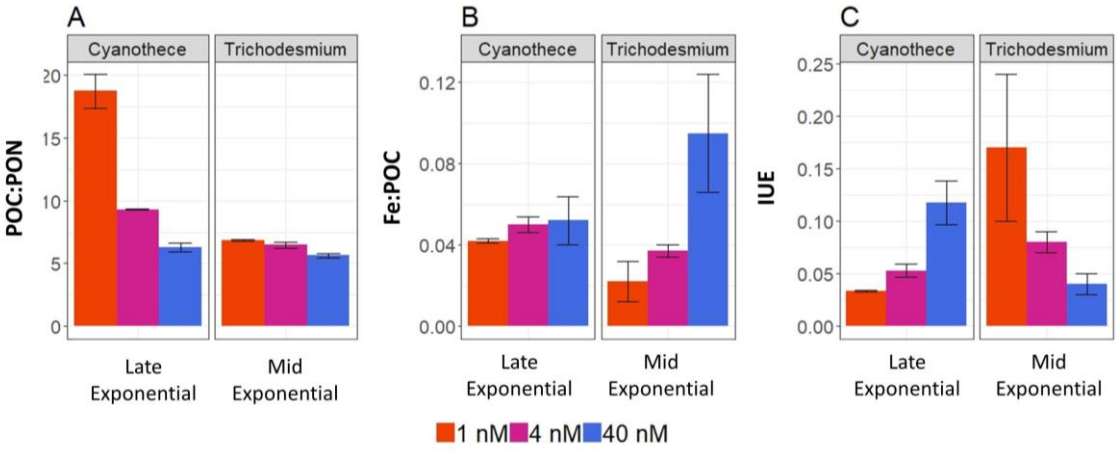

Fig. 4.3: Elemental ratios of *Cyanothece* and *Trichodesmium* during the late and mid exponential phase respectively. Bars indicate the mean values (± SD) calculated from three independent biological replicates per iron treatment of A) particulate organic carbon to nitrogen (POC:PON) in mol mol^{-1}, B) particulate iron to particulate organic carbon (PFe:POC) in mmol mol^{-1}, and of the C) iron use efficiencies (IUE) in mol Fe (mol C)$^{-1}$ s^{-1}. Colors indicate the three DFe treatments (1, 4 and 40 nM).

The relatively constant ratios of Fe:POC among the DFe treatments of *Cyanothece* suggested that this species was not able to adapt to low Fe supply. This trend is further supported by the values of the Fe use efficiencies (IUE), which indicate the units carbon produced per unit Fe per unit time, thus representing growth. Values of IUE of *Cyanothece* increased with Fe supply (Fig. 4.3C). Hence, the reduced IUE of *Cyanothece* in the 1nM and 4nM cutlures resulted in declines in nitrogen (PON) production and thus increased POC:PON ratios compared to the 40 nM DFe treatment.

Table 4.2: Basic biochemical measurements growth rate, variable fluorescence and photosynthetic parameters (Fv:Fm), particulate organic carbon (POC), particulate organic nitrogen (PON), chlorophyll *a* (chl *a*), heme *b* and nitrogen fixation rates over the course of the experiment for *Cyanothece* and *Trichodesmium*. The numbers correspond to the average value ± SD of each parameter for three biological replicates per dissolved iron (DFe) treatment

	DFe (nM)	Growth Rate (day^{-1})	Fv:Fm	POC ($\mu mol\ L^{-1}$)	PON ($\mu mol\ L^{-1}$)	P ($\mu mol\ L^{-1}$)	Fe ($nmol\ L^{-1}$)	Chl *a* ($nmol\ L^{-1}$)	Heme *b* ($pmol\ L^{-1}$)	N_2 Fixation Rates ($nmol\ N\ L^{-1}\ day^{-1}$)
Cyanothece										
Early Exp.	1		0.254 ± 0.006	23.2 ± 1.4	3.5 ± 0.67			0.50 ± 0.26	2.7 ± 0.0	2.2 ± 0.39
	4		0.389 ± 0.004	32.3 ± 3.8	5.3 ± 0.55			1.0 ± 0.16	2.6 ± 0.0	11.9 ± 0.89
	40		0.422 ± 0.035	80.5 ± 14.3	14.9 ± 2.0			7.0 ± 0.62	21.1 ± 2.5	60.1 ± 10.9
Late Exp.	1	0.116 ± 0.007	0.238 ± 0.016	35.1 ± 0.8	1.9 ± 0.12	0.33 ± 0.03	1.5 ± 0.01	1.4 ± 0.57	6.6 ± 1.4	4.6 ± 0.38
	4	0.248 ± 0.002	0.382 ± 0.006	84.0 ± 2.4	9.0 ± 0.23	0.88 ± 0.07	4.2 ± 0.18	10.3 ± 2.3	17.4 ± 1.4	25.8 ± 1.1
	40	0.471 ± 0.025	0.398 ± 0.015	472 ± 41.6	74.7 ± 2.9	5.33 ± 1.24	28.1 ± 5.6	36.7 ± 2.7	12.0 ± 0.0	254 ± 37.4
Trichodesmium										
Early Exp.	1		0.259 ± 0.006	35.0 ± 1.6	4.3 ± 0.33			1.8 ± 0.12	<0.6	6.0 ± 1.7
	4		0.277 ± 0.004	60.1 ± 10.4	10.0 ± 1.4			3.0 ± 0.54	<0.6	23.1 ± 2.1
	40		0.244 ± 0.021	21.8 ± 7.1	5.5 ± 0.60			1.2 ± 0.70	<0.6	10.7 ± 6.8
Late Exp.	1	0.216 ± 0.019	0.262 ± 0.007	53.7 ± 2.4	7.8 ± 0.2	0.36 ± 0.04	1.2 ± 0.61	4.2 ± 0.85	<0.6	17.4 ± 3.6
	4	0.254 ± 0.015	0.294 ± 0.002	117 ± 7.2	18.1 ± 0.5	1.16 ± 0.03	4.3 ± 0.45	11.4 ± 2.5	<0.6	58.3 ± 2.4
	40	0.454 ± 0.085	0.274 ± 0.021	90.1 ± 37.7	19.0 ± 6.8	1.12 ± 0.02	7.4 ± 0.42	23.9 ± 10.9	<0.6	75.6 ± 32.1

In contrast, *Trichodesmium*, as shown previously, optimized Fe use under low Fe conditions (Berman-Frank et al., 2001a; Kustka et al., 2003) since the IUE decreased with increasing Fe supply. Therefore, *Trichodesmium* maintained a constant nitrogen production as indicated by the POC:PON values which were close to the canonical Redfield ratio of 6.6 (Redfield, 1958) (Fig. 4.3C).

The different IUEs suggested that the two species potentially localized the available Fe into different Fe-proteins during Fe limitation which would include localization of Fe into heme or non-heme cofactors (Chappell and Webb, 2010; Saito et al., 2011; Shi et al., 2007). In general, strategies of Fe-localization during Fe limitation could potentially be linked to restricted production of active nitrogenase enzymes for N_2 fixation (i.e. non-heme Fe) and thus reduction of the nitrogen fixation rates and/or restriction of the photosynthetic units produced (heme Fe) and thereby overall photosynthesis rates (Berman-Frank et al., 2001a, 2007). Here, we examined further Fe localization into non-heme cofactors by investigating the expression patterns of the *nifH* gene and by measuring the nitrogen fixation rates.

Table 4.3: Average fold changes ± error (method, $2^{-\Delta\Delta Ct}$, Livak and Schmittgen, 2001) in gene expression of *nifH, petB* and heme oxygenases (*hmox, hmo1, hmo2*) for *Cyanothece* and *Trichodesmium* in the early and late exponential phase. The Ct values for Cyanothece were normalized to the expression of the 16S rRNA (Gaudana et al., 2013)whereas Ct values for Trichodesmium were normalized to rnpB (Chappell and Webb, 2010; Shi et al., 2007). For each gene, the ΔΔCt and $2^{-\Delta\Delta Ct}$ values derive from species - individual calibration of the ΔCt values with the corresponding 40 nM DFe treatment of the early exponential phase.

Species/ Growth Phase	DFe (nM)	*nifH*	*petB*	*hmox*	*hmo1*	*hmo2*
Cyanothece						
Early	1	-10.1 ± 3.6	-37.6 ± 28.6		20.0 ± 11.1	-17.7 ± 8.6
Exponential	4	-10.1 ± 4.2	-23.5 ± 7.9		161 ± 46.9	-12.8 ± 2.7
	40	1.0	1.0		1.0	1.0
Late	1	-101 ± 35.4	-1871 ± 567		1.9 ± 0.68	-2113 ± 792
Exponential	4	-1.6 ± 0.38	-7.1 ± 2.9		53.1 ± 14.8	-395 ± 90.9
	40	-1.1 ± 1.3	1.3 ± 1.4		-19.4 ± 4.6	-9.5 ± 6.1
Trichodesmium						
Early	1	-2.0 ± 0.74	1.9 ± 0.72	-1.9 ± 0.62		
Exponential	4	-1.4 ± 0.34	2.4 ± 0.60	-2.3 ± 0.60		
	40	1.0	1.0	1.0		
Late	1	-2.5 ± 0.39	12.9 ± 2.0	-2.7 ± 0.12		
Exponential	4	-3.2 ± 0.77	9.6 ± 3.5	-1.1 ± 1.1		
	40	1.8 ± 0.22	22.1 ± 9.3	1.6 ± 0.36		

For both *Cyanothece* and *Trichodesmium*, the *nifH* gene was downregulated in the 1 nM and 4 nM DFe treatments, compared to the 40nM treatment (Table 4.3, Fig. 4.4A) over the course of the experiment. In *Cyanothece*, the downregulation was in general more pronounced in the 1 nM DFe treatment and the fold change of *nifH* between the low Fe treatments (1 nM and 4 nM) was comparable in the early exponential phase. However,

during the late exponential phase, *nifH* was further downregulated in *Cyanothece* 1 nM cultures (Table 4.3), in contrast to the 4nM treatment, where transcripts of *nifH* increased, suggesting a recovery trend of the 4 nM cultures (Fig. 4.4A). Fold changes of *nifH* for *Trichodesmium* ranged within the same order of magnitude among DFe treatments. The fold change in *nifH* expression for *Trichodesmium* was comparable to the values reported by Shi et al., 2007 whilst, to our knowledge, there are no published data regarding fold changes in *nifH* for *Cyanothece* under Fe limitation.

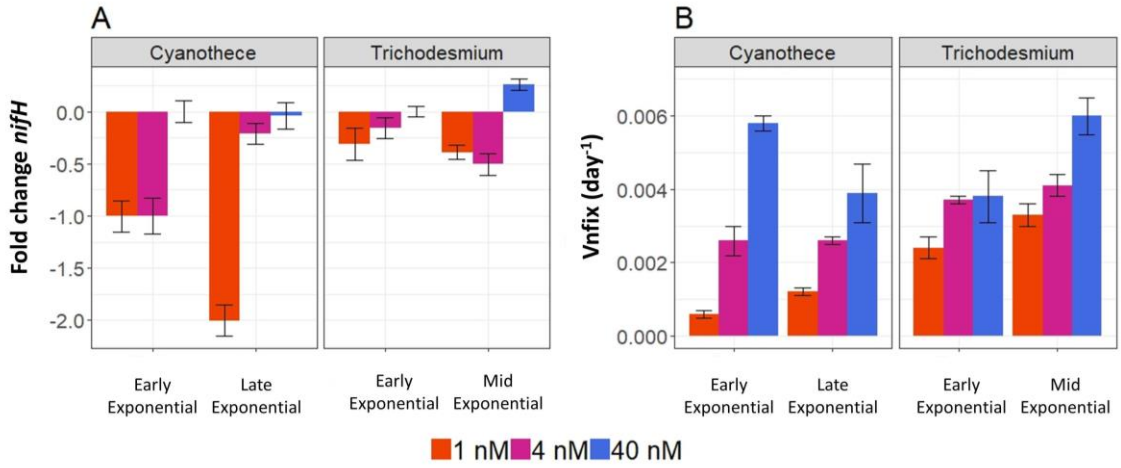

Fig. 4.4: Nitrogen fixation associated measurements during the early and the mid/late exponential phase for *Cyanothece* and *Trichodesmium*. Bars represent mean values calculated from three independent biological replicates per DFe treatment for both species. Colors indicate the three DFe treatments (1, 4 and 40 nM). A) Mean fold change in *nifH* gene expression using the relative comparison method $2^{-\Delta\Delta Ct}$ (Livak and Schmittgen, 2001). The Ct values for *Cyanothece* were normalized to the expression of the *16S rRNA* (Gaudana et al., 2013) whereas Ct values for *Trichodesmium* were normalized to *rnpB* (Chappell and Webb, 2010; Shi et al., 2007). The fold change derives after a species - individual calibration of the ΔCt values with the corresponding 40 nM DFe treatment of the early exponential phase. Note that for comparison reasons between the two species, the fold changes are presented in log scale in this graph. B) Mean values (± SD) of nitrogen-specific growth rate via nitrogen fixation (Vnfix).

Although we did not quantify the abundance of nitrogenase, we observed that the downregulation of *nifH* was associated with declines in nitrogen fixation rates (Table 4.2) for both species with low Fe supply. For *Cyanothece*, the nitrogen fixation rates ranged from 1.70 to 301 nmol N L^{-1} day^{-1} (n=18) and for *Trichodesmium* from 4.25 to 117 nmol N L^{-1} day^{-1} (n=18). The lowest nitrogen fixation rates were determined for both species in the 1 nM DFe treatment and the highest in the 40 nM DFe treatment. Increases in nitrogen fixation rates with increasing DFe supply were observed for *Trichodesmium* also by Berman-Frank et al. (2001), however a comparison of the absolute nitrogen fixation rates determined in our study is not possible since different methods were used for the rate quantification (Berman-Frank et al., 2001a). In addition, we calculated the nitrogen-specific growth rate via nitrogen fixation (V_{nfix}, day^{-1}), which standardizes the rate of nitrogen fixation against the quantity of PON and negates the effect of varying biomass. The V_{nfix} ranged from 0.0005 to 0.006 (day^{-1}) for *Cyanothece* and 0.002 to 0.006 (day^{-1}) for *Trichodesmium*. Values of the V_{nfix} increased with increasing Fe supply.

In general, both the nitrogen fixation rates and the V_{nfix} were higher in the mid/late exponential phase compared to the early exponential phase for both species, except for the 40 nM *Cyanothece* culture (Fig. 4.4B), which was likely to have already entered the stationary phase, since the phosphate concentrations was exhausted. Furthermore, the analysis of variance showed statistically significant differences in V_{nfix} with varying DFe concentrations in both *Cyanothece* ($F_{(2,15)}$ = 41.42, p<0.01) and *Trichodesmium* ($F_{(2,15)}$ = 8.1, p<0.01) attributed mainly to the differences between the 1 nM and the 40 nM treatments.

Our findings suggested that the activity of nitrogenase was restricted during Fe limitation in both species and agreed with previous studies that have documented decreases in *nifH* expression, nitrogenase abundance and nitrogen fixation rates with low Fe supply on the transcriptomic and protein level for *Trichodesmium* (Berman-Frank et al., 2001a; Chappell and Webb, 2010; Richier et al., 2012; Shi et al., 2007; Snow et al., 2015a) and other unicellular diazotroph species (Jacq et al., 2014; Saito et al., 2011).

Reduced Fe supply is also known to influence photosynthesis rates although some studies documented that *Trichodesmium* conserves photosynthesis at low Fe (Chappell and Webb, 2010; Richier et al., 2012; Shi et al., 2007; Snow et al., 2015a). Since heme *b* is a cofactor in two photosynthetic proteins (cytochrome b_{559} in PSII and cytochrome b_6 in cyt b_6f), modifications in the photosynthetic apparatus could potentially be linked to changes in the heme *b* pool, whereas restriction of the nitrogen fixation activity is linked to changes in the non heme-based nitrogenase. Hence, here we examined further how Fe limitation influenced heme *b* production, utilization and breakdown and thus potential patterns of preferential Fe distribution between the processes of photosynthesis and nitrogen fixation.

4.3.3 Heme *b* production restricted during Fe limitation

Heme *b* production is indicative of Fe localization in the electron reactions of photosynthesis and respiration. We determined the concentrations of heme *b*, which exhibited the highest concentrations in *Cyanothece* cultures ranging from 2.60 to 25.5 pmol L^{-1} over the course of the experiment (n=22, all DFe treatments). Overall heme yields in *Cyanothece* were lower than observed for other marine phytoplankton, grown at similar total DFe concentrations (Gledhill et al., 2015; Honey et al., 2013). Furthermore, the ratio heme *b*:POC ranged from 0.004 to 0.35 μmol mol^{-1} for *Cyanothece*. Both heme *b* and heme *b*:POC were lower in the low Fe treatments during the early exponential phase (Fig. 4.5B) and increased during the late exponential phase whereas the 40 nM DFe treatment followed the opposite trend, likely because this treatment was phosphorus limited at this point. The analysis of variance showed statistically significant differences in heme *b* distribution related to DFe ($F_{(2,20)}$ = 5.0, p< 0.05).

Our observations for *Cyanothece* are consistent with previous studies, which have reported that values of heme *b*: POC lower than 0.10 μmol mol^{-1} are indicative of Fe limitation in the field (Gledhill et al., 2013; Honey et al., 2013; Louropoulou et al., submitted) and in culture for other phytoplankton classes and species (Gledhill et al., 2015; Honey et al., 2013). Nevertheless, *Cyanothece* appeared to have a lower requirement for heme than *Synechococcus*, even under Fe replete conditions (Honey et al., 2013). Furthermore, the increase of heme *b*:POC in *Cyanothece* from the early to the late exponential phase and the parallel downregulation of *nifH* expression accompanied by decrease in nitrogen fixation rates implied that *Cyanothece* potentially localizes the available Fe into heme-containing proteins.

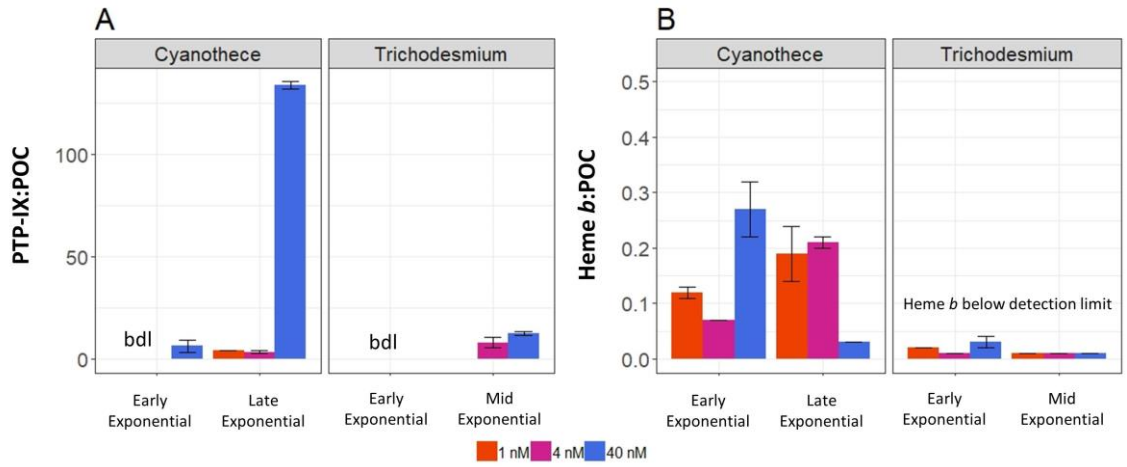

Fig. 4.5: Heme *b* production patterns under varying DFe concentrations for *Cyanothece* and *Trichodesmium* cultures during the early and mid/late exponential phase as indicated by the abundance of A) Protoporphyrin-IX (heme *b* precursor) relative to particulate organic carbon (PTP-IX:POC), and B) Heme *b* relative to POC (heme *b*:POC, μmol mol^{-1}). Bars indicate the mean values (± SD) calculated from three independent biological replicates per DFe treatment for both species. Colors indicate the three DFe treatments (1, 4 and 40 nM).

Surprisingly, heme *b* was below the detection limit (0.03 nmol L^{-1}) in *Trichodesmium* cultures for all DFe treatments and all sampling points, suggesting final concentrations lower than 0.60 pmol L^{-1} for 50 mL filtration volume. We obtained good recoveries of chl *a* (ca. 100 %) and other pigments during our LC-MS analysis (data not shown), thus we can exclude poor heme *b* recoveries based on poor extraction efficiency. The apparently low heme *b* quotas observed for *Trichodesmium* might be resulting from a higher rate of heme *b* degradation during the extraction and analysis, perhaps resulting from high levels of reactive oxygen species (Ho, 2013).

The fluctuations in heme *b* concentrations during Fe limitation may potentially be attributed to reductions in the biosynthesis pathways, which we examined further. We were able to identify in the LS-MS spectra the precursor protoporphyrin IX (PTP-IX) for both species. PTP-IX is only a precursor in one of the possible heme synthesis pathways (Dailey et al., 2017) which thus according to our findings both *Cyanothece* and *Trichodesmium* employ for heme *b* production.

Regarding the heme *b* production patterns during Fe limitation, PTP-IX:POC exhibited the highest abundance during the mid (*Trichodesmium*) and late (*Cyanothece*) exponential phase in the 40 nM DFe treatment (Fig. 4.5A). PTP-IX:POC was undetectable for the 1 nM and 4 nM DFe treatments in the early exponential phase in both species. Lower PTP-IX:POC was determined for the 4 nM *Cyanothece* culture of the late exponential phase compared to the 40 nM culture. These results suggest possible disruptions in heme biosynthesis during Fe limitation in both species (Fig. 4.6). Furthermore, the high PTP-IX content of the 40 nM *Cyanothece* cultures during the late exponential phase was also indicative of PTP-IX accumulation because of interruption of heme *b* production due to phosphate limitation and thus explaining the low heme *b*: POC values.

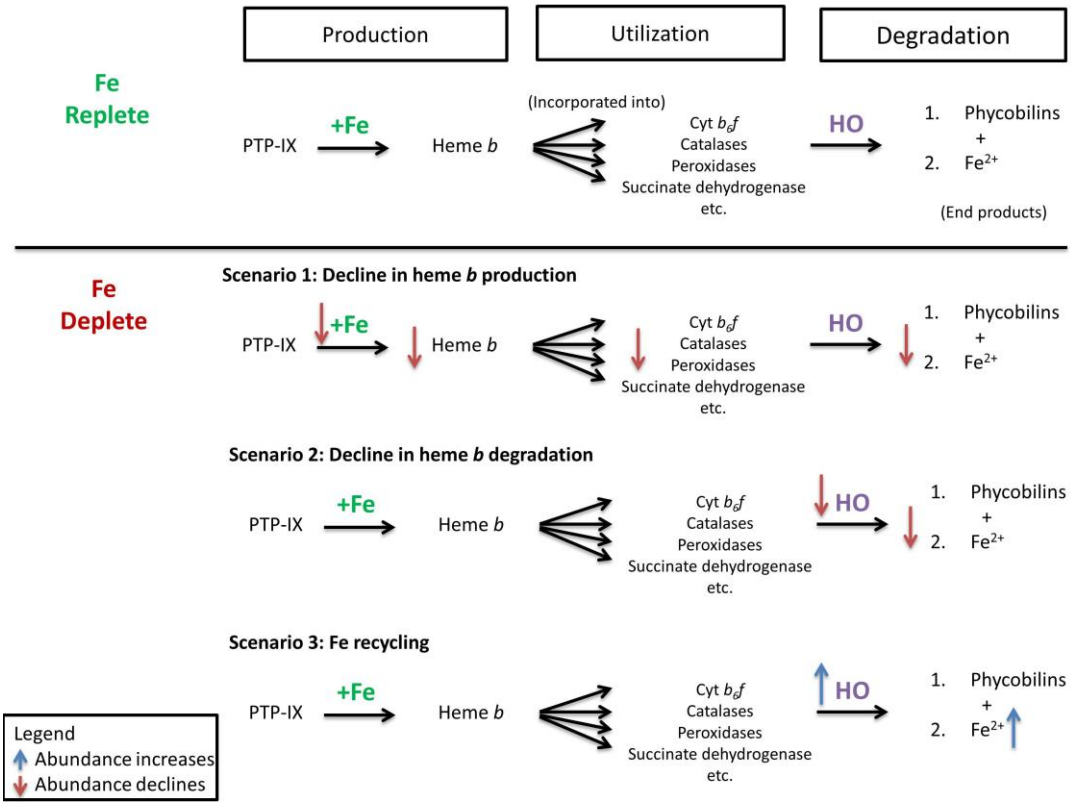

Fig. 4.6: Conceptual diagram of heme *b* production, utilization and degradation processes during Fe replete and Fe deplete conditions. Blue and red arrows indicate increase and decrease in intracellular concentrations respectively. Under Fe-replete conditions, heme *b* is synthesized from the precursor protoporphyrin-IX (PTX-IX) after insertion of Fe^{2+} into the porphyrin ring. Once produced, heme *b* is incorporated into various proteins within the cell. Heme *b* is further metabolized (degraded) by heme oxygenase (HO) for the production of phycobilins and release of Fe^{2+}. Three scenarios describe potential changes in heme *b* production, utilization and degradation patters under Fe-deplete conditions. Scenario 1: Heme *b* production may decline and this will originate from the low Fe^{2+} concentrations. This results in declines in all heme *b*- containing proteins and in declines of the abundance of the breakdown products. Scenario 2: Heme *b* breakdown may decline which will result in decreases in the phycobilins and Fe^{2+}. In this case the levels of heme *b*-containing proteins remain unchanged. Scenario 3: The HOs are activated for Fe recycling purposes. Note that in reality, these processes may occur in combination.

4.3.4 Implications of Fe limitation and heme *b* abundance on the photosynthetic apparatus

As indicators of heme *b* use in the electron transport chain and of photosynthetic apparatus activity, we measured the abundance of chl *a*, F_v:F_m, and expression patterns of the *petB* gene, which encodes the heme *b* containing b_6 - subunit of the cytochrome b_6f.

Chlorophyll *a* ranged from 0.24 to 39.4 nmol L^{-1} in *Cyanothece* cultures and from 0.51 to 34.7 nmol L^{-1} in *Trichodesmium* cultures. Despite some fluctuations among treatments in the initial growth stage, highest chl *a* concentrations were determined for both species in the 40 nM DFe cultures (Table 4.2) during the late exponential phase. Chl *a*:POC ranged from 10.1 to 153 µmol mol^{-1} in *Cyanothece* and 34.5 to 243 µmol mol^{-1} *Trichodesmium* cultures. A gradient increase of the chl *a*:POC ratio with increasing Fe was observed in the early exponential phase for *Cyanothece* and in the mid exponential phase for *Trichodesmium* (Fig. 4.7). Furthermore, in *Cyanothece* in the late exponential phase, the chl *a*:POC of the 4 nM DFe treatment exceeded the value of the 40 nM DFe treatment. The analysis of variance, showed statistically significant relationship between chl *a*:POC and Fe concentrations only in *Cyanothece* ($F_{(2, 22)}$= 4.2, $p<0.05$, n=18).

The apparent photosynthetic efficiency of PSII (F_v:F_m) for *Cyanothece* was lowest for the 1 nM DFe treatment, intermediate for the 4 nM DFe treatment and highest for the 40 nM DFe treatment (Fig. 4.7). Hence, the F_v:F_m was statistically significant among the treatments ($F_{(2,87)}$ = 138, $p<0.01$). In contrast, F_v:F_m for *Trichodesmium* was largely invariant in response to supplied DFe (Fig. 4.7) and did not exhibit any statistically significant relationship with DFe. Thus, the statistically significant difference in the F_v:F_m of *Cyanothece* suggested that the impact of low Fe on the photosynthetic apparatus was larger compared to *Trichodesmium.* Furthermore *Trichodesmium* appeared to have better PSII photochemical efficiencies across varying DFe treatments. Indeed, Shi et al. (2007) reported that in the initial growth stages Fe-stress developed gradually and F_v:F_m did not vary among DFe treatments, thus implying that our *Trichodesmium* cultures were still in the Fe-stress development phase on both sampling days. However, under fully developed Fe-stress conditions, F_v:F_m of *Trichodesmium* demonstrated an Fe-dependent behavior as reported by Richier et al. (2012).

Similarly to F_v:F_m, the fold changes of *petB* gene expression (Fig. 4.7C) showed a contrasting behavior between the two species. For *Cyanothece*, *petB* was downregulated in both the early and late exponential phase in the low DFe treatments (Table 4.3). The downregulation increased further in the 1 nM DFe and decreased in the 4 nM treatment in the late exponential phase. In contrast, the *petB* gene was upregulated in *Trichodesmium* in all DFe treatments and both growth phases whilst the fold change increased by one order of magnitude from the early to the mid exponential phase (Table

4.3, Fig. 4.7). Furthermore, the fold changes in *petB* expression for *Trichodesmium* ranged within the same order of magnitude and was comparable to the data reported by Shi et al. (2007).

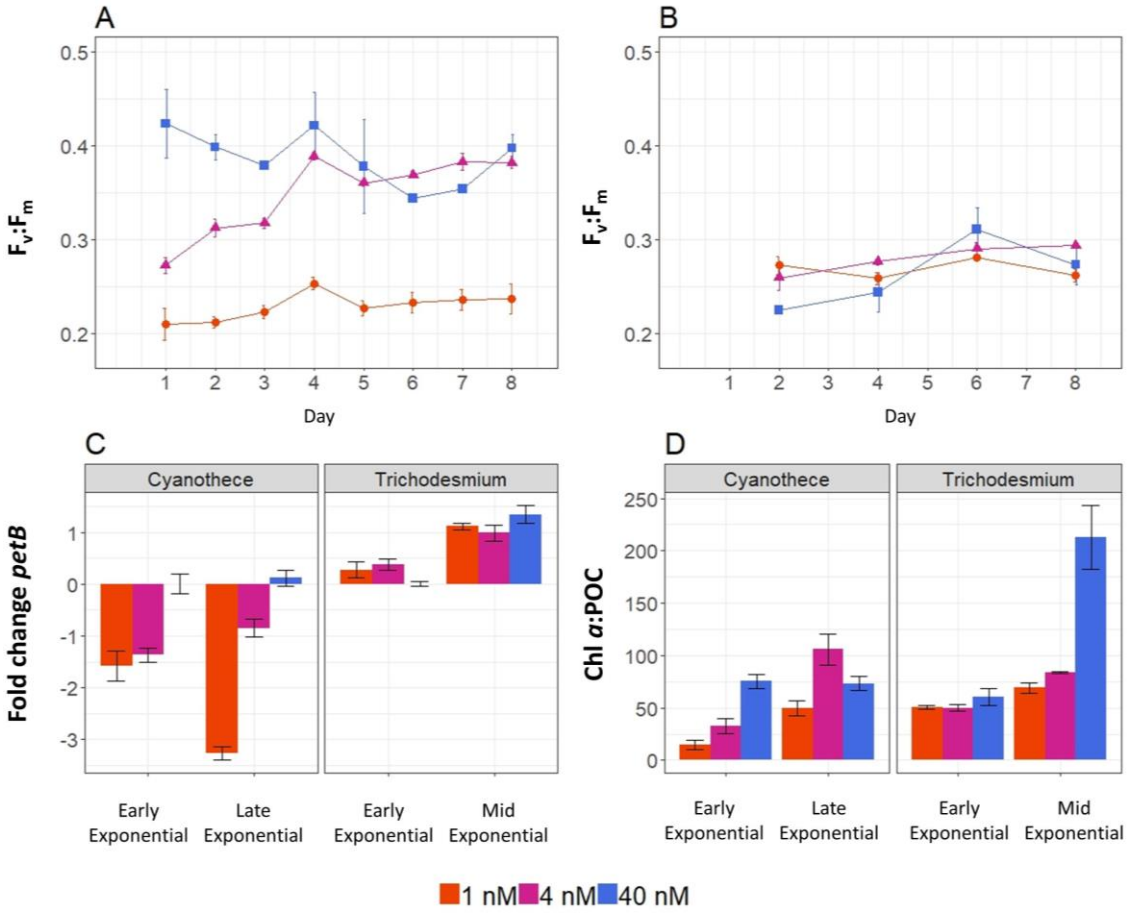

Fig. 4.7: Parameters associated with photosynthetic activity and heme *b* utilization during the early and mid/late exponential phase for *Cyanothece* and *Trichodesmium*. Dots and bars indicate mean (± SD) values calculated from three independent biological replicates per DFe treatment for both species. Colors indicate the three DFe treatments (1, 4 and 40 nM). Subplots A) and B) illustrate the photosynthetic efficiency ($F_v:F_m$) for *Cyanothece* and *Trichodesmium* respectively as measured using Fast Repetition Rate Fluorometry (FRRF). C) Mean fold change in *petB* gene expression using the relative comparison method $2^{-\Delta\Delta Ct}$ (Livak and Schmittgen, 2001). The Ct values for *Cyanothece* were normalized to the expression of the *16S rRNA* (Gaudana et al., 2013) whereas Ct values for *Trichodesmium* were normalized to *rnpB* (Chappell and Webb, 2010; Shi et al., 2007). The fold change derives after a species - individual calibration of the ΔCt values with the corresponding 40 nM DFe treatment of the early exponential phase. Note that for comparison reasons between the two species, the fold changes are presented in log scale in this graph. D) Chlorophyll *a* – to – particulate organic carbon (Chl *a*: POC, µmol mol^{-1}).

The upregulation of the *petB* gene in *Trichodesmium* suggested that the abundance of the production of heme *b*-containing cyt b_6f was enhanced, thus we assumed that the heme *b*:POC ratio would either increase or remain stable over the course of the experiment. We cannot confirm this assumption, since heme *b* was not detected during the LC-MS analysis and the calculation of the heme *b*:POC ratio was not precise. However, it is established via both proteomic and transcriptomic analyses (Richier et al., 2012; Shi et al., 2007; Snow et al., 2015a) that *Trichodesmium* during Fe limitation restricts the production of the Fe-rich nitrogenase to promote energy production via

photosynthesis. Later in the growth stages, declines in the photosystems occur (Richier et al., 2012; Shi et al., 2007). Hence, our data (upregulation of *petB*) in accordance with previous studies imply that *Trichodesmium* employs a preferential allocation of the available Fe into the photosynthetic apparatus and thus to the heme-containing centers at the cost of nitrogen fixation.

Regarding heme *b* utilization in *Cyanothece*, we observed an increase in the ratio heme *b*:POC in the low-Fe (1 nM and 4 nM DFe) cultures from the early to the late exponential phase which started from Fe-limitation indicative levels (~0.10 μmol mol^{-1}) and increased to values determined for Fe-replete phytoplankton cultures (>0.20 μmol mol^{-1}) (Gledhill et al., 2015; Honey et al., 2013). These results implied that heme *b* concentrations increased in both low Fe treatments (i.e. 1 nM and 4 nM DFe) which could potentially result in an increase in cytochrome b_6 abundance. However, we observed a contrasting behavior between the two low Fe treatments regarding the expression patterns of *petB*; in the 1 nM DFe treatment *petB* transcripts decreased further in the late exponential phase suggesting that these cultures experienced severe Fe-stress without possessing mechanisms of regulating the expression of *petB* for energy conservation via photosynthesis. Although previous work suggests that most of the Fe is utilized in the photosynthetic apparatus (Raven, 1988, 1990) by phytoplankton, our findings suggest that this is not the case for the Fe-starved *Cyanothece* and that heme *b* was not utilized in the photosynthetic apparatus. Since our analysis protocol also allows for the extraction of heme *b* from peroxidase and succinate dehydrogenase (Gledhill et al., 2013), which supplies electrons for respiration, we assumed that heme *b* was likely used for these purposes. In contrast to the 1 nM DFe cultures, the transcripts of *petB* for the 4 nM DFe cultures increased in the late compared to the early exponential phase (Fig. 4.7, Table 4.3) which also resulted into an increase in F_v:F_m. This pattern implied that part of the available Fe was utilized for production of the heme *b*-containing cytochrome b_6f while it could also potentially be interpreted as a recovery process from Fe-stress. Therefore, we observed an increase in the photosynthetic activity and one order of magnitude increase in the chl *a*:POC ratio in the 4 nM DFe cultures between the early and the late exponential phase.

The changes in heme *b*:POC levels for *Cyanothece* and the upregulation of the *petB* gene for *Trichodesmium*, which most likely results in changes of heme *b* abundance, led us to the assumption that the heme *b* pool was likely controlled by the expression of the HO during Fe limitation (Fig. 4.6). Hence, we examined the relative expression of HO, assuming that HO regulation contributes to Fe conservation within the cells (Saito et al., 2011). Furthermore, the behavior in the 4 nM DFe cultures suggested enhancement of the photosystem proteins (heme *b*-containing and chl *a*) and strategies that may potentially be employed to recover from Fe-stress.

4.3.5 Heme *b* degradation decreases during Fe limitation

On a transcriptional level, the genes encoding HO (*hmox Trichodesmium*, *hmo2 Cyanothece*) were downregulated in both species in the 1 nM and 4 nM DFe treatments compared to the 40 nM treatment (Table 4.3, Fig. 4.8A). The downregulation was more pronounced in the 1 nM DFe treatment during the late exponential phase. Despite the clear downregulation of the *hmo2* and *hmox* genes for the Fe deficient cultures of *Cyanothece* and *Trichodesmium*, respectively, there was no statistically significant relationship between the fold changes of these genes and heme *b* concentrations or heme *b*:POC.

In cyanobacteria hemes are used to produce phycobilins required for light harvesting (Richaud and Zabulon, 1997). Hence, the downregulation of HO implied that that heme *b* degradation and thus phycobilin production decreased in the Fe-starved cultures (Fig. 4.6). Both *Cyanothece* and *Trichodesmium* appeared to be able to regulate their heme *b* pool by reducing the HO activity on a transcriptional level in order to maintain energy production and photosynthesis. Further analysis on the heme-derived degradation products would shed light on whether phycobilin abundance thus phycobilisome production decreased during Fe limitation.

In general, the hemoprotein pool is considered labile and subject to regulations first because free hemes are toxic (Espinas et al., 2012) but also to accommodate the basic biochemical processes under varying Fe conditions expressed by modifications in the HO activity (Saito et al., 2011; Snow et al., 2015a). In *Trichodesmium*, proteomic analysis has shown that HO levels decrease in Fe-deplete conditions (Snow et al., 2015a) which agrees with our findings. Regarding the unicellular diazotrophs, proteomic analyses in *Crocosphaera watsonii* showed that the diurnal oscillations in the hemoprotein pool (required during photosynthesis) were expressed by activation of HO2 during the nitrogen fixation time (night) and inactivation during the photosynthesis time (day) (Saito et al., 2011). Similar diurnal oscillations between nitrogen fixation and photosynthesis were also determined for the unicellular *Cyanothece* (Stöckel et al., 2008; Toepel et al., 2009), implying that *Cyanothece* likely also possesses the ability to regulate the hemoprotein pool via altering the HO transcription. Although these studies in unicellular diazotrophs were carried out under Fe-replete conditions, diurnal oscillations in HOs may also allow for Fe conservation during Fe limitation (Saito et al., 2011).

The unicellular cyanobacterial diazotrophs possess more than one HO which often behave in an opposite manner (Frankenberg-Dinkel, 2004; Saito et al., 2011). In our study, the gene encoding *hmo1* of *Cyanothece*, exhibited a contrasting behavior compared to *hmo2* thus raising questions about its function and link to heme *b* regulation during Fe-limitation.

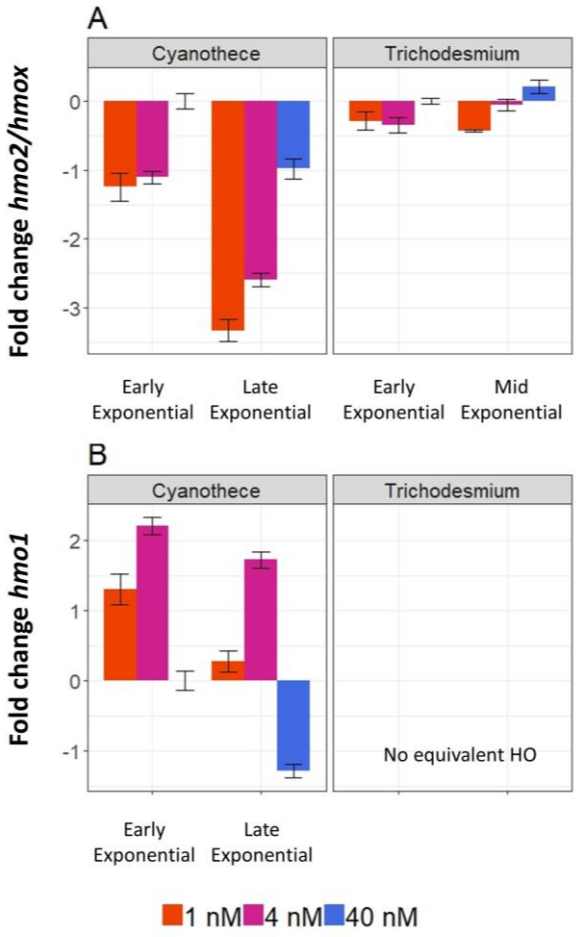

Fig. 4.8: Transcriptional regulation of heme *b* degradation with varying Fe concentrations. Fold change in gene expression of A) *hmo2* (*Cyanothece*) and *hmox* (*Trichodesmium*), and B) *hmo1* (*Cyanothece*), during the early and mid/late exponential phase. Bars indicated the mean (± SD) values calculated from three independent biological replicates per DFe treatment for both species. Colors indicate the three DFe treatments (1, 4 and 40 nM). The fold change in gene expression of *hmo2*, *hmox*, and *hmo1* was calculated using the relative comparison method $2^{-\Delta\Delta Ct}$ (Livak and Schmittgen, 2001). The Ct values for *Cyanothece* were normalized to the expression of the *16S rRNA* (Gaudana et al., 2013) whereas Ct values for *Trichodesmium* were normalized to *rnpB* (Chappell and Webb, 2010; Shi et al., 2007). For each gene, the fold change derives after a species - individual calibration of the ΔCt values with the corresponding 40 nM DFe treatment of the early exponential phase. Note that for comparison reasons between the two species, the fold changes are presented in log scale in this graph.

4.3.6 Heme oxygenase activated for Fe acquisition in *Cyanothece*?

In contrast to the *hmo2* gene, *hmo1* was upregulated in low DFe *Cyanothece* cultures (Table 4.3, Fig. 4.8B) whilst in the DFe sufficient treatment *hmo1* was downregulated (late exponential phase). Furthermore, the upregulation of *hmo1* was more pronounced in the early exponential phase compared to the late exponential phase for both low DFe cultures; the fold changes shifted from 20.0 ± 11.1 (early exponential) to 1.9 ± 0.68 (late exponential) in the 4 nM DFe treatment and from 161 ± 46.9 (early exponential) to 53.1 ± 14.8 (late exponential) for the 1 nM DFe treatment. These results implied the activation of a HO only during Fe-limiting conditions. Currently, upregulation in the expression of *hmo1* gene as a result of Fe depletion was only determined for red algae (Richaud and Zabulon, 1997). However, at the protein level, (Saito et al., 2011) showed

that the two HOs of *Crocosphaera* behave in an opposite manner, similar to our observation.

Despite complete assimilation of the available Fe from the growth media, the increase of the heme *b*:POC and chl *a*:POC ratios in both low Fe *Cyanothece* cultures from the early to the late exponential phase pointed to an increase in the heme/Fe reservoirs. We thereby suggest that the increase in *hmo1* gene expression and activation of HO1 enzyme was linked to Fe acquisition processes.

The primary role of the HOs is the removal of the Fe atom from the porphyrin ring which leads to cleavage of the porphyrin and production of biliverdin and bilirubin (Frankenberg-Dinkel, 2004; Frankenberg et al., 2003). Thus, the activation of HO1 by *Cyanothece* is likely an adaptation strategy to Fe starvation employed for recycling purposes of the intracellular heme-bound Fe (Saito et al., 2011). In the unicellular *Crocosphaera*, alternating expression between HO1 and HO2 on a diurnal cycle allowed for the release of Fe from hemes and subsequent utilization in other Fe-protein pools (Saito et al., 2011). Unicellular *Cyanothece* may be also employing a similar strategy, which can also be diurnal, for more efficient utilization of the available Fe during Fe limitation.

Another potential explanation for the upregulation of *hmo2* is that this particular HO is localized in the cytoplasm of *Cyanothece* cells that can be employed during exogenous heme uptake and functions after the extracellular hemes are transported through the membrane into the cell. This behavior has already been documented for other bacterial species (Hopkinson et al., 2008; Roe et al., 2013; Septer et al., 2011; Weaver et al., 2003). Hence, this implies that HOs in *Cyanothece* are potentially located in different areas within the cell (SI Figure 8); thus phycobilisome production via heme *b* degradation takes place in the plastid (Migita et al., 2003; Muramoto, 1999; Terry et al., 2002) whereas Fe acquisition takes place in the cytoplasm (Hopkinson et al., 2008; Roe et al., 2013; Septer et al., 2011; Weaver et al., 2003).

4.4 Conclusions

In this study we examined the heme *b* production, utilization and degradation processes under different DFe treatments in two diazotroph species *Cyanothece* and *Trichodesmium* in order to identify patterns of Fe utilization in the hemoprotein pool and its optimization during Fe-limitation. *Cyanothece* appeared to experience more severe Fe-stress, not being able to its Fe use efficiencies (IUE) under Fe limitation whereas *Trichodesmium* was more efficient in dealing with low DFe supply. This contrast likely arises from the different cell morphology or habitat-specific behavior since *Trichodesmium* grows in environments where Fe supply is fluctuating and is able to modify its IUE in order to maintain nitrogen production and survive.

Regarding heme *b*, Fe limitation restricts production of the heme *b* co-factor as both the precursor PTP-IX and heme *b*:POC ratios were low in low Fe cultures. However, our data also implied that both species possess Fe optimization strategies which result in modifications in the utilization of the heme *b* cofactor thus in the hemoprotein pool. *Trichodesmium* enhances photosynthetic activity during Fe-limitation by localizing the available Fe into the heme *b*-containing cytochrome b_6f and by reducing the Fe utilization in nitrogenase. *Cyanothece* also increased heme *b* utilization under Fe limitation but these increases were not linked to the cytochrome b_6f or the photosynthetic apparatus.

The optimization of the hemoprotein pool is likely linked to the regulation of HOs under Fe limitation. Here, we confirmed on a transcriptional level that HOs remain downregulated under Fe-stress in both species which potentially occurs for conservation of the photosynthetic activity and survival. Interestingly, we also observed increase in the transcripts in one HO in *Cyanothece* and in the heme *b*:POC ratios thus implying increase of the heme *b* cofactor in the low Fe cultures despite the complete assimilation of the DFe in the culture media. Hence, HO may also be linked to intracellular Fe recycling or extracellular Fe-acquisition processes. Both mechanisms involve on of previously produced hemoproteins and release of the Fe atoms from the hemoproteins into the cell. This finding also enhances previous assumptions of Fe acquisition mechanisms by prokaryotes using hemophores (Wandersman and Delepelaire, 2004) in conjunction with HOs thus raising questions about the exact role of HOs and of hemes for Fe nutrition of cyanobacteria.

4.5 Acknowledgements

The authors would like to thank Kerstin Nachtingall and Allanah Paul for the measurement of nitrogen fixation rates and for helping us with nitrogen fixation data processing. We acknowledge also the support of Max Planck Institute for Marine Microbiology Bremen for measurement of isotopic nitrogen composition. We also thank Nicole Pinnow for the technical support provided during the molecular analyses. Finally, thanks to the Helmholtz Research School for Ocean System Science and Technology (HOSST) for the financial support to EL.

5. Overall conclusions and outlook

5.1 Summary and resulting conclusions

Heme *b* is one of the most important Fe-containing biomolecules for marine phytoplankton. The processes that influence heme *b* concentrations in the ocean are still uncertain, although some studies in the past indicated that biomass, Fe supply and/or community composition (Bellworthy et al., 2017; Gledhill et al., 2013; Honey et al., 2013) may be the most significant driving forces. Even though it is well documented that Fe limitation leads to decreases in growth, photosynthesis and nitrogen fixation rates of phytoplankton (e.g. Geider and La Roche, 1994; Greene et al., 1992; King and Barbeau, 2007; Shi et al., 2007; Sunda and Huntsman, 1997) and declines in the abundance of hemoproteins (e.g. Allen et al., 2008; Fu and Bell, 2003; Richier et al., 2012; Snow et al., 2015; Strzepek and Harrison, 2004a) details on the impact of low Fe supply on the heme *b* cofactor is limited. Three studies documented that low Fe supply leads to decreases in heme *b* concentrations and quotas (Gledhill et al., 2013, 2015; Honey et al., 2013) and that some high-latitude species may be able to modify their heme *b* pool to conserve their growth (Gledhill et al., 2015).

The aim of this study was to expedite the knowledge regarding i) the factors driving heme *b* concentrations in the natural environment and ii) the impact of Fe limitation on the abundance, production, utilization and degradation processes of heme *b* in phytoplankton.

Chapter 2 examines the concentrations of heme *b* during the spring bloom in the subpolar and subtropical North Atlantic Ocean (GEOVIDE cruise, GEOTRACES GA01 section) in order to investigate its utility as a proxy for identifying Fe-limited phytoplankton communities *in situ*. This chapter provides a systematical examination of the relationship between heme *b* abundance and phytoplankton group assemblages. In Chapter 3 includes an investigation of the processes driving heme *b* abundance in various biogeochemical regions of the Atlantic Ocean and extends knowledge of heme *b* distributions to the under-sampled South Atlantic. Chapter 4 examines the impact of Fe limitation on heme *b* production, utilization and degradation processes in the two popular diazotroph species *Cyanothece* and *Trichodesmium* in order to identify the regulation potential of the heme *b* pool during Fe-limitation.

5.2 Overall conclusions

The overarching conclusions arising from the Chapters 2, 3 and 4 of this dissertation are the following;

1) Heme *b* concentrations decline during Fe limitation

2) Heme *b* and particularly the ratio heme *b*-to-POC can serve as proxies of Fe limitation in field studies; a value of 0.10 μmol mol^{-1} is indicative of Fe limited phytoplankton
3) The proportion of heme *b* relative to biogenic Fe is indicative of the amount of available Fe utilized in the heme *b* pool by the extant phytoplankton communities in the field
4) The heme *b* pool can be regulated during Fe limitation for growth conservation in diatoms, prymnesiophytes and diazotrophs
5) Heme *b* regulation depends on the absolute Fe requirements of each phytoplankton group and can be expressed by a decline in heme *b* abundance and utilization of Fe into other protein pools
6) Heme *b* regulation can originate at the transcript level via modifications in production, utilization and degradation processes
7) The regulation of the heme oxygenases (HOs) likely controls the levels of the intracellular heme *b* and under Fe limitation heme metabolism decreases
8) Heme oxygenases may also be linked to Fe acquisition processes in some diazotrophs, other prokaryotes and/or eukaryotes either by intracellular Fe recycling or exogenous Fe uptake via membrane transport by heme-receptor proteins

5.2.1 Iron supply drives heme *b* abundance in the Atlantic Ocean

In the past, the lowest heme *b* concentrations in the field were reported for i) the post-bloom Fe-limited Iceland Basin in 2007 (Gledhill et al., 2013), ii) the Southern Ocean (Gledhill et al., 2015), where Fe supply is low, and iii) the Tropical Atlantic Ocean which was associated with changes in atmospheric Fe fluxes (Honey, 2012; Schlosser et al., 2014). Hence, Fe supply was considered to play significant role in defining heme *b* distributions in the natural environment (Gledhill et al., 2013, 2015; Honey et al., 2013).

The current study demonstrated and confirmed that Fe supply largely controls heme *b* concentrations in the Atlantic Ocean (Chapters 2 and 3). Thus, low heme *b* concentrations (<1.0 pmol L^{-1}) were determined in areas of the Atlantic Ocean characterized by low Fe supply or exhaustion of the ambient Fe; these areas were the Irminger Basin during the spring bloom (Chapter 2), which is known to exhibit seasonal Fe limitation (Macey et al., 2014; Ryan-Keogh et al., 2013; Sanders et al., 2005), and the subtropical South Atlantic gyre (Chapter 3), which receives low amount of Fe-containing dessert particles (Jickells et al., 2005; Schlosser et al., 2014; Rijkenberg et al., 2014) thus phytoplankton is characterized as Fe-nitrogen co-limited (Browning et al., 2017a; Moore et al., 2013).

The ratio heme *b* relative to particulate organic carbon (POC) was consistently lower than 0.10 μmol mol^{-1} in these areas (Chapter 2 and 3) and indicative of Fe limitation according to laboratory culturing experiments (Gledhill et al., 2013, 2015; Honey et al.,

2013). Hence, this PhD project identified the value 0.10 μmol mol^{-1} of the ratio heme *b*:POC as indicative of Fe-limited phytoplankton and documented that heme *b*:POC can serve as a reliable indicator of Fe limitation since it appeared not to be influenced by species- specific processes which potentially involve modifications in the hemoprotein and/or other protein pools.

However, when Fe supply and availability are adequate, biomass levels drive heme *b* concentrations. In general, previous studies have shown that elevated heme *b* concentrations characterized oceanographic regions with high biomass in the North Atlantic (Gledhill et al., 2013; Honey et al., 2013) and Southern Oceans (Gledhill et al., 2013, 2015) and that the vertical distribution of heme *b* followed a similar trend to POC and chlorophyll *a* (Honey et al., 2013). In this study, the highest heme *b* concentrations were observed in regions with high productivity (Chapters 2 and 3), which were the subpolar North Atlantic, Celtic Sea, Coastal Tropical North Atlantic and stations located in the Angola and Benguela Currents.

The observations and conclusions of this PhD project regarding the forces that drive heme *b* in the Atlantic Ocean can be summarized in Fig. 5.1. This figure illustrates the major processes in the ocean Fe cycle emphasizing on the Atlantic Ocean (Tagliabue et al., 2017). Hence, heme *b* concentrations and relative to POC ratios decline in areas remote from atmospheric Fe sources or in the seasonally Fe limited subpolar areas, trends observed here in Chapters 2 and 3. In areas characterized by increased atmospheric Fe-containing dust supply, heme *b* concentrations depend on the biomass levels.

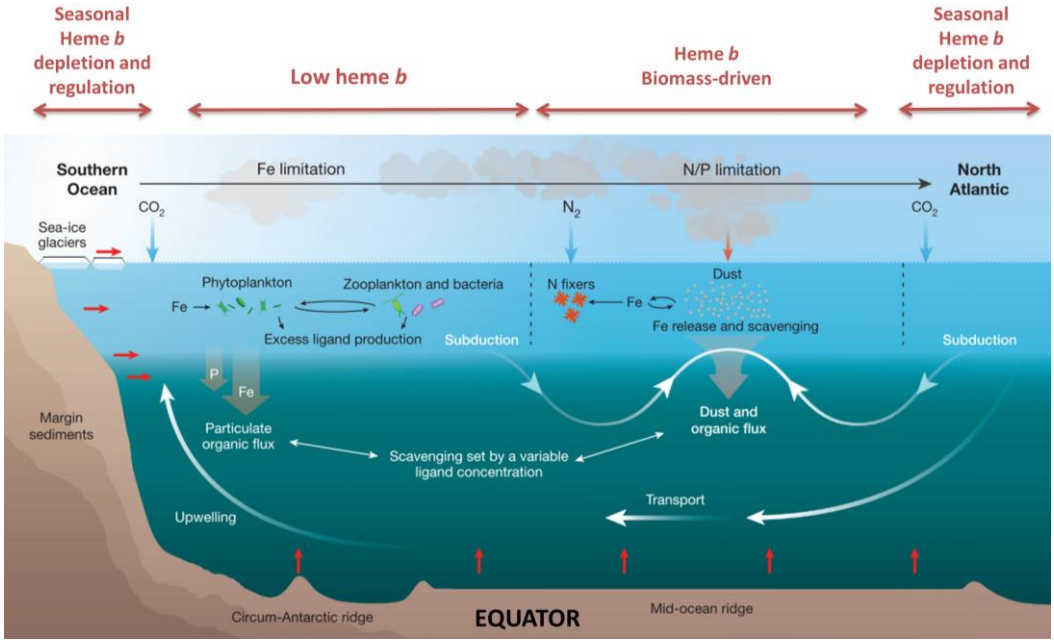

Fig. 5.1: Schematic representation of how heme *b* concentrations change in the Atlantic Ocean. Note that patterns of heme *b* refer to the Surface Mixed Layer (SML). Adapted from (Tagliabue et al., 2017) for parallel representation of the major processes of Fe cycling with emphasis on the Atlantic Ocean.

5.2.2 Field heme *b* relative to total biogenic Fe can be indicative of Fe utilization patterns and nutrient status of the extant phytoplankton communities

Laboratory experiments with cultured phytoplankton in the past demonstrated a great variability among different phytoplankton classes and species in the proportion of the total biogenic Fe utilized in heme *b* (Gledhill et al., 2013, 2015; Honey et al., 2013) (see Chapter 1). For example prokaryotes (e.g. marine cyanobacteria) exhibited lower heme *b* content relative to the total biogenic Fe compared to haptophytes and diatoms (Honey et al., 2013). Hypothetically this trend could be extrapolated to the natural environment suggesting that the extant phytoplankton groups potentially influence heme *b* abundance. To date, the link between heme *b* abundance relative to the biogenic Fe pool and microbial community assemblages was not documented.

This PhD project demonstrated (Chapter 3) that modelled heme *b* concentrations relative to biogenic Fe (heme *b*:Fe_{bio}) fluctuated from 0.17 to 9.1%. This range was comparable to previous culturing observations for species with low heme *b* content and species growing in low Fe (≤0.50 nmol L^{-1}) or nitrate culturing media (Gledhill et al., 2015; Honey, 2012; Honey et al., 2013). Thus, the differences in heme *b*:Fe_{bio} determined in Chapter 3 can be ascribed to the microbial community composition of each region, to differences among species involving heme *b* pool regulation and finally phytoplankton nutrient status.

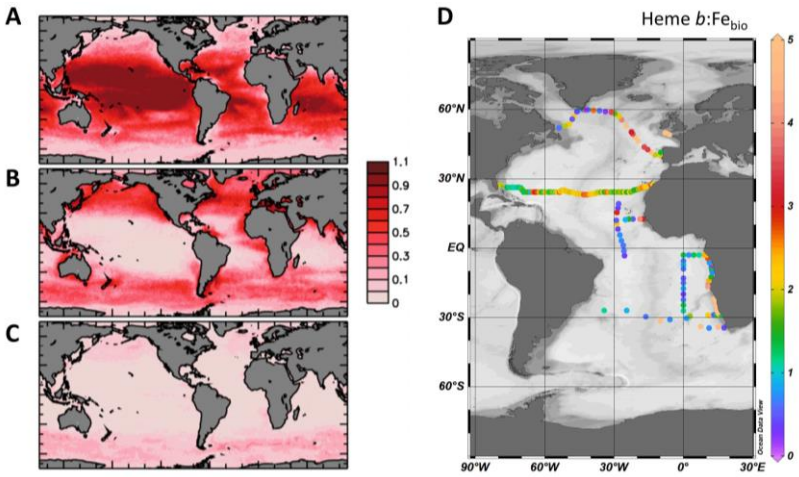

Fig. 5.2: Heme *b* proportion relative to the total biogenic Fe pool is indicative Fe utilization patterns of extant phytoplankton groups in the natural environment. Panels A, B and C represent picophytoplankton, haptophyte and diatom pools respectively in the ocean surface (fraction of time) after Le Quéré et al. (2016). Panel C illustrates heme *b*-to-biogenic Fe (%) based on data from Chapter 3.

Figure 5.2 illustrates the abundance of A) picophytoplankton, B) haptophytes and C) diatoms in the ocean surface. Regarding the spatial distribution of heme *b*:Fe_{bio} in the Atlantic Ocean, the highest values of heme *b*:Fe_{bio} were observed in high latitude areas where diatom or haptophyte species are mostly dominant. In contrast, the lowest heme *b*:Fe_{bio} were observed in the picophytoplankton dominated areas. These findings reconcile the previous laboratory observations (Gledhill et al., 2015; Honey, 2012;

Honey et al., 2013) with measurements for field phytoplankton populations thus confirming laboratory observations in the natural environment. Finally, heme *b*:Fe_{bio} can be used as an indicator of microbial community composition and of Fe utilization patterns in the hemoprotein pool by extant phytoplankton groups. Hence, this dissertation contributed to the knowledge of how the available Fe is utilized by phytoplankton in the natural environment.

5.2.3 The heme *b* pool can be optimized during Fe limitation for Fe conservation

Although Fe limitation generally leads to decreases in heme *b* concentrations and normalized to carbon ratios (Gledhill et al., 2013, 2015; Honey et al., 2013), the low concentrations and quotas of heme *b* are not always accompanied by decreases in biomass or growth; this example was observed in the field in the area of Irminger Basin (Chapter 2) and in Iceland Basin in 2005 (Gledhill et al., 2013). Furthermore, in culture by Gledhill et al. (2015) showed that open ocean prymnesiophytes and diatoms (*Emiliania huxleyi*, *Phaeocystis antarctica*, *Chaetoceros brevis*) maintained their growth rates despite reduced intracellular heme *b* concentrations under Fe limitation (i.e. DFe $\leq$ 0.5 nmol L^{-1}).

Conservation of biomass-indicative parameters and parallel heme *b* depletion may be considered one of the Fe regulation mechanisms of phytoplankton triggered by changing ambient Fe conditions and expressed by allocation of the available Fe away from the heme *b* pool (Gledhill et al., 2015). By now it is well established that phytoplankton possesses diverse mechanisms of adaptation to Fe limitation aiming for Fe conservation and thus survival (Morrissey and Bowler, 2012). These include modifications in the stoichiometric ratios (e.g. Fe to carbon) (Sunda and Huntsman, 1995) and/or preferential allocation of Fe into selected Fe containing molecules (Nunn et al., 2013; Shi et al., 2007; Smith et al., 2016; Snow et al., 2015a; Strzepek and Harrison, 2004).

It is documented in this PhD project, that the reduction and regulation of heme *b* in field phytoplankton populations was not a class- or species- specific response to Fe limitation. Hence, different phytoplankton groups are able to regulate heme *b* in order to optimize and conserve Fe use. Furthermore, this study showed that heme *b* regulation depends on the overall absolute Fe requirements of each extant phytoplankton group.

Studies have already indicated that individual Fe requirements of phytoplankton groups potentially induce shifts in assemblages from larger-sized to smaller-sized populations in the high-latitude areas (Boyd et al., 2012; Ryan-Keogh et al., 2013, 2017; Strzepek et al., 2012). Fig. 5.3 represents a model of how heme *b* relative to biomass potentially changes during these shifts in phytoplankton assemblages from larger-sized diatom to smaller-sized prymnesiophyte populations in the high-latitude subpolar North Atlantic Ocean according to the Fe drawdown rates. Thus, in mixed phytoplankton communities, heme *b* regulation may occur at several time points during the bloom progression and

the whole community will become progressively limited when the species with the lowest Fe requirement can no longer satisfy its subsistence Fe quota. This reconciles the findings presented in Chapter 2 for the diatom dominated Irminger Basin (Chapter 2) and in literature for the prymnesiophyte dominated Iceland Basin (Gledhill et al., 2013; Poulton et al., 2010).

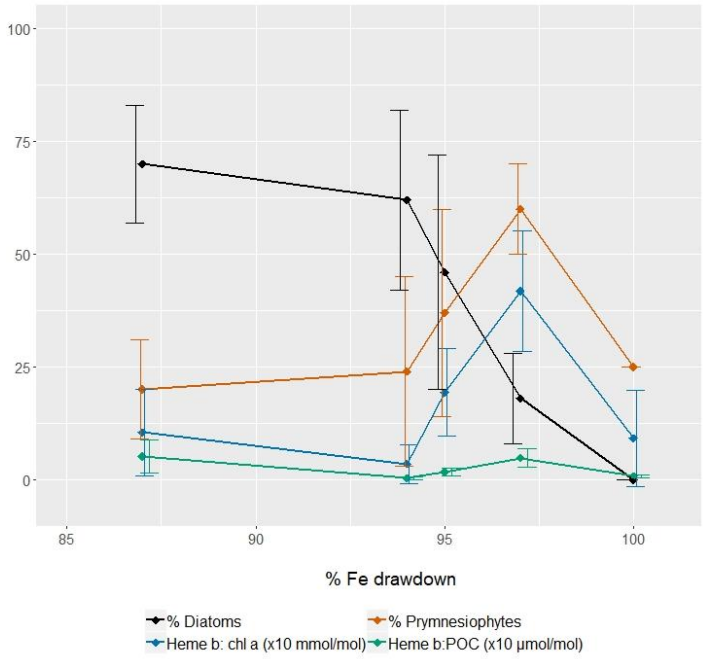

Fig. 5.3: *Heme b abundance and regulation in the high-latitude subpolar North Atlantic Ocean during the bloom progression. Shifts in phytoplankton assemblages from diatoms to prymnesiophytes may occur due to the class-dependent requirements in Fe as the bloom progresses* (Boyd et al., 2012; Ryan-Keogh et al., 2013, 2017; Strzepek et al., 2012). *Heme b regulation is likely to occur when the absolute ambient Fe concentrations decline as an adaptation mechanism for more efficient utilization of the available Fe. Regulation will be expressed by depletion of cellular heme b relative to POC and chl a thus exhibiting decrease in the heme b:POC and increase in the chl a:heme b ratios.*

Diazotrophs also possess the ability of modifying their intracellular Fe quotas (Berman-Frank et al., 2001a; Sunda and Huntsman, 1995) and of distributing Fe into selected Fe-protein pools in order to conserve their growth (Berman-Frank et al., 2001a, 2001b; Chappell and Webb, 2010; Saito et al., 2011; Shi et al., 2007; Snow et al., 2015a). Various studies showed via transcriptomic or proteomic analysis that the filamentous diazotroph *Trichodesmium* localizes the available Fe into the photosynthetic apparatus causing reduction in nitrogenase and thus nitrogen fixation activity (Chappell and Webb, 2010; Richier et al., 2012; Shi et al., 2007; Snow et al., 2015a). Unicellular diazotrophs are known to employ diurnal oscillations in nitrogen fixation and carbon fixation (Jacq et al., 2014; Saito et al., 2011; Stöckel et al., 2008) in order to separate nitrogenase from oxygen, which however also lead to Fe recycling and regulation of the hemoprotein pool (Saito et al., 2011).

The current study (Chapter 4) examined the impact of Fe limitation on *Cyanothece* and *Trichodesmium* species. Although Fe limitation resulted in declines in heme *b*

production in both species, the general response of the two diazotrophs to Fe limitation and implications on the heme *b* utilization differed.

The Fe use efficiencies (IUE) indicate how much biomass (i.e. units carbon) is produced per unit Fe per unit time (Raven, 1988) and thus IUEs are indicative of growth and effective utilization of the available Fe. In this study, *Cyanothece* experienced more severe Fe-stress and was not capable of modifying successfully its stoichiometric ratios (Fe to carbon) resulting into low IUEs. In contrast, *Trichodesmium* was more efficient in dealing with low Fe supply and had higher IUEs.

This contrast in IUEs between the two species led to different heme *b* utilization and regulation strategies; *Trichodesmium* increased expression of the heme *b*-containing cytochrome b_6f of the photosynthetic apparatus by reducing the Fe content of nitrogenase resulting into declines in nitrogen fixation rates as observed previously (Chappell and Webb, 2010; Richier et al., 2012; Shi et al., 2007; Snow et al., 2015a). *Cyanothece* allocated the available Fe away from the nitrogen fixation apparatus and into the heme *b* inventories, which however were not linked to enhancement of the cytochrome b_6f or of photosynthetic efficiencies.

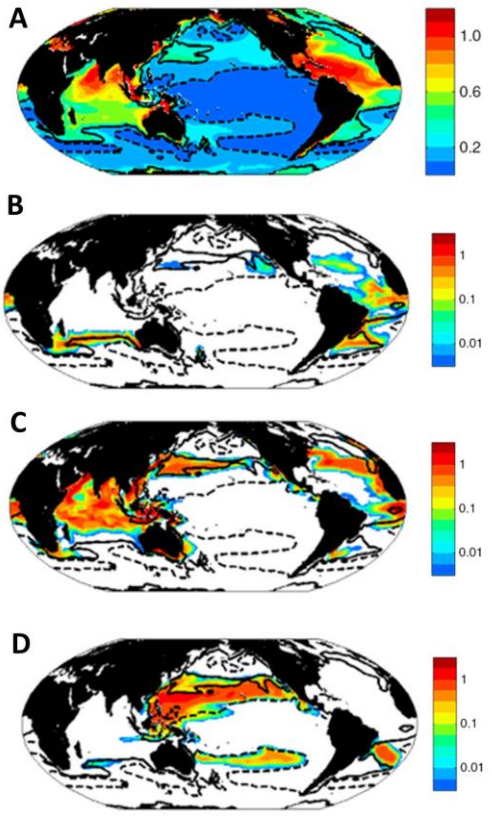

Fig. 5.4: Example of how Fe supply in conjunction with Fe requirements, Fe use efficiencies (IUE) and available optimization strategies may be critical in controlling the geographical abundance of diazotrophs after Saito et al. (2011). Subplot A illustrates modelled Fe concentrations in nmol L^{-1}. Subplots B, C and D illulstrate the predicted abundance (in mg C m^{-3}) of *Trichodesmium*-analogs, of non-hotbunking unicellular diazotrophs and of hotbunking unicellular diazotrophs (analogs of Crocosphaera watsonii) respectively. Dashed and solid contours indicate 0.1 nmol L^{-1} and 0.3 nmol L^{-1} Fe respectively.

The manner in which the two diazotrophs utilized the available Fe into the heme *b* pool implies that the Fe regulation strategies likely originate from the different cell morphology or from habitat-specific considerations (Berman-Frank et al., 2001a; Shaked and Lis, 2012). Saito et al. (2011) demonstrated that diurnal oscillations Fe-containing proteins and sharing of Fe between photosynthesis and nitrogen fixation allow *Crocosphaera sp.* to inhabit regions characterized by lower Fe concentrations. Similarly, high Fe demand and the ability to utilize Fe from dust particles (Polyviou et al., 2018; Rubin et al., 2011; Snow et al., 2015b) allow *Trichodesmium* to grow in areas characterized by elevated Fe atmospheric inputs. Hence, the findings of this study agree with previous studies suggesting that IUE and Fe-regulation strategies that diazotrophs possess are critical in defining the geographical distribution of diverse diazotrophs species (Fig. 5.4) according to Fe supply (Berman-Frank et al., 2007; Moore et al., 2009; Saito et al., 2014). Finally, the contrasting trends in the expression of the two HOs implied that *Cyanothece* may be one of the unicellular diazotrophs employing "hotbunking" for more efficient Fe-utilization.

5.2.4 Heme *b* synthesis and metabolism can be regulated at a transcript level for Fe conservation

The regulation of intracellular Fe concentrations may be originating from modifications in the expression of genes encoding proteins involved in the production, utilization or even degradation of Fe-containing cofactors. In general, changes at the transcription level are considered adaptation mechanisms of phytoplankton to Fe-limitation and have been observed in various phytoplankton species including cyanobacteria (e.g. Chappell and Webb, 2010; Ludwig and Bryant, 2012; Shi et al., 2007) and diatoms (Allen et al., 2008; Cohen et al., 2017, 2018; Marchetti et al., 2012; Smith et al., 2016). Heme oxygenase is the enzyme responsible for the metabolism of heme *b* (Beale and Cornejo, 1991; Frankenberg-Dinkel, 2004) and is considered to contribute to Fe conservation within the cells (Saito et al., 2011). Proteomic analysis in *Trichodesmium* demonstrated that the levels of HO increase in Fe-replete conditions (Snow et al., 2015a) and in unicellular diazotrophs (*Crocosphaera watsonii*), two HOs participate in diurnal oscillations of the hemoprotein pool for the separation of oxygenic photosynthesis with nitrogen fixation (Saito et al., 2011).

This PhD project (Chapter 4) showed that the genes encoding HO in *Trichodesmium* and *Cyanothece* remained downregulated when the concentration of Fe in the culturing media was low. Hence, this study demonstrated that the intracellular heme *b* concentrations can be controlled by changes in the expression of HO for conservation of the produced hemes and thus growth.

Some organisms possess more than one isoforms of HO (see Chapter 1) (Frankenberg-Dinkel, 2004). Interestingly, two studies in eukaryotic phytoplankton (Richaud and Zabulon, 1997; Smith et al., 2016) showed that the expression of a gene encoding HO

increased as a result of Fe depletion. Furthermore, Saito et al. (2011) documented via proteomic analysis that the two HOs of *Crocosphaera watsonii* behave in an opposite manner, meaning that when one HO was active the other was inactive and vice versa.

Here, the transcripts of one HO (*hmo1*) in *Cyanothece* increased during Fe limitation in contrast to the second HO (*hmo2*). An increase in the ratio of heme *b* relative to biomass was also observed implying that heme *b*-Fe increased despite the complete assimilation of the dissolved Fe from the culturing media.

The findings of this study imply that HOs may have two important roles in cyanobacteria; 1) the production of phycobilins for light harvesting and 2) the release of Fe from porphyrins. Hence, heme degradataion via HOs is of primary importance and during Fe limitation appeared to cause disruptions in HO activity which may have negative implications on phytoplankton's status. Furthermore, HOs remove the Fe atom from the porphyrin ring (Frankenberg-Dinkel, 2004; Frankenberg et al., 2003), therefore the activation of HO during Fe limitation by *Cyanothece* may be linked to recycling processes of the intracellular heme-bound Fe (Saito et al., 2011) or to Fe acquisition processes via exogenous heme uptake and transport through the membranes using heme-receptor proteins as observed for other bacterial species (Hopkinson et al., 2008; Roe et al., 2013; Septer et al., 2011; Weaver et al., 2003). The localization of HOs within the cell may be thus critical in defining their role, since HOs have been identified in the plasmid (Migita et al., 2003; Muramoto, 1999; Terry et al., 2002) and in the cytoplasm (Hopkinson et al., 2008; Roe et al., 2013; Septer et al., 2011; Weaver et al., 2003). Finally, this study enhances the previous assumptions (Hopkinson et al., 2008; Roe et al., 2013; Septer et al., 2011; Weaver et al., 2003) of Fe-uptake mechanisms via hemes employed by prokaryotes.

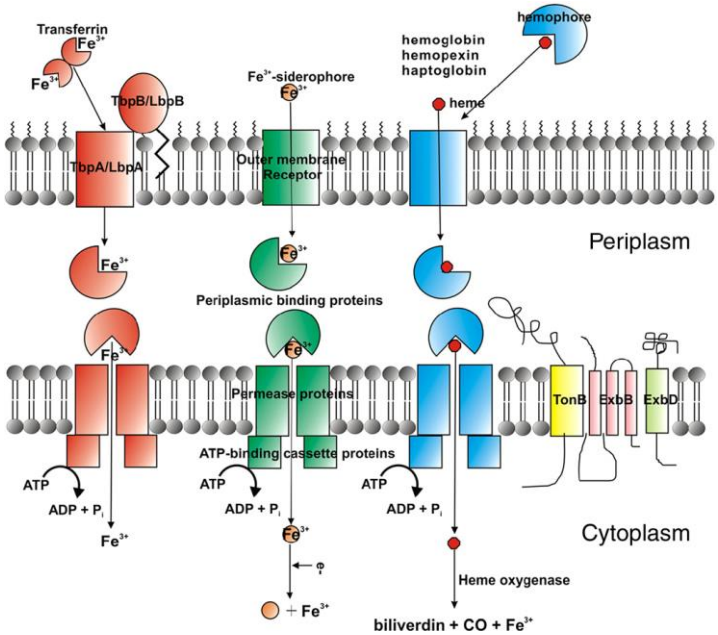

Fig. 5.5: Schematic representation of Fe uptake in Gram-negative bacteria after Krewulak and Vogel (2008). There are numerous Fe uptake pathways in Gram-negative bacteria which include Fe uptake from transferrin, siderophores,

or heme. All of these uptake pathways require an outer-membrane receptor, a periplasmic binding protein (PBP), and inner membrane ATP-binding cassette (ABC) transporter. Not all bacteria have all three systems; but some have more than one type.

5.3 Take home messages

This dissertation enhanced the previously published studies by giving a complete overview of the heme *b* abundance in the Atlantic Ocean, by identifying some of the processes driving the heme *b* abundance in cultured and field phytoplankton populations and by demonstrating that the heme *b* pool is subject to regulations for Fe conservation in diverse phytoplankton groups. Hence, this project contributed to the field of marine biogeochemistry by advancing the knowledge on the impact of Fe limitation on marine phytoplankton and on the physiological responses and adaptation potential of phytoplankton to changing Fe supply.

This study also contributed to the establishment of a simple method for the identification of Fe limited phytoplankton in the field which accounts for the ability of phytoplankton to optimize Fe use. Therefore, this study can provide a starting point for more detailed exploration of other oceanic areas. Finally, findings of this and future studies on hemes could potentially be implemented into global biogeochemical models and help us predict the implications of altering Fe fluxes on phytoplankton physiology and key biogeochemical cycles.

5.4 Future directions and outlook

5.4.1 Validation of heme *b* cut-off values of Fe limitation

This study demonstrated that heme *b* concentrations and quotas are a sign of Fe limited phytoplankton and provide an overview of the cellular activity of marine microbes *in situ*. Although Chapters 2 and 3 alongside previously published laboratory experiments (Gledhill et al., 2013, 2015; Honey et al., 2013) provided a solid documentation of the heme *b* concentrations and quotas that are indicative of Fe limitation, a comparison of the heme *b* method to other biomarkers or methods for mapping Fe limited phytoplankton would help establishing the cut-off values for Fe-limited phytoplankton. For example, heme *b* could be measured in field populations and compared to the established Fe-stress biomarkers such as flavodoxin (LaRoche et al., 1996), ferredoxin (Pankowski and McMinn, 2009), IdiA (Saito et al., 2014; Webb et al., 2001) and ISIP (Morrissey et al., 2015). Heme *b* concentrations and quotas could also be monitored during incubation bioassay experiments with Fe additions in field populations (Browning et al., 2014a; Moore et al., 2008; Nielsdóttir et al., 2009), even though sometimes bioassay experiments may not be representative of the mixed phytoplankton communities due to the positive response of faster growing organisms (e.g. diatoms) to nutrient additions (Price et al., 1994). Nevertheless, such comparisons with Fe stress biomarkers or Fe-addition incubation experiments would reinforce the current

observations that heme *b* is a good indicator of Fe limitation whilst validating this straightforward and method for mapping Fe limited phytoplankton.

5.4.2 Wider application of heme *b*

This work documented that heme *b* can be a reliable indicator of the status of marine microbes in terms of Fe availability and can contribute to the identification of Fe utilization strategies of marine phytoplankton. To date we possess field data only from the Atlantic Ocean thus this is sole oceanic region where we know how microbes utilize Fe in the heme *b* pool and how they respond to Fe supply. Therefore, it would be particularly interesting in the future to explore the abundance of heme *b* in other oceanic regions and identify the physiological status or Fe regulation strategies of other microbial communities.

Some areas worth exploring would be the Indian Ocean due to projected increased atmospheric Fe fluxes (Fig. 5.6) which may have a significant contribution to marine productivity and thus heme *b* utilization in the photosynthetic apparatus. Finally, application of heme *b* in areas remote from any atmospheric Fe sources like the Southern and the Pacific Oceans (Fig. 5.6) would enhance our knowledge about the adaptation-potential of other phytoplankton species to Fe limitation. Finally, this information could be incorporated into global biogeochemical models and reinforce the predictions on how oceanic Fe availability influences carbon sequestration patterns and in extent the climate.

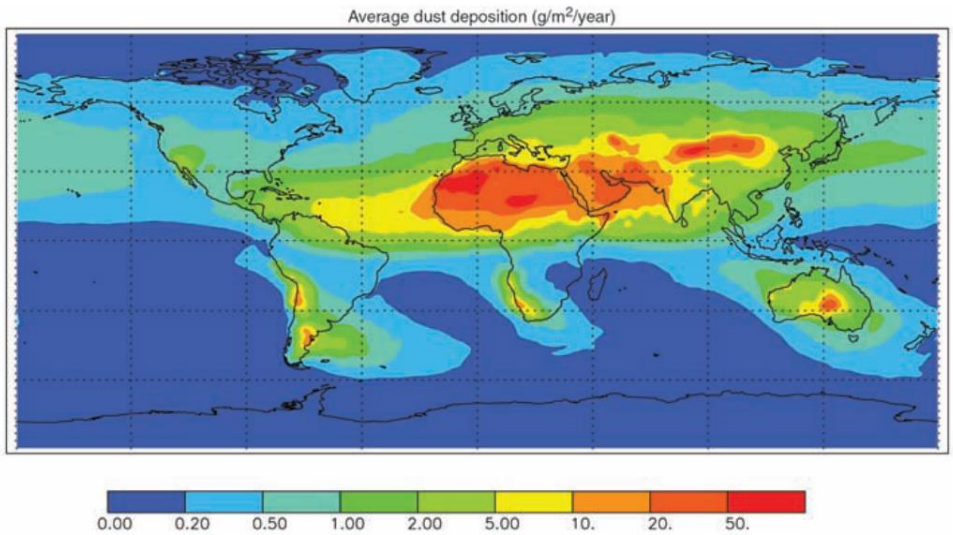

Fig. 5.6: *Dust fluxes to the world oceans after Jickells et al. (2005). Estimates are based on a composite of three published modeling studies that match satellite optical depth, in situ concentration, and deposition observations* (Ginoux et al., 2001; Mahowald and Luo, 2003; Tegen et al., 2004). *Percentage inputs to ocean basins based on this figure are as follows: North Atlantic, 43%; South Atlantic, 4%; North Pacific, 15%; South Pacific, 6%; Indian, 25%; and Southern Ocean, 6%*

5.4.3 Monitoring of heme *b* during an open-ocean bloom

Chapter 2 demonstrated that heme *b* depletion may be a regulatory mechanism of Fe allocation away from the hemoprotein pool serving for Fe conservation. Heme *b* depletion and regulation is likely to occur during shifts in phytoplankton populations as the bloom progresses as a result of the absolute Fe requirements of each phytoplankton group (Boyd et al., 2012; Ryan-Keogh et al., 2013, 2017; Strzepek et al., 2012) (e.g. shifts from diatoms to haptophytes). This finding suggests that this trend is likely to be observed multiple times during the bloom progression (Fig. 5.3) and would depend on Fe drawdown rates.

A limitation of the study presented in Chapter 2 is that sampling was carried out during a research expedition thus relying on one sampling point at a specific time. Therefore, a short-term effect cannot be eliminated from the findings and the interpretation of the results illustrated in Chapter 2. However, Bellworthy et al. (2017) monitored heme *b* abundance in a mesocosm experiment and showed that heme *b* concentrations were variable in time throughout the bloom progression whilst they decreased rapidly under nutrient depletion. Taking this into account, as a plan to advance the research presented in this thesis, the monitoring of heme *b* in concert with the community composition (e.g. identification of species 16S rDNA amplicon sequencing) over the course of an open-ocean phytoplankton bloom would shed light and confirm the statement mentioned in Chapter 2 and illustrated in Fig. 5.3. Such experiment would establish the idea that once the subsistence heme *b* quotas (and related Fe quota) can no longer be supported, the extant population becomes Fe limited. Hence, the whole community will become progressively limited only when the species with the lowest Fe requirement can no longer satisfy its subsistence Fe quota.

5.4.4 How is heme *b* regulated?

Heme *b* is contained in the cytochromes b_6f and b_{559} of photosystem II (PSII) and in nitrate reductase (Hogle et al., 2014). Chapter 2 illustrated that eukaryotic phytoplankton populations of Irminger Basin exhibited low heme *b* concentrations which, however were regulated for Fe and growth conservation. Hence, the reduction in heme *b* could be ascribed to regulation and decreases in the abundance of the cytochromes b_6f and b_{559} of the PSII apparatus (Greene et al., 1992; Strzepek and Harrison, 2004), which would reconcile the findings presented in Chapter 2 with the findings of Macey et al. (2014) who reported increases in chl *a* to PSII ratio in the Irminger Basin. Furthermore, the reduction of heme *b* in Irminger Basin (Chapter 2) could also be linked to reduction of nitrate reductase due to the switch from nitrate to ammonium utilization (Price et al., 1991; Timmermans et al., 1994) by the extant diatoms.

The identification of the molecular strategies of Fe regulation and of the origins of heme *b* regulation in the field was beyond the scope of this project. However, both

transcriptomic and proteomic analyses in field phytoplankton populations could be powerful tools for identification on how the available ambient Fe is utilized in the heme *b* pool and how production, utilization and degradation processes are influenced during Fe limitation.

To date, transcriptomic and proteomic analysis in diatom species (*Thalassiosira pseudonada*, *Thalassiosira oceanica and Pseudo-nitzschia granii*) showed that the heme *b*-containing cytochrome b_6f is downregulated whilst the expression of the PSII proteins remained stable (Cohen et al., 2018; Lommer et al., 2012; Nunn et al., 2013). In addition, molecular analysis in diatoms also showed that both the gene expression and activity of nitrate reductases decreased under low Fe conditions and that the abundance of ammonium transporter (AMT) proteins increased (Cohen et al., 2017; Marchetti et al., 2012; Nunn et al., 2013; Timmermans et al., 1994). Therefore, in order to fully establish how the ambient Fe is distributed into the heme *b* inventory and how the heme *b* pool is optimized during Fe limitation, the determination of transcripts and abundance of the heme *b*-containing proteins, such as cytochrome *b6* and nitrate reductase would provide useful information.

Finally, apart from the obvious heme *b*-containing proteins, other molecules are also associated with heme *b* abundance and cycling. For example, molecular analysis on i) associated proteins such as the ammonium transporters (AMT), that would indicate shifts to ammonium nutrition and declines in the heme *b*-containing nitrate reductase, and/or ii) proteins involved in the production or degradation of heme *b* (e.g. ferrochelatase or HO activity), may also be helpful in establishing heme *b* cycling patterns during Fe limitation in mixed phytoplankton communities. Finally, quantification of heme *b* precursors (e.g. PTP-IX) and breakdown products (e.g. bilirubin), which were identified at a preliminarily level in this study, may be useful in further investigations.

5.4.5 The role of heme oxygenases

This project showed a contrasting behavior between genes encoding two different HOs in the diazotroph *Cyanothece*. However, to date, little information exists regarding the processes involving HOs in eukaryotic phytoplankton (Richaud and Zabulon, 1997; Smith et al., 2016). Future research projects could incorporate in both field and laboratory experiments transcriptomic and proteomic investigations in eukaryotes for monitoring of the gene expression of HO, the actual protein levels alongside with the concentrations of heme *b* and its degradation products (e.g. bilirubin). This would expand the knowledge regarding HO to other phytoplankton classes and species rather than just bacteria.

We know that HOs are responsible for the cleavage of the porphyrin ring and release of Fe(II) (Frankenberg-Dinkel, 2004). Some studies have raised the hypothesis that HOs may also be involved in Fe acquisition processes in prokaryotes (Hopkinson et al.,

2008; Roe et al., 2013; Wandersman and Delepelaire, 2004) and diatoms (Smith et al., 2016) because of increases in the levels of some HOs during Fe limitation. The current project enhanced this hypothesis, thus it would be highly interesting to identify in future experiments which exactly is the role of HOs. This could be achieved for example by identification of membrane receptors for heme (Hopkinson et al., 2008) or single-cell imaging techniques for monitoring the distribution of Fe within the cells of diverse phytoplankton species.

5.4.6 Further experiments addressing previous assumptions and models

Studies in unicellular diazotrophs indicated that the hemoprotein pool is subject to diel variations (Saito et al., 2011) and that hemoproteins are labile protein pools (Espinas et al., 2012). Monitoring of heme *b* in cultured and/or field phytoplankton during day-night experiments would shed light on potential hemoprotein regulation strategies which can also be independent of Fe availability. The ideas mentioned in the previous sections (5.4.4, 5.4.5) could be implemented in such experiment (i.e. monitoring of HOs, nitrate reductase, cytochrome b_6f) providing information on what are the normal heme *b* diel cycling processes and how these potentially change during Fe limitation.

One limitation mentioned in Chapter 4 was the difficulty in maintaining and collecting samples from the two cultured species in the same growth phase thus complicating the interspecies comparison. The use of chemostats would improve the experimental conditions in studies involving cultured phytoplankton since the cultures would remain constantly in the exponential phase thus facilitating the sampling procedures and later on the interpretation of results. Furthermore, the use of chemostats would likely eliminate the variability in heme *b* resulting from the acclimation to the media after inoculation.

Finally, heme *b* is a very essential Fe-containing molecule but not the exclusively important heme cofactor within an organism. Future studies and research could focus on the development of analytical techniques for the determination of other heme structures such as heme *c*, which is the prosthetic group of the *c*-type cytochromes performing electron transfer (Bowman and Bren, 2008; Chapman et al., 1997). This would advance our knowledge regarding Fe utilization in the hemoprotein pool by phytoplankton and improve our current assessments of what is the impact of Fe limitation in the hemoprotein pool.

Bibliography

Achterberg, E. P., Moore, C. M., Henson, S. A., Steigenberger, S., Stohl, A., Eckhardt, S., et al. (2013). Natural iron fertilization by the Eyjafjallajökull volcanic eruption. *Geophys. Res. Lett.* 40, 921–926. doi:10.1002/grl.50221.

Achterberg, E. P., Steigenberger, S., Marsay, C. M., Lemoigne, F. A. C., Painter, S. C., Baker, A. R., et al. (2018). Iron Biogeochemistry in the High Latitude North Atlantic Ocean. *Sci. Rep.* 8, 1–15. doi:10.1038/s41598-018-19472-1.

Allen, A. E., LaRoche, J., Maheswari, U., Lommer, M., Schauer, N., Lopez, P. J., et al. (2008). Whole-cell response of the pennate diatom Phaeodactylum tricornutum to iron starvation. *Proc. Natl. Acad. Sci.* 105, 10438–10443. doi:10.1073/pnas.0711370105.

Allen, A. E., Ward, B. B., and Song, B. (2005). Characterization of diatom (bacillariophyceae) nitrate reductase genes and their detection in marine phytoplankton communities. *J. Phycol.* 41, 95–104. doi:10.1111/j.1529-8817.2005.04090.x.

Allnutt, F. C. T., and Bonner, W. D. (1987). Evaluation of Reductive Release as a Mechanism for Iron Uptake from Ferrioxamine B by Chlorella vulgaris *Plant Physiol.* 85, 751 LP – 756. doi:10.1104/pp.85.3.751.

Aminot, A., and Kerouel, R. (2007). *Dosage automatique des nutriments dans les eaux marines*. Quae ed.

Anderson, M. A., and Morel, F. M. M. (1982). The influence of aqueous iron chemistry on the uptake of iron by the coastal diatom Thalassiosira weissflogii. *Limnol. Oceanogr.* 27, 789–813. doi:10.4319/lo.1982.27.5.0789.

Aumont, O., Ethé, C., Tagliabue, A., Bopp, L., and Gehlen, M. (2015). PISCES-v2: An ocean biogeochemical model for carbon and ecosystem studies. *Geosci. Model Dev.* 8, 2465–2513. doi:10.5194/gmd-8-2465-2015.

Baker, A. R., and Croot, P. L. (2010). Atmospheric and marine controls on aerosol iron solubility in seawater. *Mar. Chem.* 120, 4–13. doi:10.1016/j.marchem.2008.09.003.

Beale, S. I. (1993). Biosynthesis of Phycobilins. *Chem. Rev.* 93, 785–802. doi:10.1021/cr00018a008.

Beale, S. I. (2007). "Biosynthesis of Open-Chain Tetrapyrroles in Plants, Algae, and Cyanobacteria," in *Ciba Foundation Symposium 180 - The Biosynthesis of the Tetrapyrrole Pigments* Novartis Foundation Symposia., 156–176. doi:10.1002/9780470514535.ch9.

Beale, S. I., and Cornejo, J. (1984). Enzymatic heme oxygenase activity in soluble extracts of the unicellular red alga, Cyanidium caldarium. *Arch. Biochem. Biophys.* 235, 371–384. doi:10.1016/0003-9861(84)90210-8.

Beale, S. I., and Cornejo, J. (1991). Biosynthesis of Phycobilins. *J. Biol. Chem.* 266, 22328–22332.

Beale, S. I., and Yeh, J. I. (1999). Deconstructing heme. *Nat. Struct. Biol.* 6, 903–905.

doi:10.1038/13264.

Behrenfeld, M. J., Bale, A. J., Kolber, Z. S., Aiken, J., and Falkowski, P. G. (1996). Confirmation of iron limitation of phytoplankton photosynthesis in the equatorial Pacific Ocean. *Nature* 383, 508–511. doi:10.1038/383508a0.

Behrenfeld, M. J., Boss, E., Siegel, D. A., and Shea, D. M. (2005). Carbon-based ocean productivity and phytoplankton physiology from space. *Global Biogeochem. Cycles* 19, 1–14. doi:10.1029/2004GB002299.

Behrenfeld, M. J., Westberry, T. K., Boss, E. S., O'Malley, R. T., Siegel, D. A., Wiggert, J. D., et al. (2009). Satellite-detected fluorescence reveals global physiology of ocean phytoplankton. *Biogeosciences* 6, 779–794. doi:10.5194/bg-6-779-2009.

Bellworthy, J., Gledhill, M., Esposito, M., and Achterberg, E. P. (2017). Abundance of the iron containing biomolecule, heme b, during the progression of a spring phytoplankton bloom in a mesocosm experiment. *PLoS One* 12, e0176268. doi:10.1371/journal.pone.0176268.

Bergman, B., Sandh, G., Lin, S., Larsson, J., and Carpenter, E. J. (2013). Trichodesmium - a widespread marine cyanobacterium with unusual nitrogen fixation properties. *FEMS Microbiol. Rev.* 37, 286–302. doi:10.1111/j.1574-6976.2012.00352.x.

Berman-Frank, I., Cullen, J. T., Shaked, Y., Sherrell, R. M., and Falkowski, P. G. (2001a). Iron availability, cellular iron quotas, and nitrogen fixation in Trichodesmium. *Limnol. Oceanogr.* 46, 1249–1260. doi:10.4319/lo.2001.46.6.1249.

Berman-Frank, I., Lundgren, P., Chen, Y. B., Kupper, H., Kolber, Z., Bergman, B., et al. (2001b). Segregation of nitrogen fixation and oxygenic photosynthesis in the marine cyanobacterium Trichodesmium. *Science (80-.).* 294, 1534–1537. doi:10.1126/science.1064082.

Berman-Frank, I., Quigg, A., Finkel, Z. V., Irwin, A. J., and Haramaty, L. (2007). Nitrogen-fixation strategies and Fe requirements in cyanobacteria. *Limnol. Oceanogr.* 52, 2260–2269. doi:10.4319/lo.2007.52.5.2260.

Bernroitner, M., Zamocky, M., Furtmüller, P. G., Peschek, G. A., and Obinger, C. (2009). Occurrence, phylogeny, structure, and function of catalases and peroxidases in cyanobacteria. *J. Exp. Bot.* 60, 423–440. doi:10.1093/jxb/ern309.

Bibby, T. S., Nield, J., and Barber, J. (2001). Iron deficiency induces the formation of an antenna ring around trimeric photosystem I in cyanobacteria. *Nature* 412, 743.

Blaby-Haas, C. E., and Merchant, S. S. (2012). The ins and outs of algal metal transport. *Biochim. Biophys. Acta - Mol. Cell Res.* 1823, 1531–1552. doi:10.1016/j.bbamcr.2012.04.010.

Bowie, A. R., Lannuzel, D., Remenyi, T. A., Wagener, T., Lam, P. J., Boyd, P. W., et al. (2009). Biogeochemical iron budgets of the Southern Ocean south of Australia: Decoupling of iron and nutrient cycles in the subantarctic zone by the summertime supply. *Global Biogeochem. Cycles* 23, 1–14. doi:10.1029/2009GB003500.

Bowie, A. R., Maldonado, M. T., Frew, R. D., Croot, P. L., Achterberg, E. P., Mantoura, R. F. C., et al. (2008). Topical Studies in Oceanography : The fate of added iron during a mesoscale fertilisation experiment in the Southern Ocean.

Deep Sea Res. Part II 48, 2703–2743. doi:10.1016/S0967-0645(01)00015-7.

Bowler, C., Vardi, A., and Allen, A. E. (2009). Oceanographic and Biogeochemical Insights from Diatom Genomes. *Ann. Rev. Mar. Sci.* 2, 333–365. doi:10.1146/annurev-marine-120308-081051.

Bowman, S. E. J., and Bren, K. L. (2008). The chemistry and biochemistry of hemec: functional bases for covalent attachment. *Nat. Prod. Rep.* 25, 1118–1130. doi:10.1039/B717196J.

Boyd, P. W., Arrigo, K. R., Strzepek, R., and Van Dijken, G. L. (2012). Mapping phytoplankton iron utilization: Insights into Southern Ocean supply mechanisms. *J. Geophys. Res. Ocean.* 117, 1–18. doi:10.1029/2011JC007726.

Boyd, P. W., and Ellwood, M. J. (2010). The biogeochemical cycle of iron in the ocean. *Nat. Geosci.* 3, 675–682. doi:10.1038/ngeo964.

Boyd, P. W., Jickells, T., Law, C. S., Blain, S., Boyle, E. A., Buesseler, K. O., et al. (2007). Mesoscale Iron Enrichment Experiments 1993-2005: Synthesis and Future Directions. *Science (80-.).* 315, 612–617. doi:10.1126/science.1131669.

Boyd, P. W., Watson, A. J., Law, C. S., Abraham, E. R., Trull, R., Murdoch, R., et al. (2000). Phytoplankton bloom upon mesoscale iron fertilization of polar Southern Ocean waters. *Nature* 407, 695–702. doi:10.1038/35037500.

Browning, T. J., Achterberg, E. P., Rapp, I., Engel, A., Bertrand, E. M., Tagliabue, A., et al. (2017a). Nutrient co-limitation at the boundary of an oceanic gyre. *Nature* 551, 242–246. doi:10.1038/nature24063.

Browning, T. J., Achterberg, E. P., Yong, J. C., Rapp, I., Utermann, C., Engel, A., et al. (2017b). Iron limitation of microbial phosphorus acquisition in the tropical North Atlantic. *Nat. Commun.* 8, 15465. doi:10.1038/ncomms15465.

Browning, T. J., Bouman, H. A., Moore, C. M., Schlosser, C., Tarran, G. A., Woodward, E. M. S., et al. (2014a). Nutrient regimes control phytoplankton ecophysiology in the South Atlantic. *Biogeosciences* 11, 463–479. doi:10.5194/bg-11-463-2014.

Browning, T. J., Bouman, H. A., and Moore, M. C. (2014b). Satellite-detected fluorescence: decouplingnonphotochemical quenching from ironstress signals in the South Atlantic and Southern Ocean. *Global Biogeochem. Cycles* 28, 510–524. doi:10.1002/2013GB004773.

Brzezinski, M. A., Krause, J. W., and Goericke R., L. M. R. and S. M. R. B. R. M. B. K. A. F. P. (2015). Enhanced silica ballasting from itron stress sustrains carbon export in a frontal zone within the California Current. *J. Geophys. Res. Ocean.* 120, 4654–4669. doi:10.1002/2015JC010829.

Butler, A. (2005). Marine Siderophores and Microbial Iron Mobilization. *Biometals* 18, 369–374. doi:10.1007/s10534-005-3711-0.

Butler, A., and Theisen, R. M. (2010). Iron(III)–siderophore coordination chemistry: Reactivity of marine siderophores. *Coord. Chem. Rev.* 254, 288–296. doi:https://doi.org/10.1016/j.ccr.2009.09.010.

Capone, D. G. (1997). Trichodesmium, a Globally Significant Marine Cyanobacterium. *Science (80-.).* 276, 1221–1229. doi:10.1126/science.276.5316.1221.

Capone, D. G. (2001). Marine nitrogen fixation: what's the fuss? *Curr. Opin.*

Microbiol. 4, 341–348. doi:10.1016/S1369-5274(00)00215-0.

Capone, D. G., Burns, J. A., Montoya, J. P., Subramaniam, A., Mahaffey, C., Gunderson, T., et al. (2005). Nitrogen fixation by Trichodesmium spp.: An important source of new nitrogen to the tropical and subtropical North Atlantic Ocean. *Global Biogeochem. Cycles* 19, 1–17. doi:10.1029/2004GB002331.

Caporaso, J. G., Bittinger, K., Bushman, F. D., Desantis, T. Z., Andersen, G. L., and Knight, R. (2010a). PyNAST: A flexible tool for aligning sequences to a template alignment. *Bioinformatics* 26, 266–267. doi:10.1093/bioinformatics/btp636.

Caporaso, J. G., Kuczynski, J., Stombaugh, J., Bittinger, K., Bushman, F. D., Costello, E. K., et al. (2010b). QIIME allows analysis of high-throughput community sequencing data. *Nat. Methods* 7, 335–336. doi:10.1038/nmeth.f.303.

Caughey, W. S., Barlow, C. H., O'Keeffe, D. H., and O'Toole, M. C. (1973). Spectroscopic studies of cis and trans effects in hemes and hemins. *Ann. N. Y. Acad. Sci.* 206, 296–309. doi:10.1111/j.1749-6632.1973.tb43218.x.

Caughey, W. S., Smythe, G. A., O'Keeffe, D. H., Maskasky, J. E., and Smith, M. I. (1975). Heme A of cytochrome c oxicase. Structure and properties: comparisons with hemes B, C, and S and derivatives. *J. Biol. Chem.* 250, 7602–7622.

Chapman, S. K., Daff, S., and Munro, A. W. (1997). "Heme: The most versatile redox centre in biology?," in *Metal Sites in Proteins and Models: Iron Centres*, eds. H. A. O. Hill, P. J. Sadler, and A. J. Thomson (Berlin, Heidelberg: Springer Berlin Heidelberg), 39–70. doi:10.1007/3-540-62870-3_2.

Chappell, P. D., Moffett, J. W., Hynes, A. M., and Webb, E. A. (2012). Molecular evidence of iron limitation and availability in the global diazotroph Trichodesmium. *ISME J.* 6, 1728–1739. doi:10.1038/ismej.2012.13.

Chappell, P. D., and Webb, E. A. (2010). A molecular assessment of the iron stress response in the two phylogenetic clades of Trichodesmium. *Environ. Microbiol.* 12, 13–27. doi:10.1111/j.1462-2920.2009.02026.x.

Charlson, R. J., Lovelock, J. E., Andreae, M. O., and Warren, S. G. (1987). Oceanic phytoplankton, atmospheric sulphur, cloud albedo and climate. *Nature* 326, 655–661. doi:10.1038/326655a0.

Chen, Y.-B., Zehr, J. P., and Mellon, M. (1996). Growth and nitrogen fixation of the diazotrophic filamentous nonheterocystous cyanobacterium trichodesmium sp. Ims 101 in defined media: evidence for a circadian rhythm. *J. Phycol.* 32, 916–923. doi:10.1111/j.0022-3646.1996.00916.x.

Chever, F., Sarthou, G., Bucciarelli, E., Blain, S., and Bowie, A. R. (2010). An iron budget during the natural iron fertilisation experiment KEOPS (Kerguelen Islands, Southern Ocean). *Biogeosciences* 7, 455–468. doi:10.5194/bg-7-455-2010.

Coale, K. H., Wang, X., Tanner, S. J., and Johnson, K. S. (2003). Phytoplankton growth and biological response to iron and zinc addition in the Ross Sea and Antarctic Circumpolar Current along 170°W. *Deep. Res. Part II Top. Stud. Oceanogr.* 50, 635–653. doi:10.1016/S0967-0645(02)00588-X.

Cohen, N. R., Ellis, K. A., Lampe, R. H., McNair, H., Twining, B. S., Maldonado, M. T., et al. (2017). Diatom Transcriptional and Physiological Responses to Changes in Iron Bioavailability across Ocean Provinces. *Front. Mar. Sci.* 4, 360. doi:10.3389/fmars.2017.00360.

Cohen, N. R., Gong, W., Moran, D. M., McIlvin, M. R., Saito, M. A., and Marchetti, A. (2018). Transcriptomic and proteomic responses of the oceanic diatom Pseudo-nitzschia granii to iron limitation. *Environ. Microbiol.* 20, 3109–3126. doi:10.1111/1462-2920.14386.

Comeau, A. M., Douglas, G. M., and Langille, M. G. I. (2017). Microbiome Helper: a Custom and Streamlined Workflow for Microbiome Research. *mSystems* 2. doi:10.1128/mSystems.00127-16.

Comeau, A. M., Harding, T., Galand, P. E., Vincent, W. F., and Lovejoy, C. (2012). Vertical distribution of microbial communities in a perennially stratified Arctic lake with saline, anoxic bottom waters. *Sci. Rep.* 2, 604. doi:10.1038/srep00604.

Cornah, J. E., Terry, M. J., and Smith, A. G. (2003). Green or red: what stops the traffic in the tetrapyrrole pathway? *Trends Plant Sci.* 8, 224–230. doi:10.1016/S1360-1385(03)00064-5.

Cornejo, J., and Beale, S. I. (1988). Algal heme oxygenase from Cyanidium caldarium. Partial purification and fractionation into three required protein components. *J. Biol. Chem.* 263, 11915–11921.

Cornejo, J., and Beale, S. I. (1997). Phycobilin biosynthetic reactions in extracts of cyanobacteria. *Photosynth. Res.* 51, 223–230.

Cornejo, J., Willows, R. D., and Beale, S. I. (1998). Phytobilin biosynthesis: Cloning and expression of a gene encoding soluble ferredoxin-dependent heme oxygenase from Synechocystis sp. PCC 6803. *Plant J.* 15, 99–107. doi:10.1046/j.1365-313X.1998.00186.x.

Crane, B. R., Siegel, L. M., and Getzoff, E. D. (1995). Sulfite Reductase Structure at 1.6 : Evolution and Catalysis for Reduction of Inorganic Anions. *Science (80-.).* 270, 59–67. doi:10.1126/science.270.5233.59.

Cullen, J. J. (1982). The Deep Chlorophyll Maximum: Comparing Vertical Profiles of Chlorophyll a. *Can. J. Fish. Aquat. Sci.* 39, 791–803. doi:10.1139/f82-108.

Cullen, J. J. (1991). Hypotheses to explain high-nutrient conditions in the open sea. *Limnol. Oceanogr.* 36, 1578–1599. doi:10.4319/lo.1991.36.8.1578.

da Silva, J. J. R. F., and Williams, R. J. P. (2001). *The Biological Chemistry of the Elements: The Inorganic Chemistry of Life*. OUP Oxford Available at: https://books.google.de/books?id=qXbKF1Pw_GsC.

Dailey, H. A., Dailey, T. A., Gerdes, S., Jahn, D., Jahn, M., O'Brian, M. R., et al. (2017). Prokaryotic Heme Biosynthesis: Multiple Pathways to a Common Essential Product. *Microbiol. Mol. Biol. Rev.* 81, 1–62. doi:10.1128/MMBR.00048-16.

Dailey, H. A., and Gerdes, S. (2015). HemQ: An iron-coproporphyrin oxidative decarboxylase for protoheme synthesis in Firmicutes and Actinobacteria. *Arch. Biochem. Biophys.* 574, 27–35. doi:10.1016/j.abb.2015.02.017.

Dailey, H. A., Gerdes, S., Dailey, T. A., Burch, J. S., and Phillips, J. D. (2015). Noncanonical coproporphyrin-dependent bacterial heme biosynthesis pathway that does not use protoporphyrin. *Proc. Natl. Acad. Sci.* 112, 2210 LP – 2215. doi:10.1073/pnas.1416285112.

de Baar, H. J. W., Boyd, P. W., Coale, K. H., Landry, M. R., Tsuda, A., Assmy, P., et

al. (2005). Synthesis of iron fertilization experiments: From the iron age in the age of enlightenment. *J. Geophys. Res. C Ocean.* 110, 1–24. doi:10.1029/2004JC002601.

Decelle, J., Romac, S., Stern, R. F., Bendif, E. M., Zingone, A., Audic, S., et al. (2015). PhytoREF: A reference database of the plastidial 16S rRNA gene of photosynthetic eukaryotes with curated taxonomy. *Mol. Ecol. Resour.* 15, 1435–1445. doi:10.1111/1755-0998.12401.

Diaz, J. M., and Plummer, S. (2018). Production of extracellular reactive oxygen species by phytoplankton: past and future directions. *J. Plankton Res.* doi:10.1093/plankt/fby039.

Dos Santos, P. C., Dean, D. R., Hu, Y., and Ribbe, M. W. (2004). Formation and Insertion of the Nitrogenase Iron−Molybdenum Cofactor. *Chem. Rev.* 104, 1159–1174. doi:10.1021/cr020608l.

Duggen, S., Olgun, N., Croot, P., Hoffmann, L., Dietze, H., Delmelle, P., et al. (2010). The role of airborne volcanic ash for the surface ocean biogeochemical iron-cycle: A review. *Biogeosciences* 7, 827–844. doi:10.5194/bg-7-827-2010.

Dutkiewicz, S., Follows, M. J., and Parekh, P. (2005). Interactions of the iron and phosphorus cycles: A three-dimensional model study. *Global Biogeochem. Cycles* 19, 1–22. doi:10.1029/2004GB002342.

Elder, G. H., and Roberts, A. G. (1995). Uroporphyrinogen decarboxylase. *J. Bioenerg. Biomembr.* 27, 207–214. doi:10.1007/BF02110035.

Elrod, V. A., Berelson, W. M., Coale, K. H., and Johnson, K. S. (2004). The flux of iron from continental shelf sediments: A missing source for global budgets. *Geophys. Res. Lett.* 31. doi:10.1029/2004GL020216.

Erdner, D. L., and Anderson, D. M. (1999). Ferredoxin and flavodoxin as biochemical indicators of iron limitation during open-ocean iron enrichment. *Limnol. Oceanogr.* 44, 1609–1615. doi:10.4319/lo.1999.44.7.1609.

Espinas, N. A., Kobayashi, K., Takahashi, S., Mochizuki, N., and Masuda, T. (2012). Evaluation of Unbound Free Heme in Plant Cells by Differential Acetone Extraction. *Plant Cell Physiol.* 53, 1344–1354. doi:10.1093/pcp/pcs067.

Falkowski, P., Falkowski, P., Scholes, R. J., Boyle, E., Canadell, J., Canfield, D., et al. (2011). The Global Carbon Cycle : A Test of Our Knowledge of Earth as a System. *Science (80-.).* 291, 290–296. doi:10.1126/science.290.5490.291.

Falkowski, P. G. (1994). The role of phytoplankton photosynthesis in global biogeochemical cycles. *Photosynth. Res.* 39, 235–258. doi:10.1007/BF00014586.

Falkowski, P. G. (1997). Evolution of the Nitrogen-Cycle and Its Influence on the Biological Sequestration of CO2 in the Ocean. *Nature* 387, 272–275.

Falkowski, P., and Kiefer, D. A. (1985). Chlorophyll a fluorescence in phytoplankton: relationship to photosynthesis and biomass. *J. Plankton Res.* 7, 715–731. doi:10.1093/plankt/7.5.715.

Falkowski, P., and Kolber, Z. (1995). Variations in Chlorophyll Fluorescence Yields in Phytoplankton in the World Oceans. *Funct. Plant Biol.* 22, 341. doi:10.1071/PP9950341.

Ferreira, G. C. (1999). Ferrochelatase. *Int. J. Biochem. Cell Biol.* 31, 995–1000.

doi:10.1016/S1357-2725(99)00066-7.

Field, C. B., Behrenfeld, M. J., Randerson, J. T., and Falkowski, P. (1998). Primary Production of the Biosphere: Integrating Terrestrial and Oceanic Components. *Science (80-.).* 281, 237 LP – 240. doi:10.1126/science.281.5374.237.

Finzi-Hart, J. a, Pett-Ridge, J., Weber, P. K., Popa, R., Fallon, S. J., Gunderson, T., et al. (2009). Fixation and fate of C and N in the cyanobacterium Trichodesmium using nanometer-scale secondary ion mass spectrometry. *Proc. Natl. Acad. Sci. U. S. A.* 106, 6345–50. doi:10.1073/pnas.0810547106.

Fischer, K., Barbier, G. G., Hecht, H.-J., Mendel, R. R., Campbell, W. H., and Schwarz, G. (2005). Structural basis of eukaryotic nitrate reduction: crystal structures of the nitrate reductase active site. *Plant Cell* 17, 1167–1179. doi:10.1105/tpc.104.029694.

Fragoso, G. M., Poulton, A. J., Yashayaev, I. M., Head, E. J. H., and Purdie, D. A. (2017). Spring phytoplankton communities of the Labrador Sea (2005-2014): Pigment signatures, photophysiology and elemental ratios. *Biogeosciences* 14, 1235–1259. doi:10.5194/bg-14-1235-2017.

Fragoso, G. M., Poulton, A. J., Yashayaev, I. M., Head, E. J. H., Stinchcombe, M. C., and Purdie, D. A. (2016). Biogeographical patterns and environmental controls of phytoplankton communities from contrasting hydrographical zones of the Labrador Sea. *Prog. Oceanogr.* 141, 212–226. doi:10.1016/j.pocean.2015.12.007.

Frankenberg-Dinkel, N. (2004). Bacterial Heme Oxygenases. *Antioxid. Redox Signal.* 6, 825–834. doi:10.1089/ars.2004.6.825.

Frankenberg, N., Erskine, P. T., Cooper, J. B., Shoolingin-Jordan, P. M., Jahn, D., and Heinz, D. W. (1999). High resolution crystal structure of a Mg2+-dependent porphobilinogen synthase. *J. Mol. Biol.* 289, 591–602. doi:10.1006/jmbi.1999.2808.

Frankenberg, N., Moser, J., and Jahn, D. (2003). Bacterial heme biosynthesis and its biotechnological application. *Appl. Microbiol. Biotechnol.* 63, 115–127. doi:10.1007/s00253-003-1432-2.

Fraser, J. M., Tulk, S. E., Jeans, J. A., Campbell, D. A., Bibby, T. S., and Cockshutt, A. M. (2013). Photophysiological and Photosynthetic Complex Changes during Iron Starvation in Synechocystis sp. PCC 6803 and Synechococcus elongatus PCC 7942. *PLoS One* 8, e59861. doi:10.1371/journal.pone.0059861.

Fu, F. X., and Bell, P. R. F. (2003). Growth, N2 fixation and photosynthesis in a cyanobacterium, Trichodesmium sp., under Fe stress. *Biotechnol. Lett.* 25, 645–649. doi:10.1023/A:1023068232375.

Gao, Y., Smith, G. J., and Alberte, R. S. (1993). Nitrate Reductase from the Marine Diatom Skeletonema costatum (Biochemical and Immunological Characterization). *Plant Physiol.* 103, 1437–1445. doi:10.1104/pp.103.4.1437.

Gaudana, S. B., Krishnakumar, S., Alagesan, S., Digmurti, M. G., Viswanathan, G. A., Chetty, M., et al. (2013). Rhythmic and sustained oscillations in metabolism and gene expression of Cyanothece sp. ATCC 51142 under constant light. *Front. Microbiol.* 4, 1–11. doi:10.3389/fmicb.2013.00374.

Geider, R. J. (1999). Complex lessons of iron uptake. *Nature* 400, 815–816. doi:10.1038/23582.

Geider, R. J., and La Roche, J. (1994). The role of iron in phytoplankton photosynthesis, and the potential for iron-limitation of primary productivity in the sea. *Photosynth. Res.* 39, 275–301. doi:10.1007/BF00014588.

Gerringa, L. J. A., Alderkamp, A.-C., Laan, P., Thuróczy, C.-E., De Baar, H. J. W., Mills, M. M., et al. (2012). Iron from melting glaciers fuels the phytoplankton blooms in Amundsen Sea (Southern Ocean): Iron biogeochemistry. *Deep Sea Res. Part II Top. Stud. Oceanogr.* 71–76, 16–31. doi:10.1016/j.dsr2.2012.03.007.

Ginoux, P., Chin, M., Tegen, I., Prospero, J. M., Holben, B., Dubovik, O., et al. (2001). Sources and distributions of dust aerosols simulated with the GOCART model. *J. Geophys. Res. Atmos.* 106, 20255–20273. doi:10.1029/2000JD000053.

Giordano, M., Norici, A., and Hell, R. (2005). Sulfur and phytoplankton: acquisition, metabolism and impact on the environment. *New Phytol.* 166, 371–382. doi:10.1111/j.1469-8137.2005.01335.x.

Gledhill, M. (2007). The determination of heme b in marine phyto- and bacterioplankton. *Mar. Chem.* 103, 393–403. doi:10.1016/j.marchem.2006.10.008.

Gledhill, M. (2014). The detection of iron protoporphyrin (heme b) in phytoplankton and marine particulate material by electrospray ionisation mass spectrometry - comparison with diode array detection. *Anal. Chim. Acta* 841, 33–43. doi:10.1016/j.aca.2014.06.045.

Gledhill, M., Achterberg, E. P., Honey, D. J., Nielsdottir, M. C., and Rijkenberg, M. J. A. (2013). Distributions of particulate Heme b in the Atlantic and Southern Oceans - Implications for electron transport in phytoplankton. *Global Biogeochem. Cycles* 27, 1072–1082. doi:10.1002/2013GB004639.

Gledhill, M., and Buck, K. N. (2012). The organic complexation of iron in the marine environment: A review. *Front. Microbiol.* 3, 1–17. doi:10.3389/fmicb.2012.00069.

Gledhill, M., Gerringa, L. J. A., Laan, P., and Timmermans, K. R. (2015). Heme b quotas are low in Southern Ocean phytoplankton. *Mar. Ecol. Prog. Ser.* 532, 29–40. doi:10.3354/meps11345.

Goldman, S. J., Lammers, P. J., Berman, M. S., and Sanders-Loehr, J. (1983). Siderophore-mediated iron uptake in different strains of Anabaena sp. *J. Bacteriol.* 156, 1144–1150.

Greene, R. M., Geider, R. J., Kolber, Z., and Falkowski, P. G. (1992). Iron-Induced Changes in Light Harvesting and Photochemical Energy Conversion Processes in Eukaryotic Marine Algae. *Plant Physiol.* 100, 565–575. doi:10.1104/pp.100.2.565.

Greene, R. M., Kolber, Z. S., Swift, D. G., Tindale, N. W., and Falkowski, P. G. (1994). Physiological limitation of phytoplankton photosynthesis in the eastern equatorial Pacific determined from variability in the quantum yield of fluorescence. *Limnol. Oceanogr.* 39, 1061–1074. doi:10.4319/lo.1994.39.5.1061.

Guskov, A., Kern, J., Gabdulkhakov, A., Broser, M., Zouni, A., and Saenger, W. (2009). Cyanobacterial photosystem II at 2.9-Å resolution and the role of quinones, lipids, channels and chloride. *Nat. Struct. Mol. Biol.* 16, 334–342. doi:10.1038/nsmb.1559.

Harrison, W. G., Børsheim, K. Y., Li, W. K. W., Maillet, G. L., Pepin, P., Sakshaug, E., et al. (2013). Phytoplankton production and growth regulation in the Subarctic North Atlantic: A comparative study of the Labrador Sea-Labrador/Newfoundland

shelves and Barents/Norwegian/Greenland seas and shelves. *Prog. Oceanogr.* 114, 26–45. doi:10.1016/j.pocean.2013.05.003.

Hart, G. J., and Battersby, A. R. (1985). Purification and properties of uroporphyrinogen III synthase (co-synthetase) from Euglena gracilis. *Biochem. J.* 232, 151–160. doi:10.1042/bj2320151.

Hart, G. J., Miller, A. D., Leeper, F. J., and Battersby, A. R. (1987). Biosynthesis of the natural porphyrins: proof that hydroxymethylbilane synthase (porphobilinogen deaminase) uses a novel binding group in its catalytic action. *J. Chem. Soc. Chem. Commun.*, 1762–1765. doi:10.1039/C39870001762.

Henson, S. A., Dunne, J. P., and Sarmiento, J. L. (2009). Decadal variability in North Atlantic phytoplankton blooms. *J. Geophys. Res. Ocean.* 114, 1–11. doi:10.1029/2008JC005139.

Henson, S. A., Sanders, R., Holeton, C., and Allen, J. T. (2006). Timing of nutrient depletion, diatom dominance and a lower-boundary estimate of export production for Irminger Basin, North Atlantic. *Mar. Ecol. Prog. Ser.* 313, 73–84. doi:10.3354/meps313073.

Hickman, A. E., Moore, C. M., Sharples, J., Lucas, M. I., Tilstone, G. H., Krivtsov, V., et al. (2012). Primary production and nitrate uptake within the seasonal thermocline of a stratified shelf sea. *Mar. Ecol. Prog. Ser.* 463, 39–57. doi:10.3354/meps09836.

Ho, T.-Y. (2013). Nickel limitation of nitrogen fixation in Trichodesmium. *Limnol. Oceanogr.* 58, 112–120. doi:10.4319/lo.2013.58.1.0112.

Ho, T.-Y., Quigg, A., Finkel, Z. V., Milligan, A. J., Wyman, K., Falkowski, P. G., et al. (2003). The elemental composition of some marine phytoplankton. *J. Phycol.* 39, 1145–1159. doi:10.1111/j.0022-3646.2003.03-090.x.

Hogle, S. L., Dupont, C. L., Hopkinson, B. M., King, A. L., Buck, K. N., Roe, K. L., et al. (2018). Pervasive iron limitation at subsurface chlorophyll maxima of the California Current. *Proc. Natl. Acad. Sci.* 115, 13300–13305. doi:10.1073/pnas.1813192115.

Hogle, S. L. S., Barbeau, K. a, and Gledhill, M. (2014). Heme in the marine environment: from cells to the iron cycle. *Metallomics* 6, 1107–1120. doi:10.1039/C4MT00031E.

Hogle, S. L., Thrash, J. C., Dupont, C. L., and Barbeau, K. A. (2016). Trace Metal Acquisition by Marine Heterotrophic Bacterioplankton with Contrasting Trophic Strategies. *Appl. Environ. Microbiol.* 82, 1613 LP – 1624. doi:10.1128/AEM.03128-15.

Hohmann-Marriott, M. F., and Blankenship, R. E. (2011). Evolution of Photosynthesis. *Annu. Rev. Plant Biol.* 62, 515–548. doi:10.1146/annurev-arplant-042110-103811.

Holm-Hansen, O., and Hewes, C. D. (2004). Deep chlorophyll-a maxima (DCMs) in Antarctic waters: I. Relationships between DCMs and the physical, chemical, and optical conditions in the upper water column. *Polar Biol.* 27, 699–710. doi:10.1007/s00300-004-0641-1.

Honey, D. J. (2012). Heme b in marine cyanobacteria and the (sub-) tropical North Atlantic. Available at: https://eprints.soton.ac.uk/id/eprint/359063.

Honey, D. J., Gledhill, M., Bibby, T. S., Legiret, F. E., Pratt, N. J., Hickman, A. E., et al. (2013). Heme b in marine phytoplankton and particulate material from the North Atlantic Ocean. *Mar. Ecol. Prog. Ser.* 483, 1–17. doi:10.3354/meps10367.

Hopkinson, B. M., Roe, K. L., and Barbeau, K. A. (2008). Heme uptake by Microscilla marina and evidence for heme uptake systems in the genomes of diverse marine bacteria. *Appl. Environ. Microbiol.* 74, 6263–6270. doi:10.1128/AEM.00964-08.

Hopwood, M. J., Carroll, D., Browning, T. J., Meire, L., Mortensen, J., Krisch, S., et al. (2018). Non-linear response of summertime marine productivity to increased meltwater discharge around Greenland. *Nat. Commun.* 9. doi:10.1038/s41467-018-05488-8.

Howard, J. B., and Rees, D. C. (1996). Structural Basis of Biological Nitrogen Fixation. *Chem. Rev.* 96, 2965–2982. doi:10.1021/cr9500545.

Huot, Y., Franz, B. A., and Fradette, M. (2013). Estimating variability in the quantum yield of Sun-induced chlorophyll fluorescence: A global analysis of oceanic waters. *Remote Sens. Environ.* 132, 238–253. doi:10.1016/j.rse.2013.01.003.

Hutchins, D. A., Franck, V. M., Brzezinski, M. A., and Bruland, K. W. (1999). Inducing phytoplankton iron limitation in iron-replete coastal waters with a strong chelating ligand. *Limnol. Oceanogr.* 44, 1009–1018. doi:10.4319/lo.1999.44.4.1009.

Jacq, V., Ridame, C., L'Helguen, S., Kaczmar, F., and Saliot, A. (2014). Response of the unicellular diazotrophic cyanobacterium Crocosphaera watsonii to iron limitation. *PLoS One* 9. doi:10.1371/journal.pone.0086749.

Jaffe, E. K. (1995). Porphobilinogen synthase, the first source of Heme's asymmetry. *J. Bioenerg. Biomembr.* 27, 169–179. doi:10.1007/BF02110032.

Jaffe, E. K. (2004). The porphobilinogen synthase catalyzed reaction mechanism. *Bioorg. Chem.* 32, 316–325. doi:10.1016/j.bioorg.2004.05.010.

Jickells, T. D., An, Z. S., Andersen, K. K., Baker, A. R., Bergametti, G., Brooks, N., et al. (2005). Global Iron Connections Between Desert Dust, Ocean Biogeochemistry, and Climate. *Science (80-.).* 308, 67–71. doi:10.1126/science.1105959.

Joos, F., Sarmiento, J. L., and Siegenthaler, U. (1991). Estimates of the effect of Southern Ocean iron fertilization on atmospheric CO2 concentrations. *Nature* 349, 772–775. doi:10.1038/349772a0.

Kara, A. B., Rochford, P. A., and Hurlburt, H. E. (2000). An optimal definition for ocean mixed layer depth. *J. Geophys. Res. Ocean.* 105, 16803–16821. doi:10.1029/2000JC900072.

Karl, D., Michaels, A., Bergman, B., Capone, D. G., Carpenter, E. J., Letelier, R., et al. (2002). Dinitrogen fixation in the world's oceans. *Biogeochemistry* 57–58, 47–98. doi:10.1023/A:1015798105851.

King, A. L., and Barbeau, K. (2007). Evidence for phytoplankton iron limitation in the southern California Current System. *Mar. Ecol. Prog. Ser.* 342, 91–103. doi:10.3354/meps342091.

King, A. L., Sañudo-Wilhelmy, S. A., Boyd, P. W., Twining, B. S., Wilhelm, S. W., Breene, C., et al. (2012). A comparison of biogenic iron quotas during a diatom spring bloom using multiple approaches. *Biogeosciences* 9, 667–687.

doi:10.5194/bg-9-667-2012.

Koch, M., Breithaupt, C., Kiefersauer, R., Freigang, J., Huber, R., and Messerschmidt, A. (2004). Crystal structure of protoporphyrinogen IX oxidase: a key enzyme in haem and chlorophyll biosynthesis. *EMBO J.* 23, 1720–1728. doi:10.1038/sj.emboj.7600189.

Kolber, Z. S., Barber, R. T., Coale, K. H., Fitzwateri, S. E., Greene, R. M., Johnson, K. S., et al. (1994). Iron limitation of phytoplankton photosynthesis in the equatorial Pacific Ocean. *Nature* 371, 145. doi:10.1038/371145a0.

Kolber, Z. S., Prášil, O., and Falkowski, P. G. (1998). Measurements of variable chlorophyll fluorescence using fast repetition rate techniques: defining methodology and experimental protocols. *Biochim. Biophys. Acta - Bioenerg.* 1367, 88–106. doi:10.1016/S0005-2728(98)00135-2.

Kopylova, E., Noe, L., and Touzet, H. (2012). SortMeRNA: Fast and accurate filtering of ribosomal RNAs in metatranscriptomic data. *Bioinformatics* 28, 3211–3217. doi:10.1093/bioinformatics/bts611.

Kraemer, S. M. (2004). Iron oxide dissolution and solubility in the presence of siderophores. *Aquat. Sci.* 66, 3–18. doi:10.1007/s00027-003-0690-5.

Krewulak, K. D., and Vogel, H. J. (2008). Structural biology of bacterial iron uptake. *Biochim. Biophys. Acta - Biomembr.* 1778, 1781–1804. doi:10.1016/j.bbamem.2007.07.026.

Krishnakumar, S., Gaudana, S. B., Viswanathan, G. A., Pakrasi, H. B., Wangikar, P. P., and Louis, S. (2013). Rhythm of Carbon and Nitrogen Fixation in Unicellular Cyanobacteria Under Turbulent and Highly Aerobic Conditions. 110, 2371–2379. doi:10.1002/bit.24882.

Kupper, H., Setlik, I., Seibert, S., Prasil, O., Setlikova, E., Strittmatter, M., et al. (2008). Iron limitation in the marine cyanobacterium Trichodesmium reveals new insights into regulation of photosynthesis and nitrogen fixation. *New Phytol.* 179, 784–798. doi:10.1111/j.1469-8137.2008.02497.x.

Kurisu, G. (2003). Structure of the Cytochrome b6f Complex of Oxygenic Photosynthesis: Tuning the Cavity. *Science (80-.).* 302, 1009–1014. doi:10.1126/science.1090165.

Kustka, A., Carpenter, E. J., and Sañudo-Wilhelmy, S. A. (2002). Iron and marine nitrogen fixation: progress and future directions. *Res. Microbiol.* 153, 255–262. doi:10.1016/S0923-2508(02)01325-6.

Kustka, A., Saudo-Wilhelmy, S., Carpenter, E. J., Capone, D. G., and Raven, J. A. (2003). A revised estimate of the iron use efficiency of nitrogen fixation, with special reference to the marine cyanobacterium Trichodesmium spp. (Cyanophyta). *J. Phycol.* 39, 12–25. doi:10.1046/j.1529-8817.2003.01156.x.

Lampe, R. H., Mann, E. L., Cohen, N. R., Till, C. P., Thamatrakoln, K., Brzezinski, M. A., et al. (2018). Different iron storage strategies among bloom-forming diatoms. *Proc. Natl. Acad. Sci.* 115, E12275–E12284. doi:10.1073/pnas.1805243115.

Langlois, R. J., Hümmer, D., and LaRoche, J. (2008). Abundances and distributions of the dominant nifH phylotypes in the Northern Atlantic Ocean. *Appl. Environ. Microbiol.* 74, 1922–1931. doi:10.1128/AEM.01720-07.

LaRoche, J., Boyd, P. W., McKay, R. M. L., and Geider, R. J. (1996). Flavodoxin as an in situ marker for iron stress in phytoplankton. *Nature* 382, 802. doi:10.1038/382802a0.

Layer, G., Pierik, A. J., Trost, M., Rigby, S. E., Leech, H. K., Grage, K., et al. (2006). The Substrate Radical of Escherichia coli Oxygen-independent Coproporphyrinogen III Oxidase HemN. *J. Biol. Chem.* 281, 15727–15734. doi:10.1074/jbc.M512628200.

Le Quéré, C., Buitenhuis, E. T., Moriarty, R., Alvain, S., Aumont, O., Bopp, L., et al. (2016). Role of zooplankton dynamics for Southern Ocean phytoplankton biomass and global biogeochemical cycles. *Biogeosciences* 13, 4111–4133. doi:10.5194/bg-13-4111-2016.

Lis, H., Shaked, Y., Kranzler, C., Keren, N., and Morel, F. M. M. (2015). Iron bioavailability to phytoplankton: An empirical approach. *ISME J.* 9, 1003–1013. doi:10.1038/ismej.2014.199.

Liu, X., and Millero, F. J. (1999). The solubility of iron hydroxide in sodium chloride solutions. *Geochim. Cosmochim. Acta* 63, 3487–3497. doi:10.1016/S0016-7037(99)00270-7.

Liu, X., and Millero, F. J. (2002). The solubility of iron in seawater. *Mar. Chem.* 77, 43–54. doi:10.1016/S0304-4203(01)00074-3.

Livak, K. J., and Schmittgen, T. D. (2001). Analysis of relative gene expression data using real-time quantitative PCR and the 2-ΔΔCT method. *Methods* 25, 402–408. doi:10.1006/meth.2001.1262.

Lobo, S. A. L., Scott, A., Videira, M. A. M., Winpenny, D., Gardner, M., Palmer, M. J., et al. (2015). Staphylococcus aureus haem biosynthesis: characterisation of the enzymes involved in final steps of the pathway. *Mol. Microbiol.* 97, 472–487. doi:10.1111/mmi.13041.

Lochte, K., Ducklow, H. W., Fasham, M. J. R., and Stienen, C. (1993). Plankton succession and carbon cycling at 47°N 20°W during the JGOFS North Atlantic Bloom Experiment. *Deep Sea Res. Part II Top. Stud. Oceanogr.* 40, 91–114. doi:10.1016/0967-0645(93)90008-B.

Lommer, M., Specht, M., Roy, A.-S., Kraemer, L., Andreson, R., Gutowska, M. A., et al. (2012). Genome and low-iron response of an oceanic diatom adapted to chronic iron limitation. *Genome Biol.* 13, R66. doi:10.1186/gb-2012-13-7-r66.

Lorrain, A., Savoye, N., Chauvaud, L., Paulet, Y.-M., and Naulet, N. (2003). Decarbonation and preservation method for the analysis of organic C and N contents and stable isotope ratios of low-carbonated suspended particulate material. *Anal. Chim. Acta* 491, 125–133. doi:10.1016/S0003-2670(03)00815-8.

Louropoulou, E., Gledhill, M., Browning, T. J., Desai, D., Menzel Barraqueta, J.-L., Tonnard, M., et al. Regulation of the phytoplankton heme b iron pool during the North Atlantic spring bloom. *Accept. Front. Microbiol.*

Lübben, M., and Morand, K. (1994). Novel prenylated hemes as cofactors of cytochrome oxidases. Archaea have modified hemes A and O. *J. Biol. Chem.* 269, 21473–21479.

Ludwig, M., and Bryant, D. A. (2012). Acclimation of the global transcriptome of the cyanobacterium Synechococcus sp. strain PCC 7002 to nutrient limitations and

different nitrogen sources. *Front. Microbiol.* 3, 1–15. doi:10.3389/fmicb.2012.00145.

Luo, Y.-W., Doney, S. C., Anderson, L. A., Benavides, M., Berman-Frank, I., Bode, A., et al. (2012). Database of diazotrophs in global ocean: abundance, biomass and nitrogen fixation rates. *Earth Syst. Sci. Data* 4, 47–73. doi:10.5194/essd-4-47-2012.

Macey, A. I., Ryan-Keogh, T., Richier, S., Moore, C. M., and Bibby, T. S. (2014). Photosynthetic protein stoichiometry and photophysiology in the high latitude north atlantic. *Limnol. Oceanogr.* 59, 1853–1864. doi:10.4319/lo.2014.59.6.1853.

Mahowald, N. M., Engelstaedter, S., Luo, C., Sealy, A., Artaxo, P., Benitez-Nelson, C., et al. (2009). Atmospheric Iron Deposition: Global Distribution, Variability, and Human Perturbations. *Ann. Rev. Mar. Sci.* 1, 245–278. doi:10.1146/annurev.marine.010908.163727.

Mahowald, N. M., and Luo, C. (2003). A less dusty future? *Geophys. Res. Lett.* 30. doi:10.1029/2003GL017880.

Malatesta, F., Antonini, G., Sarti, P., and Brunori, M. (1995). Structure and function of a molecular machine: cytochrome c oxidase. *Biophys. Chem.* 54, 1–33. doi:https://doi.org/10.1016/0301-4622(94)00117-3.

Maldonado, M. T., Allen, A. E., Chong, J. S., Lin, K., Leus, D., Karpenko, N., et al. (2006). Copper-dependent iron transport in coastal and oceanic diatoms. *Limnol. Oceanogr.* 51, 1729–1743. doi:10.4319/lo.2006.51.4.1729.

Maldonado, M. T., and Price, N. M. (1999). Utilization of iron bound to strong organic ligands by plankton communities in the subarctic Pacific Ocean. *Deep Sea Res. Part II Top. Stud. Oceanogr.* 46, 2447–2473. doi:10.1016/S0967-0645(99)00071-5.

Maldonado, M. T., and Price, N. M. (2001). Reduction and transport of organically bound iron by Thalassiosira oceanica (Bacillariophyceae). *J. Phycol.* 37, 298–310. doi:10.1046/j.1529-8817.2001.037002298.x.

Maldonado, M. T., Strzepek, R. F., Sander, S., and Boyd, P. W. (2005). Acquisition of iron bound to strong organic complexes, with different Fe binding groups and photochemical reactivities, by plankton communities in Fe-limited subantarctic waters. *Global Biogeochem. Cycles* 19. doi:10.1029/2005GB002481.

Marchetti, A., and Cassar, N. (2009). Diatom elemental and morphological changes in response to iron limitation: A brief review with potential paleoceanographic applications. *Geobiology* 7, 419–431. doi:10.1111/j.1472-4669.2009.00207.x.

Marchetti, A., Schruth, D. M., Durkin, C. A., Parker, M. S., Kodner, R. B., Berthiaume, C. T., et al. (2012). Comparative metatranscriptomics identifies molecular bases for the physiological responses of phytoplankton to varying iron availability. *Proc. Natl. Acad. Sci.* 109, E317 LP-E325. doi:10.1073/pnas.1118408109.

Martin, J. H. (1990). Glacial-interglacial CO2 change: The Iron Hypothesis. *Paleoceanography* 5, 1–13. doi:10.1029/PA005i001p00001.

Mayfield, J. A., Dehner, C. A., and DuBois, J. L. (2011). Recent advances in bacterial heme protein biochemistry. *Curr. Opin. Chem. Biol.* 15, 260–266. doi:10.1016/j.cbpa.2011.02.002.

McDonald, D., Price, M. N., Goodrich, J., Nawrocki, E. P., Desantis, T. Z., Probst, A., et al. (2012). An improved Greengenes taxonomy with explicit ranks for ecological and evolutionary analyses of bacteria and archaea. *ISME J.* 6, 610–618. doi:10.1038/ismej.2011.139.

Mercier, C., Boyer, F., Bonin, A., and Coissac, E. (2013). SUMATRA and SUMACLUST: fast and exact comparison and clustering of sequences. in *SeqBio 2013*, eds. T. Lecroq and H. Touzet (Montpellier).

Migita, C. T., Zhang, X., and Yoshida, T. (2003). Expression and characterization of cyanobacterium heme oxygenase, a key enzyme in the phycobilin synthesis: Properties of the heme complex of recombinant active enzyme. *Eur. J. Biochem.* 270, 687–698. doi:10.1046/j.1432-1033.2003.03421.x.

Mignot, A., Claustre, H., Uitz, J., Poteau, A., Ortenzio, F. D., and Xing, X. (2014). Understanding the seasonal dynamics of phytoplankton biomass and the deep chlorophyll maximum in oligotrophic environments: A Bio-Argo float investigation. *Global Biogeochem. Cycles* 28, 856–876. doi:10.1002/2013GB004781.

Milgrom, L. R. (1997). *The Colours of Life: An introduction to the chemistry of porphyrins and related compounds*. Oxford: Oxford university press doi:10.1023/A:1007100414820.

Millero, F. J., Sotolongo, S., and Izaguirre, M. (1987). The oxidation kinetics of Fe(II) in seawater. *Geochim. Cosmochim. Acta* 51, 793–801. doi:10.1016/0016-7037(87)90093-7.

Millero, F. J., Yao, W., and Aicher, J. (1995). The speciation of Fe(II) and Fe(III) in natural waters. *Mar. Chem.* 50, 21–39. doi:10.1016/0304-4203(95)00024-L.

Milligan, A. J., Berman-Frank, I., Gerchman, Y., Dismukes, G. C., and Falkowski, P. G. (2007). Light-dependent oxygen consumption in nitrogen-fixing Cyanobacteria plays a key role in nitrogenase protection. *J. Phycol.* 43, 845–852. doi:10.1111/j.1529-8817.2007.00395.x.

Mills, M. M., Ridame, C., Davey, M., La Roche, J., and Geider, R. J. (2004). Iron and phosphorus co-limit nitrogen fixation in the eastern tropical North Atlantic. *Nature* 429, 292–294. doi:10.1038/nature02550.

Mochizuki, N., Tanaka, R., Grimm, B., Masuda, T., Moulin, M., Smith, A. G., et al. (2010). The cell biology of tetrapyrroles : a life and death struggle. *Trends Plant Sci.* 15, 488–498. doi:10.1016/j.tplants.2010.05.012.

Mohamed, K. N., Steigenberger, S., Nielsdottir, M. C., Gledhill, M., and Achterberg, E. P. (2011). Dissolved iron(III) speciation in the high latitude North Atlantic Ocean. *Deep. Res. Part I Oceanogr. Res. Pap.* 58, 1049–1059. doi:10.1016/j.dsr.2011.08.011.

Mohr, W., Großkopf, T., Wallace, D. W. R., and LaRoche, J. (2010). Methodological underestimation of oceanic nitrogen fixation rates. *PLoS One* 5, 1–7. doi:10.1371/journal.pone.0012583.

Monterey, G. I., and Levitus, S. (1997). *Seasonal variability of Mixed Layer Depth for the World Ocean*. Washington, D.C: U.S. Govt. Print. Off.

Montoya, J. P., Voss, M., Kahler, P., and Capone, D. G. (1996). A Simple , High-Precision , High-Sensitivity Tracer Assay for N (inf2) Fixation . These include :

A Simple , High-Precision , High-Sensitivity Tracer Assay for N 2 Fixation. *Appl. Environ. Microbiol.* 62, 986–993.

Moore, C. M., Lucas, M. I., Sanders, R., and Davidson, R. (2005). Basin-scale variability of phytoplankton bio-optical characteristics in relation to bloom state and community structure in the Northeast Atlantic. *Deep Sea Res. Part I Oceanogr. Res. Pap.* 52, 401–419. doi:10.1016/j.dsr.2004.09.003.

Moore, C. M., Mills, M. M., Achterberg, E. P., Geider, R. J., LaRoche, J., Lucas, M. I., et al. (2009). Large-scale distribution of Atlantic nitrogen fixation controlled by iron availability. *Nat. Geosci.* 2, 867–871. doi:10.1038/ngeo667.

Moore, C. M., Mills, M. M., Arrigo, K. R., Berman-Frank, I., Bopp, L., Boyd, P. W., et al. (2013). Processes and patterns of oceanic nutrient limitation. *Nat. Geosci* 6, 701–710. doi:10.1038/ngeo1765.

Moore, C. M., Mills, M. M., Langlois, R., Milne, A., Achterberg, E. P., La Roche, J., et al. (2008). Relative influence of nitrogen and phosphorus availability on phytoplankton physiology and productivity in the oligotrophic sub-tropical North Atlantic Ocean. *Limnol. Oceanogr.* 53, 291–305. doi:10.4319/lo.2008.53.1.0291.

Moore, C. M., Mills, M. M., Milne, A., Langlois, R., Achterberg, E. P., Lochte, K., et al. (2006a). Iron limits primary productivity during spring bloom development in the central North Atlantic. *Glob. Chang. Biol.* 12, 626–634. doi:10.1111/j.1365-2486.2006.01122.x.

Moore, C. M., Seeyave, S., Hickman, A. E., Allen, J. T., Lucas, M. I., Planquette, H., et al. (2007). Iron-light interactions during the CROZet natural iron bloom and EXport experiment (CROZEX) I: Phytoplankton growth and photophysiology. *Deep. Res. Part II Top. Stud. Oceanogr.* 54, 2045–2065. doi:10.1016/j.dsr2.2007.06.011.

Moore, C. M., Suggett, D. J., Hickman, A. E., Kim, Y.-N., Tweddle, J. F., Sharples, J., et al. (2006b). Phytoplankton photoacclimation and photoadaptation in response to environmental gradients in a shef sea. *Limnol. Oceanogr.* 51, 936–949. doi:10.4319/lo.2006.51.2.0936.

Moore, J. K., and Doney, S. C. (2007). Iron availability limits the ocean nitrogen inventory stabilizing feedbacks between marine denitrification and nitrogen fixation. *Global Biogeochem. Cycles* 21, 1–12. doi:10.1029/2006GB002762.

Moore, J. K., Doney, S. C., Glover, D. M., and Fung, I. Y. (2002). Iron cycling and nutrient-limitation patterns in surface waters of the world ocean. *Deep. Res. Part II Top. Stud. Oceanogr.* 49, 463–507. doi:10.1016/S0967-0645(01)00109-6.

Morel, F. M. M. (2008). The co-evolution of phytoplankton and trace element cycles in the oceans. *Geobiology* 6, 318–324. doi:10.1111/j.1472-4669.2008.00144.x.

Morel, F. M. M., and Price, N. M. (2003). The Biogeochemical Cycles of Trace Metals. *Science (80-.).* 300, 944–947. doi:10.1126/science.1083545.

Morrissey, J., and Bowler, C. (2012). Iron utilization in marine cyanobacteria and eukaryotic algae. *Front. Microbiol.* 3, 1–13. doi:10.3389/fmicb.2012.00043.

Morrissey, J., Sutak, R., Paz-Yepes, J., Tanaka, A., Moustafa, A., Veluchamy, A., et al. (2015). A Novel Protein, Ubiquitous in Marine Phytoplankton, Concentrates Iron at the Cell Surface and Facilitates Uptake. *Curr. Biol.* 25, 364–371. doi:10.1016/j.cub.2014.12.004.

Muramoto, T. (1999). The Arabidopsis Photomorphogenic Mutant hy1 Is Deficient in Phytochrome Chromophore Biosynthesis as a Result of a Mutation in a Plastid Heme Oxygenase. *PLANT CELL ONLINE* 11, 335–348. doi:10.1105/tpc.11.3.335.

Muramoto, T. (2002). Expression and Biochemical Properties of a Ferredoxin-Dependent Heme Oxygenase Required for Phytochrome Chromophore Synthesis. *PLANT Physiol.* 130, 1958–1966. doi:10.1104/pp.008128.

Nakano, S., Takahashi, M., Sakamoto, A., Morikawa, H., and Katayanagi, K. (2012). Structure-function relationship of assimilatory nitrite reductases from the leaf and root of tobacco based on high-resolution structures. *Protein Sci.* 21, 383–395. doi:10.1002/pro.2025.

Nielsdóttir, M. C., Bibby, T. S., Moore, C. M., Hinz, D. J., Sanders, R., Whitehouse, M., et al. (2012). Seasonal and spatial dynamics of iron availability in the Scotia Sea. *Mar. Chem.* 130–131, 62–72. doi:10.1016/j.marchem.2011.12.004.

Nielsdóttir, M. C., Moore, C. M., Sanders, R., Hinz, D. J., and Achterberg, E. P. (2009). Iron limitation of the postbloom phytoplankton communities in the Iceland Basin. *Global Biogeochem. Cycles* 23, 1–13. doi:10.1029/2008GB003410.

Nunn, B. L., Faux, J. F., Hippmann, A. A., Maldonado, M. T., Harvey, H. R., Goodlett, D. R., et al. (2013). Diatom Proteomics Reveals Unique Acclimation Strategies to Mitigate Fe Limitation. *PLoS One* 8, e75653. doi:10.1371/journal.pone.0075653.

Olsen, A., Brown, K. R., Chierici, M., Johannessen, T., and Neill, C. (2008). Sea-surface CO 2 fugacity in the subpolar North Atlantic. *Biogeosciences* 5, 535–547. doi:10.5194/bg-5-535-2008.

Ortiz de Montellano, P. (2000). The mechanism of heme oxygenase. *Curr. Opin. Chem. Biol.* 4, 221–227. doi:10.1016/S1367-5931(99)00079-4.

Pabortsava, K., Lampitt, R. S., Benson, J., Crowe, C., McLachlan, R., Le Moigne, F. A. C., et al. (2017). Carbon sequestration in the deep Atlantic enhanced by Saharan dust. *Nat. Geosci.* 10, 189–194. doi:10.1038/ngeo2899.

Paczuska, L., and Kosakowska, A. (2003). Is iron a limiting factor of Nodularia spumigena blooms ? *Oceanologia* 45, 679–692.

Pankowski, A., and Mcminn, A. (2008). Iron availability regulates growth, photosynthesis, and production of ferredoxin and flavodoxin in Antarctic sea ice diatoms. *Aquat. Biol.* 4, 273–288. doi:10.3354/ab00116.

Pankowski, A., and McMinn, A. (2009). Development of immunoassays for the iron-regulated proteins ferredoxin and flavodoxin in polar microalgae. *J. Phycol.* 45, 771–783. doi:10.1111/j.1529-8817.2009.00687.x.

Peers, G., and Price, N. M. (2006). Copper-containing plastocyanin used for electron transport by an oceanic diatom. *Nature* 441, 341–344. doi:10.1038/nature04630.

Pfreundt, U., Kopf, M., Belkin, N., Berman-Frank, I., and Hess, W. R. (2014). The primary transcriptome of the marine diazotroph Trichodesmium erythraeum IMS101. *Sci. Rep.* 4, 6187. doi:10.1038/srep06187.

Pfreundt, U., Stal, L. J., Voß, B., and Hess, W. R. (2012). Dinitrogen fixation in a unicellular chlorophyll d-containing cyanobacterium. *ISME J.* 6, 1367–1377. doi:10.1038/ismej.2011.199.

Pinto, F. L., Thapper, A., Sontheim, W., and Lindblad, P. (2009). Analysis of current

and alternative phenol based RNA extraction methodologies for cyanobacteria. *BMC Mol. Biol.* 10, 79. doi:10.1186/1471-2199-10-79.

Piola, A. R., Möller, O. O., Guerrero, R. A., and Campos, E. J. D. (2008). Variability of the subtropical shelf front off eastern South America: Winter 2003 and summer 2004. *Cont. Shelf Res.* 28, 1639–1648. doi:10.1016/j.csr.2008.03.013.

Polyviou, D., Baylay, A. J., Hitchcock, A., Robidart, J., Moore, C. M., and Bibby, T. S. (2018). Desert Dust as a Source of Iron to the Globally Important Diazotroph Trichodesmium. *Front. Microbiol.* 8. doi:10.3389/fmicb.2017.02683.

Poulson, R., and Polglase, W. J. (1975). The enzymic conversion of protoporphyrinogen IX to protoporphyrin IX. Protoporphyrinogen oxidase activity in mitochondrial extracts of Saccharomyces cerevisiae. *J. Biol. Chem.* 250, 1269–1274.

Poulton, A. J., Charalampopoulou, A., Young, J. R., Tarran, G. A., Lucas, M. I., and Quartly, G. D. (2010). Coccolithophore dynamics in non-bloom conditions during late summer in the central Iceland Basin (July-August 2007). *Limnol. Oceanogr.* 55, 1601–1613. doi:10.4319/lo.2010.55.4.1601.

Price, N. M., Ahner, B. A., and Morel, F. M. M. (1994). The equatorial Pacific Ocean: Grazer-controlled phytoplankton populations in an iron-limited ecosystem1. *Limnol. Oceanogr.* 39, 520–534. doi:10.4319/lo.1994.39.3.0520.

Price, N. M., Andersen, L. F., and Morel, F. M. M. (1991). Iron and nitrogen nutrition of equatorial Pacific plankton. *Deep Sea Res. Part A, Oceanogr. Res. Pap.* 38, 1361–1378. doi:10.1016/0198-0149(91)90011-4.

R Core Team (2016). R: A Language and Environment for Statistical Computing. Available at: https://www.r-project.org.

Ras, J., Claustre, H., Uitz, J., Ras, J., Claustre, H., and Spatial, J. U. (2008). Spatial variability of phytoplankton pigment distributions in the Subtropical South Pacific Ocean : comparison between in situ and predicted data. *Biogeosciences* 5, 353–369. doi:10.5194/bg-5-353-2008.

Ratliff, M., Zhu, W., Deshmukh, R., Wilks, A., and Stojiljkovic, I. (2001). Homologues of neisserial heme oxygenase in gram-negative bacteria: degradation of heme by the product of the pigA gene of Pseudomonas aeruginosa. *J. Bacteriol.* 183, 6394–6403. doi:10.1128/JB.183.21.6394-6403.2001.

Raven, J. A. (1988). The iron and molybdenum use efficiencies of plant growth with different energy, carbon and nitrogen sources. *New Phytol.* 109, 279–287. doi:10.1111/j.1469-8137.1988.tb04196.x.

Raven, J. A. (1990). Predictions of Mn and Fe use efficiencies of phototrophic growth as a function of light availability for growth and of C assimilation pathway. *New Phytol.* 116, 1–18. doi:10.1111/j.1469-8137.1990.tb00505.x.

Raven, J. A., Evans, M. C. W., and Korb, R. E. (1999). The role of trace metals in photosynthetic electron transport in O-2-evolving organisms. *Photosynth. Res.* 60, 111–150. doi:10.1023/a:1006282714942.

Reddy, K. J., Haskell, J. B., Sherman, D. M., and Sherman, L. A. (1993). Unicellular, aerobic nitrogen-fixing cyanobacteria of the genus Cyanothece. *J. Bacteriol.* 175, 1284–1292. doi:10.1128/jb.175.5.1284-1292.1993.

Redfield, A. C. (1958). The biological control of chemical factors in the environment.

Am. Sci. 46, 230A–221.

Resing, J. A., Sedwick, P. N., German, C. R., Jenkins, W. J., Moffett, J. W., Sohst, B. M., et al. (2015). Basin-scale transport of hydrothermal dissolved metals across the South Pacific Ocean. *Nature* 523, 200–203. doi:10.1038/nature14577.

Reynolds, C. S. (2006). *The Ecology of Phytoplankton*. Cambridge: Cambridge University Press doi:10.1017/CBO9780511542145.

Rhie, G., and Beale, S. I. (1992). Biosynthesis of phycobilins. Ferredoxin-supported nadph-independent heme oxygenase and phycobilin-forming activities from Cyanidium caldarium. *J. Biol. Chem.* 267, 16088–16093.

Rhie, G. E., and Beale, S. I. (1995). Phycobilin Biosynthesis: Reductant Requirements and Product Identification for Heme Oxygenase from Cyanidium caldarium. *Arch. Biochem. Biophys.* 320, 182–194. doi:https://doi.org/10.1006/abbi.1995.1358.

Richardson, D. J. (2000). Bacterial respiration: a flexible process for a changing environment. *Microbiology* 146, 551–571. doi:10.1099/00221287-146-3-551.

Richaud, C., and Zabulon, G. (1997). The heme oxygenase gene (pbsA) in the red alga Rhodella violacea is discontinuous and transcriptionally activated during iron limitation. *Proc. Natl. Acad. Sci.* 94, 11736–11741. doi:10.1073/pnas.94.21.11736.

Richier, S., Macey, A. I., Pratt, N. J., Honey, D. J., Moore, C. M., and Bibby, T. S. (2012). Abundances of iron-binding photosynthetic and nitrogen-fixing proteins of Trichodesmium both in culture and in situ from the North Atlantic. *PLoS One* 7, Richier, S., Macey, A. I., Pratt, N. J., Honey, D. doi:10.1371/journal.pone.0035571.

Richter, O.-M. H., and Ludwig, B. (2009). Electron transfer and energy transduction in the terminal part of the respiratory chain — Lessons from bacterial model systems. *Biochim. Biophys. Acta - Bioenerg.* 1787, 626–634. doi:10.1016/j.bbabio.2009.02.020.

Rijkenberg, M. J. A., Middag, R., Laan, P., Gerringa, L. J. A., van Aken, H. M., Schoemann, V., et al. (2014). The Distribution of Dissolved Iron in the West Atlantic Ocean. *PLoS One* 9, e101323. doi:10.1371/journal.pone.0101323.

Rijkenberg, M. J. A., Steigenberger, S., Powell, C. F., Haren, H., Patey, M. D., Baker, A. R., et al. (2012). Fluxes and distribution of dissolved iron in the eastern (sub-) tropical North Atlantic Ocean. *Global Biogeochem. Cycles* 26. doi:10.1029/2011GB004264.

Roe, K. L., Hogle, S. L., and Barbeau, K. A. (2013). Utilization of Heme as an Iron Source by Marine Alphaproteobacteria in the Roseobacter Clade. *Appl. Environ. Microbiol.* 79, 5753–5762. doi:10.1128/AEM.01562-13.

Rognes, T., Flouri, T., Nichols, B., Quince, C., and Mahé, F. (2016). VSEARCH: a versatile open source tool for metagenomics. *PeerJ* 4. doi:10.7717/peerj.2584.

Rubin, M., Berman-Frank, I., and Shaked, Y. (2011). Dust- and mineral-iron utilization by the marine dinitrogen-fixer Trichodesmium. *Nat. Geosci.* 4, 529–534. doi:10.1038/ngeo1181.

Rue, E. L., Bay, M., and Kenneth, W. B. (1997). The role of organic complexation on ambient iron chemistry in the equatorial Pacific Ocean and the response of a mesoscale iron addition experiment. 901–910.

Ryan-Keogh, T. J., DeLizo, L. M., Smith, W. O., Sedwick, P. N., McGillicuddy, D. J., Moore, C. M., et al. (2017). Temporal progression of photosynthetic-strategy in phytoplankton in the Ross Sea, Antarctica. *J. Mar. Syst.* 166, 87–96. doi:10.1016/j.jmarsys.2016.08.014.

Ryan-Keogh, T. J., Macey, A. I., Nielsdóttir, M. C., Lucas, M. I., Steigenberger, S. S., Stinchcombe, M. C., et al. (2013). Spatial and temporal development of phytoplankton iron stress in relation to bloom dynamics in the high-latitude North Atlantic Ocean. *Limnol. Oceanogr.* 58, 533–545. doi:10.4319/lo.2013.58.2.0533.

Saito, M. A., Bertrand, E. M., Dutkiewicz, S., Bulygin, V. V, Moran, D. M., Monteiro, F. M., et al. (2011). Iron conservation by reduction of metalloenzyme inventories in the marine diazotroph Crocosphaera watsonii. *Proc. Natl. Acad. Sci. U. S. A.* 108, 2184–9. doi:10.1073/pnas.1006943108.

Saito, M. A., McIlvin, M. R., Moran, D. M., Goepfert, T. J., DiTullio, G. R., Post, A. F., et al. (2014). Multiple nutrient stresses at intersecting Pacific Ocean biomes detected by protein biomarkers. *Science (80-.).* 345, 1173–1177. doi:10.1126/science.1256450.

Sanders, R., Brown, L., Henson, S., and Lucas, M. (2005). New production in the Irminger Basin during 2002. 55, 291–310. doi:10.1016/j.jmarsys.2004.09.002.

Sanders, R., Henson, S. A., Koski, M., De La Rocha, C. L., Painter, S. C., Poulton, A. J., et al. (2014). The Biological Carbon Pump in the North Atlantic. *Prog. Oceanogr.* 129, 200–218. doi:10.1016/j.pocean.2014.05.005.

Sarmiento, J. L., and Gruber, N. (2004). *Ocean biogeochemical dynamics*. Princeton University Press.

Sarmiento, J. L., Gruber, N., Brzezinski, A., and Dunne, J. P. (2003). High latitude controls of thermohaline nutrients and low latitude biological productivity. *Nature* 427, 56–60. doi:10.1038/nature02127.

Sarthou, G., Lherminier, P., Achterberg, E. P., Alonso-Pérez, F., Bucciarelli, E., Boutorh, J., et al. (2018). Introduction to the French GEOTRACES North Atlantic Transect (GA01): GEOVIDE cruise. *Biogeosciences Discuss.* 2018, 1–24. doi:10.5194/bg-2018-312.

Sarthou, G., Timmermans, K. R., Blain, S., and Tréguer, P. (2005). Growth physiology and fate of diatoms in the ocean: A review. *J. Sea Res.* 53, 25–42. doi:10.1016/j.seares.2004.01.007.

Sarthou, G., Vincent, D., Christaki, U., Obernosterer, I., Timmermans, K. R., and Brussaard, C. P. D. (2008). The fate of biogenic iron during a phytoplankton bloom induced by natural fertilisation: Impact of copepod grazing. *Deep. Res. Part II Top. Stud. Oceanogr.* 55, 734–751. doi:10.1016/j.dsr2.2007.12.033.

Schlitzer, R. (2018). Ocean Data View. Available at: http://odv.awi.de.

Schlosser, C., Klar, J. K., Wake, B. D., Snow, J. T., Honey, D. J., Woodward, E. M. S., et al. (2014). Seasonal ITCZ migration dynamically controls the location of the (sub)tropical Atlantic biogeochemical divide. *Proc. Natl. Acad. Sci. U. S. A.* 111, 1438–42. doi:10.1073/pnas.1318670111.

Schmitt, M. P. (1997). Utilization of host iron sources by Corynebacterium diphtheriae: identification of a gene whose product is homologous to eukaryotic heme oxygenases and is required for acquisition of iron from heme and hemoglobin. *J.*

Bacteriol. 179, 838–845. doi:10.1128/jb.179.3.838-845.1997.

Schorsch, M., Kramer, M., Goss, T., Eisenhut, M., Robinson, N., Osman, D., et al. (2018). A unique ferredoxin acts as a player in the low-iron response of photosynthetic organisms. *Proc. Natl. Acad. Sci.* 115, E12111–E12120. doi:10.1073/pnas.1810379115.

Schröder, I., Johnson, E., and de Vries, S. (2003). Microbial ferric iron reductases. *FEMS Microbiol. Rev.* 27, 427–447. doi:10.1016/S0168-6445(03)00043-3.

Septer, A. N., Wang, Y., Ruby, E. G., Stabb, E. V, and Dunn, A. K. (2011). The haem-uptake gene cluster in Vibrio fischeri is regulated by Fur and contributes to symbiotic colonization. *Environ. Microbiol.* 13, 2855–2864. doi:10.1111/j.1462-2920.2011.02558.x.

Shaked, Y., Kustka, A. B., and Morel, F. M. M. (2005). A general kinetic model for iron acquisition by eukaryotic phytoplankton. *Limnol. Oceanogr.* 50, 872–882. doi:10.4319/lo.2005.50.3.0872.

Shaked, Y., and Lis, H. (2012). Disassembling iron availability to phytoplankton. *Front. Microbiol.* 3, 1–26. doi:10.3389/fmicb.2012.00123.

Shekhawat, G. S., and Verma, K. (2010). Haem oxygenase (HO): An overlooked enzyme of plant metabolism and defence. *J. Exp. Bot.* 61, 2255–2270. doi:10.1093/jxb/erq074.

Shi, D., Kranz, S. a., Kim, J.-M., and Morel, F. M. M. (2012). Ocean acidification slows nitrogen fixation and growth in the dominant diazotroph Trichodesmium under low-iron conditions. *Proc. Natl. Acad. Sci.* 109, E3094–E3100. doi:10.1073/pnas.1216012109.

Shi, T., Sun, Y., and Falkowski, P. G. (2007). Effects of iron limitation on the expression of metabolic genes in the marine cyanobacterium Trichodesmium erythraeum IMS101. *Environ. Microbiol.* 9, 2945–2956. doi:10.1111/j.1462-2920.2007.01406.x.

Shoolingin-Jordan, P. M. (1995). Porphobilinogen deaminase and uroporphyrinogen III synthase: Structure, molecular biology, and mechanism. *J. Bioenerg. Biomembr.* 27, 181–195. doi:10.1007/BF02110033.

Singh, A. K., McIntyre, L. M., and Sherman, L. A. (2003). Microarray analysis of the genome-wide response to iron deficiency and iron reconstitution in the cyanobacterium Synechocystis sp. PCC 6803. *Plant Physiol.* 132, 1825–1839. doi:10.1104/pp.103.024018.

Singleton, C., White, G. F., Todd, J. D., Marritt, S. J., Cheesman, M. R., Johnston, A. W. B., et al. (2010). Heme-responsive DNA Binding by the Global Iron Regulator Irr from Rhizobium leguminosarum. *J. Biol. Chem.* 285, 16023–16031. doi:10.1074/jbc.M109.067215.

Smith, S. R., Gillard, J. T. F., Kustka, A. B., McCrow, J. P., Badger, J. H., Zheng, H., et al. (2016). Transcriptional Orchestration of the Global Cellular Response of a Model Pennate Diatom to Diel Light Cycling under Iron Limitation. *PLOS Genet.* 12, e1006490. doi:10.1371/journal.pgen.1006490.

Snow, J. T., Polyviou, D., Skipp, P., Chrismas, N. A. M., Hitchcock, A., Geider, R., et al. (2015a). Quantifying integrated proteomic responses to iron stress in the globally important marine diazotroph Trichodesmium. *PLoS One* 10, 1–24.

doi:10.1371/journal.pone.0142626.

Snow, J. T., Schlosser, C., Woodward, E. M. S., Mills, M. M., Achterberg, E. P., Mahaffey, C., et al. (2015b). Environmental controls on the biogeography of diazotrophy and Trichodesmium in the Atlantic Ocean. *Global Biogeochem. Cycles* 29, 865–884. doi:10.1002/2015GB005090.

Sohm, J. A., Webb, E. A., and Capone, D. G. (2011). Emerging patterns of marine nitrogen fixation. *Nat. Rev. Microbiol.* 9, 499–508. doi:10.1038/nrmicro2594.

Soria-Dengg, S., and Horstmann, U. (1995). Ferrioxamines B and E as iron sources for the marine diatom Phaeodactylum tricornutum. *Mar. Ecol. Prog. Ser.* 127, 269–277.

Stöckel, J., Welsh, E. A., Liberton, M., Kunnvakkam, R., Aurora, R., and Pakrasi, H. B. (2008). Global transcriptomic analysis of Cyanothece 51142 reveals robust diurnal oscillation of central metabolic processes. doi:10.1073/pnas.0711068105.

Stolpe, B., and Hassellöv, M. (2009). Nanofibrils and other colloidal biopolymers binding trace elements in coastal seawater: Significance for variations in element size distributions. *Limnol. Oceanogr.* 55, 187–202. doi:10.4319/lo.2010.55.1.0187.

Stroupe, M. E., and Getzoff, E. D. (2009). "The Role of Siroheme in Sulfite and Nitrite Reductases BT - Tetrapyrroles: Birth, Life and Death," in, eds. M. J. Warren and A. G. Smith (New York, NY: Springer New York), 375–389. doi:10.1007/978-0-387-78518-9_24.

Strzepek, R. F., and Harrison, P. J. (2004). Photosynthetic architecture differs in coastal and oceanic diatoms. *Nature* 431, 689–692. doi:10.1038/nature02954.

Strzepek, R. F., Hunter, K. A., Frew, R. D., Harrison, P. J., and Boyd, P. W. (2012). Iron-light interactions differ in Southern Ocean phytoplankton. *Limnol. Oceanogr.* 57, 1182–1200. doi:10.4319/lo.2012.57.4.1182.

Strzepek, R. F., Maldonado, M. T., Hunter, K. A., Frew, R. D., and Boyd, P. W. (2011). Adaptive strategies by Southern Ocean phytoplankton to lessen iron limitation: Uptake of organically complexed iron and reduced cellular iron requirements. *Limnol. Oceanogr.* 56, 1983–2002. doi:10.4319/lo.2011.56.6.1983.

Stumm, W., and Morgan, J. J. (1995). *Aquatic chemistry: chemical equilibria and rates in natural waters*. John Wiley & Sons.

Suggett, D. J., Moore, C. M., Hickman, A. E., and Geider, R. J. (2009). Interpretation of fast repetition rate (FRR) fluorescence: Signatures of phytoplankton community structure versus physiological state. *Mar. Ecol. Prog. Ser.* 376, 1–19. doi:10.3354/meps07830.

Sugishima, M., Migita, C. T., Zhang, X., Yoshida, T., and Fukuyama, K. (2004). Crystal structure of heme oxygenase-1 from cyanobacterium Synechocystis sp. PCC 6803 in complex with heme. *Eur. J. Biochem.* 271, 4517–4525. doi:10.1111/j.1432-1033.2004.04411.x.

Sunda, W. G. (2012). Feedback interactions between trace metal nutrients and phytoplankton in the ocean. *Front. Microbiol.* 3, 1–22. doi:10.3389/fmicb.2012.00204.

Sunda, W. G., and Hardison, D. R. (2010). Evolutionary tradeoffs among nutrient acquisition, cell size, and grazing defense in marine phytoplankton promote

ecosystem stability. *Mar. Ecol. Prog. Ser.* 401, 63–76. doi:10.3354/meps08390.

Sunda, W. G., and Huntsman, S. A. (1995). Iron Uptake and Growth Limitation in Oceanic and Coastal Phytoplankton. *Mar. Chem.* 50, 189–206. doi:10.1016/0304-4203(95)00035-p.

Sunda, W. G., and Huntsman, S. A. (1997). Interrelated influence of iron, light and cell size on marine phytoplankton growth light and cell size on marine phytoplankton growth. *Nature* 390, 389–392. doi:10.1038/37093.

Sunda, W. G., Price, N. M., and Morel, F. M. M. (2005). Trace metal ion buffers and their use in culture studies. *Algal Cult. Tech.* 4, 35–63.

Sunda, W. G., Swift, D. G., and Huntsman, S. A. (1991). Low iron requirement for growth in oceanic phytoplankton. *Nature* 351, 55–57. doi:10.1038/351055a0.

Swart, S., Thomalla, S. J., and Monteiro, P. M. S. (2015). The seasonal cycle of mixed layer dynamics and phytoplankton biomass in the Sub-Antarctic Zone: A high-resolution glider experiment. *J. Mar. Syst.* 147, 103–115. doi:10.1016/j.jmarsys.2014.06.002.

Tagliabue, A., and Arrigo, K. R. (2006). Processes governing the supply of iron to phytoplankton in stratified seas. *J. Geophys. Res. Ocean.* 111, 1–14. doi:10.1029/2005JC003363.

Tagliabue, A., Aumont, O., DeAth, R., Dunne, J. P., Dutkiewicz, S., Galbraith, E., et al. (2016). How well do global ocean biogeochemistry models simulate dissolved iron distributions? *Global Biogeochem. Cycles* 30, 149–174. doi:10.1002/2015GB005289.

Tagliabue, A., Bowie, A. R., Boyd, P. W., Buck, K. N., Johnson, K. S., and Saito, M. A. (2017). The integral role of iron in ocean biogeochemistry. *Nature* 543, 51–59. doi:10.1038/nature21058.

Tagliabue, A., Hawco, N. J., Bundy, R. M., Landing, W. M., Milne, A., Morton, P. L., et al. (2018). The Role of External Inputs and Internal Cycling in Shaping the Global Ocean Cobalt Distribution: Insights From the First Cobalt Biogeochemical Model. *Global Biogeochem. Cycles* 32, 594–616. doi:10.1002/2017GB005830.

Tagliabue, A., and Resing, J. (2016). Impact of hydrothermalism on the ocean iron cycle. *Philos. Trans. R. Soc. A Math. Phys. Eng. Sci.* 374, 20150291. doi:10.1098/rsta.2015.0291.

Takahashi, H., Kopriva, S., Giordano, M., Saito, K., and Hell, R. (2011). Sulfur Assimilation in Photosynthetic Organisms: Molecular Functions and Regulations of Transporters and Assimilatory Enzymes. *Annu. Rev. Plant Biol.* 62, 157–184. doi:10.1146/annurev-arplant-042110-103921.

Tegen, I., Werner, M., Harrison, S. P., and Kohfeld, K. E. (2004). Relative importance of climate and land use in determining present and future global soil dust emission. *Geophys. Res. Lett.* 31. doi:10.1029/2003GL019216.

Terry, M. J., Linley, P. J., and Kohchi, T. (2002). Making light of it: the role of plant haem oxygenases in phytochrome chromophore synthesis. *Biochem. Soc. Trans.* 30, 604 LP – 609. doi:10.1042/bst0300604.

Terzulli, A., and Kosman, D. J. (2010). Analysis of the High-Affinity Iron Uptake System at the Chlamydomonas reinhardtii Plasma Membrane. *Eukaryot. Cell* 9,

815–826. doi:10.1128/EC.00310-09.

Thomas, L. N., Tandon, A., and Mahadevan, A. (2013). Submesoscale Processes and Dynamics. *Ocean Model. an Eddying Regime*. doi:10.1029/177GM04.

Timmermans, K. R., Davey, M. S., Van der Wagt, B., Snoek, J., Geider, R. J., Veldhuis, M. J. W., et al. (2001a). Co-limitation by iron and light of Chaetoceros brevis, C. dichaeta and C. calcitrans (Bacillariophyceae). *Mar. Ecol. Prog. Ser.* 217, 287–297. doi:10.3354/meps217287.

Timmermans, K. R., Gerringa, L. J. A., Baar, H. J. W. De, Wagt, B. Van Der, Veldhuis, M. J. W., Jong, J. T. M. De, et al. (2001b). Growth Rates of Large and Small Southern Ocean Diatoms in Relation to Availability of Iron to availability Ocean diatoms in relation of Growth rates of large and small Southern iron in natural seawater. *Limnology* 46, 260–266.

Timmermans, K. R., Stolte, W., and de Baar, H. J. W. (1994). Iron-mediated effects on nitrate reductase in marine phytoplankton. *Mar. Biol.* 121, 389–396. doi:10.1007/BF00346749.

Timmermans, K. R., Van Der Wagt, B., and De Baar, H. J. W. (2004). Growth rates, half-saturation constants, and silicate, nitrate, and phosphate depletion in relation to iron availability of four large, open-ocean diatoms from the Southern Ocean. *Limnol. Oceanogr.* 49, 2141–2151. doi:10.4319/lo.2004.49.6.2141.

Toepel, J., McDermott, J. E., Summerfield, T. C., and Sherman, L. A. (2009). Transcriptional analysis of the unicellular, diazotrophic cyanobacterium Cyanothece sp. ATCC 51142 grown under short day/night cycles. *J. Phycol.* 45, 610–620. doi:10.1111/j.1529-8817.2009.00674.x.

Tonnard, M., Planquette, H., Bowie, A. R., van der Merwe, P., Gallinari, M., Desprez de Gésincourt, F., et al. (2018). Dissolved iron in the North Atlantic Ocean and Labrador Sea along the GEOVIDE section (GEOTRACES section GA01). *Biogeosciences Discuss.*, 1–53. doi:10.5194/bg-2018-147.

Tripathy, B. C., Sherameti, I., and Oelmüller, R. (2010). Siroheme. *Plant Signal. Behav.* 5, 14–20. doi:10.4161/psb.5.1.10173.

Twining, B. S., and Baines, S. B. (2013). The Trace Metal Composition of Marine Phytoplankton. *Ann. Rev. Mar. Sci.* 5, 191–215. doi:10.1146/annurev-marine-121211-172322.

Twining, B. S., Baines, S. B., Fisher, N. S., and Landry, M. R. (2004). Cellular iron contents of plankton during the Southern Ocean Iron Experiment (SOFeX). *Deep. Res. Part I Oceanogr. Res. Pap.* 51, 1827–1850. doi:10.1016/j.dsr.2004.08.007.

Unno, M., Matsui, T., and Ikeda-Saito, M. (2007). Structure and catalytic mechanism of heme oxygenase. *Nat. Prod. Rep.* 24, 553–570. doi:10.1039/b604180a.

Ussher, S. J., Achterberg, E. P., and Worsfold, P. J. (2004). Marine Biogeochemistry of Iron. *Environ. Chem.* 1, 67. doi:10.1071/EN04053.

Ussher, S. J., Worsfold, P. J., Achterberg, E. P., Laës, A., Blain, S., Laan, P., et al. (2007). Distribution and redox speciation of dissolved iron on the European continental margin. *Limnol. Oceanogr.* 52, 2530–2539. doi:10.4319/lo.2007.52.6.2530.

Vassiliev, I. R., Kolber, Z., Wyman, K. D., Mauzerall, D., Shukla, V. K., and

Falkowski, P. G. (1995). Effects of Iron Limitation on Photosystem II Composition and Light Utilization in Dunaliella tertiolecta. *Plant Physiol.* 109, 963–972. doi:10.1104/pp.109.3.963.

Vavilin, D. V, and Vermaas, W. F. J. (2002). Regulation of the tetrapyrrole biosynthetic pathway leading to heme and chlorophyll in plants and cyanobacteria. *Physiol. Plant.* 115, 9–24. doi:10.1034/j.1399-3054.2002.1150102.x.

Verardo, D. J., Froelich, P. N., and McIntyre, A. (1990). Determination of organic carbon and nitrogen in marine sediments using the Carlo Erba NA-1500 analyzer. *Deep Sea Res. Part A. Oceanogr. Res. Pap.* 37, 157–165. doi:10.1016/0198-0149(90)90034-S.

Vu, T. T., Stolyar, S. M., Pinchuk, G. E., Hill, E. A., Kucek, L. A., Brown, R. N., et al. (2012). Genome-scale modeling of light-driven reductant partitioning and carbon fluxes in diazotrophic unicellular cyanobacterium Cyanothece sp. ATCC 51142. *PLoS Comput. Biol.* 8. doi:10.1371/journal.pcbi.1002460.

Wandersman, C., and Delepelaire, P. (2004). Bacterial Iron Sources: From Siderophores to Hemophores. *Annu. Rev. Microbiol.* 58, 611–647. doi:10.1146/annurev.micro.58.030603.123811.

Wang, Y.-P., and Lei, Q.-Y. (2018). Metabolite sensing and signaling in cell metabolism. *Signal Transduct. Target. Ther.* 3, 30. doi:10.1038/s41392-018-0024-7.

Ward, B., Capone, D., and Zehr, J. (2007). What's New in the Nitrogen Cycle? *Oceanography* 20, 101–109. doi:10.5670/oceanog.2007.53.

Weaver, R., Kirchman, D., and Hutchins, D. (2003). Utilization of iron/organic ligand complexes by marine bacterioplankton. *Aquat. Microb. Ecol.* 31, 227–239. doi:10.3354/ame031227.

Webb, E. A., Moffett, J. W., and Waterbury, J. B. (2001). Iron Stress in Open-Ocean Cyanobacteria (Synechococcus, Trichodesmium, and Crocosphaera spp.): Identification of the IdiA Protein. *Appl. Environ. Microbiol.* 67, 5444–5452. doi:10.1128/AEM.67.12.5444-5452.2001.

Wells, M. L., Price, N. M., and Bruland, K. W. (1995). Iron chemistry in seawater and its relationship to phytoplankton: a workshop report. *Mar. Chem.* 48, 157–182. doi:10.1016/0304-4203(94)00055-I.

Welschmeyer, N. A. (1994). Fluorometric analysis of chlorophyll a in the presence of chlorophyll b and pheopigments. *Limnol. Oceanogr.* 39, 1985–1992. doi:10.4319/lo.1994.39.8.1985.

Whitby, F. G., Phillips, J. D., Hill, C. P., McCoubrey, W., and Maines, M. D. (2002). Crystal Structure of a Biliverdin IXα Reductase Enzyme–Cofactor Complex. *J. Mol. Biol.* 319, 1199–1210. doi:10.1016/S0022-2836(02)00383-2.

Wilks, A. (2002). Heme Oxygenase: Evolution, Structure, and Mechanism. *Antioxid. Redox Signal.* 4, 603–614. doi:10.1089/15230860260220102.

Wolf, H. U., Lang, W., and Zander, R. (1984). Alkaline haematin D-575, a new tool for the determination of haemoglobin as an alternative to the cyanhaemiglobin method. II. Standardisation of the method using pure chlorohaemin. *Clin. Chim. Acta* 136, 95–104. doi:10.1016/0009-8981(84)90251-1.

Yang, J., Sangwan, I., Lindemann, A., Hauser, F., Hennecke, H., Fischer, H.-M., et al. (2006). Bradyrhizobium japonicum senses iron through the status of haem to regulate iron homeostasis and metabolism. *Mol. Microbiol.* 60, 427–437. doi:10.1111/j.1365-2958.2006.05101.x.

Zamocky, M., Furtmüller, P. G., and Obinger, C. (2008). Evolution of catalases from bacteria to humans. *Antioxid. Redox Signal.* 10, 1527–1548. doi:10.1089/ars.2008.2046.

Zander, R., Lang, W., and Wolf, H. U. (1984). Alkaline haematin D-575, a new tool for the determination of haemoglobin as an alternative to the cyanhaemiglobin method. I. description of the method. *Clin. Chim. Acta* 136, 83–93. doi:10.1016/0009-8981(84)90250-X.

Zehr, J. (1997). Structural analysis of the Trichodesmium nitrogenase iron protein: implications for aerobic nitrogen fixation activity. *FEMS Microbiol. Lett.* 153, 303–309. doi:10.1016/S0378-1097(97)00259-0.

Zehr, J. P. (2011). Nitrogen fixation by marine cyanobacteria. *Trends Microbiol.* 19, 162–173. doi:10.1016/j.tim.2010.12.004.

Zehr, J. P., and Ward, B. B. (2002). Nitrogen Cycling in the Ocean : New Perspectives on Processes and Paradigms MINIREVIEW Nitrogen Cycling in the Ocean : New Perspectives on Processes and Paradigms. *Appl. Environ. Microbiol.* 68, 1015–1024. doi:10.1128/AEM.68.3.1015.

Zhang, D., Kobert, K., Flouri, T., and Stramatakis, A. (2014). PEAR: A fast and accurate Illumina Paired-End reAd mergeR. *Bioinformatics* 30, 614–620. doi:10.1093/bioinformatics/btt593.

Zhu, W., Hunt, D. J., Richardson, A. R., and Stojiljkovic, I. (2000). Use of heme compounds as iron sources by pathogenic neisseriae requires the product of the hemO gene. *J. Bacteriol.* 182, 439–447. doi:10.1128/jb.182.2.439-447.2000.

Zubkov, M. V, Sleigh, M. A., Tarran, G. A., Burkill, P. H., and Leakey, R. J. . (1998). Picoplanktonic community structure on an Atlantic transect from 50°N to 50°S. *Deep Sea Res. Part I Oceanogr. Res. Pap.* 45, 1339–1355. doi:10.1016/S0967-0637(98)00015-6.

Supplementary Information

SI Table 1: Results of Spearman's rank correlation for heme *b*, chlorophyll *a* (chl *a*), Particulate Organic Carbon (POC), Particulate Organic Nitrogen (PON), nitrate and dissolved iron (DFe) overall for the GEOVIDE cruise. All correlations shown exhibited $p<0.01$.

	Heme *b*	**Chl *a***	**POC**	**PON**	**Nitrate**
Chl *a*	0.41 (153)				
POC	0.42 (165)	0.88 (296)			
PON	0.40 (165)	0.87 (295)	0.93 (346)		
Nitrate	-0.31 (84)	-0.54(136)	-0.54(151)	-0.5(151)	
DFe	-0.07 (91)		-0.29(176)	-0.3(175)	0.28 (397)

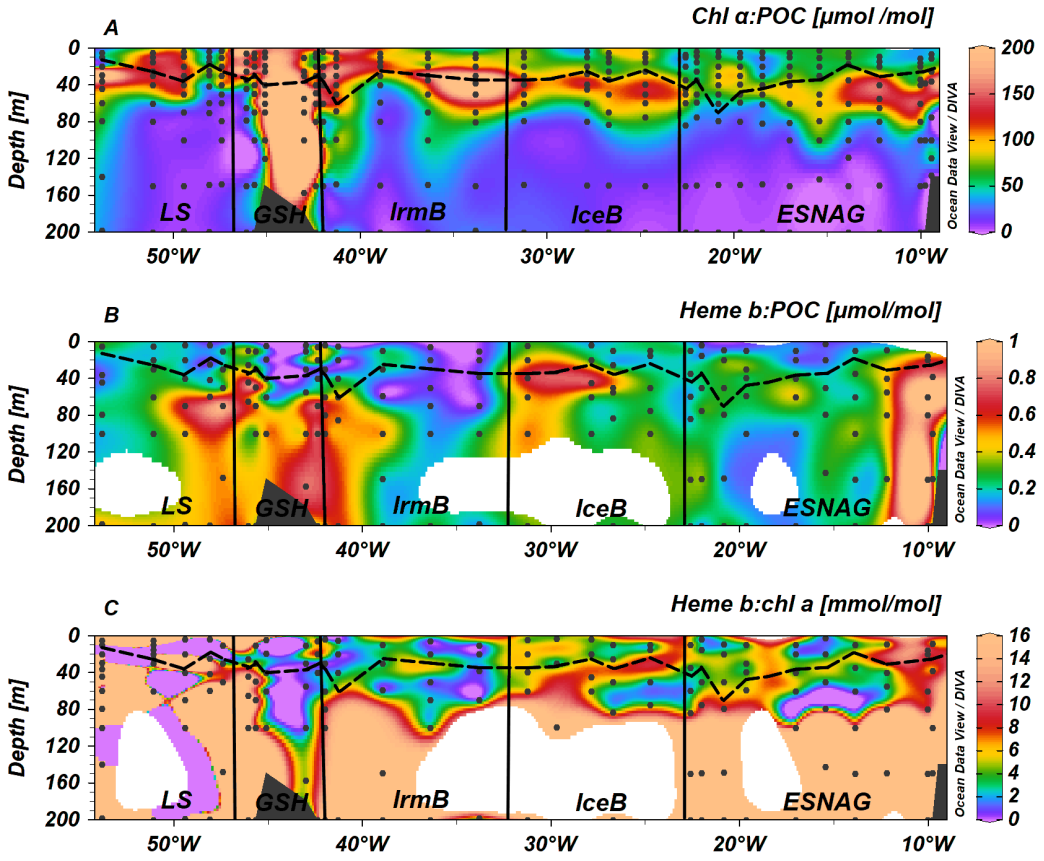

SI Fig. 1: Cross-sectional profiles across the GEOVIDE transect of the ratios A) Chrorophyll *a* (chl *a*) to Particulate Organic Carbon (POC), B) Heme *b* to POC, and C) heme *b* to chl *a*. Dashed lines indicate the Surface Mixed Layer (SML) and dots indicate the stations and depths where samples were taken. Letter annotations indicate the five oceanographic regions; Eastern Subropical North Atlantic Gyre (ESNAG), Iceland Basin (IceB), Irminger Basin (IrmB), Greenland Shelf (GSH) and Labrador Sea (LS).

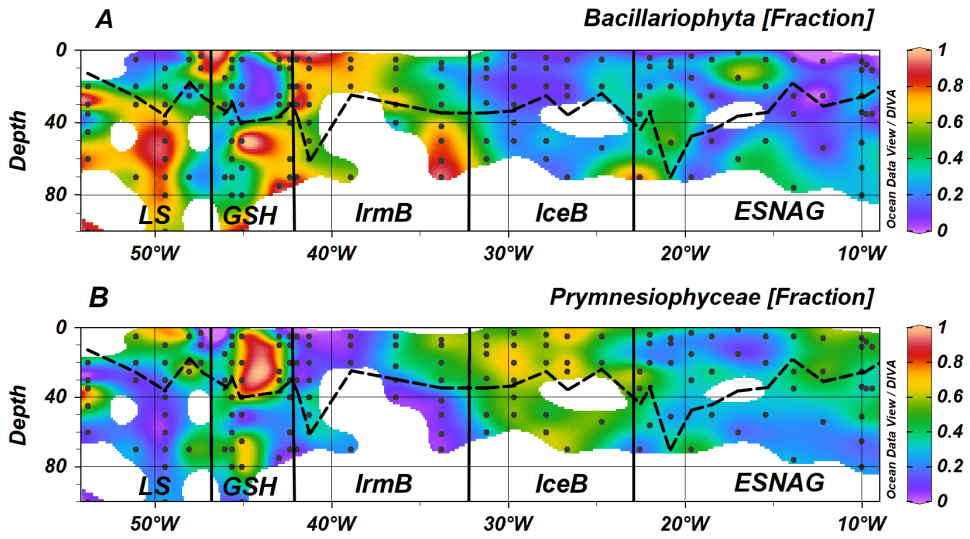

SI Fig. 2: Cross-sectional distribution of the relative abundance along the GEOVIDE transect of A) Bacillariophyta (diatoms), and B) Prymnesiophyceae. Dashed lines indicate the Surface Mixed Layer (SML) and dots indicate the stations and depths where samples were taken. Letter annotations indicate the five oceanographic regions; Eastern Subtropical North Atlantic Gyre (ESNAG), Iceland Basin (IceB), Irminger Basin (IrmB), Greenland Shelf (GSH) and Labrador Sea (LS).

SI Table 2: List of accession numbers as determined by Chloroplast (cp) 16S rRNA sequencing. New OTUs will be deposited to the GenBank.

AACY020080403	EF575247	GQ452891	HQ671788	JN976406
AB164407	EF575250	GQ452893	HQ671819	JN977301
AB196966	EF575303	GQ903342	HQ671832	JP297615
AB196967	EU005664	GU061402	HQ671857	JQ013153
AB199885	EU005687	GU061466	HQ671873	JQ013163
AB199887	EU005693	GU061468	HQ671892	JQ013176
AB200263	EU268091	GU061833	HQ671893	JQ269285
AF001655	EU394562	GU062154	HQ671898	JQ347416
AF172719	EU592338	GU119599	HQ671918	JQ586285
AF514855	EU805127	GU119711	HQ671968	JQ712399
AM259746	EU805239	GU119856	HQ672013	JQ753195
AM690833	EU919835	GU119858	HQ672015	JX015718
AY135682	EU919855	GU119861	HQ672034	JX015817
AY702176	FJ002166	GU119871	HQ672070	JX016173
DQ395642	FJ002174	GU208415	HQ672084	JX016292
EF573661	FJ002180	GU234935	HQ672098	JX016404
EF573710	FJ002195	GU940753	HQ672103	JX016417
EF573851	FJ002202	HM057648	HQ672106	JX016502
EF573980	FJ002206	HM057655	HQ672112	JX016595
EF574021	FJ002214	HM057658	HQ672114	JX016622
EF574253	FJ002228	HM057665	HQ672126	JX016649
EF574408	FJ002231	HM057706	HQ672137	JX016811
EF574443	FJ002238	HM057742	HQ672159	JX016902
EF574473	FJ425629	HM057746	HQ672178	JX016925
EF574510	FJ456816	HM057791	HQ672197	JX016969
EF574561	FJ612433	HM127595	HQ672204	JX017139
EF574585	FJ649257	HM594190	HQ672210	JX017189
EF574660	FJ745174	HM594191	HQ672216	JX297813
EF574672	FJ745242	HQ671772	JF272023	JX537814
EF574676	FJ826098	HQ203795	JF272162	JX537830
EF574682	FJ826213	HQ203812	JF272166	JX537894
EF574706	FJ826217	HQ203931	JF277129	JX537910
EF574730	FJ826341	HQ203940	JF277140	JX559213
EF574742	FJ826342	HQ203943	JF277152	KC425548
EF574745	FJ849120	HQ230156	JF344318	KC425580
EF574836	FN396639	HQ241996	JF830226	NC_007288
EF574861	FN396684	HQ242008	JN207202	NC_012097
EF574864	FN396754	HQ242211	JN207221	U32670
EF574908	GQ250620	HQ242461	JN207230	U32671
EF574962	GQ340169	HQ242621	JN457994	U70723
EF575130	GQ347890	HQ242646	JN625650	X82156
EF575192	GQ348575	HQ671746	JN874342	

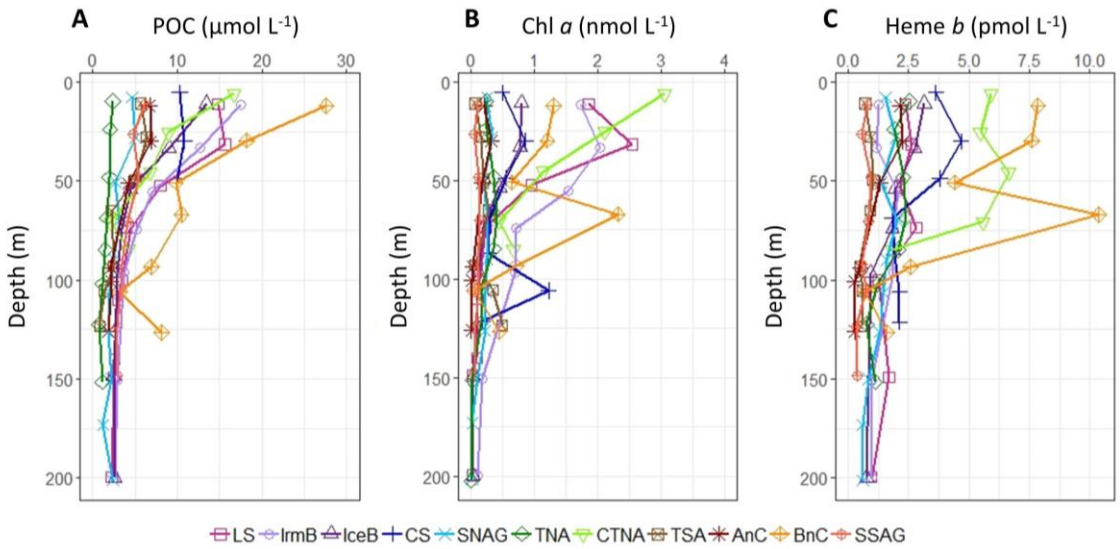

SI Fig. 3: Average depth profiles for particulate organic carbon (POC), chlorophyll *a* and heme *b*. Dots represent the average concentration of each parameter in each depth horizon from 0 down to 220m. Colours indicate the oceanographic region; Labrador Sea (LS), Labrador Sea (LS), Irminger Basin (IrmB), Iceland Basin (IceB), Celtic Sea (CS), Subtropical North Atlantic Gyre (SNAG), Tropical North Atlantic (TNA), Coastal Tropical North Atlantic (CTNA), Tropical South Atlantic (TSA), Angola Current (AnC), Benguella Current (BnC) and Subtropical South Atlantic Gyre (SSAG).

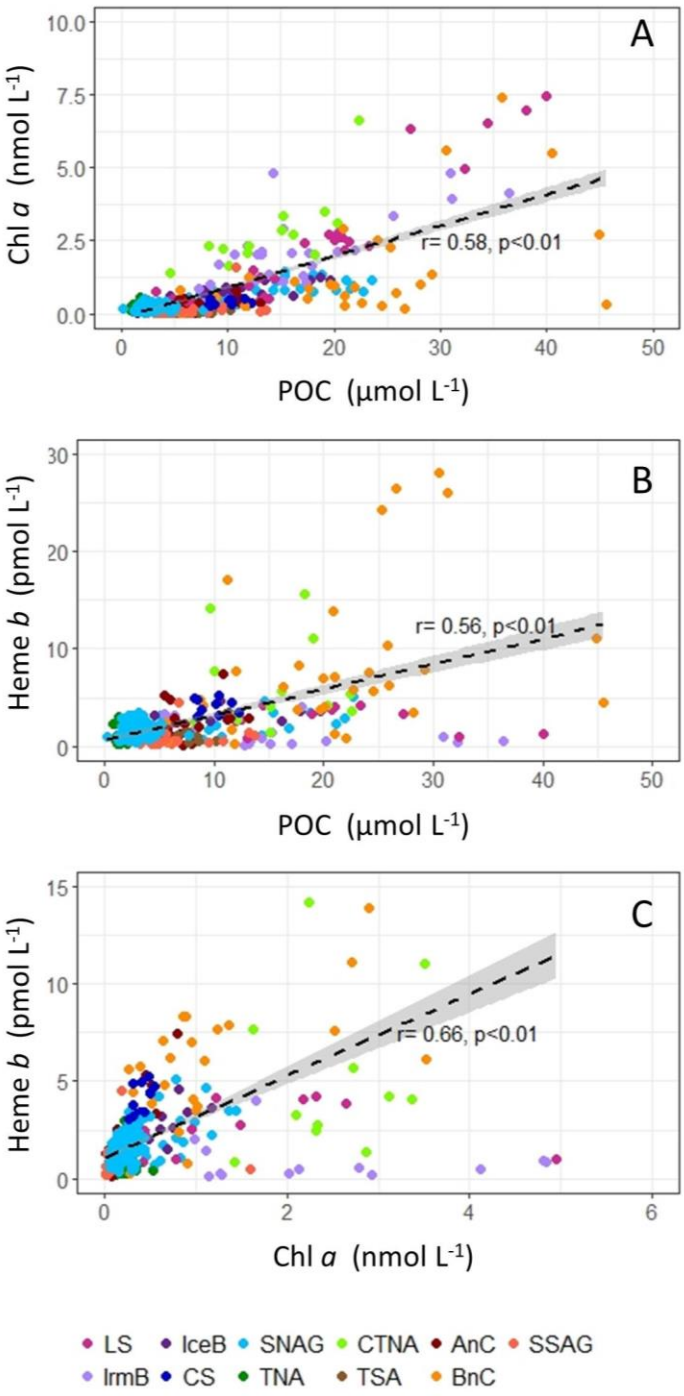

SI Fig. 4: Scatter plots of A) chlorophyll *a* versus particulate organic carbon (POC), B) heme *b* versus POC and C) heme *b* versus chlorophyll *a* for the surface mixed layer (SML). Dots indicate data points and colours indicate the oceanographic regions. Letter annotations indicate the correlation coefficients after Spearman's rho rank test. Irminger Basin (IrmB) and the subtropical South Atlantic (SSAG) were excluded from the correlations.

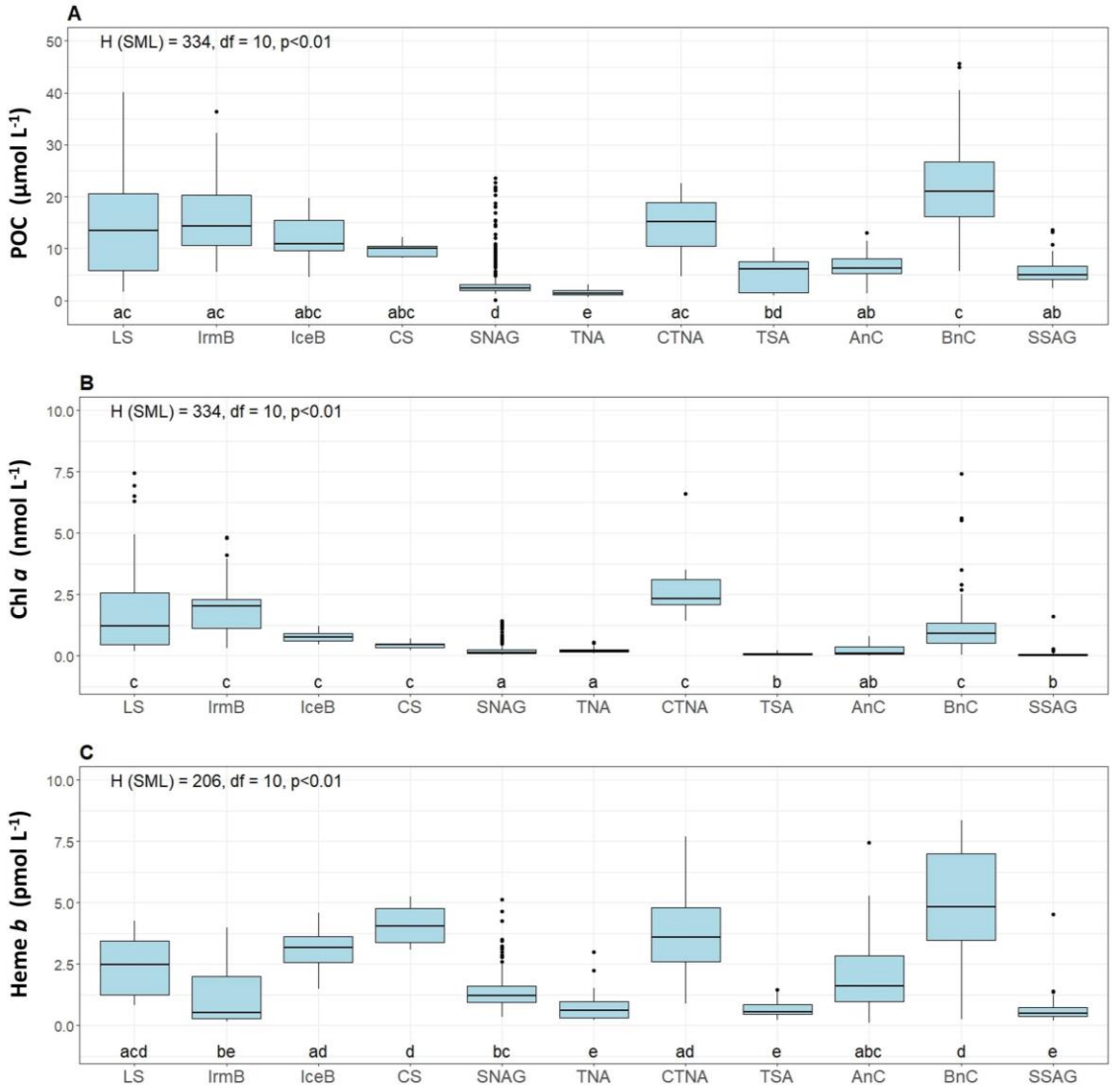

SI Fig. 5: Boxplots of distributions in the surface mixed layer (SML) of A) Particulate Organic Carbon (POC), B) Chlorophyll *a*, and C) heme *b* for the eleven oceanographic regions; Labrador Sea (LS), Labrador Sea (LS), Irminger Basin (IrmB), Iceland Basin (IceB), Celtic Sea (CS), Subtropical North Atlantic Gyre (SNAG), Tropical North Atlantic (TNA), Coastal Tropical North Atlantic (CTNA), Tropical South Atlantic (TSA), Angola Current (AnC), Benguella Current (BnC) and Subtropical South Atlantic Gyre (SSAG). On top of sub-plots A, B and C the result of the Kruskal-Wallis test is annotated. Letters (letters a to c) below the boxes indicate the Compact Letter Display (cld) of the statistically significant different groups in the SML after a Post-hoc test for multiple comparisons of groups.

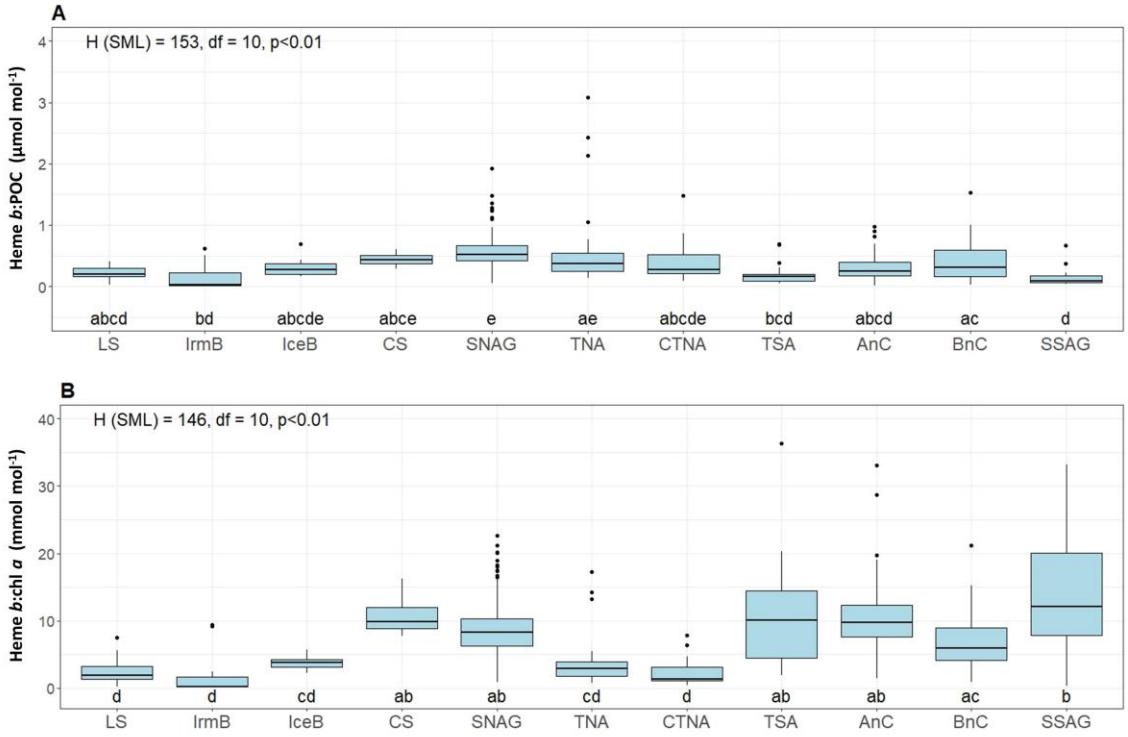

SI Fig. 6: Boxplots of distributions in the surface mixed layer (SML) of the ratios A) heme *b*:POC, and B) heme *b*:chl *a* for the eleven oceanographic regions; Labrador Sea (LS), Labrador Sea (LS), Irminger Basin (IrmB), Iceland Basin (IceB), Celtic Sea (CS), Subtropical North Atlantic Gyre (SNAG), Tropical North Atlantic (TNA), Coastal Tropical North Atlantic (CTNA), Tropical South Atlantic (TSA), Angola Current (AnC), Benguella Current (BnC) and Subtropical South Atlantic Gyre (SSAG). On top of sub-plots A and B the result of the Kruskal-Wallis test is annotated. Letters (letters a to c) below the boxes indicate the Compact Letter Display (cld) of the statistically significant different groups in the SML after a Post-hoc test for multiple comparisons of groups.

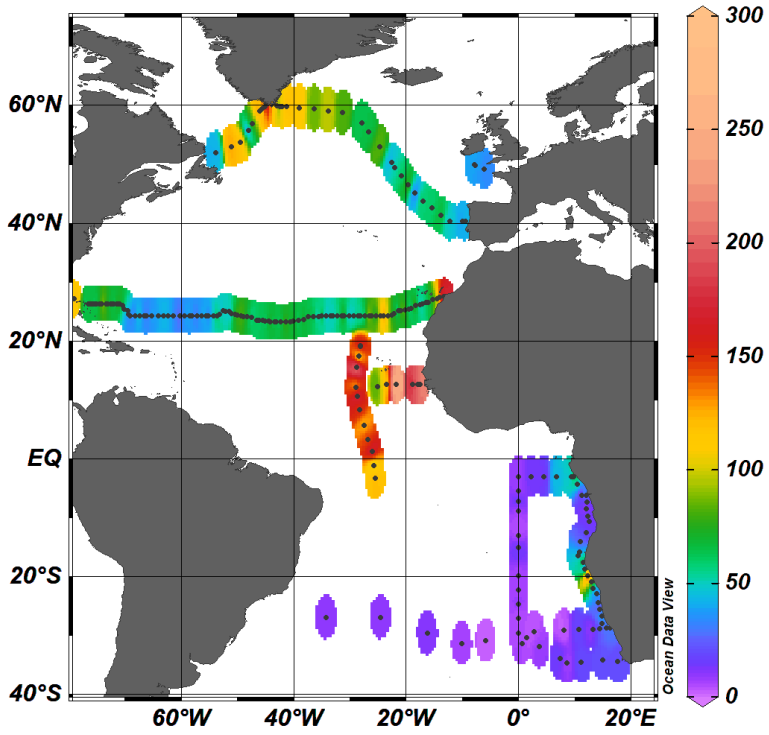

SI Fig. 7: Surface plot of the median values in the Surface Mixed Layer (SML) of chlorophyll *a* to particulate organic carbon (chl a:POC) ratio. Dots indicate the sampled stations.

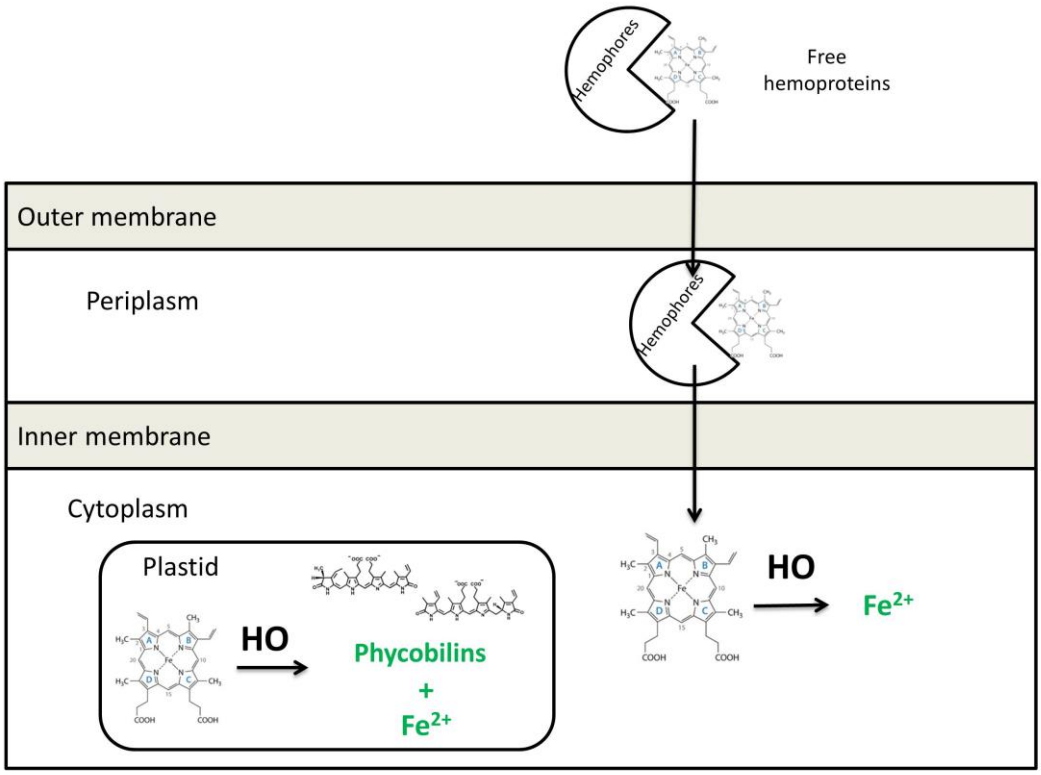

SI Fig.8: Schematic of the heme oxygenase (HO) functions within the cells of *Cyanothece*. Two HOs are potentially localized in different areas of the cell; in the cytoplasm HOs are associated with Fe acquisition processes via degrading extracellular hemes, which are transported in the cell through the membranes. In the plasmid, HOs are responsible for the production of phycobilins which are subsequently used in the phycobiliproteins of the light harvesting apparatus. Uptake of the extracelluar hemes occurs potentially via hemophores and transport through the membranes is achieved via receptor proteins (Krewulak and Vogel, 2008; Wandersman and Delepelaire, 2004).

Declaration

I, Evangelia Louropoulou, hereby declare that I have written this Ph.D. thesis independently, under compliance of the rules for good scientific practice of the German Research Foundation. I declare that I have used only the sources, the data and the support that I have clearly mentioned. Moreover, I assure that this Ph.D. thesis has not been submitted for the conferral of a degree elsewhere, and that none of my academic degrees has ever been withdrawn. Published or submitted for publication manuscripts are identified at the relevant places.

Kiel, June 2019

_____

(Evangelia Louropoulou)